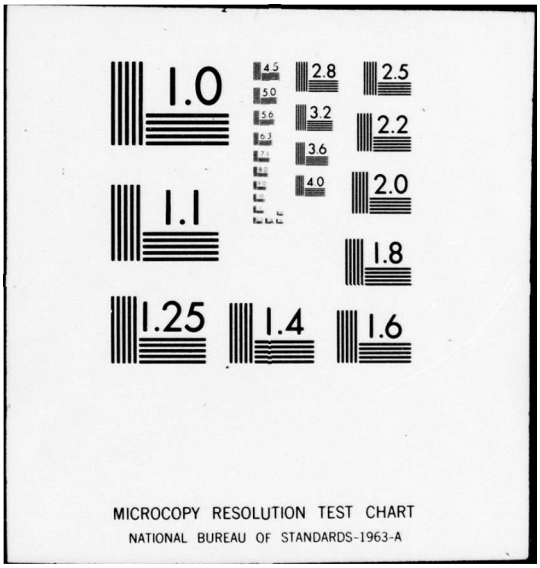
AD-A055 436 CALIFORNIA UNIV LOS ANGELES DEPT OF ATMOSPHERIC SCIENCES F/G 20/1
PROBLEMS AND TECHNIQUES OF SOUND RANGING.(U)
AUG 77 M G WURTELE, J ROE

UNCLASSIFIED DAAD07-75-C-0087

NL

1 OF 3
AD
A055 436




1.0
1.1
1.25
1.4
1.6
1.8
2.0
2.2
2.5
2.8
3.2
3.6
4.0
4.5
5.0
5.6
6.3
MICROCOPY RESOLUTION TEST CHART
NATIONAL BUREAU OF STANDARDS-1963-A

FOR FURTHER TRAN

(6) PROBLEMS AND TECHNIQUES OF SOUND RANGING,

(10) M. G. Wurtele and John Roe

(9) Final Report,

Contract No. DAAD07-75-C-0087
(15)

AUGUST 1977

(11) Aug 77

(12) 216p.

AD A055436

DDC
RECEIVED
JUN 15 1978
E

AD No.
DDC FILE COPY

Department of Atmospheric Sciences
University of California
Los Angeles, CA 90024

78 06 14 005
409 787

TABLE OF CONTENTS

Partial contents:

Section 1. Introduction

2. A Complete and Geometrically Accurate Formulation of the Basic Sound-Ranging Equations;

3. Ray Theory, Diffraction, and Scattering;

4. The Effect of an Absorbant Ground Surface, or Plane vs. Spherical Waves and Pulses;

5. The Effect of a Stratified Atmosphere;

6. The Effect of a Terrain Obstacle;

7. The Propagation of a Howitzer Blast; and

8. Analysis of PASS Data.

9. A More General View of the Sound-Ranging Problem

10. Conclusions and Recommendations

11. References

ACCESSION for
NTIS White Section
DDC Buff Section
UNANNOUNCED
JUSTIFICATION per Letter on File
BY
DISTRIBUTION/AVAILABILITY CODES
Dist. AVAIL. and/or SPECIAL
A

A

78 06 14 005

1. INTRODUCTION

The principles upon which sound ranging is based were formulated in the second decade of the century, during World War I and remain equally the basis for the techniques as they exist today. The fundamental assumption is that the sound rays proceed spherically outward from the source to the receivers, moving with the local speed of sound as modified by the wind velocity, along a shortest pathlength, regardless of terrain, character of ground surface, and stratification of the atmosphere. The field procedures, as set forth in FM 6-122 (1964), are designed as follows. The measured differences in arrival times are recorded, then modified successively by a temperature correction, a curvature correction, and a wind correction, all calculated from graphical devices.

The continued use of sound ranging by artillery services throughout the world for more than a half-century testify to the essential validity of these assumptions and to the techniques adopted for their field application. However, it does not follow that a reconsideration of the physics involved cannot lead to an improvement in the accuracy of results under certain conditions of atmosphere and terrain.

It was therefore the philosophy of the principal investigator to attack the entire problem of sound ranging ab initio--from the ground up, both figuratively and literally (since important results are obtained for certain types of ground cover). The following questions are thus asked and answered in this report:

(1) How valid is the assumption of linear propagation of a signal rising from the firing of an 8-inch howitzer?

(2) How important is the directional effect of the howitzer, that is, does the sound propagate as a spherical wave?

(3) To construct the most accurate formulation of the basic sound ranging formulas and program them for digital computer.

(4) What is the effect of atmospheric density and temperature stratification?

(5) What is the value of "ray tracing" in sound ranging?

(6) What is the effect of an absorbant ground surface, such as ploughed earth or meadow-land?

(7) What is the effect of terrain obstacles, in particular, hills of hundreds of meters in elevation?

(8) Is it possible to use any of the signal information received, other than the time of arrival?

In considering and answering these questions we have used digital computation of the full non-linear equations of motion; analytic formulations followed by digital evaluation of the results, and data from the Artillery Meteorological Comparisons of the Atmospheric Sciences Laboratory, at White Sands Missile Range, Oct/Nov, 1974.

Throughout the work, the consideration was uppermost to incorporate all results in operational form for sound ranging. However, this is not always possible at the present time because of the lack of empirical studies of sound transmission in the

low frequency range employed by current sound ranging instrumentation.

Readers interested in results rather than methods may turn to the section titled Conclusions and Recommendations.

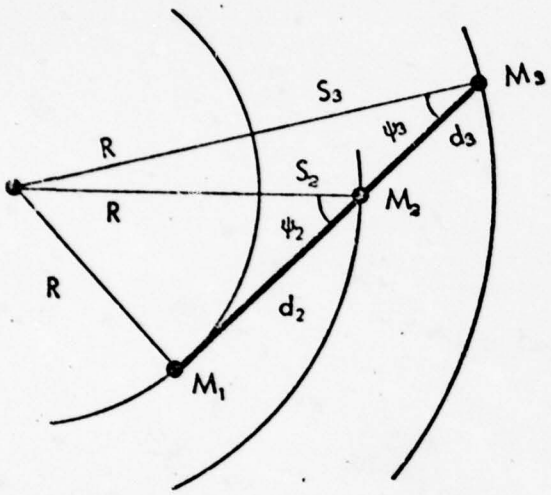
2. A COMPLETE AND GEOMETRICALLY ACCURATE FORMULATION OF THE BASIC SOUND-RANGING EQUATION

The sound ranging computational routine of FM6-122 was devised for field use before the development of small electronic programmable calculators. Thus we shall derive all formulas in this report under the assumption that such calculators will be available under field conditions. The calculating routines are not long or involved, and the necessary programs are provided in this report.

First, we shall derive two alternative formulations of the basic geometric formulas. In Figure 2.1, S is the sound-source, R the distance to the microphone M_1, and $R+s_2$ and $R+s_3$ the distances from M_2 and M_3 respectively. The three microphones are assumed to be in a straight line, separated by distances d_2 and d_3. Applying the law of cosines to the traingles SM_1M_3 and SM_2M_3, we have, respectively,

$$\begin{aligned} R^2 &= (R+s_3)^2 + (d_2+d_3)^2 - 2(R+s_3)(d_2+d_3)\cos\psi_3 \\ (R+s_2)^2 &= (R+s_3)^2 + d_3^2 - 2d_3(R+s_3)\cos\psi_3 \end{aligned} \qquad (2.1)$$

Elimination of $\cos\psi_3$ yields the formula for R,



If $d_2 = d_3 = d$

$$2\,d\cos\psi_3 = \frac{2S_2S_3(S_3 - S_2) + 2d^2(4S_2 - 3S_3)}{4S_2S_3 - 2S_2^2 - S_3 - 2d^2}$$

$$\left[2R = \frac{S_3^2 - 2S_2^2 - 2d^2}{2S_2 - S_3}\right]$$

Figure 2.1 Geometry of the Sound-Ranging Problem.

78 06 14 005

$$2R = \frac{d_2 d_3 (d_2 + d_3) + (d_2 + d_3) s_2^2 - d_2 s_3^2}{- d_3 s_3 + (s_3 - s_2)(d_2 + d_3)} \qquad (2.2)$$

If we now, for simplicity, take the case in which the microphones are equally spaced,

$$d_2 = d_3 = d ,$$

we have the simpler relation,

$$2R = \frac{2d^2 + 2s_2^2 - s_3^2}{s_3 - 2s_2} \qquad (2.3a)$$

These relations for R may be substituted into a law-of-cosines (2.1) to obtain the corresponding formulas for $\cos \psi_3$. Letting

$$D = d_2 + d_3$$

we have

$$D \cos \psi_3 = \frac{d_3^2 D s_3 + D(s_3 - s_2)(s_2 s_3 - D^2)}{D s_2 (2s_3 - s_2) - d_2 d_3 D - d_2 s_3^2}$$

and for the case of equally spaced microphones,

$$2d \cos \psi_3 = \frac{2d^2 (4s_2 - 3s_3) + 2s_2 s_3 (s_3 - s_2)}{4s_2 s_3 - 2s_2^2 - s_3^2 - 2d^2} \qquad (2.3b)$$

In the sequel we shall assume equally-spaced microphones so that the formulas are shorter. There is no principled difficulty of deriving any of the formulas for the general case of arbitrary spacing or, for that matter, of arbitrary, rather than straight line, configuration.

A second derivation is based upon the geometric theorem that the locus of a point, the difference in distance of which from two given points is constant, is a hyperbola, with the two points as foci, thus a single pair of microphones determine that the source S lies on a certain hyperbola, and a second pair, another hyperbola. The intersection of these two hyperbolas uniquely specifies the source location.

Consider the line of the three equally-spaced microphones to be the x-axis, with the origin located midway between M_1 and M_2 (Figure 2.2). Thus M_1 is located at $x = -d/2$, M_2 at $x = d/2$ and M_3 at $x = 3d/2$. The hyperbola with foci at $(\pm d/2, 0)$ and with constant distance s_2 has the equation for M_1 and M_2

$$\frac{x^2}{s_2^2} - \frac{y^2}{d^2 - s_2^2} = \frac{1}{4}$$

The corresponding equation for M_2 and M_3 is obtained by applying the same formula at the point $x = -d$, that is by letting $x' = x + d$ with

$$\frac{x'^2}{s'^2} - \frac{y^2}{d^2 - s'^2} = \frac{1}{4}$$

(Here of course $s' = s_3 - s_2$ in terms of Figure 2.1). We have two equations in

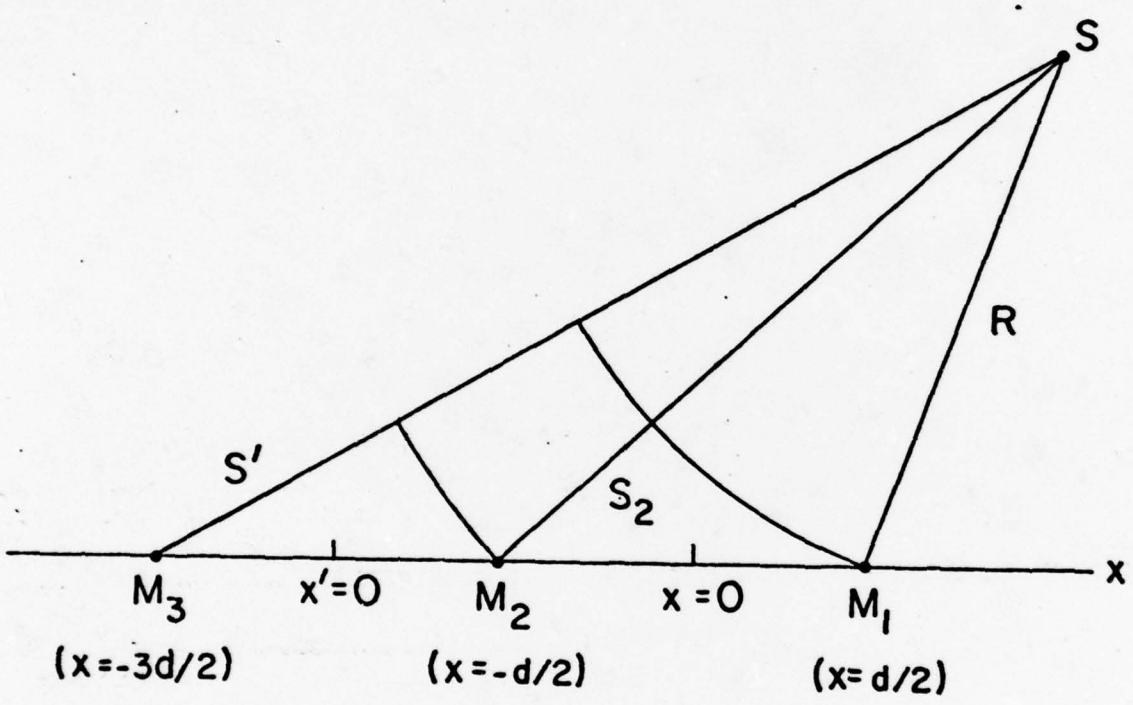


Figure 2.2 Alternative Geometry of the Sound-Ranging Problem.

two unknowns, and by elimination we obtain

$$x = \frac{s_2^2}{d} \frac{(d^2 - s'^2)}{(s'^2 - s^2)} \left\{ 1 \pm \left[1 + \frac{d^2(s^2 - s_2^2)}{s_2^2 (d^2 - s'^2)} + \frac{s'^2}{4s_2^2} \frac{(s'^2 - s^2)^2}{(d^2 - s'^2)^2} \right]^{\frac{1}{2}} \right\} \tag{2.4a}$$

where the minus sign is used if M_2 is closer to s than M_1 (i.e., if the signal arrives first at M_2). This value for x is then substituted into the formula

$$y = \left[\frac{(d^2 - s_2^2)}{s_2^2} x^2 - \frac{1}{4}(d^2 - s_2^2) \right]^{\frac{1}{2}} \tag{2.4b}$$

to obtain the coordinate of s normal to the base line.

The formulations (2.3) and (2.4) are exactly equivalent, the former giving the result in polar, the latter in cartesian, coordinates. We shall refer to polar coordinates hereafter, since these are the natural expression of range and azimuth.

We now turn to the problem that really concerns us in this report: how to specify the distances s_2 and s_3 from the time-differences of the signal arrivals at M_1, M_2, and M_3. If the spherical sound wave is perfectly reflected by the ground and is not diffracted, scattered, or advected, then

$$s_i = C \Delta t_i \qquad i = 2, 3 \tag{2.5}$$

where Δt_i is the time difference in the arrival of the signal at M_i and M_{i-1}.

To the extent that these assumptions are invalid in any particular event, or that instrumental error effects the value of the Δt_i, the basic sound ranging formulas (2.3) will give results more or less in error.

It does not require detailed error analysis to see that a small percentual error in estimating the s_i will lead to a small percentual error in calculating $\cos \psi_3$ by (2.3b), but a large percentual error in calculating R by (2.3a). To take a simple instance, let

$$d = 2 \text{ km}, \qquad R = 7.07 \text{ km}, \qquad \cos \psi_3 = 0.874$$

corresponding to true values of $s_2 = 1.531$ and $s_3 = 3.225$. If we use the estimates $s_2 = 1.53$ and $s_3 = 3.25$--an error of less than one percent--we obtain

$$\cos \psi_3 \doteq 0.862 \qquad R \doteq 5.58$$

an error of about one percent in $\cos \psi_3$ and 21 percent in R. It cannot improve the accuracy to use different but equivalent formulas--for example, (2.4), in cartesian coordinates. The great sensitivity of the calculations to input errors is inherent in any ranging system using the given information inputs, to wit, the signal-arrival time differences.

All this is well known to persons acquainted with sound ranging or any other type of ranging. It is restated here for completness and emphasis. There are two approaches to reluction of error that will be considered in this report:

(1) A more consistent and--it is hoped--accurate formulation of the effect of a wind field; and (2) a suggested means of incomporating the effects of diffraction

by each of a number of physical sources: atmospheric temperature gradients; an absorbant ground surface; and surface irregularities such as hills. In each case it will be shown that under certain conditions in nature significant errors could arise by failure to take account of the accompanying effects in a proper way.

Distortion by a constant wind field

The geometry of the sound ranging problem is so complicated in the case of even a uniform wind that we must begin the derivation from scratch in order to keep track of all approximations. Let the speed of the wind by U, directed along the x-axis, without loss of generality. The wave front is then given by the equation (Whitham, 1974, pp. 254-259)

$$(x - Ut)^2 + y^2 = c^2 t^2. \tag{2.6}$$

We may rewrite this equation in terms of R, the distance from the source:

$$R^2 - 2x\,Ut = (c^2 - U^2)\, t^2 \tag{2.7}$$

This configuration is illustrated in Figure 2.3 for the two points M_1 and M_2. The observed data are U, θ , and the time difference $t_2 - t_1$. Obviously it is necessary to make simplifying assumptions. The single assumption we shall make is that the Mach number is small, that is

$$U^2 \ll c^2$$

or

$$U^2 t^2 < R^2. \tag{2.8}$$

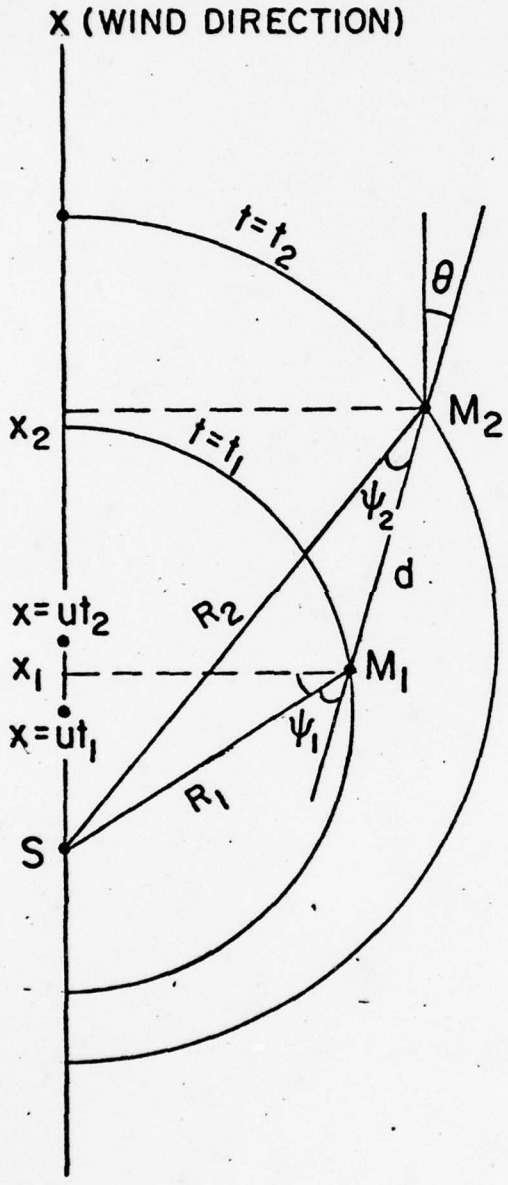


Figure 2.3 Geometry of Wind Correction.

No approximations are made concerning the curvature. Given this assumption, we can write (2.7) in the form

$$R \doteq ct\left[1 + \frac{2xU}{c^2t}\right]^{\frac{1}{2}}$$

$$\doteq ct\left[1 + M\frac{x}{R}\right] \tag{2.9}$$

If we now apply this result at the two stations M_1 and M_2, we have

$$s_2 = R_2 - R_1 \doteq c(t_2 - t_1) + U\left[\frac{x_2}{R_2}t_2 - \frac{x_1}{R_1}t_1\right] \tag{2.10}$$

or letting $\Delta t_2 = t_2 - t_1$, and using the first order approximation,

$$Ut \doteq MR ,$$

we have

$$s_2 \doteq c\Delta t_2 + M(x_2 - x_1)$$

or

$$s_2 \doteq c\Delta t_2 + Md\cos\theta \tag{2.11}$$

with a similar approximation for s_3. When these relations are substituted into the ranging equations, a result is obtained valid to the first order in the Mach number with no approximations as to the curvature, that is, no assumptions that d/R or $(x_2 - x_1)/R$ are small. It would be possible to carry out the approximations to the

second order in the Mach number, or to work implicit equations of form (2.7). However, the present approximations are satisfactory in almost all cases in nature.

In any event, the ranging formulas as here written are a consistent approximation. They are programmed in FORTRAN, with a listing provided in Appendix A. It should be emphasized that this simple program is well within the capability of current hand-held programmable computers, an ideal and flexible piece of field equipment.

3. RAY THEORY, DIFFRACTION, AND SCATTERING

It was mentioned in Section 1 that sound ranging is based upon the assumption that a ray travels along the ground surface with the local speed of sound. It is the purpose of this section to relate this assumption to the theory of ray-tracing, and to the theories of diffraction and scattering.

The fundamental partial differential equations for families of sound wave fronts and for the associated ray paths were set forth formally by Milne (1921). We may gain insight into their structure by taking a simple instance of two-dimensional propagation, say, in the (x,z)-plane, with the speed of sound varying only in the z-direction. This is, of course, a reasonably realistic direction.

The ray-path equations are then (Milne, 1921, p. 102)

$$\frac{dz}{dx} = \tan\theta, \tag{3.1a}$$

together with the refraction equation,

$$c(z) \sin\theta_o = C_o \sin\theta . \tag{3.1b}$$

Here θ is the angle of the ray with the vertical, $c(z)$ is the stratified sound speed, and the subscript zero denotes initial values for the ray being traced. The integral formulation of (3.1) is

$$x = x_o + \sin\theta_o \int_{z_o}^{z} \frac{c(z)dz}{c_o^2 - \sin^2\theta_o c^2} , \tag{3.2}$$

This is consistent with our qualitative understanding that rays are deflected concavely toward lower temperatures. For example, if c decreases upward, (3.2) shows that for

Figure 3.1 (following page) Ray Structure for Various Atmospheric Lapse Rates of Temperature (after Franck and Sager (1974)).

Abscissa is horizontal direction and ordinate is vertical. Plotted lines are rays, labelled in degrees of initial inclination to vertical. Stippled areas are zones of silence. The temperature structures in each of the cases are:

4a. Lapse rate is 80 percent dry adiabatic.

4b. Temperature inversion surface to 85 m.

4c. Temperature inversion surface to 151 m.

4d. Temperature inversion surface to 200 m.

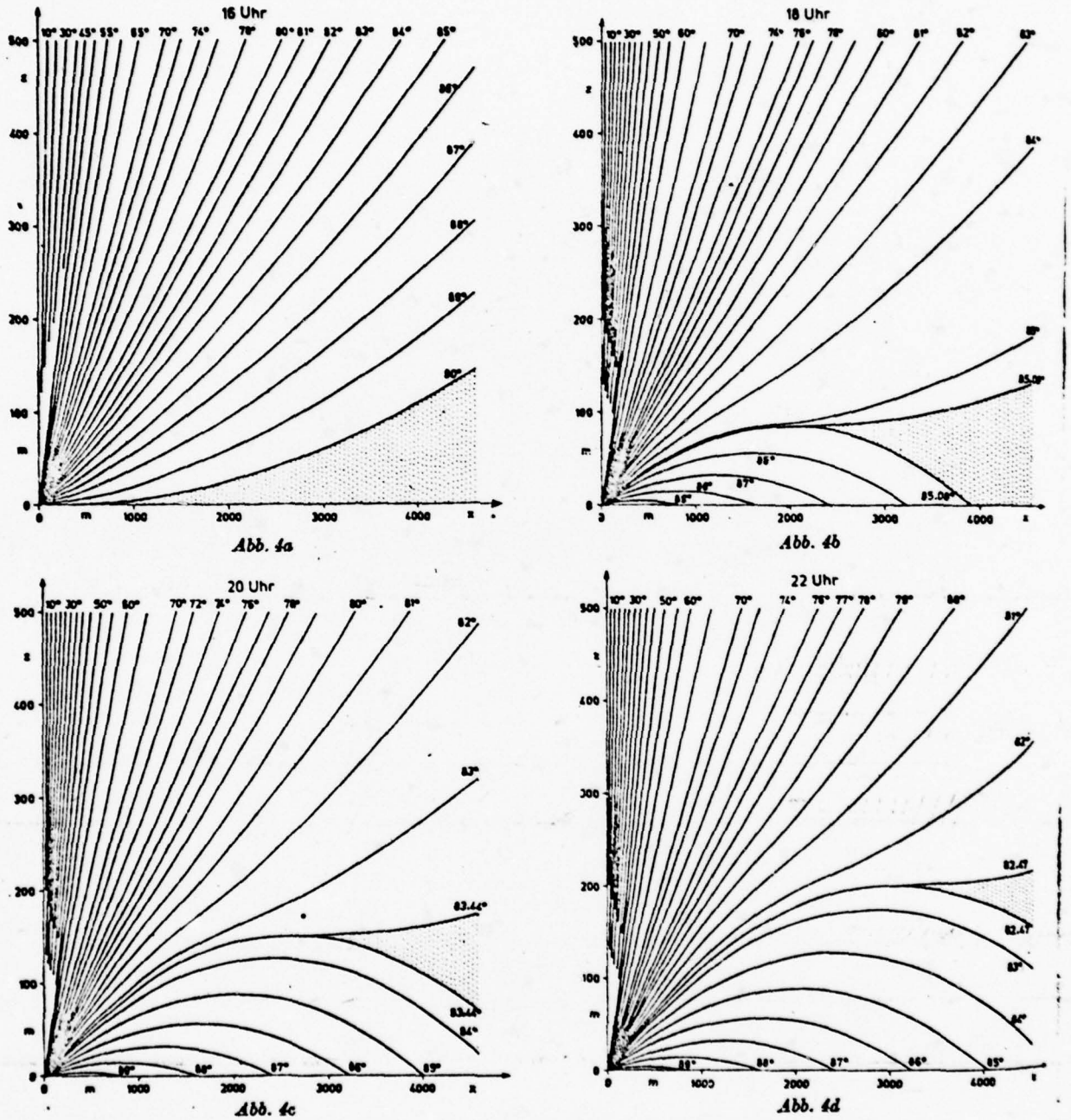


Abb. 4a *Abb. 4b* *Abb. 4c* *Abb. 4d*

Abb. 4. Schallverteilung bei bodennaher Schallquelle vor (a) und während der Bodeninversion (b bis h)

Figure 3.1

$\theta_o > 0$, then x and z increase together, that is the ray is concave upward. Points at which rays are oriented horizontally define the beginning of shadow areas into which the rays given by (3.2) cannot penetrate. Such ray patterns are often calculated for atmospheric conditions. For example, Franck and Sager (1975) exhibit their ray calculations (Figure 3.1) for temperature profiles at different times of day, indicating the shadow zones, the sound source being at ground level.

Calculations such as these are correct as far as they go; but they must not be interpreted as presenting a complete picture of sound transmission. Formulations of the ray equations, whether in simplified models like (3.1) or in terms of the most general geometric optics, describe the complete problem only in an unlimited medium. If a boundary is present, the boundary condition becomes part of the problem, and the equations must be reformulated. The shadow boundary is defined as before, but now the disturbance propagates over the boundary into the shadow with the local sound speed. The wave fronts and rays in the shadow area are said to be diffracted. This state of affairs is diagramatically represented in Figure 3.2. The most complete presentation of the methods of geometrical acoustics is that of Friedlander (1958).

Thus the basic sound ranging assumption is in a strict sense more valid than the limited ray theory such as that developed in Milne (1921) and applied by Franck and Sager (1975). However, despite its correctness as concerns arrival time, this assumption gives no indication of the amplitude signature of the arriving signal. We shall see that diffraction drastically alters the wave or pulse form, and that this alteration may produce significant errors if ignored in sound ranging procedures.

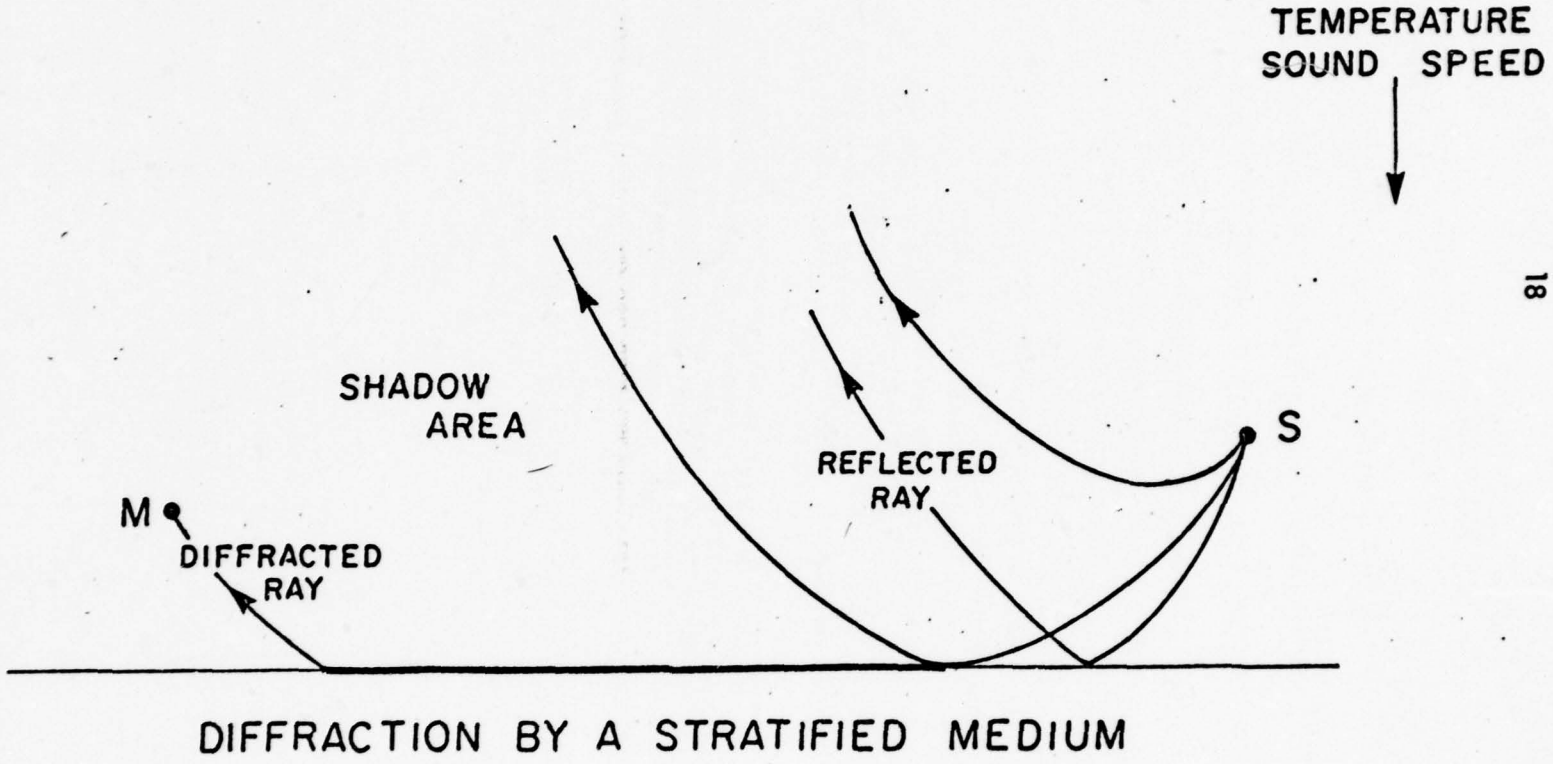


Figure 3.2 Schematic Representation of Ray Diffraction in a Stratified Medium.

What has been said above of a stratified atmosphere is equally applicable to the problem of propagation over an obstacle or over an absorbing surface. A transmitted pulse propagates into the geometric shadow as a diffracted pulse. Although the physical mechanisms are similar, there are quantitative differences, and calculations must be performed separately for each physical model.

There is, of course, another fundamental objection to simple ray-tracing, which is applicable also to geometric acoustics in general. If the scatterer--whether it be a temperature gradient or a solid obstacle--has a characteristic length of the order of the wave length of the scattered signal, geometric acoustics becomes a poor or invalid approximation to the true solution. It is possible to treat this approximation as a first one and then to modify it. However, for purposes of this study, we shall drop entirely the physical model of rays and ray-tracing and consider each case as a boundary-value problem of mathematical physics.

4. THE EFFECT OF AN ABSORBANT GROUND SURFACE, OR PLANE vs. SPHERICAL WAVES AND PULSES

When a sound source radiates in the atmosphere, the sound travels outward radially as a spherical wave or pulse. After this signal has traveled for some minimum time, the distance from the source will be large with respect to any length scale involved in the problem. At this point, one might be tempted to ask, can the model adopted be that of a plane wave?

A first response could be that spherical and plane waves have very different dynamics, one amplitude falling off inversely with the distance and the other maintaining its amplitude unchanged as it propagates.

However, this difference of behavior is presently of little importance in sound ranging, and we turn to consider a much more fundamental objection to the plane wave model. In any problem of artillery sound ranging, the presence of the boundary surface of the earth is a fundamental consideration, and we must be careful to treat properly the problem of propagation near a solid boundary. It is an elementary result of acoustics (Morse and Ingard, 1968, p. 262) that the reflection coefficient of a plane wave at a solid boundary (called "locally reacting")

$$c_r = \frac{z\cos\theta - 1}{z\cos\theta + 1} \quad , \tag{4.1}$$

where z is the relative impedance of the boundary, ρc that of the air, and θ the zenith angle of incidence. If z is finite and $\theta = \frac{\pi}{2}$, then $c_r = -1$, and the reflected wave exactly cancels the incident wave. A plane wave cannot propagate along a boundary

of finite impedance. On the other hand, if z is infinite, then $c_r = 1$ for all angles of incidence, and the reflected wave is in phase with the incident wave, doubling the amplitude.

The only way out of this dilemma is to adopt an adequate physical model: that of a spherical wave proceeding from a point source and interacting with the boundary of arbitrary impedance. The spherical wave is mathematically decomposable into a continuous spectrum of plane waves impinging upon the plane with every angle of incidence θ. Each of these plane waves is reflected with the coefficient given by (4.1); so that when these are summed over all θ, the resultant wave is capable of propagation along a plane boundary without cancelation. When the impedance z is very large in magnitude, the spherical wave propagates almost undistorted, except that its amplitude is doubled by reflection.

It should be mentioned that another type of solid boundary--in addition to the locally reacting--is physically possible, called a boundary of "extended reaction". This is analogous to a two-media system in which the ground is interpeted as a medium that responds as an acoustic system to the passage of the atmospheric wave. The coefficient of reflection in this case is given by (Morse and Ingard, 1968, pp. 266 ff)

$$c_r = \frac{m\cos\theta - \sqrt{n^2 - \sin^2\theta}}{m\cos\theta + \sqrt{n^2 - \sin^2\theta}}$$

where $m = \rho_1/\rho$ and $n = c/c_1$, the subscripted quantities referring to the bounding medium. The locally reacting surface leading to (4.1), we interpret as one which permits penetration by air motions, but does not transmit horizontally an acoustic wave.

This may be realized, for example, by a ploughed field, or a meadow in which the soil is kept loose by the grassy growth.

The treatment of the problem of a spherical wave propagating over a plane surface of finite impedance has a long history. It was first solved by Rudnick (1947), who applied the Sommerfeld solution for electromagnetic waves to the acoustic case of a surface of extended reaction. Later Lawhead and Rudnick (1951) and Ingard (1951) investigated also the same problem for a locally-reacting surface. These and other early studies are reported in textbook form by Brekhovskikh (1960, Ch. 4).

Interest in the subject has recently revived, and a new burst of research activity has introduced new methods and increased our detailed knowledge of the solutions--see, for example, Delaney and Bazley (1970); Wenzel (1974); Chien and Soroka (1975); Thomasson (1976); and Donato (1976a, 1976b).

The points of emphasis here are (1) that especially when dealing with regions near a boundary, the plane wave approximation may be inadequate and misleading, and (2) that models involving spherical wave propagation near a boundary quickly lead to problems at or beyond the current state of the art in mathematical analysis. In the ensuing treatment, we shall take care that our approximations are valid physically as well as mathematically.

The analyses referred to above have in common that they apply to monochromatic *radiation from* an acoustic source. For our sound ranging problem, a much more realistic model is the pulse, involving the complete spectrum of waves. This is particularly

important given the fundamental role of the signal arrival time in current techniques. We shall thus restrict our attention to pulse propagation.

The basic analytical work here was performed by Doak (1952). It differs from the techniques in the monochromatic case by treating an initial-value problem and studying the signature of the signal at various distances from the source as a function of time.

We assume a simple unit step-function pressure pulse in three dimensions

$$p = \frac{H(t - R/c)}{4\pi R} \tag{4.2}$$

where $H(t)$ is the heaviside step-function,

$$\begin{aligned} H(t) &= 0 \qquad && t<0 \\ &= 1, && t>0 \end{aligned} \tag{4.3}$$

and R is the distance from the source. The source is assumed to be an arbitrary distance above a uniform locally-reacting horizontal plane of finite impedance z, so that the reflection coefficient c_r for each component wave in the pulse (4.2) is given by (4.1). The mathematics involves a number of coordinate transformations, but is entirely straightforward. For details, the reader is referred to Doak's (195?) paper. The general result may be written in the form

$$p = \frac{H(t- R/c)}{4\pi R} + \frac{H(t- r/c)}{4\pi r}$$

$$- \frac{2}{4\pi c} H(t- r/c) \int_1^{\tau} F(\theta, \lambda)d\lambda \tag{4.4}$$

where $\tau = ct/r$ and $F(\theta, \lambda)$ is the inverse Laplace transform representing the pulse as diffracted by the absorbing boundary:

$$F(\theta,\lambda) = \frac{1}{2\pi i}\int_B \frac{\exp[s(t-r\lambda/c)]}{[(1+z\lambda\cos\theta)^2+z^2(\lambda^2(\lambda^2-1)\sin^2\theta]^{\frac{1}{2}}}\,ds \qquad (4.5)$$

Here B is the Bromwich path in the complex plane, with all singularities of the integrand on the left.

The geometry of (4.4) is given in Figure 4.1, in full generality. For current sound ranging techniques, S coincides with S' at the surface, and M is also at the surface, so that R = r and $\theta = \pi/2$.

The evaluation of (4.5) depends on knowing the impedance z as a function of wave-frequency, that is, in this formulation, as a function of s. As a first approximation, we may make an evaluation for z = constant. In this case,

$$F(\theta,\lambda) = \frac{\delta(t-r\lambda/c)}{[(1+z\lambda\cos\theta)^2+z^2(\lambda^2-1)\sin^2\theta)]^{\frac{1}{2}}}$$

where $\delta(t)$ is the Dirac delta-function.

Substituting this expression into (4.4), we obtain

$$P = \frac{H(t-R/c)}{4\pi R} + \frac{H(t-r/c)}{4\pi r} - \frac{2H(t-r/c)}{4\pi r}[(1+z\tau\cos\theta)^2 + z^2(\tau^2-1)\sin^2\theta]^{-\frac{1}{2}} \qquad (4.6)$$

where, as before, = ct/R.

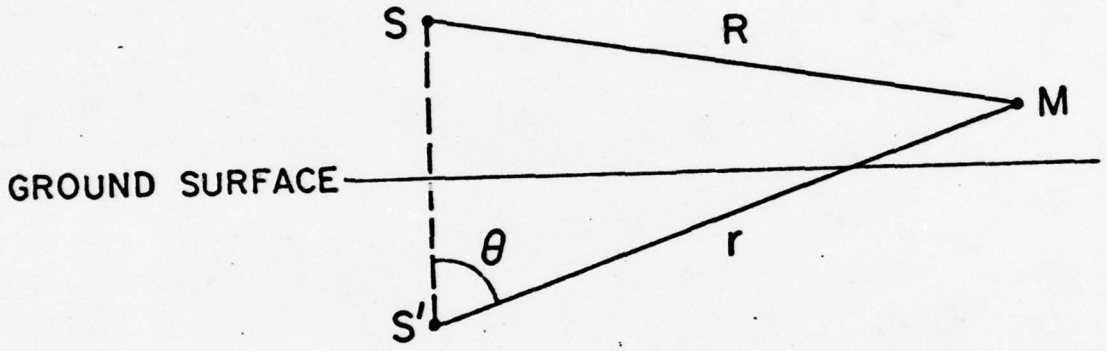


Figure 4.1 Geometry of Spherical Pulse Propagation.

The first two terms are the incident and the reflected pulses, respectively. The third term shows the effect of the locally-reacting (absorbant surface. The arrival times are those given by geometrical acoustics, but the amplitude is distorted by the diffracting effect of the surface on the reflected pulse. Just after arrival ($\tau \doteq 1$), we have

$$P \doteq \frac{1}{4\pi R} + \frac{1}{4\pi r}\left\{1 - \frac{2}{1+z\cos\theta}\right\},$$

so that for low impedance and distant points ($\theta \to \pi/2$), the diffraction can more than cancel the reflected pulse amplitude. When the signal arrival is long past ($\tau \gg 1$), we have

$$P \doteq \frac{1}{4\pi R} + \frac{1}{4\pi r}\left\{1 - 0(\tau - 1)\right\},$$

that is, the pressure is approximately the sum of the incident and reflected pulses.

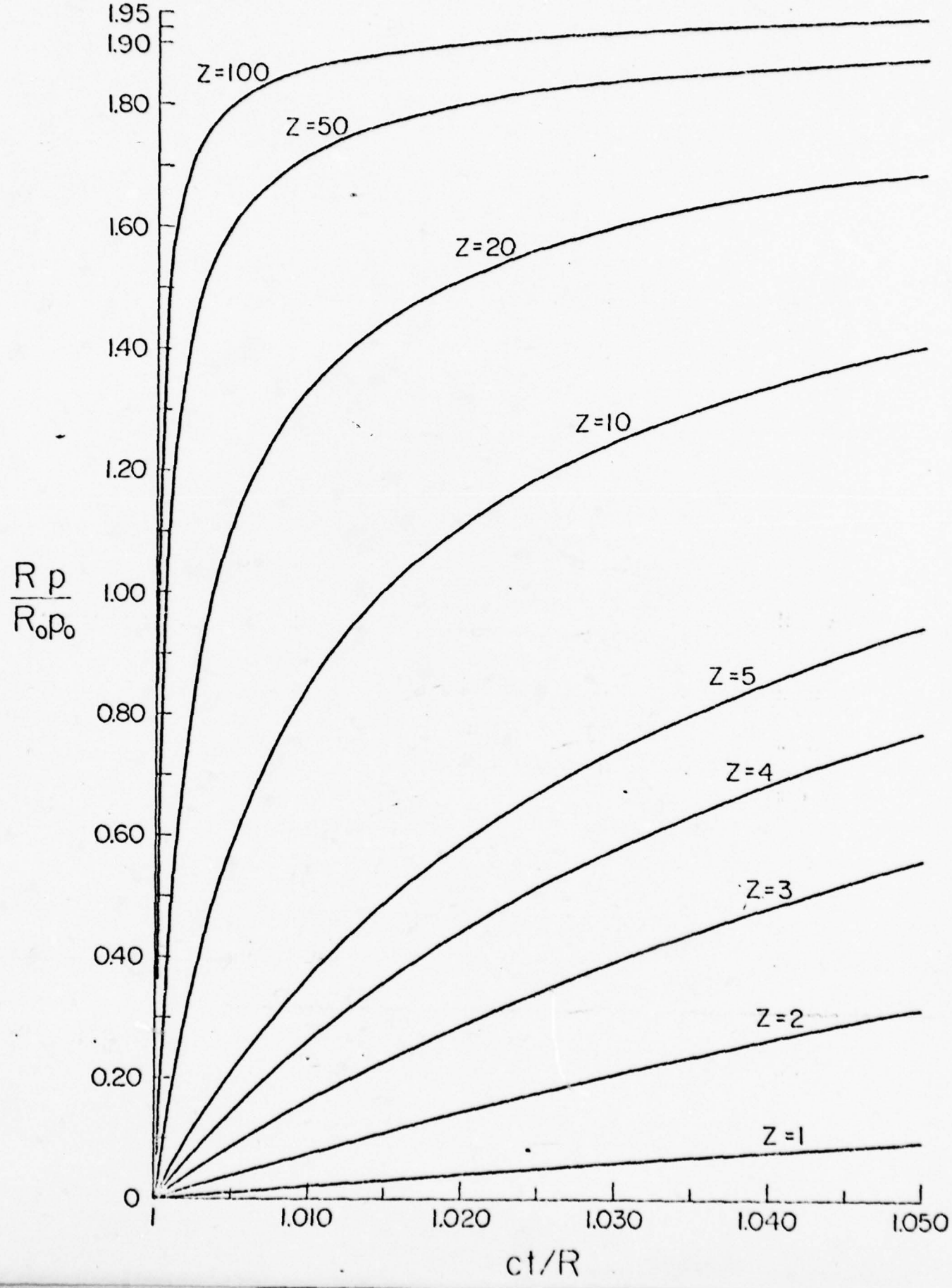
For a more detailed, quantitative analysis, we consider the special sound ranging case for which $\theta = \pi/2$, $R = r$. Thus

$$P = \frac{2H(t-R/c)}{4\pi R} - \frac{2H(t-R/c)}{4\pi R}\left[1 + z^2(\tau^2 - 1)\right]^{-\frac{1}{2}}. \qquad (4.7)$$

Incident and reflected pulses arrive simultaneously at $\tau = 1$, but at this moment the diffracted pulse exactly concels the sum of the incident and reflected pulses, so that the amplitude is zero. The diffraction dies out as time increases, but there is a non-zero time interval between the arrival time and the time that the microphone detects the signal. The magnitude of this interval will depend on the impedance of the ground surface z on the distance R of the microphone from the source, and, of course, on the sensitiveity of the microphone.

Figure 4.2 Signature of Spherical Pressure Pulse on a Surface of Finite Impedance

The abscissa shows scaled time after arrival ($ct/R = 1$) and the ordinate, scaled pressure. The curves are labeled with the relative impedance values Z.


1.95
1.90
1.80
1.60
1.40
1.20
1.00
0.80
0.60
0.40
0.20
0
Z=100
Z=50
Z=20
Z=10
Z=5
Z=4
Z=3
Z=2
Z=1
R p / R₀p₀
1
1.010
1.020
1.030
1.040
1.050
ct/R

In all sound-ranging theory to-date, it has been assumed that the signal arrival is a clearly defined event, idealized as a step function, and not a gradual increase from a zero amplitude.

The signature (4.7) has been plotted for a range of impedance values in Figure 4.2. It will be noted that the behavior is strongly dependent on the impedance. For $z = 100$, the curve is close to a step-function, and the signal rises rapidly to its maximum steady value of two. For z of the order of unity its rise is very much slower and the signature bears no resemblance to a step function. It follows that a much longer time interval $(\tau - 1)$ would pass before the signal rose to detectable level.

We may apply these results to the sound ranging problem as follows. Consider that a certain critical pressure p_c is known, which will activate the microphone system. This will be the same for M_1 and for M_2. Thus from (4.7), we obtain

$$\begin{aligned} \lambda &= R_1^{-1} - [z^2 c^2 t_1^2 - R_1^2 (z^2 - 1)]^{-\frac{1}{2}} \\ &= R_2^{-1} - [z^2 c^2 t_2^2 - R_2^2 (z^2 - 1)]^{-\frac{1}{2}} \end{aligned} \tag{4.8}$$

where λ is a known constant. Here t_1 and t_2 are not the true arrival times, but rather the times at which the signal first reaches a detectable amplitude at M_1 and M_2, respectively. What we observe therefore is, as before, the time difference $t_2 - t_1$, and from it we wish to deduce the distance difference $R_2 - R_1$.

A simple mathematical case, although extreme as a physical assumption, is that for $z = 1$. Then (4.8) becomes

$$R_2 - R_1 = C(t_2 - t_1)[(1 - \lambda R_1)(1 + \lambda c t_2)^{-1}] \tag{4.9}$$

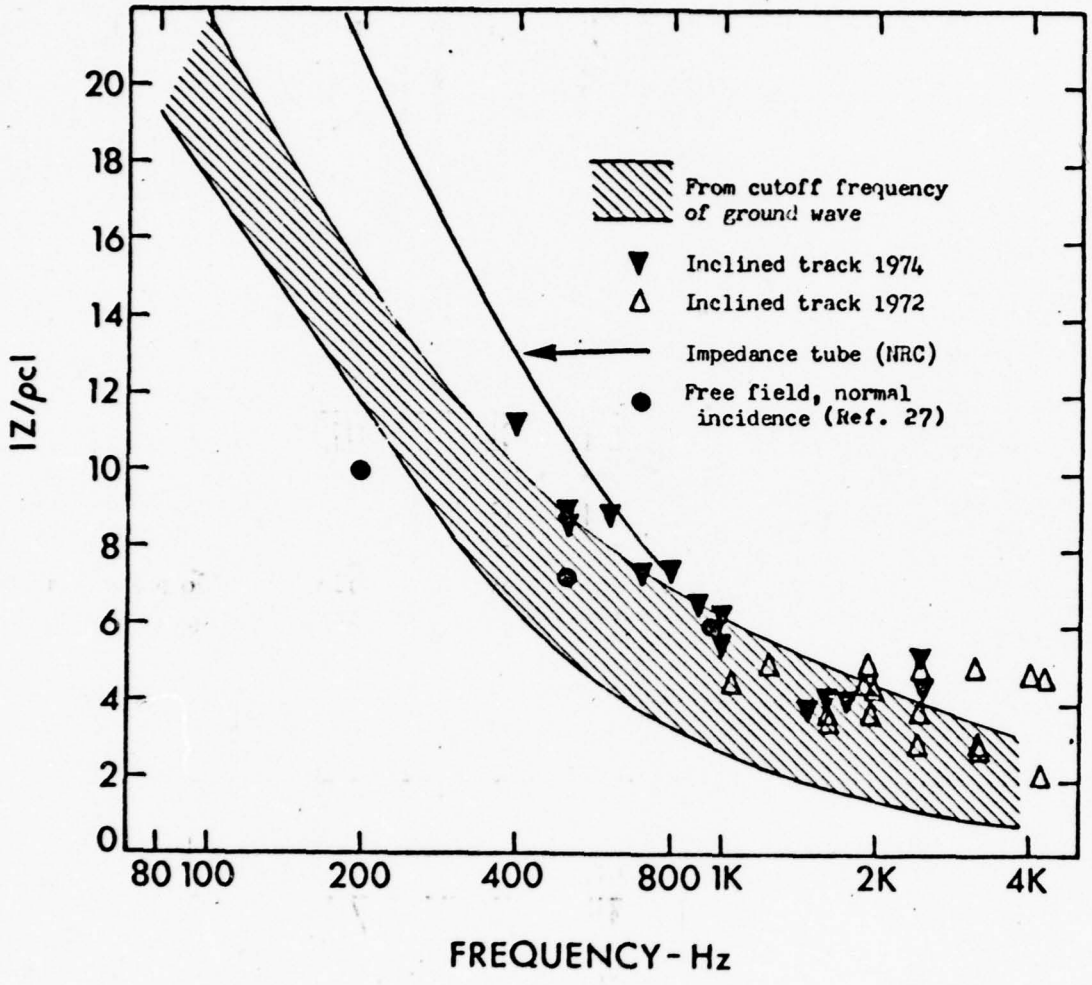


Fig. 4.3 Impedance of a Grassy Surface for Various Frequencies (after Embleton, Piercy, and Olson (1976)).

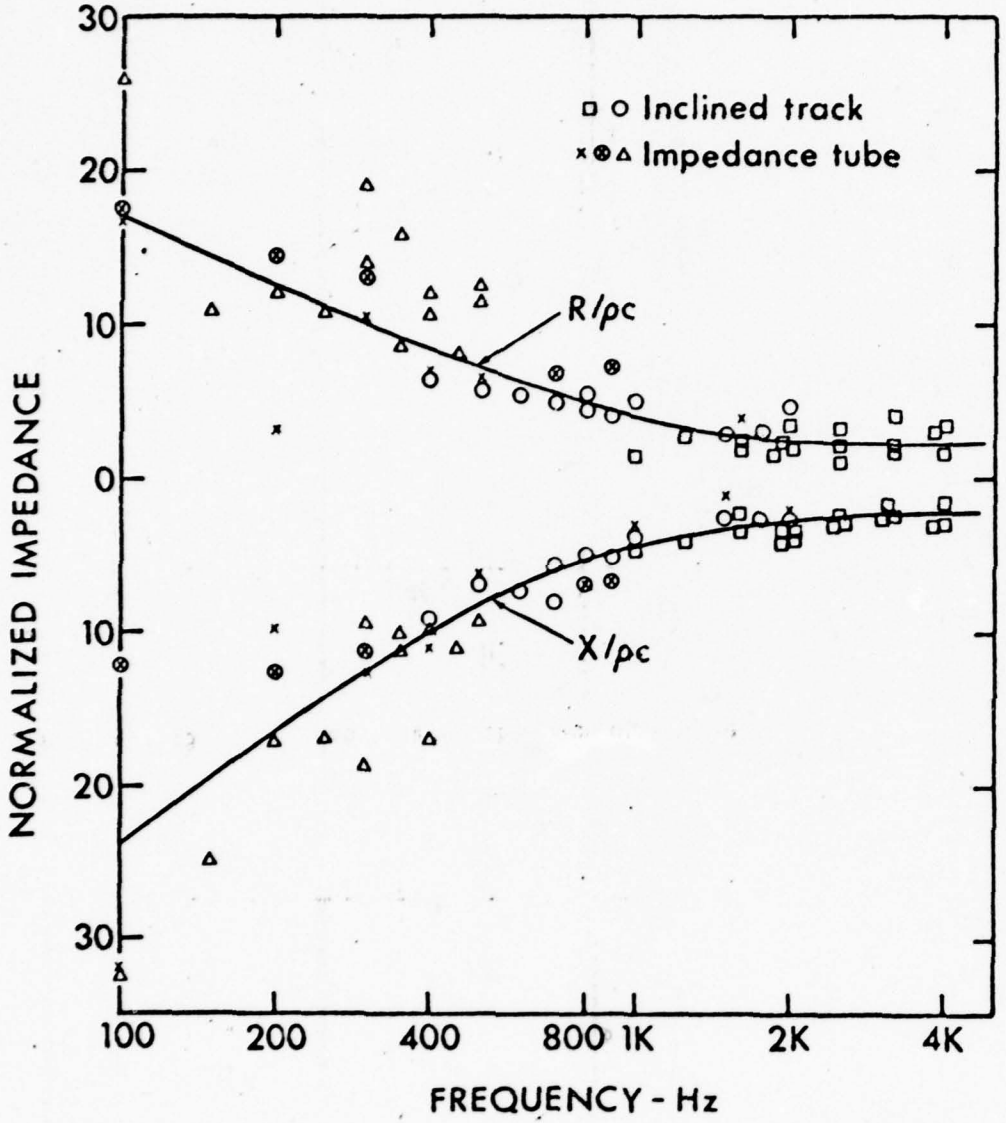


Figure 4.4 Real and Imaginary Components of Impedance of a Grassy Surface (after Embleton, Piercy, and Olson (1976)).

In (4.9), the bracketed factor on the right represents the correction due to the low impedance. The classical formula $\Delta R = c\Delta t$ is recovered by taking $\lambda \to 0$, that is, infinitely sensitive microphones.

Field Studies

Unfortunately there are no direct field studies known to the author of sound ranging over a surface of low impedance. However, problems of aircraft noise have led to some recent investigations of interest on acoustic wave under realistic outdoor conditions, for example, Dickenson and Doak (1970); Piercy and Embleton (1974); Embleton, Piercy, and Olson (1976). These field studies concentrated on noise in the relatively high frequency range, of the order of 10^2 and 10^3 Hertz. Some of the results are reproduced in Figures 4.3 and 4.4. The curves show a tendency for the impedance to increase with decreasing wave frequency, but there are not sufficient experiments at the lower frequencies to permit us to extrapolate the curves. Further, the low impedances were observed over meadowland. It is possible that a looser surface--plowed fields, forest ground cover--could reduce the impedance still further.

Propagation of an N-wave

The striking results from these experiments suggested a more realistic analytical model. The solution (4.7) is for a simple step-function pulse; this is not, however, the typical signal form projected by an artillery blast. This question will

be discussed in detail below, but we can here use the simple model of an N-wave for the early signal form:

$$\begin{aligned} N(t) &= 0 && 0 < t \\ &= 1 - \frac{2t}{T} && 0 < t < T \\ &= 0 && T < t \end{aligned} \tag{4.10}$$

The solution (4.6) can now be interpreted as an influence function for the more general solution,

$$4\pi p = 2N(t-R/c) - 2\int_0^t \frac{N'(t_1)\, H(t-\frac{R}{c}-t_1)}{\{1+z^2[\frac{c^2}{R^2}(t-t_1)^2+1]\}^{\frac{1}{2}}}\, dt\,, \tag{4.11}$$

where $N'(t)$ is the derivative of (4.10), and we have assumed propagation along the ground surface ($\theta = \pi/2$). If the integral in (4.11) is evaluated, we have

$$4\pi Rp = 2N(t-R/c) - \frac{2H(t-R/c)}{[1+z^2(\tau^2-1)]^{\frac{1}{2}}} - \frac{2H(t-R/c-T)}{[1+z^2(\tau-T^*)^2-1]^{\frac{1}{2}}}$$

$$\begin{aligned} &\frac{4}{zT^*}\ln\frac{\tau\,\tau^2-a^2}{1+z^{-1}} && 1 < \tau < 1+T^* \\ &\frac{4}{zT^*}\ln\frac{\tau+\tau^2-a^2}{\tau-T^*+(\tau-T^*)^2-a^2} && 1+T^* < \tau \end{aligned} \tag{4.12}$$

Here $\tau = ct/R$, as before, $T^* = cT/R$, and $a^2 = 1-z^{-2}$. In (4.12) the first term represents, of course, the undistorted pulse traveling with speed c, the second and third terms represent the distortion by the absorbant boundary of the impulses at $t = 0$

and $t = T$, respectively, and the fourth term represents the distortion of the linear fall-off of the signal during the period $0 < t < T$.

One would anticipate that surface absorption would have a more pronounced effect on a signal of short duration than on the single step function, and this is the case. Some calculations from (4.12) are graphed in Figure 4.5. Here we see that the $z = 1$ curve is scarcely distinguishable from the axis: the N-wave signal has been effectively wiped out. The curve for $z = 100$, on the other hand, resembles the initial disturbance very closely. This impedance is not appreciably different from total reflection in form, although the amplitude is reduced by about 30 per cent.

The formula (4.12) is much more complicated than (4.7), and implicit formulation for the sound ranging problem corresponding to (4.9) would not contribute to our intuitive understanding, and hence is not written down here. We appear to be, at this point, very far from the original sound ranging formulation; and this situation may be described as follows.

So long as the pulse is propagating undiffracted, it must arrive in advance of any reflected signals, and if it is of detectable amplitude at all, it will register at the microphone as a pulse, presumably in the form of an N-wave. However, once the pulse travels as a diffracted signal in the shadow zone, its detectable arrival times no longer satisfy the fundamental assumptions of sound ranging. The problem of sound ranging then becomes essentially an "inverse problem" of deducing local information at remote sites from information received at three or more stations. This formulation will be discussed in more detail in a later section of this report. The emphasis of this section is that such a problem can arise even if the medium is homogeneous and the

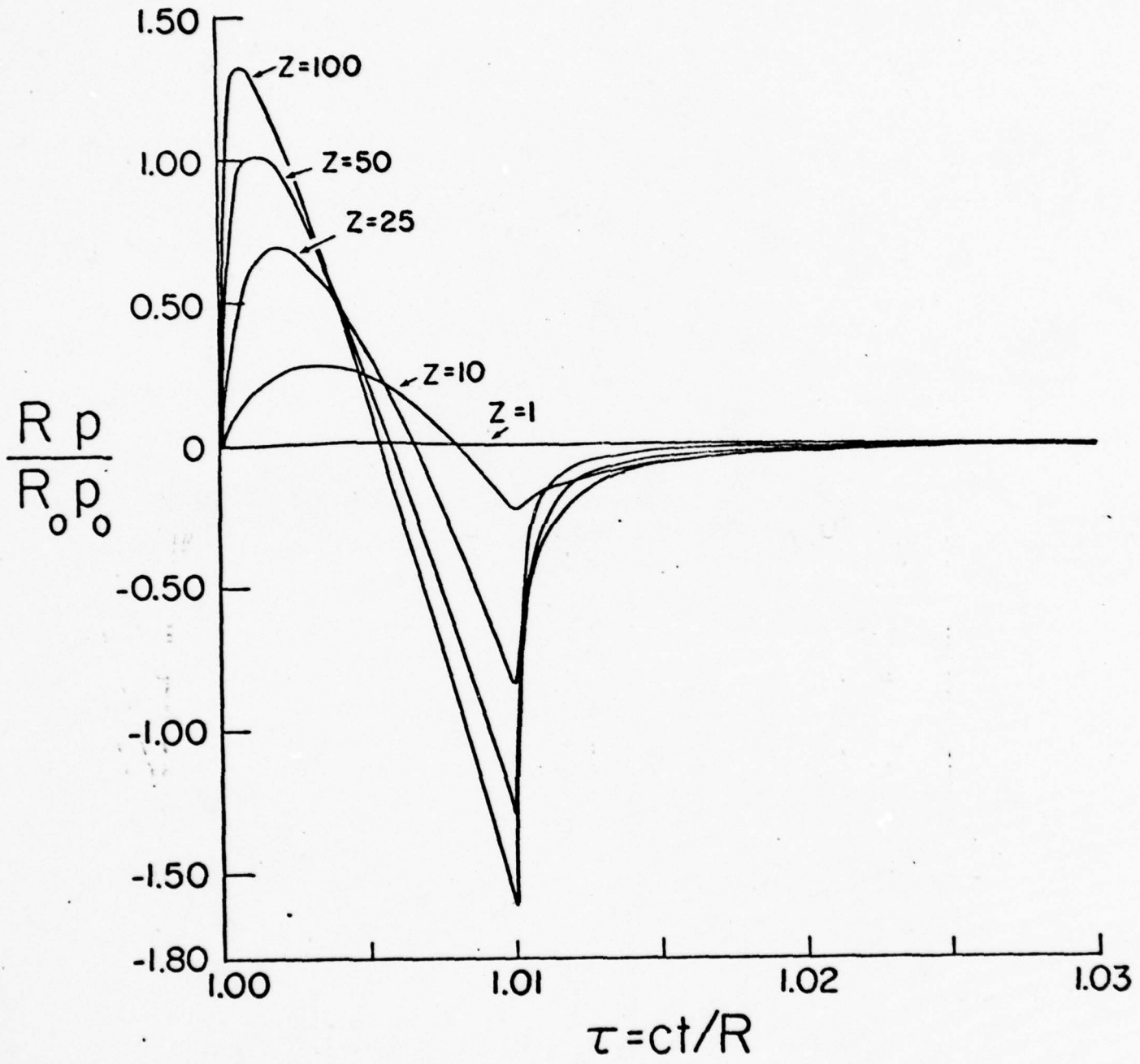


Fig. 4.5 Signature of a Spherical N-Wave on a Surface of Finite Impedance

Same as Figure 4.2 except for the imput pulse form.

terrain is level: a type of diffraction occurs whenever the earth surface has a relative impedance of the order of, say, ten or less.

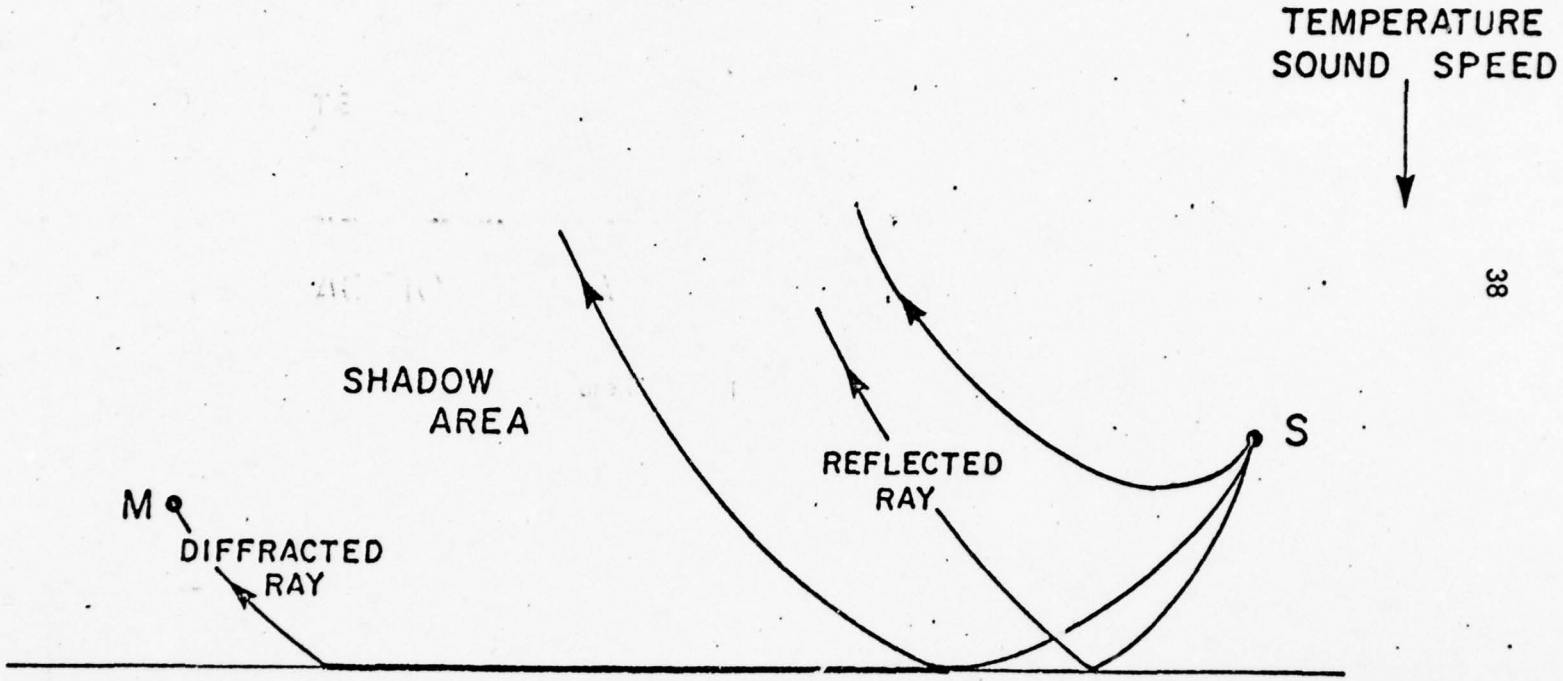
5. EFFECT OF A STRATIFIED ATMOSPHERE

In problems of diffraction and scattering that we shall consider here and below, including that of a stratified atmosphere, have this in common: they are too difficult analytically for a complete solution. However, fortunately our interest is in the time interval soon after arrival time, and for this brief period an asymptotic result is possible. This result is in a form amenable to digital evaluation, and such computations have been performed and are represented in graphical form.

As was pointed out in Section 3, simple ray theory is not applicable to a stratified atmosphere unless diffracted rays, propagating into the shadow zone, are taken into account, and the amplitude is calculated along the ray.

The proper diagramatical representation of the ray pattern is that of Figure 3.2. This is drawn, obviously, for an atmosphere in which the temperature, and so the speed of sound, decreases with height. Thus the rays are concave upward. That particular ray that is tangent to the bounding surface at its lowest point defines the shadow boundary. This figure may now be compared to Figure 3.1a. In 3.1a the source is on the boundary, and therefore the entire surface $z = 0$ is in shadow. According to scattering theory, the diffracted ray proceeds at sound speed into the shadow zone, which it is thus misleading to refer to as a "silent zone". The problem now becomes a classical eigenfunction expansion.

For a simple atmospheric model in which temperature decreases with height, a pulse-propagation solution was worked out some years ago by Friedlander (1958). It is assumed that the bounding surface is perfectly reflective.



DIFFRACTION BY A STRATIFIED MEDIUM

Figure 3.2 (Repeated)

The Green's function for the problem is the solution of the equation for a step function impulse at the origin

$$\frac{1}{c^2}\frac{\partial^2 G}{\partial t^2} - \nabla^2 G = \delta(x)\,\delta(y)\,\delta(z)\,H(t)$$

where δ is the delta function, with the boundary condition $\partial G/\partial z = 0$ at $z = 0$. Friedlander's technique is to take the Laplace transform of this equation and determine its behavior as the transform variable $s \to \infty$. This gives the form of the signal for small times after arrival, a very suitable asymptotic solution for our purposes. The analysis is straightforward, leading to the result, for $z = 0$,

$$4\pi Rp = H(\tau - 1)\exp\left[-\frac{\Gamma R}{T_o}(\tau-1)^{-\frac{1}{2}}\right], \qquad (5.1)$$

where $\tau = c_o t/R$, as before, and $\Gamma = -(dT/dz)_o$ is the lapse rate at the surface. The form of (5.1) is a special case of a more general form of diffracted time-signature,

$$Rp = A(\tau-1)^{-q}\exp\left[-B(\tau-1)^{-\frac{1}{2}}\right]. \qquad (5.2)$$

The signal starts at the arrival time $\tau = 1$ with zero amplitude and grows slowly or rapidly according to the coefficient B in the exponential. In the more general case, with the exponent q different from zero, there is an effect tending to decrease the amplitude with increasing time $\tau-1$. However, it must be remembered that expressions like (5.1) and (5.2) are derived as asymptotic expansions for $(\tau-1)$ small, and thus must not be expected to give reliable results for long times.

Some signatures have been calculated from (5.1) and are presented in Figure 5.2. We have taken the distance from the source as 3.3 km and plotted two curves, one for a lapse rate of 10 deg/km and one for 5 deg/km.

It will be noted that both signatures--unlike those of Figures 4.2 and 4.5 for low surface impedance--rise rapidly, resembling closely the original impulse $H(t - R/c)$. It is evident from (5.1) that if we were to choose a very large temperature gradient Γ, or large distance R, it would be possible to obtain signatures relatively flat at the origin. However, within the practical limits of sound ranging in the atmosphere, we may expect Figure 5.2 to be typical.

We thus conclude that it is highly unlikely that normal atmospheric temperature gradients under normal sound ranging conditions will contribute significantly to the ranging error. This conclusion is, of course, subject to revision by a study of instrumental sensitivity.

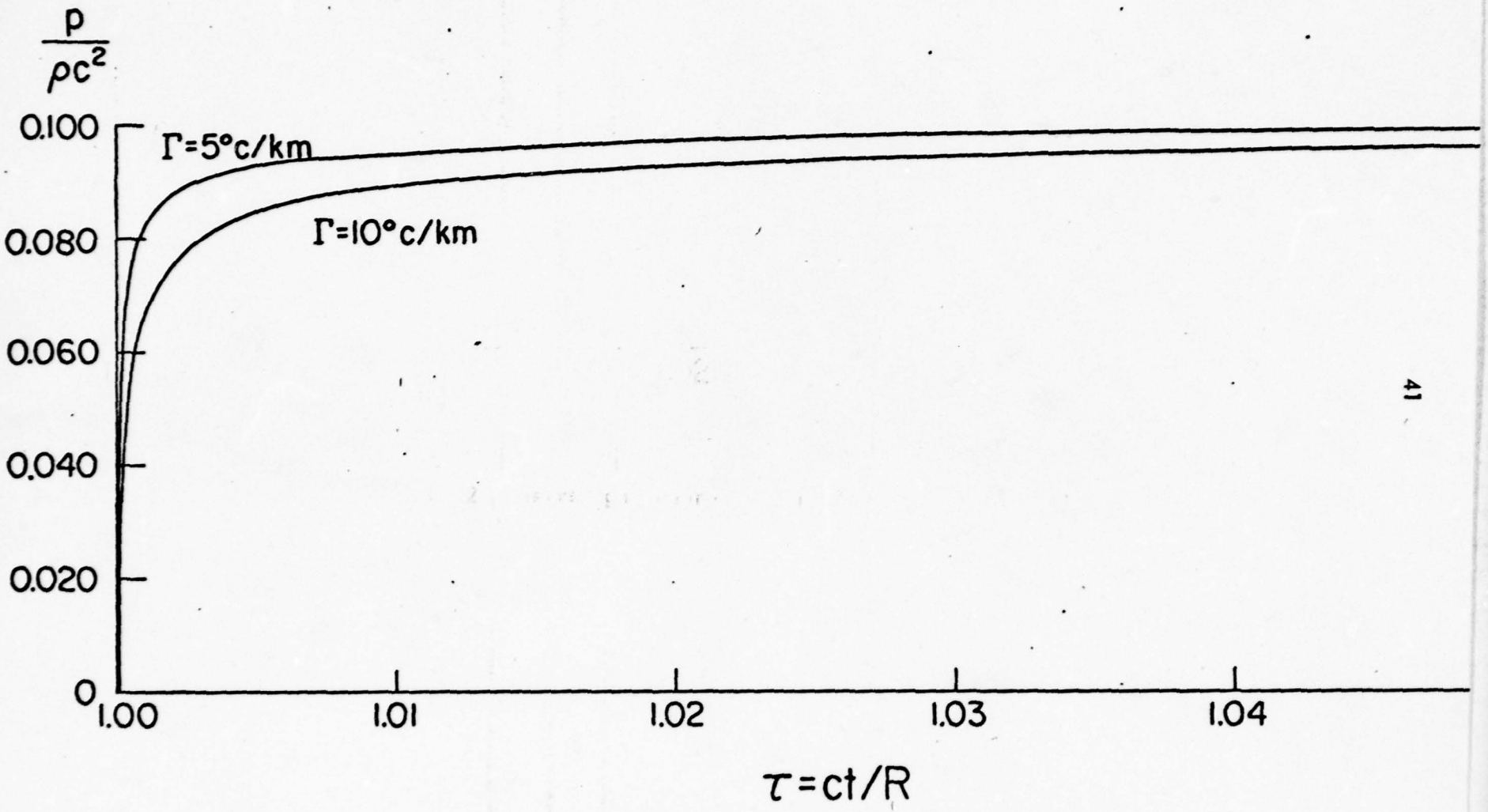


Figure 5.2 Pressure Signature in a Stratified Atmosphere.

6. THE EFFECT OF A TERRAIN OBSTACLE

It is evident that irregularities in the surface over which the sound is transmitted will have an important effect on the signal, and considerable effort has been devoted to this topic. Reflections from periodically corrugated surfaces are discussed by Meecham (1956) and by Proud et al. (1958); and a more general method of treatment is suggested by Meecham (1956).

However, we anticipate that the most satisfactory method of treating surface irregularities will be statistical, that is, by statistically parameterizing the properties of the surface. This can be done relatively simply for a single plane wave when the surface has an impedance or roughness with known variance (Morse and Ingard, 1968, pp. 441-449). We are not aware of a corresponding treatment for a spherical pulse.

Thusthe content of this section will be limited to terrain obstacles of the order of the wave length of the sound radiation, or greater. For the sound-ranging problem, the obstacle considered will be of the size of a hill or small mountain. Although the mathematics is difficult, the analysis can be done by the approximations and techniques outlined in Section 5.

Physically, the geometric optics of this problem is similar to that of a stratified atmosphere, in that our greatest interest lies in the shadow region in which only diffracted rays can penetrate. The picture is that of Figure 6.1. Again we shall find that the signal arrives with the local speed of sound, but with zero amplitude, so that time of arrival and time of detection are not identical.

For reasons explained more fully in preceding sections, the existence of the earth as a boundary along which the pulse must propagate precludes the use of any plane wave model. Thus application of the great body of analytical results on the scattering of plane waves by obstacles of various configurations is denied to us. The simplest relevant formal problem is that of a spherical pulse scattered by a cyclinder, with the assumption that the plane containing the source and the axis of the cylinder is perfectly reflecting, as is the surface of the cylinder itself. The technique is outlined by Huang (1975), extending the plane-wave results derived by Friedlander (1958). More difficult problems have been attempted. Uberall et al. (1968), McNicholas et al. (1968), and Rudgers and Überall (1970) derive formulas for scattering by non-rigid cylinders. Carlson and Hung (1974) obtain some results onthe difference in scattering cross sections of non-symmetric profiles as compared with that of the cylinder.

However, we shall restrict ourselves to the more idealized problem in which we can derive hard quantitative results. The analysis proceeds as follows. Let all distances be made non-dimensional by the radius of the cylinder a, time by a/c. Let Y be the non-dimensional distance along the axis of the cylinder, and D the distance of the source from the origin on the axis. The distance R between the source and the microphone is thus given by

$$R^2 = (X + D)^2 + Y^2.$$

This geometry is diagrammed in Figure 6.2.

Huang (1975), using the line-sourge solution of Frienlander (1958), derives the following approximations for an incident unit spherical pressure pulse. The line-source (i.e., two-dimensional solution is

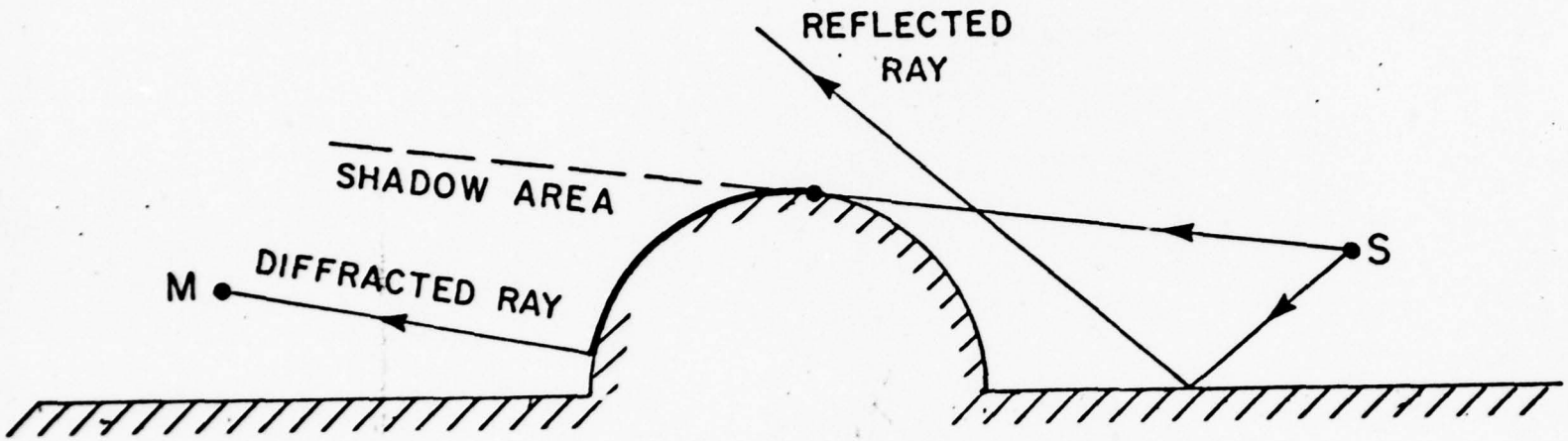


Figure 6.1 DIFFRACTION BY A HARD OBSTACLE

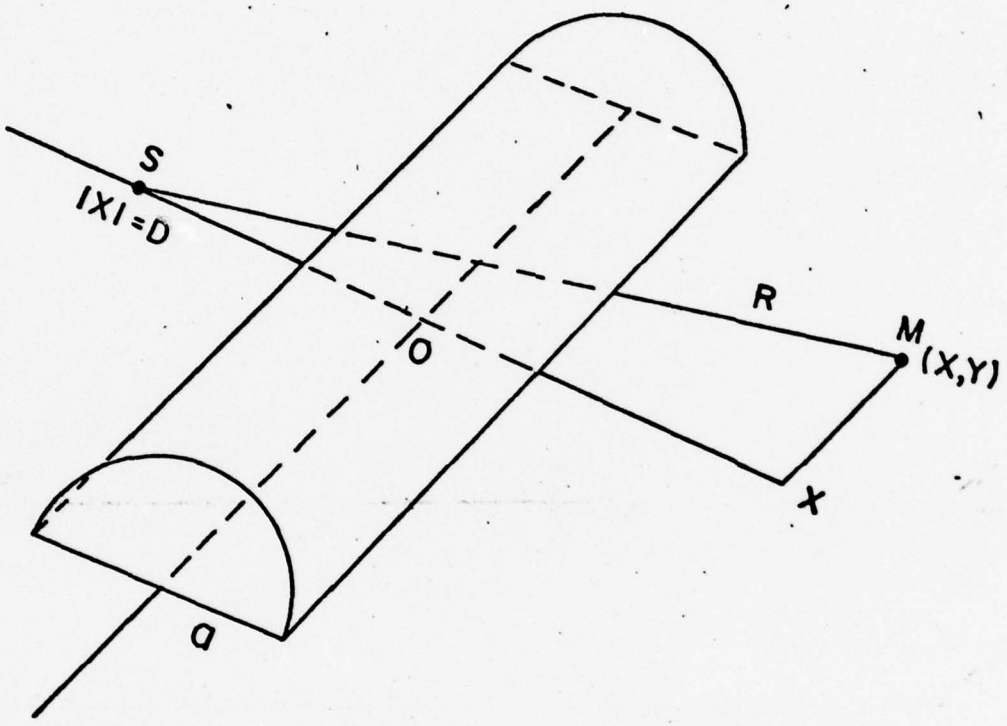


Figure 6.2 The Geometry of the Scattering of a Spherical Pulse by a Cyclinder

S is the source, M the microphone, both lying in the plane containing the axis of the cylinder. The line $\overline{SO}$ is the X-axis, normal to the axis of the cylinder. x,y, and R are scaled by the cylinder radius a.

$$F(X, t - t_a) = 0.924\,[\,X^2 - 1\,)(D^2 - 1)\,\theta_c(t - t_a)]^{-\frac{1}{4}} \cdot H(t - t_a)\exp[-0.280\,\theta_c^{3/2}(t - t_a)^{-\frac{1}{2}}] \tag{6.1}$$

where t_a is the two-dimensional arrival time aX/c, and θ_c is the shadow boundary,

$$\theta_c = \pi - \cos^{-1}\frac{1}{D} - \cos^{-1}\frac{1}{R}\,. \tag{6.2}$$

As in Section 5, the assumption has been made that $t - t_a$ is small, that is, that the signal has not long passed the position of the microphone (X,Y). The solution in three dimensions is then given by

$$P(X, Y, t - t_a) = \frac{1}{\pi}\,t(t^2 - t_a^2)^{\frac{1}{2}} \int_{-1}^{1} \frac{F\{[\,t^2 - y^2 - \frac{1}{4}(1 + \alpha)^2(t^2 - t_a^2)]^{\frac{1}{2}} - t_a\}}{t^2 - \frac{1}{4}(1 + \alpha)^2\,(t^2 - t_a^2)}\,d\alpha \tag{6.3}$$

This expression has been evaluated by numerical computation, and the various results are plotted in Figures 6.3, 6.4, 6.5, and 6.6. We note first that the larger the distance from the cylinder of source and microphone, the more the pressure trace resembles a step function, that is the smaller the influence of the obstacle. For source and microphone close in to their respective sides of the hill, the diffraction is very marked, in the usual pattern: the amplitude rises slowly from zero to a much-delayed maximum. Which point in time of such a signature the microphone would record as "arrival" is a matter for further investigation; also whether or not two different microphones would give the same answer.

Figure 6.3 Diffraction of a line-source pulse by a cylindrical ridge, computed from the analysis by Friedlander (1958). The ordinate is dimensionless pressure, the abscissa is dimensionless time after arrival. Each curve is labeled by a number pair: the distance of the source from the center of the ridge and the distance of the microphone from the center of the ridge. The result is symmetric in these two quantities, so that they need not be designated.

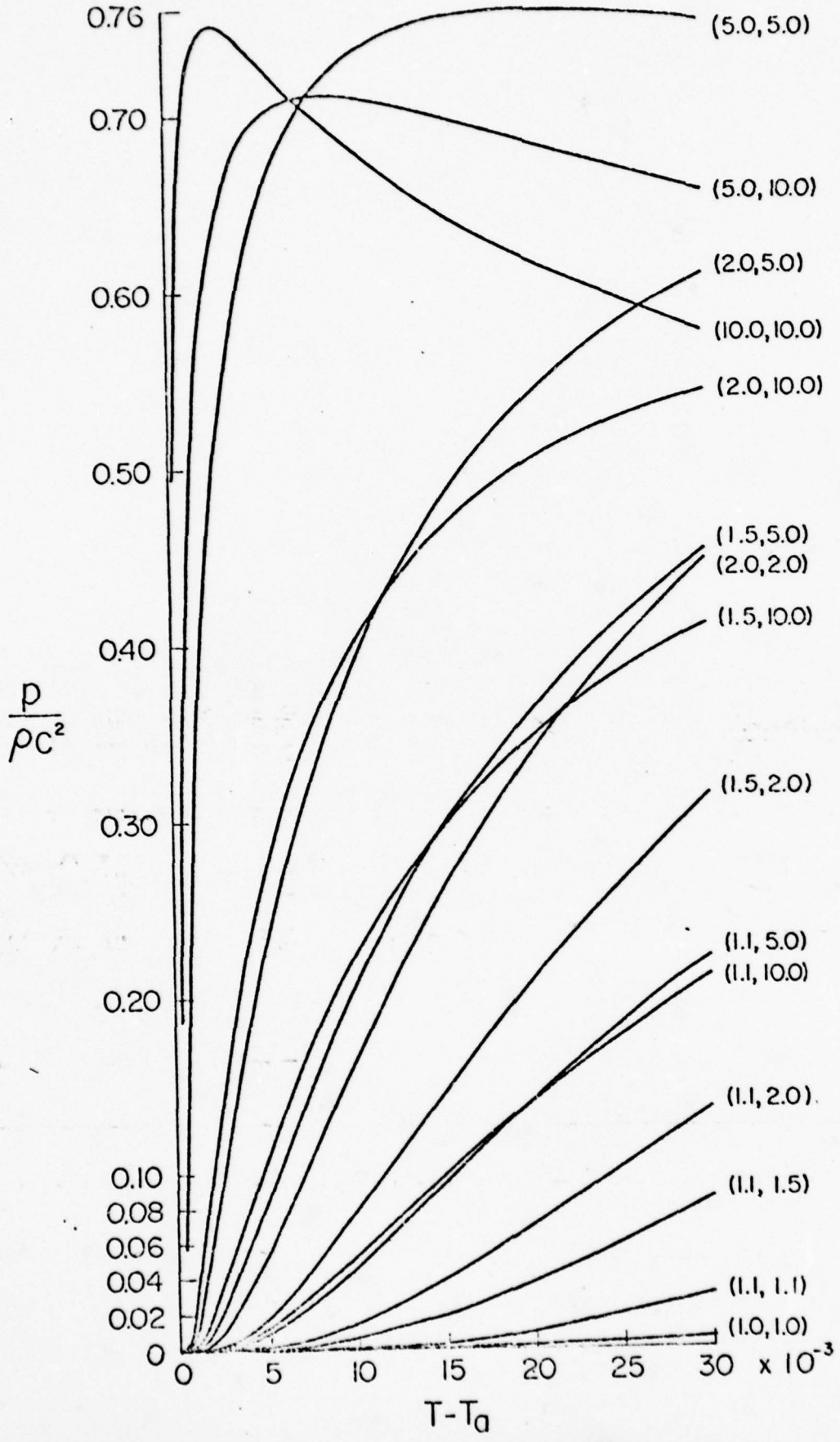

0.76
0.70
0.60
0.50
0.40
0.30
0.20
0.10
0.08
0.06
0.04
0.02
0
$\frac{p}{\rho c^2}$
0
5
10
15
20
25
30 x 10^{-3}
$T-T_a$
(5.0, 5.0)
(5.0, 10.0)
(2.0,5.0)
(10.0,10.0)
(2.0,10.0)
(1.5,5.0)
(2.0,2.0)
(1.5,10.0)
(1.5,2.0)
(1.1, 5.0)
(1.1, 10.0)
(1.1, 2.0)
(1.1, 1.5)
(1.1, 1.1)
(1.0, 1.0)

Figure 6.3

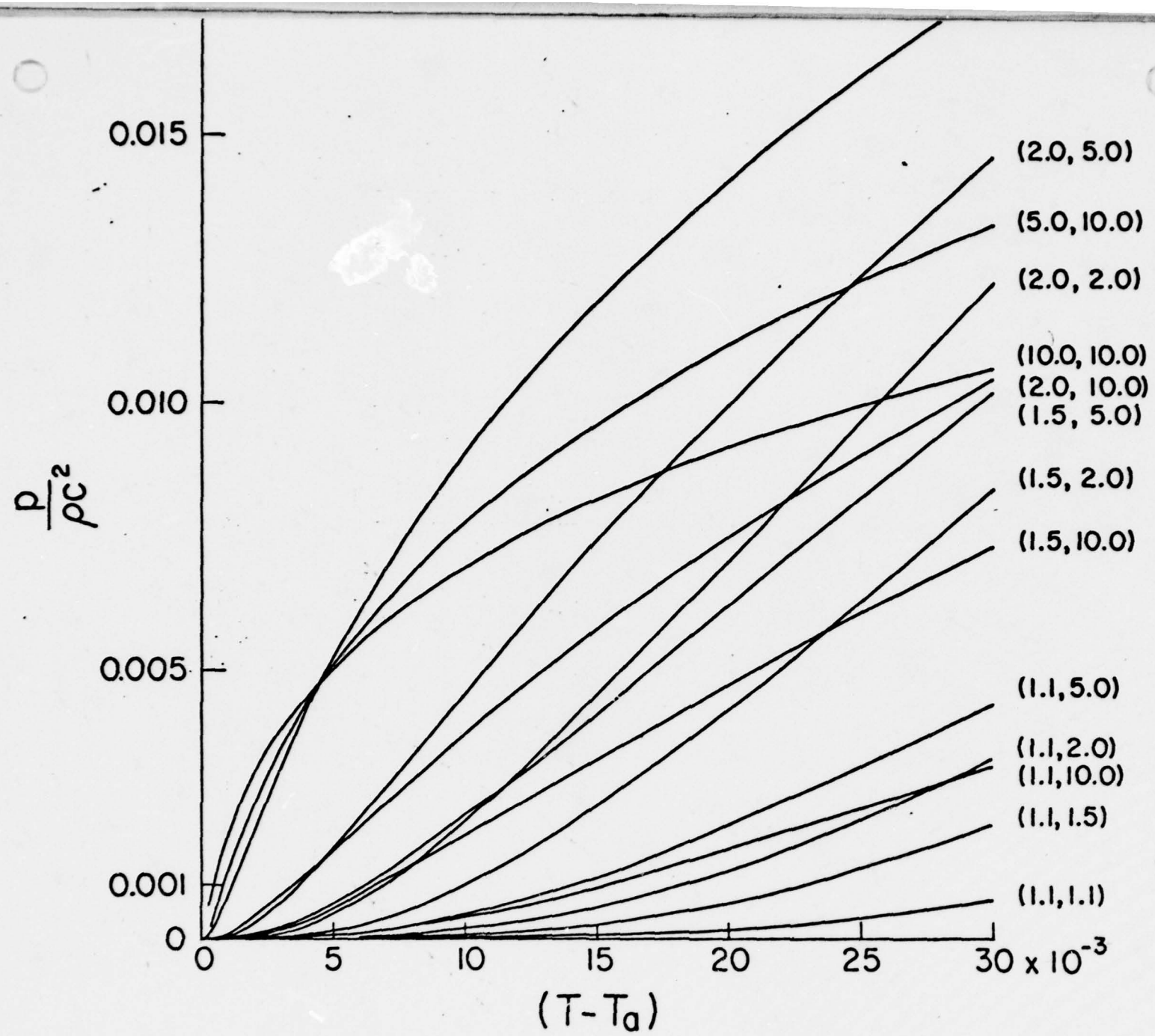


Figure 6.4 True three-dimensional diffraction of a spherical pulse by a cylindrical ridge, computed from the analysis of Huang (1975). Labelling as in Figure 6.3.

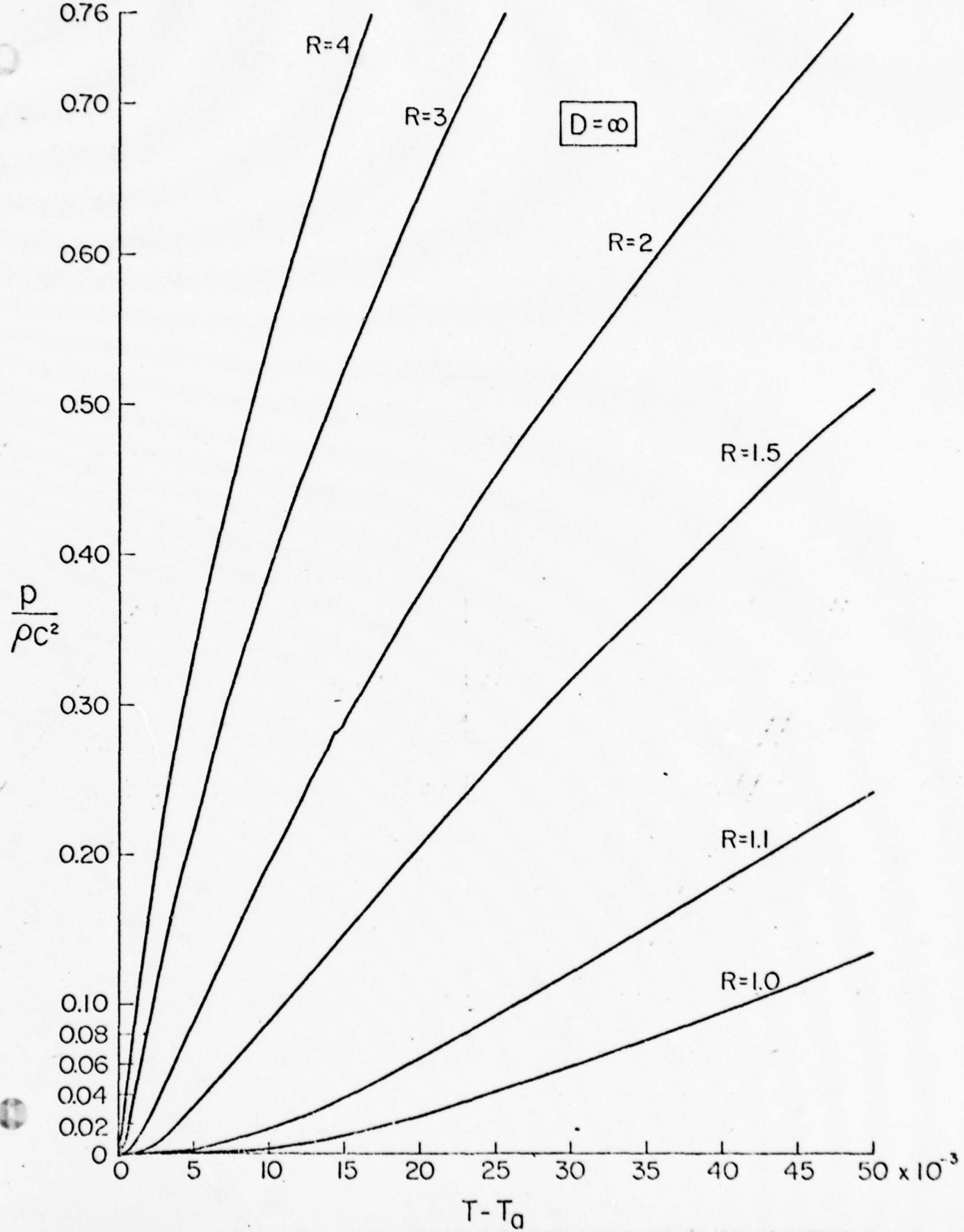


Figure 6.5 Same as Figure 6.4, for a source at "infinite" distance from the ridge.

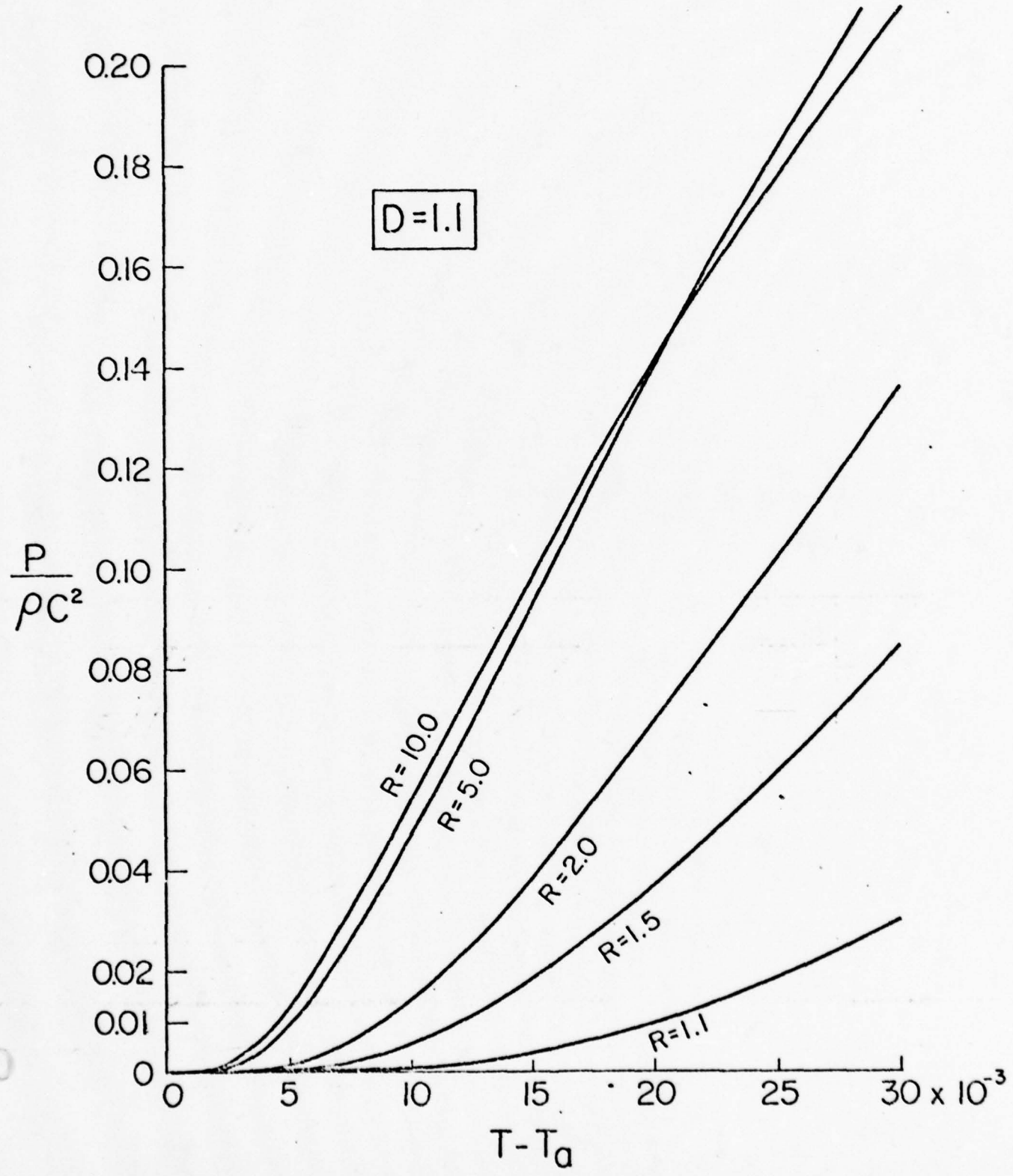


Figure 6.5 Same as Figure 6.4, for a source close-in to the beginning of the ridge.

The Simulation of a Howitzer Blast Traversing a 500-foot Hill

This computation--the first of its kind ever attempted--is structured as follows. The spherically symmetric Howitzer blast is computed out to a radial distance somewhat less than 500 feet. At this point the data from this computation serves as input into the boundary of a two dimensional grid. This input will have the form of an N-wave, as represented in the appropriate profiles of Figure 7.1. The two-dimensional zones are about one foot on a side, so that smoothing of the spherically symmetric solution is necessary. This operation wipes out the spurious numerical oscillations discussed in Section 7, so that they do not appear in the results of this Section. The smoothing is done according to a scheme that conserves both energy and momentum.

Since the solution is now two-dimensional, the velocity will have two components. A vector velocity plot thereby becomes a meaningful visualization of the motion patterns. These must be viewed with the fact in mind that the vectors represent values at their base points, and therefore may appear on occasion to penetrate the boundary. The mathematical condition at the hill is zero normal velocity component, that is, perfect reflection.

The first plot of Fig. 6.7 exhibits the grid scheme. In this plot it is resting at the bottom of the hill on the side of the source; the slope of the hill can be seen extending up to 110 feet on the right. As the pulse progresses, the grid is moved along at a speed that keeps it ahead of the front, but with enough zones to follow what form the signal will take at any given point.

The plot for Cycle 50 shows the beginning of pulse reflection from the hill, particularly pronounced where the incidence is normal. Cycle 50 shows some interesting features. The pattern of both incident and reflected waves is evident, together with their complex interaction. But also in this cycle, at the lower left, we see that the reflected wave has intersected, and been re-reflected from the grid boundary. Thus there is a triangle in this portion of the grid that contains non-physical, numerical results. This is true of all subsequent cycles; to perform the computations in any other way would be prohibitively expensive. However, this region of physical non-significance will move with the local speed of sound and therefore cannot contaminate more than a portion of the grid. In Cycle 450, for example, the reinforcement of the incident wave by the reflected, observable along a line from the wave front, is physically real. At any given point in space where this reinforcement is taking place, it would appear as an echo if there had been a sufficient period of silence since the passage of the front, or as a rumble, if not. By Cycle 850, this pattern still persists, but has become considerably more complicated. At this time the front is approaching the shadow limit, which, as calculated above, is on the hillside at an elevation of 433 feet.

By Cycle 1100, the pulse front is definitely into the shadow, and the process of diffraction has begun, although scarcely noticeable at this stage. Cycle 1300 shows a more advanced stage of diffraction: the amplitudes are overall smaller, and they rise from zero amplitude at the front relatively slowly to their maxima.

This pattern is still more in evidence at Cycle 1909, at which the pulse front has just reached the top of the hill. The scale of the velocity vectors of the earlier plots has been retained, and the diffracted field is smooth, regular, and slowly varying.

In Fig. 6.9 we see a time history at a point just five feet above the surface on top the hill. Here the pressure trace is an N-wave, but because of the diffraction it is difficult to specify a precise arrival time. Even at this distance the effect of non-linearity is significant. The distance from the source is

$$[1000^2 + 500.5^2]^{\frac{1}{2}} = 1118 \text{ ft}$$

The arrival time accroding to linear theory for the sound speed 1116.36 ft/sec would be 1.002 sec. We see from Fig. 6.9 that it is closer to 0.96

By .Cycle 2850, the pulse has proceeded about 100 feet down the far side of the hill. The diffraction effect by this stage is very significant. The pattern is such that arrival time is very difficult to define. The scale has been doubled from the previous plots, but the first maximum is very small indeed. The signal then falls off to negligiblity and rises to a second, reinforced maximum.

In the plots for Cycles 3150 and 3650 the scale has been increased by a factor of ten. These show the pulse before and after passing the 45 degree point on the hill (354 feet elevation). To show the effects of diffraction we compare the signal signatures at this point (Figure 6.8) with the symmetric point on the other side of the hill, that is the side receiving the direct radiation (Figure 6.10).

The signal arrives in Figure 6.8 as a true pulse with a sudden rise and the beginning of a decline into the N-wave configuration. However, by this time of passage of the first pulse, the reflections have begun to arrive. These take the form of oscillations with a frequency of about 100 Hz. The signature suggests a lower frequency component also, but is terminated for computational reasons, to wit, the end of the moving grid. It should be

emphasized here that these oscillations are physical and not computational. We also note that pressure and velocity are precisely in phase, a characteristic of the direct linear sound propagation.

Figure 6.10 presents a very great contrast. The distances of the two points from the source are 737 ft and 1400 ft, which would result in a direct radiation amplitude reduction of about 47 per cent. The actual computed reduction of the amplitude of the first pulse maximum is seen to be about 83 per cent, clearly an effect of the shadow.

The structure of the signal has been totally altered. The gradual rise from zero to the first maximum, typical of the diffracted pulse, makes impossible the field detection of true arrival time. None of the reflection oscillations are evident; and the second maximum exceeds the first.

Figure 6.7 (following pages). Vector plots of diffraction of Howitzer blast by a ridge.

The ridge of circular cross-section with radius of 500 feet, is centered 1000 feet from the howitzer. Plotted are the velocity vectors, scaled according to the legend. The distance coordinate (in feet) is X, the height coordinate, Y. Each plot shows the pulse front and some distance behind it. The point X = 750, Y = 433 on the hill begins the shadow zone. See text for further details.

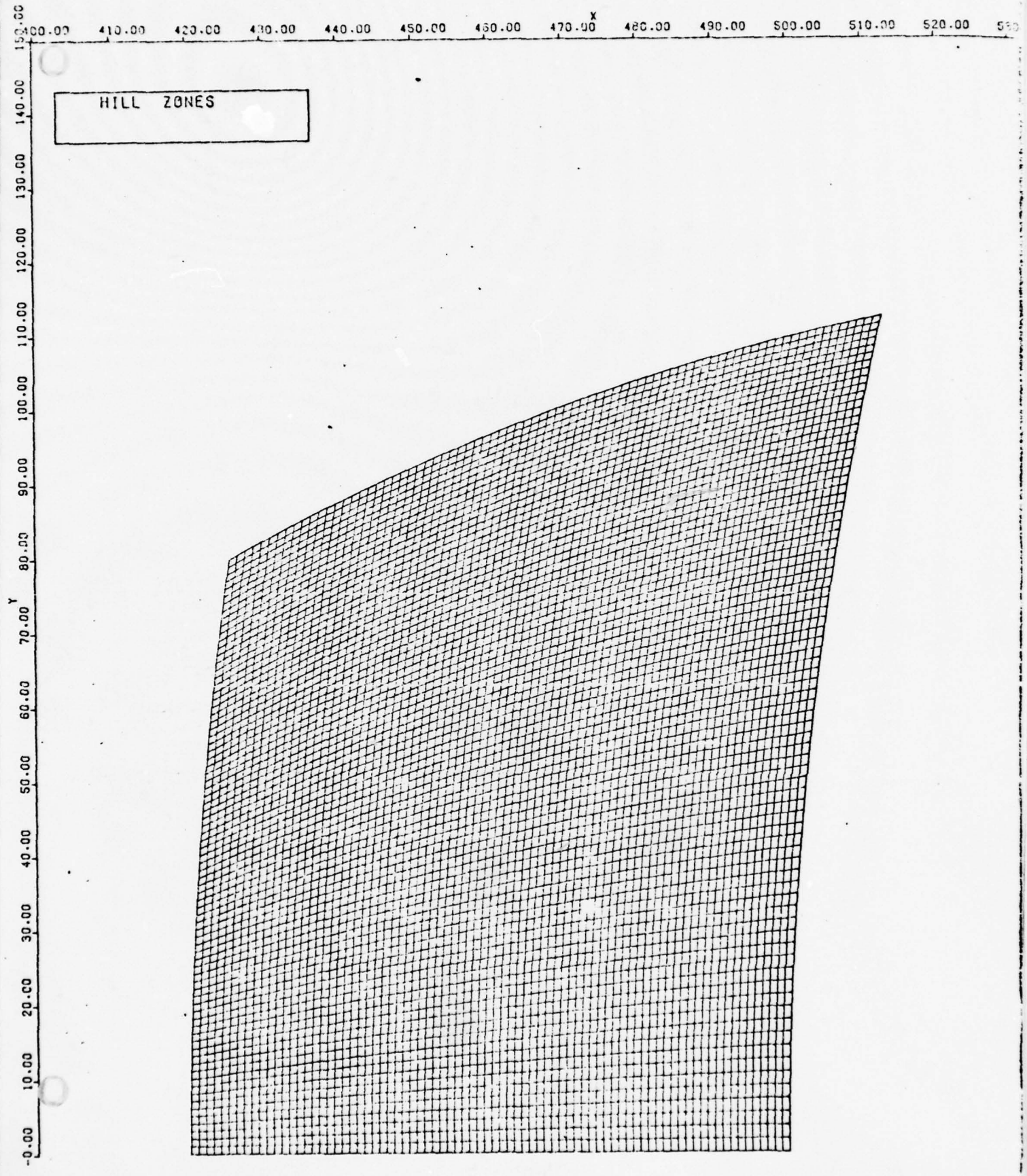

HILL ZONES
X
Y
400.00
410.00
420.00
430.00
440.00
450.00
460.00
470.00
480.00
490.00
500.00
510.00
520.00
150.00
140.00
130.00
120.00
110.00
100.00
90.00
80.00
70.00
60.00
50.00
40.00
30.00
20.00
10.00
-0.00

Figure 6.7


46-1X1
PROBLEM 4602.25 SCALE 20.0 FT/SEC
TIME 434.6142 DUMP 1 CYCLE 50
VELOCITY VECTOR PLOT
TAPE REEL 6847
DAY MONTH YEAR 25 JAN 77
TIME OF DAY 17:15:08
X
420.00
430.00
440.00
450.00
460.00
470.00
480.00
490.00
500.00
510.00
520.00
Y
150.00
140.00
130.00
120.00
110.00
100.00
90.00
80.00
70.00
60.00
50.00
40.00
30.00
20.00
10.00
0.00

Figure 6.7

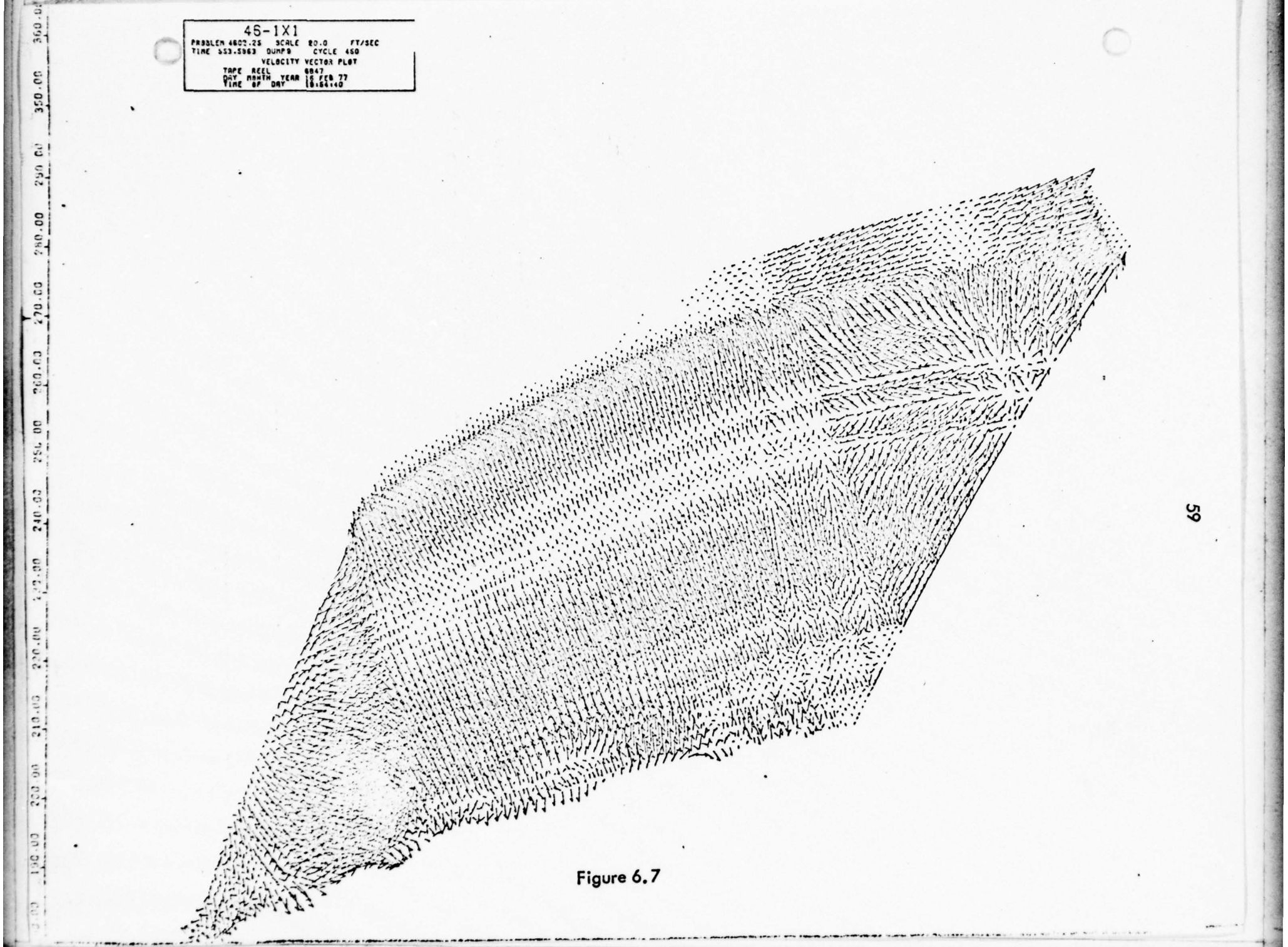

46-1X1
PROBLEM 4602.25 SCALE 20.0 FT/SEC
TIME 553.5963 DUMP9 CYCLE 450
VELOCITY VECTOR PLOT
TAPE REEL 6847
DAY MONTH YEAR 15 FEB 77
TIME OF DAY 10:54:40

Figure 6.7

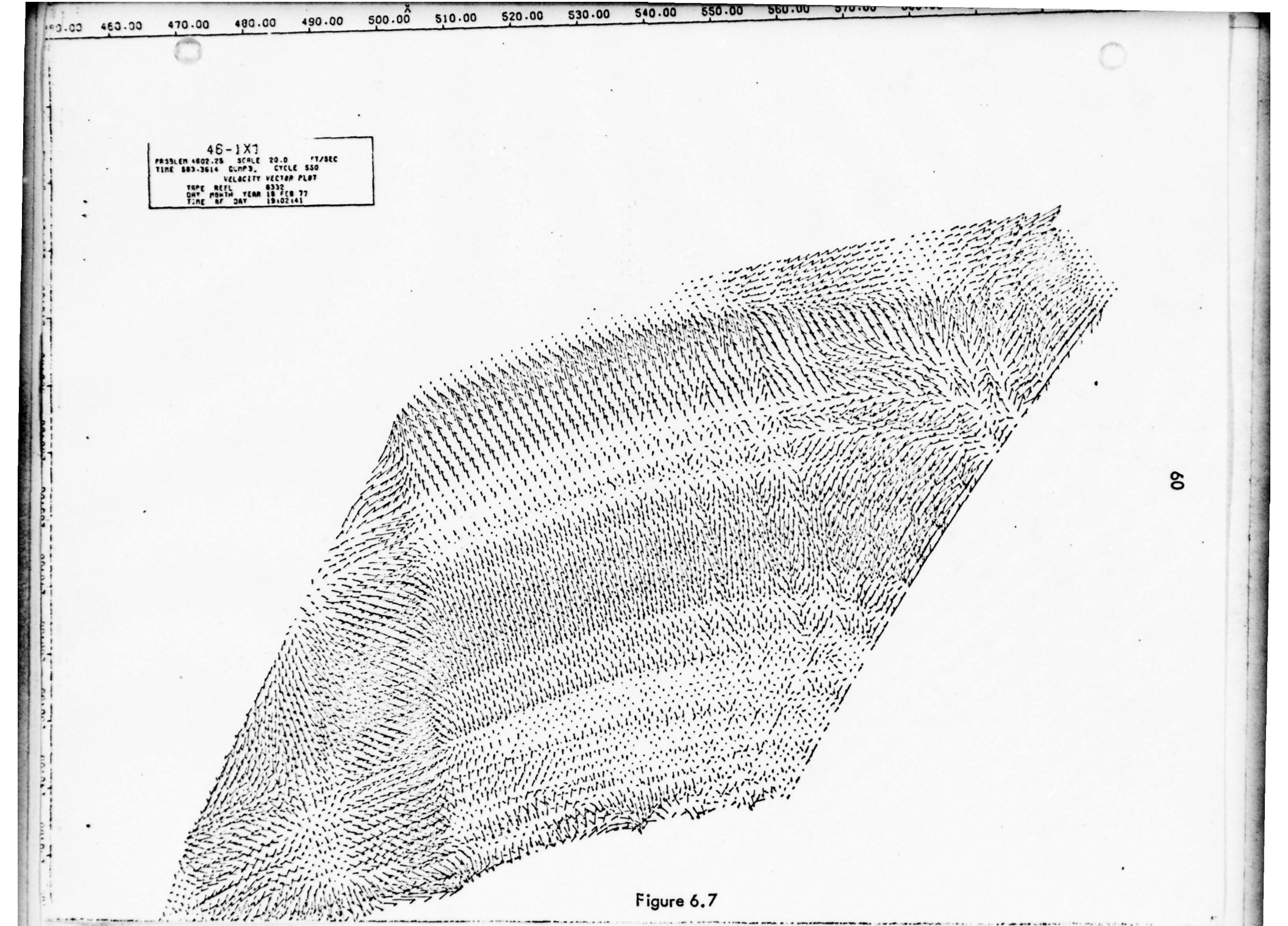

460.00
470.00
480.00
490.00
500.00
510.00
520.00
530.00
540.00
550.00
560.00
46-1X1
PROBLEM 4602.25 SCALE 20.0 FT/SEC
TIME 883.3614 DUMP3, CYCLE 550
VELOCITY VECTOR PLOT
TAPE REEL 8332
DAY MONTH YEAR 18 FEB 77
TIME OF DAY 19:02:41

Figure 6.7

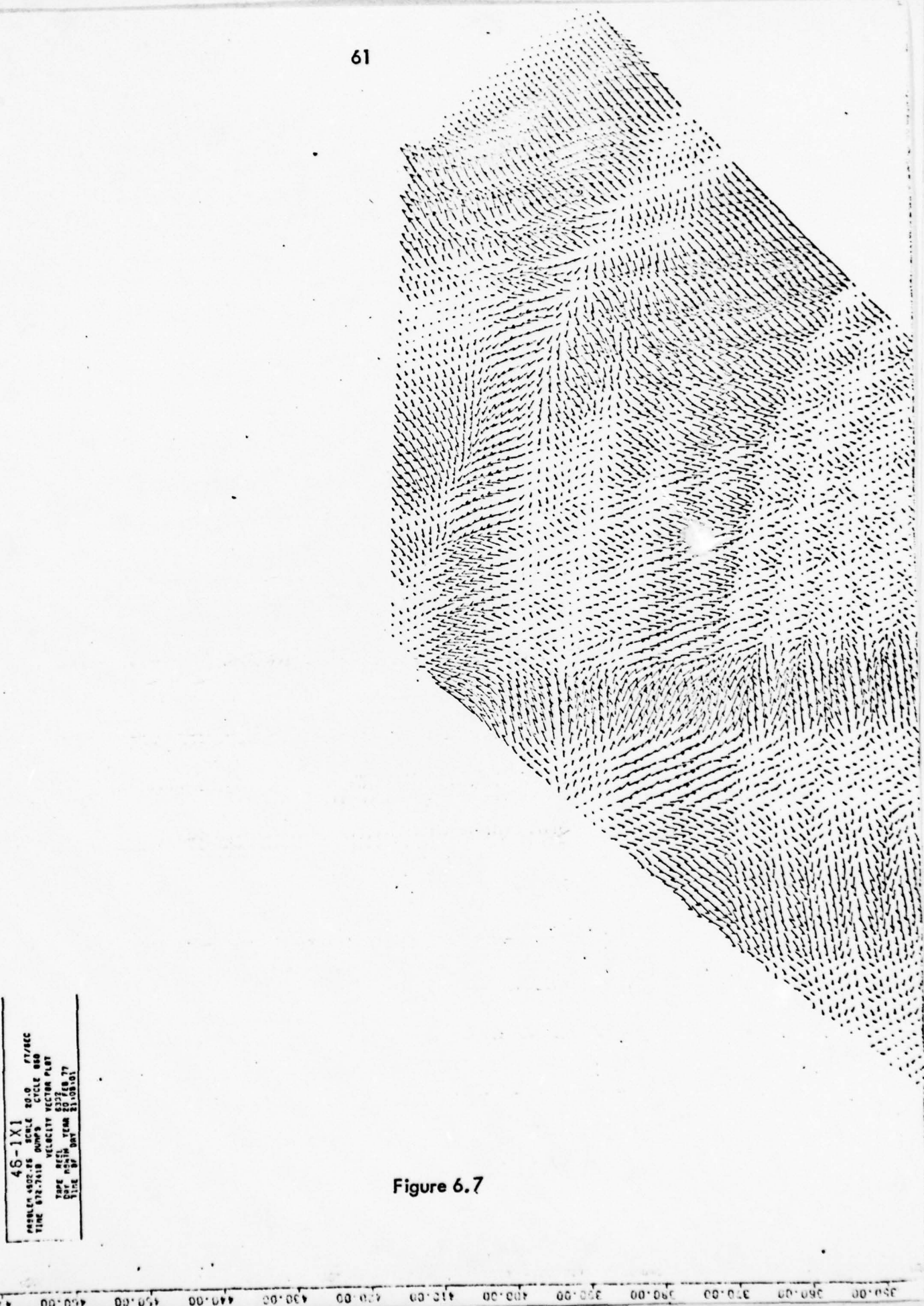

46-1X1
PROBLEM 4502.05 SCALE 20.0 FT/SEC
TIME 672.7410 DUMPS CYCLE 880
VELOCITY VECTOR PLOT
TAPE REEL 6332
DAY MONTH YEAR 20 FEB 77
TIME HP DAY 21:08:01
350.00
360.00
370.00
380.00
390.00
400.00
410.00
420.00
430.00
440.00
450.00
460.00
470.00

Figure 6.7

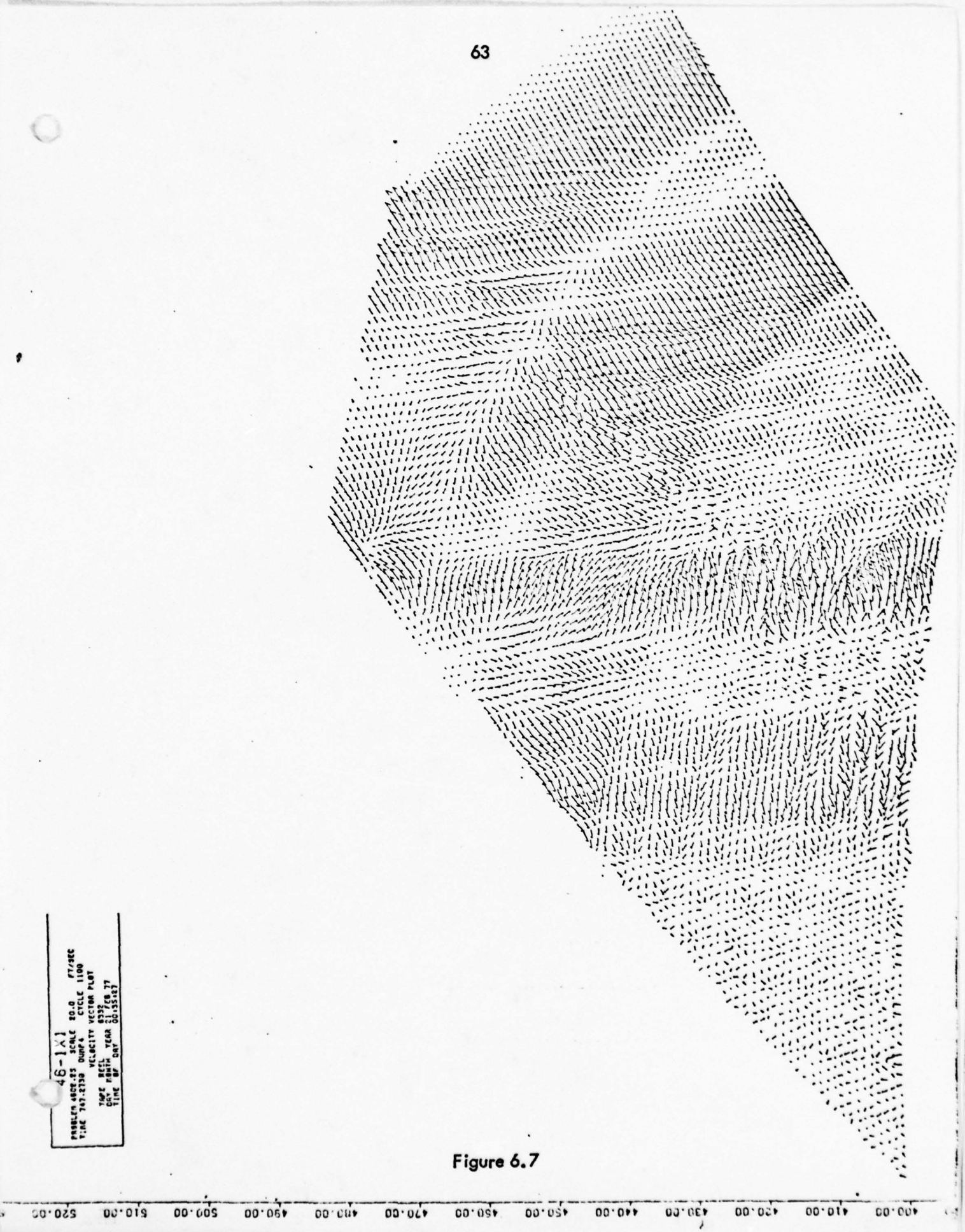

46-1X1
PROBLEM 4852.83 SCALE 20.0 FT/SEC
TIME 747.2730 QUAD4 CYCLE 1100
VELOCITY VECTOR PLOT
TAPE 8332
DAY FOUTH YEAR 77/FEB 27
TIME 00' DAY 00:55:07
400.00
410.00
420.00
430.00
440.00
450.00
460.00
470.00
480.00
490.00
500.00
510.00
520.00

Figure 6.7

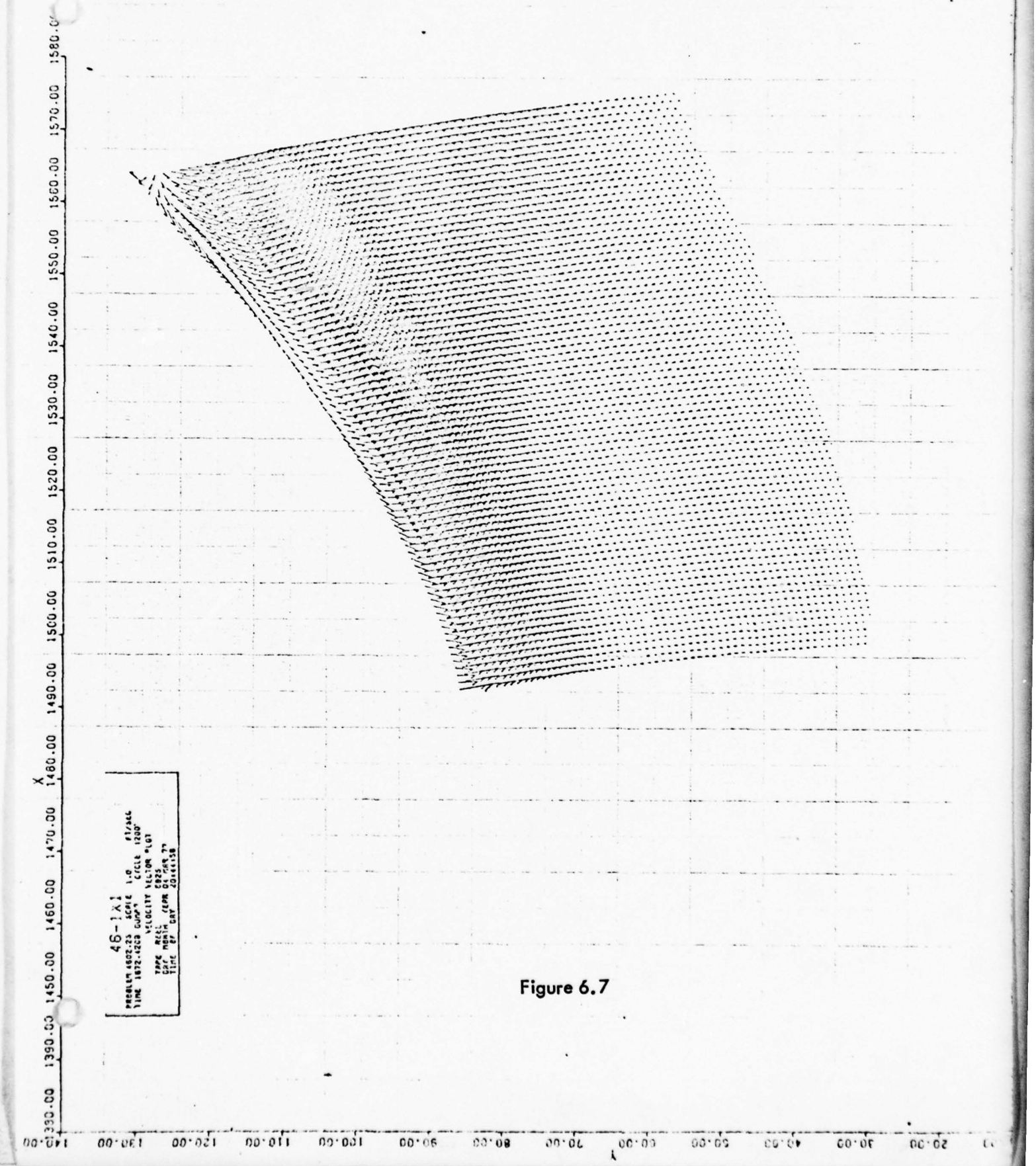

46-1X1
PROBLEM 1602.23 SCALE 1.0 FT/SEC
TIME 1872.1200 CUMPY CYCLE 1200
VELOCITY VECTOR PLOT
TAPE REEL
DSF MBATH YEAR 01 JAN 77
TIME OF DAY 20:44:58
X
Y
1580.00
1570.00
1560.00
1550.00
1540.00
1530.00
1520.00
1510.00
1500.00
1490.00
1480.00
1470.00
1460.00
1450.00
1440.00
1390.00
20.00
30.00
40.00
50.00
60.00
70.00
80.00
90.00
100.00
110.00
120.00
130.00
140.00

Figure 6.7

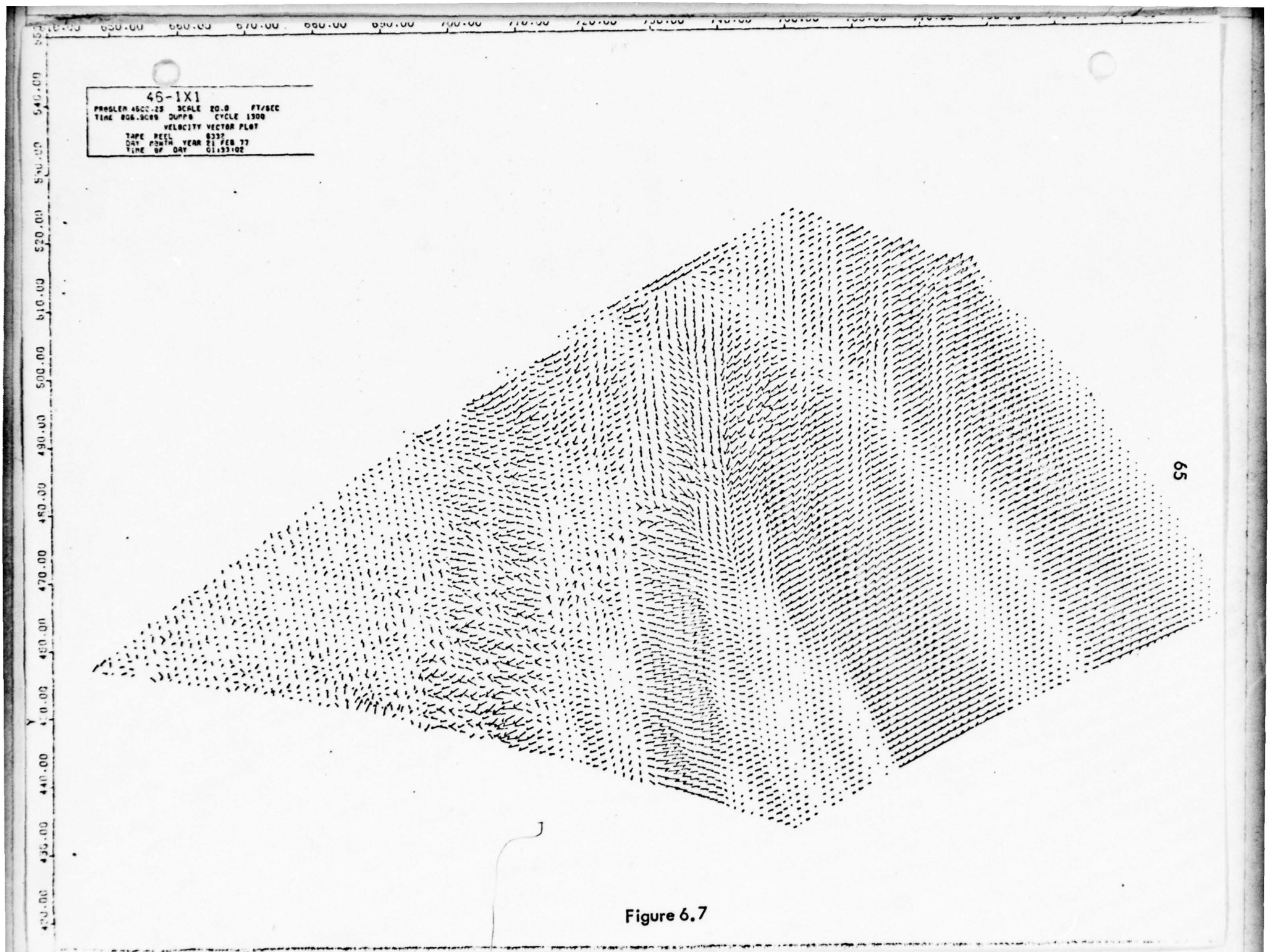

46-1X1
PROBLEM 4602.25 SCALE 20.0 FT/SEC
TIME 806.9069 DUMP8 CYCLE 1300
VELOCITY VECTOR PLOT
TAPE REEL 8332
DAY MONTH YEAR 21 FEB 77
TIME OF DAY 01:33:02

Figure 6.7

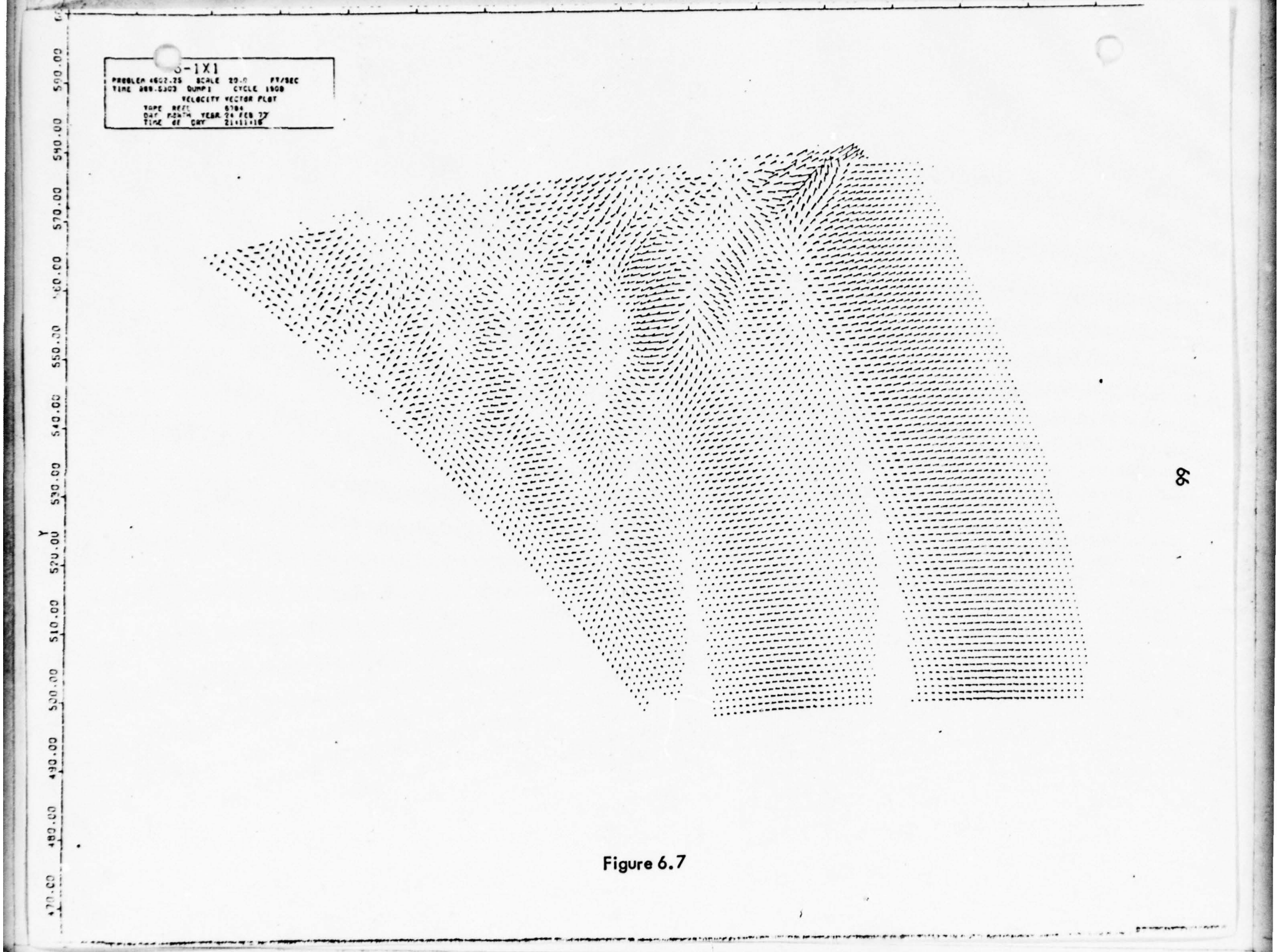

S-1X1
PROBLEM 4602.25 SCALE 20.0 FT/SEC
TIME 300.5303 DUMP1 CYCLE 1900
VELOCITY VECTOR PLOT
TAPE REEL 8184
DAY MONTH YEAR 74 FEB 27
TIME OF DAY 21:11:16
Y
590.00
540.00
490.00
440.00
390.00
340.00
290.00
240.00
190.00
140.00
90.00
40.00

Figure 6.7

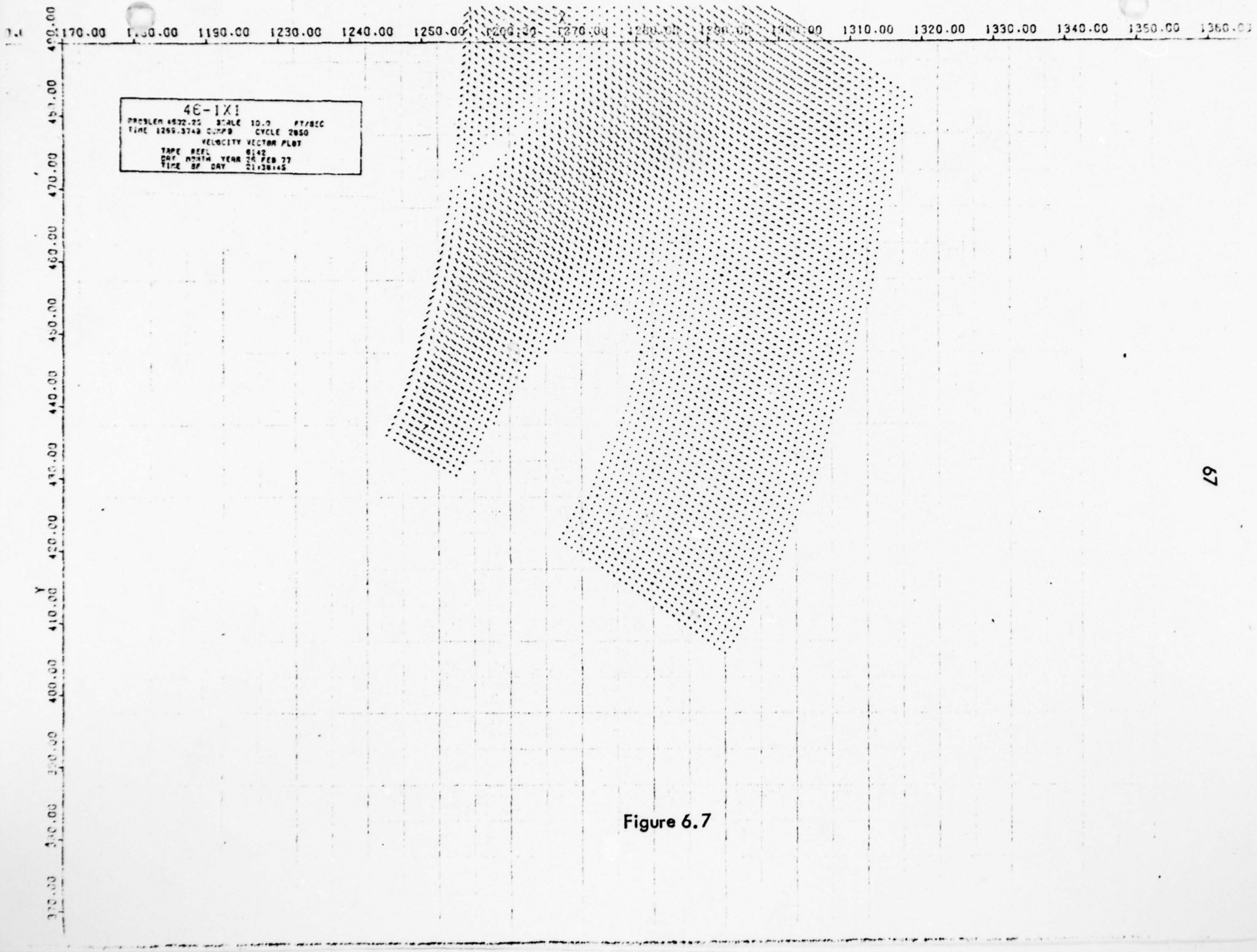

48-1X1
PROBLEM 4832.25 SCALE 10.0 FT/SEC
TIME 1269.3748 CUMPD CYCLE 2850
VELOCITY VECTOR PLOT
TAPE REEL 8142
DAY MONTH YEAR 26 FEB 77
TIME OF DAY 21:38:45
1170.00
1190.00
1230.00
1240.00
1250.00
1310.00
1320.00
1330.00
1340.00
1350.00
Y
410.00
420.00
430.00
440.00
450.00
460.00
470.00

Figure 6.7

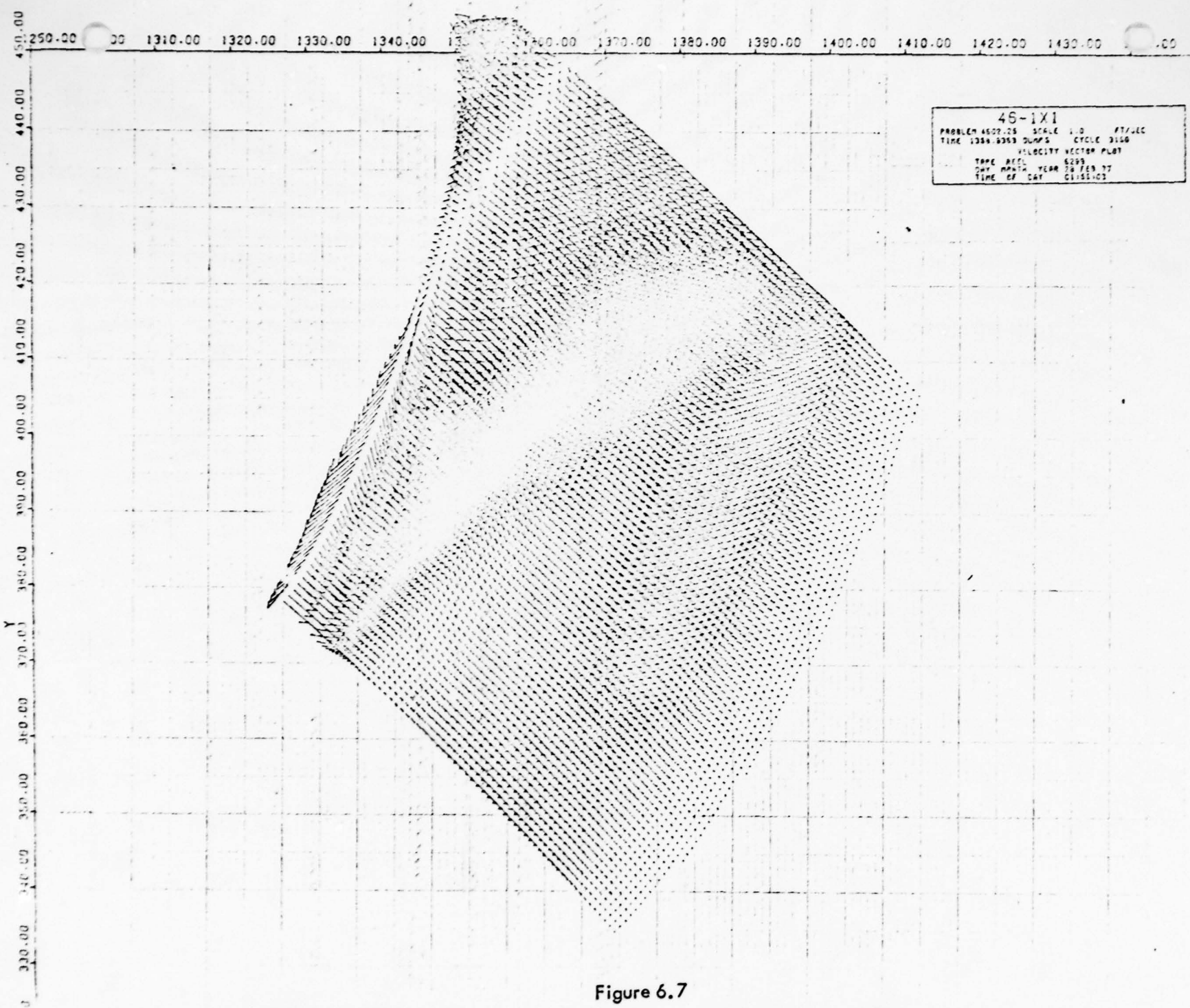
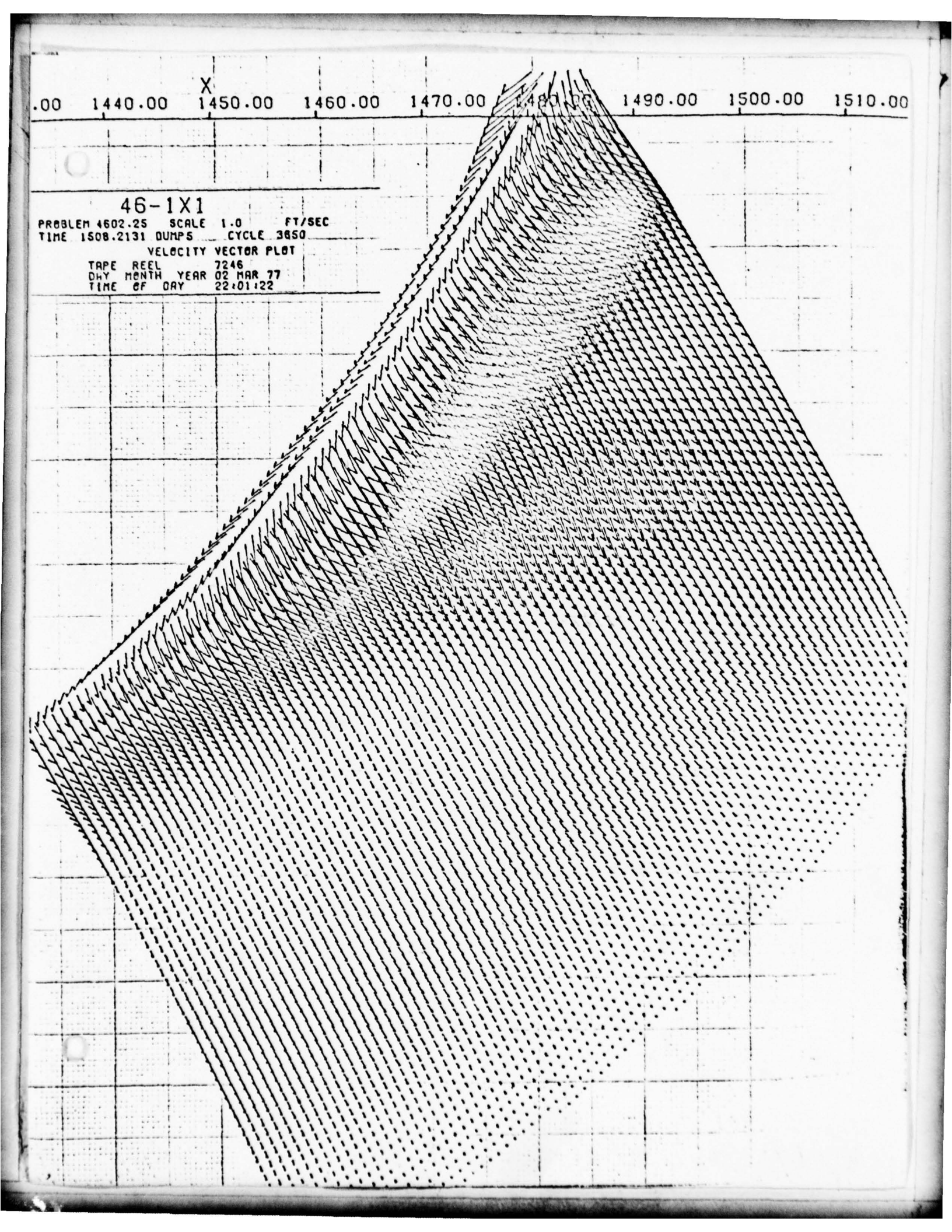

46-1X1
PROBLEM 4502.25 SCALE 1.0 FT/SEC
TIME 1356.9369 DUMPS CYCLE 3156
VELOCITY VECTOR PLOT
TAPE REEL 6293
DAY MONTH YEAR 26 FEB 77
TIME OF DAY 01:55:03
1250.00
1310.00
1320.00
1330.00
1340.00
1400.00
1410.00
1420.00
1430.00
1450.00
450.00
440.00
430.00
420.00
410.00
400.00
390.00
380.00
370.00
360.00
350.00
340.00
330.00
Y

Figure 6.7


X
.00
1440.00
1450.00
1460.00
1470.00
1490.00
1500.00
1510.00
46-1X1
PROBLEM 4602.25 SCALE 1.0 FT/SEC
TIME 1508.2131 DUMPS CYCLE 3850
VELOCITY VECTOR PLOT
TAPE REEL 7246
DAY MONTH YEAR 02 MAR 77
TIME OF DAY 22:01:22

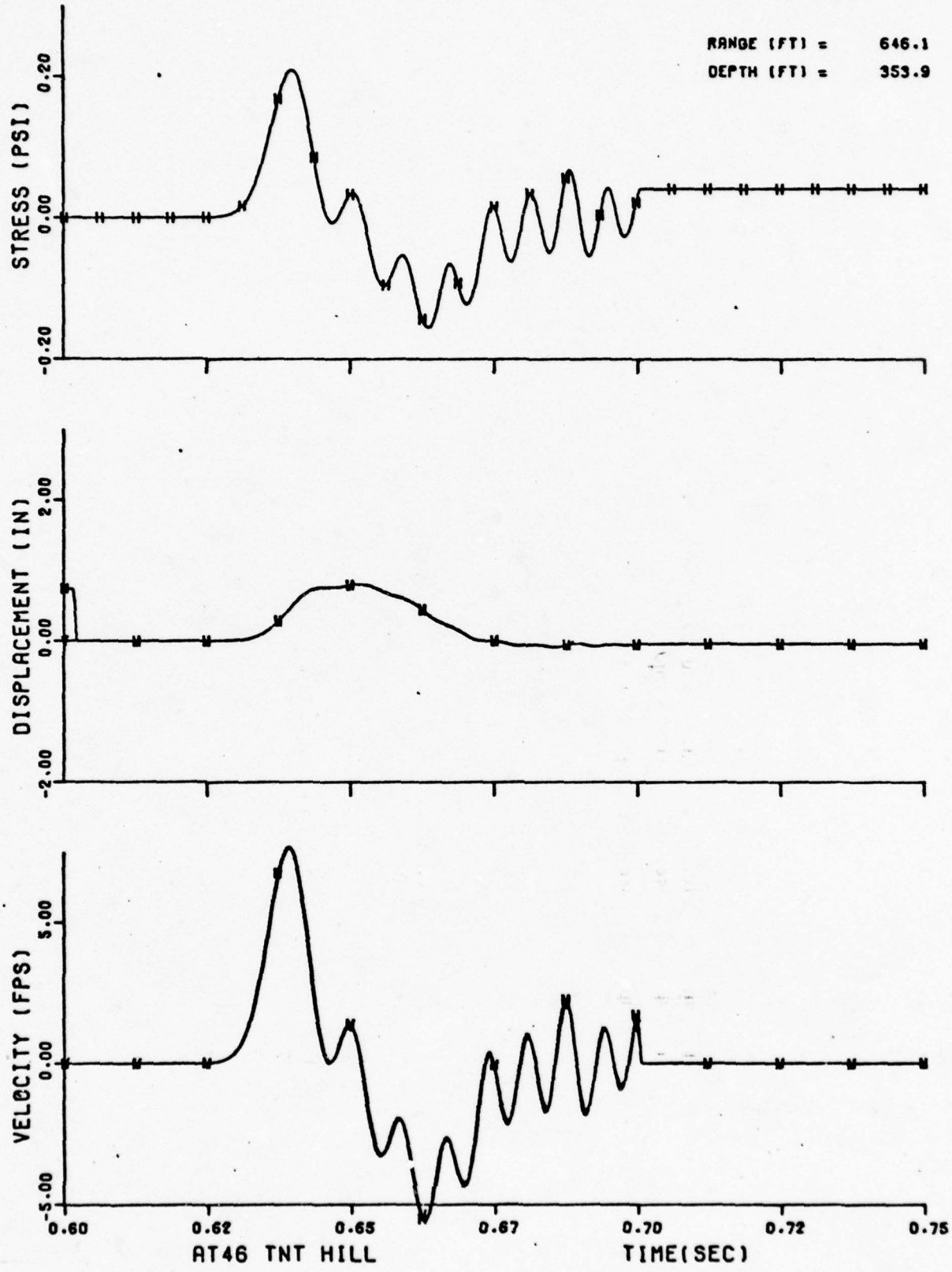


Figure 6.8 Signatures at Elevation of 354 feet on Side of Hill Nearer Source

Quantities graphed are, pressure, displacement, and velocity. Here the graphs represent time signatures at a point, the abscissa being labelled in seconds from the moment of blast.

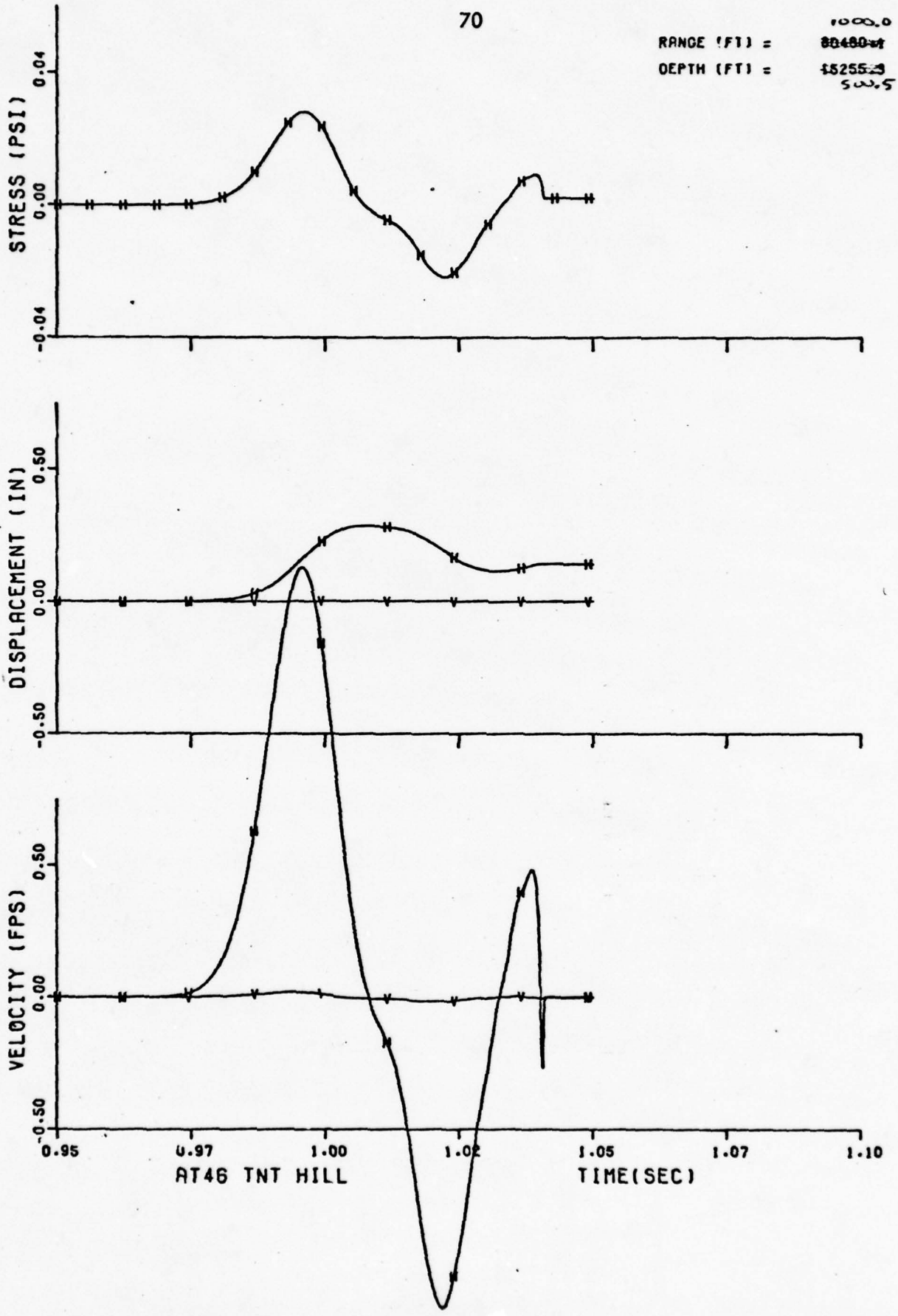


Figure 6.9 Same as Figure 6.8, but for a point just at the top of the hill.

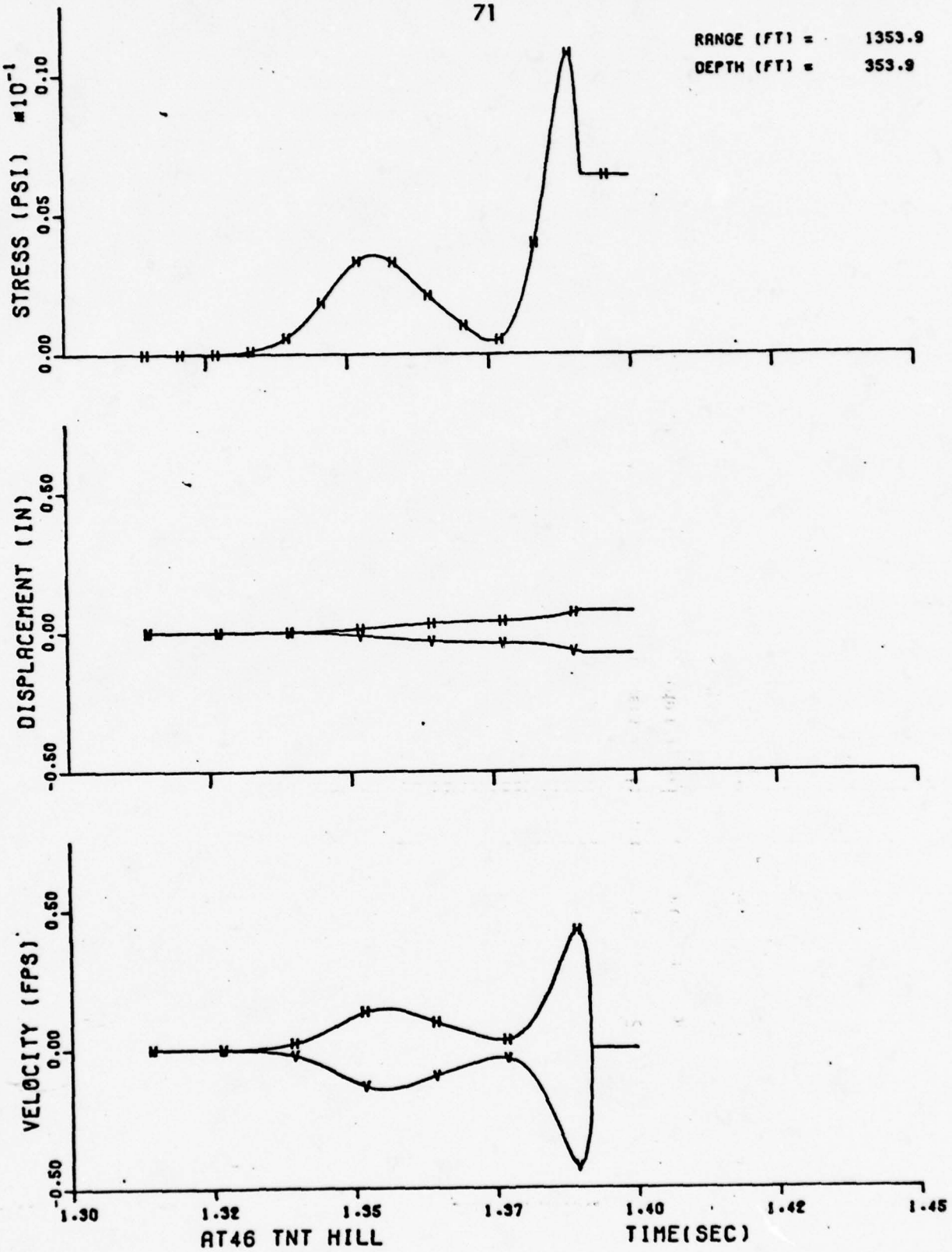


Figure 6.10 Signatures at Elevation of 354 feet on Side of Hill Further from Source. Same as Figure 6.8, at the symmetric point on the shadow side of the hill.

7. THE PROPAGATION OF A HOWITZER BLAST

The serious theoretical study of pulse propagation from an intense explosion began as classified research during the second World War. The pioneering discovery of self-similar solutions to the spherical problem was the independent work of Taylor (1946, 1950) and of Sedov (1959, Ch. 4). Building upon this work, Whitham (1950; 1974, Chs. 6,9) developed a technique--later termed "nonlinearization"--that calculates approximations based on large distance from the source, but takes into account the fact that the true characteristics are not of the linearized form $t - R/C_o$ = constant, but are some function $\tau(R,t)$ = const, to be determined. To use the linearized form might give good results near the source, but would lead to serious error for large R owing to the divergence of the true characteristics. However, for explosions of the magnitude that concern us here, the overpressure and the particle velocities are small when compared respectively to the mean pressure and the sound speed, except very near the source. The disturbance is thus always paradoxically propagating like a linear distance in one sense and like a non-linear one in another sense.

The theoretical treatment (Whitham, 1950, pp. 579 ff.) takes as a model an expanding sphere, initially of radius d, of uniform high pressure $p^o/p_o \gg 1$, where p_o is atmospheric. The uniformly valid approximation for large distance R is then as follows.

The shock front has the representation

$$c_o t = R - b(\ell n R)^{\frac{1}{2}} \qquad (7.1)$$

where $b^2 = 0.84 \frac{p^o}{p_o} d^2$. The constant b cannot really be measured, since the expanding-sphere model is not an adequate representation of the actual blast. However, if we

assume a pressure of say, 40 atmospheres in a sphere of one meter radius, we obtain $b \doteq 5.8$ m and for a distance R of, say 5 kilometers, we have

$$b(\ell n R)^{\frac{1}{2}} \doteq 16 \text{ m} \qquad (7.2)$$

For a sound speed $c_o = 330$ m/sec, this would represent a correction of 0.03 seconds on a linear arrival time of 15.15 seconds.

The reason for this is clear: during its highly nonlinear expansion, the shock travels with a speed in excess of the sound speed. The equation (7.1) shows that the linear propagation is not quite effectively achieved, even after a considerable distance and time of propagation.

However, the picture is still more complicated. After the first overpressure was has passed from the explosive gases, a rarefaction wave is propagated back into them. This is followed by a new second shock, a second rarefaction wave, a third shock, and so on until the explosive gases have been effectively reduced in energy.

Theory tells us that the second shock propagates as

$$c_o t = R + b(\ell n R)^{\frac{1}{2}}, \qquad (7.3)$$

a counterpart to (7.1). However, the details of the shock formation depend essentially on the time-geometry of the expanding sphere, and this is precisely the most unrealistic aspect of the model. Thus one proper test of the theoretical results is a full-scale computation of the explosion and of the subsequent shock propagation.

The Numerical Simulation of a Spherical Blast

There have been a number of computer simulations of spherical blast. One highly successful example is that of H. L. Brode (1959). This particular piece of

research by Brode represents the culmination of a series of similar efforts by himself and others. We have used the Afton Code (Trulio et al., 1976) to simulate a howitzer blast, using as input the parameters associated with the WSMR PASS operation, together with the most recent equations of state for explosives. The basic assumption--discussed in later sections--is that despite the essentially directional nature of a howitzer explosion, for results concerned with even moderate distances from the source, the event may be idealized as spherically symmetric. This simplifying geometry permits us to compute the expansions and rarefactions with a grid-network sufficient to resolve the details. In the early stages of the explosion, for example, it was necessary to use a zone-dimension of 7.5 cm! The physical quantities of the computation were provided by personnel of the Atmospheric Sciences Laboratory, WSMR (Blomerth, personal communication). Together with other derived parameters, they are as follows.

Initial Conditions

In undisturbed air:

density	$\rho_o = 1.225$ kg/m^3	
pressure	$p_o = 1.013$ bars	(7.4)
sound speed	$c_o = 340.25$ m /s	

In the high explosive:

radius of HE sphere	$R_E = 0.1634$ m
density	$\rho_E = 1557$ kg/m^3
specific energy	$e_E = 4.2945 \times 10^6$ joule /kg

The computation obviously requires one set of equations for the explosion and the subsequent movement of the exploded gases, and another for the resulting motions of the air. Between these two gaseous systems there will remain an interface.

The dynamic equations for the high explosive are those of Taylor (1950), with the exception of the equation of state. Because the constants, and even the form, of the equation of state for explosives are best determined empirically, we have used for this purpose the recent results of Lee et al. (1968) as the most satisfactory version to date.

The air was treated as a gamma-law gas,

$$\Delta p = \gamma \frac{p}{\rho} \Delta \rho ,$$

and integrated according to the Afton Code. The finite difference equations of this code are complex but fully documented by Trulio et al. (1976) in the User's Manual.

Two runs were performed for the spherically symmetric explosion:

(1) Using spacial zones of 7.5 cm length, the integration was carried out to 1.5 seconds.

(2) Using spacial zones of 15 cm, the integration was carried out to 6.735 sec. This result was used as the input to the computation of diffraction by a hill, reported in Section 6.

It may be mentioned at this point that to our knowledge, these computations of a blast wave are here carried out an order of magnitude further in time (and space) than any other yet performed. The computations of Brode (1959), for example, are terminated (corresponding to the data for our problem) at about 0.12 sec.

is still active dynamically in a very complicated pattern. The shock-producing process may or may not still be in operation, but the magnitudes are no longer sufficient to be detected above the computational noise.

This noise--that is, truncation error--is evident in the periodic wiggles back of each shock; and a word concerning this problem is in order. The shock front, having the theoretical form of a step function, cannot be resolved in its propagation by finite differences. The cost of discretizing the computation is that spurious oscillations are set up, and the amplitude of the shock energy maximum is diminished by the energy of these little wavelets. This situation has been examined in some detail by Wurtele (1961), who presents analytical solutions for differential-difference equations that enable us to see the structure of the numerically introduced error. By the methods of this paper, we can specify that at a time of 51 ms, the numerical oscillation should have a wave length of 6.1 zones. The dump at 51.492 shows that this is indeed the wavelength. However, in order to check further, we repeated the computation with a reduced zone length of 7.5 cm. The results are contained in Figure 7.2. A dump at the same time (51 ms) shows a finer resolution of the shocks, to be sure, but with double the number of oscillations per unit distance. This demonstrates beyond question that the oscillation is numerical and not physical.

It would be simple to remove these spurious oscillations by smoothing--a running average over a dozen zones, for example--but this would be a purely cosmetic operation, with no information gained and with new problems introduced which we would understand less well than we understand the existing numerical error. For this reason, we have graphed the computed solution with no modification at any time.

The set of graphical output in Figure 7.1 show the simulation of the blast. The upper figure (labelled stress) on each page is the overpressure, the middle is the parcel displacement, and the bottom is the (radial) velocity. Each graph represents the distribution of the quantity in space at a given time. Care must be taken in reading the magnitudes, since both the ordinate and the abscissa scales change with time in order that a satisfactory graph be presented. The zero-point also is variably placed.

With these facts in mind, we may examine the results. The first shock is evident in DUMP 1, at 0.024 ms. The dumps at 0.693 and 1.121 ms show the subsequent extreme rarefaction. In the latter graph the pressure appears to be zero--i.e. a negative one-bar overpressure--and reference to the digital output shows it to be indeed almost but not quite a vacuum.

Recalling that this is a spherical rather than a linear blast-wave, we note that the rarefaction cannot be propagated backward beyond the origin, and, according to the above-mentioned theory, a second shock must follow. This is first evident at 6.313 ms: the first shock has propagated to about 22 feet from the source; and the rarefaction extends from about 15 feet back to 5 feet, where the second shock begins. This process is repeated twice more. Reference to the dump at 51.492 ms shows an interesting situation. Four shocks are evident, at 82, 55, 46, and 36 feet. Each shock is smaller than its predecessor. The first has still a significant, though greatly reduced, overpressure (0.07 bars); and the subsequent shocks exist within a general rarefaction region, with each sub-peak pressure just zero or slightly positive. At about seven feet one notes the interface of the high explosive and the gamma-law air. The HE

We may now look at a later time, say 176.507 ms. At this point the computation within the HE was abandoned as no longer contributing significantly to the region of interest behind the shock. The first shock itself has reached 225 feet and its maximum overpressure has fallen to 0.05 bars, or 50 mb. The second and third shocks are still detectable above the computational noise, but the fourth is now lost. The velocity maximum is about 13 m sec^{-1}, small compared to the speed of sound, but certainly large for a sound wave.

The last dump, at 6701.280 sec, shows the shock front at 7520 ft. Only two shocks are now distinguishable. The spurious oscillation following the first shock is about 40 zones in wave length. Overpressure is about one-half millibar and velocity 15 cm/sec. It is this state of the system that served as input to the computation of scattering by a hill in Section 6.

In order to make connection with theory let us consider a relatively late dump, say, 70. This is at time 2.766 seconds, using the sound speed (7.4), we have

$$c_o t = 941.13 \text{ m.}$$

Now owing to numerical dispersion, we have an interval bounding the arrival time, rather than a precise time of arrival. An understanding of the numerical effects would lead us to place the shock front at DUMP 70 at 3130 feet or 954.02 m. It could not be placed at less than 3115 feet or 949.45 m. These distances translate to time differences of 0.03788 and 0.02445 sec respectively. Thus in the simulation, as in the non-linear theory, the signal arrives measurably ahead of the arrival time predicted by the basic sound-ranging assumptions.

If we wish to establish even more detailed correspondence between simulation and analysis, we may apply (7.1) to the simulation results. Using R = 954.02 m and t = 2.766 sec, we obtain a value for b,

$$b = \frac{R - c_o t}{(\ell n R)^{\frac{1}{2}}} \doteq 6.4 \text{ m}$$

This is not far from our tentative value of b = 5.8 m, calculated on the basis of a pressure of 40 atmospheres in a one-meter-radius sphere. If one examines the early dumps, he will see that although the expanding-sphere model is not really applicable, if one were forced to use it, the values assumed would be defensible.

At any rate, we see that the arrival time is distorted by the essential nonlinearily of the shock propagation. It remains to determine how great an error is introduced into sound-ranging results by this distortion.

Implications for Sound Ranging

Using some rather gross assumptions, we may estimate the ranging error involved with the nonlinearity. Let us use (7.1) with b = 6. Then if we apply (7.1) to the arrivals at R_1 and R_2, and subtract the results, we have

$$c_o \Delta t = \Delta R - b \{ [\ell n (R_2)]^{\frac{1}{2}} - [\ell n (R_1)]^{\frac{1}{2}} \} \qquad (7.6)$$

where $\Delta t = t_2 - t_1$, and $\Delta R = R_2 - R_1$. We now use the approximations--solely for the purpose of the present discussion —

$$\ell n \left(1 + \frac{\Delta R}{R_1}\right) \ll \ell n R_1$$

and

$$\frac{\Delta R}{R_1} \ll 1 .$$

Then (7.6) becomes

$$c_o \Delta t \doteq \Delta R - \frac{b}{2} \frac{\ell n(1+\frac{\Delta R}{R_1})}{(\ell n R_1)^{\frac{1}{2}}}$$

$$= \Delta R \left[1 - \frac{b}{2R_1(\ell n R_1)^{\frac{1}{2}}} \right]$$

This applies equally to the signal arrivals at R_1 and R_3. Hence we may write

$$s_i = (1 + \epsilon)\, \sigma_i \qquad i = 2,3 \qquad (7.7)$$

where, as before, $\sigma_i = c_o \Delta t_i$, and

$$1 + \epsilon = \left[1 - \frac{b}{2R_1(\ell n R_1)^{\frac{1}{2}}}\right]^{-1} \qquad (7.8)$$

It is easily estimated that for $b \sim 6$ m, the value of ϵ will be about 10^{-3}. If we substitute (7.7) into the ranging formula (2.3a), we obtain

$$2R = \frac{2d^2 - (\sigma_3^2 - 2\sigma_2^2)(1+\epsilon)^2}{(1+\epsilon)(\sigma_3 - 2\sigma_2)}$$

or to the first order in ϵ

$$R = R_o(1-\epsilon) - \epsilon \frac{\sigma_3^2 - 2\sigma_2^2}{\sigma_3 - 2\sigma_2} \qquad (7.9)$$

The correction of one-tenth per cent on R_o is perhaps bordering on negligibility, but the additive term would normally be a correction three or more times as large. It would seem that a correction factor as in (7.9) should be built into the ranging formulas and computational code. The approximations made in deriving (7.8) might affect the result, but (7.9) would always lead to a more accurate ranging estimate.

We are not quite in a position to recommend a final formulation for this correction. The evidence seems to be that a value of six for b is adequate, but further computation would be desirable.

The value of R_1 in (7.8) is, of course, unknown. In theory, an estimate could be made, R_1 computed, and then an iteration procedure performed. However, in view of the smallness of the correction in practice, this seems not worthwhile. The first estimate is probably adequate.

The amplitude, as well as the arrival time, is always measurably nonlinear in behavior. For example, the peak overpressure at any distance R is given by

$$\frac{P}{P_o} = \frac{Ad}{R(\ell n R)^{\frac{1}{2}}} \qquad (7.10)$$

where A and B are to be empirically determined Miles (1967) has gathered the available data, and for comparison with linear theory determined an "apparent exponent of decay" q such that

$$p \sim R^{-q}. \qquad (7.11)$$

In linear theory, of course, $q = 1$. Although behavior according to (7.10) can never satisfy a power law, it turns out that for typical sound-ranging distances R_1 the value of q is relatively constant, about 1.07. This and the other empirically-determined values could be introduced into (7.11) so that we can replace (7.8) by

$$\epsilon \doteq \frac{K}{R^{1.07}} \qquad (7.12)$$

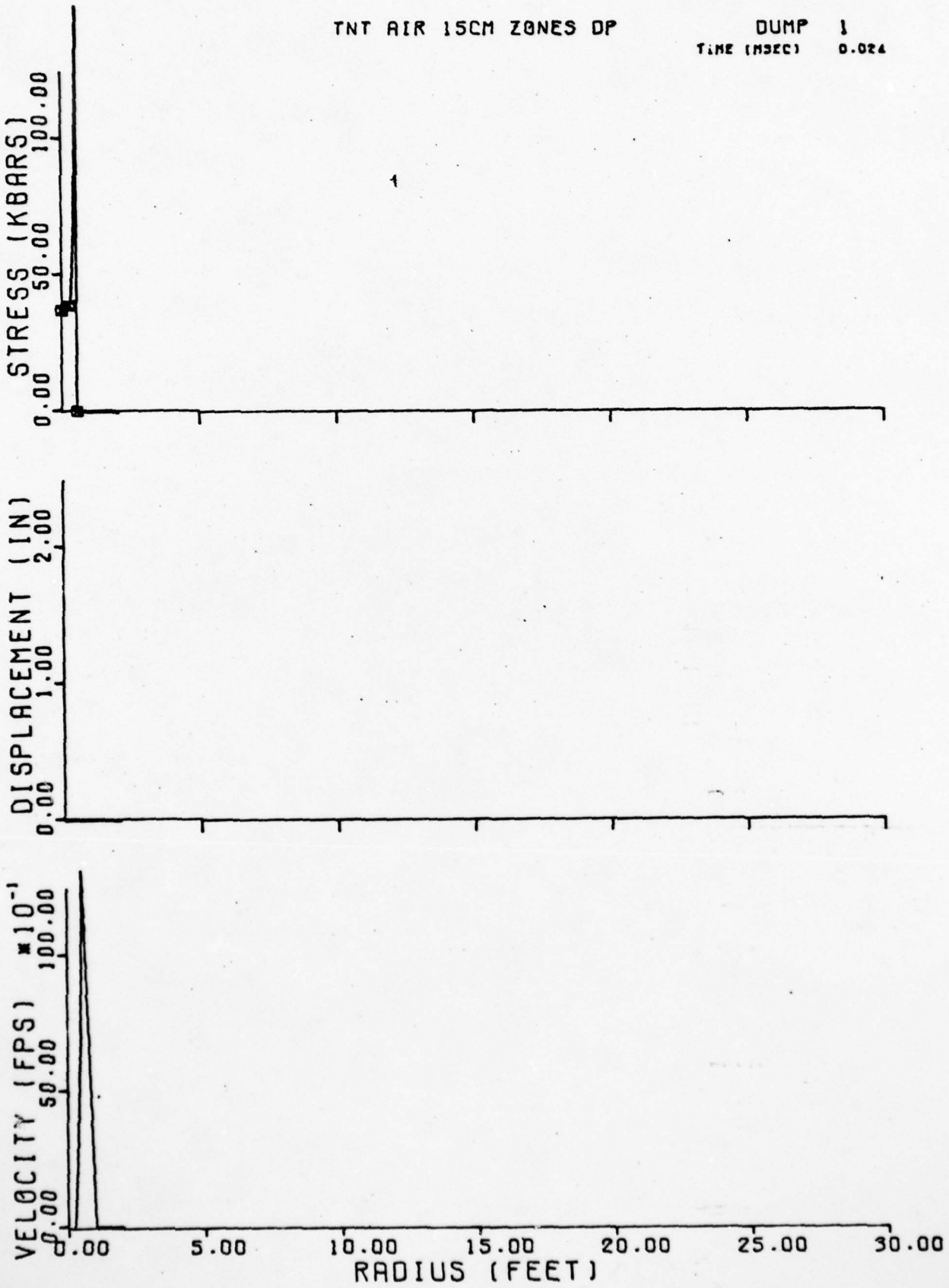
with R_1 expressed in meters, and the constant K is to be determined by field experiments.

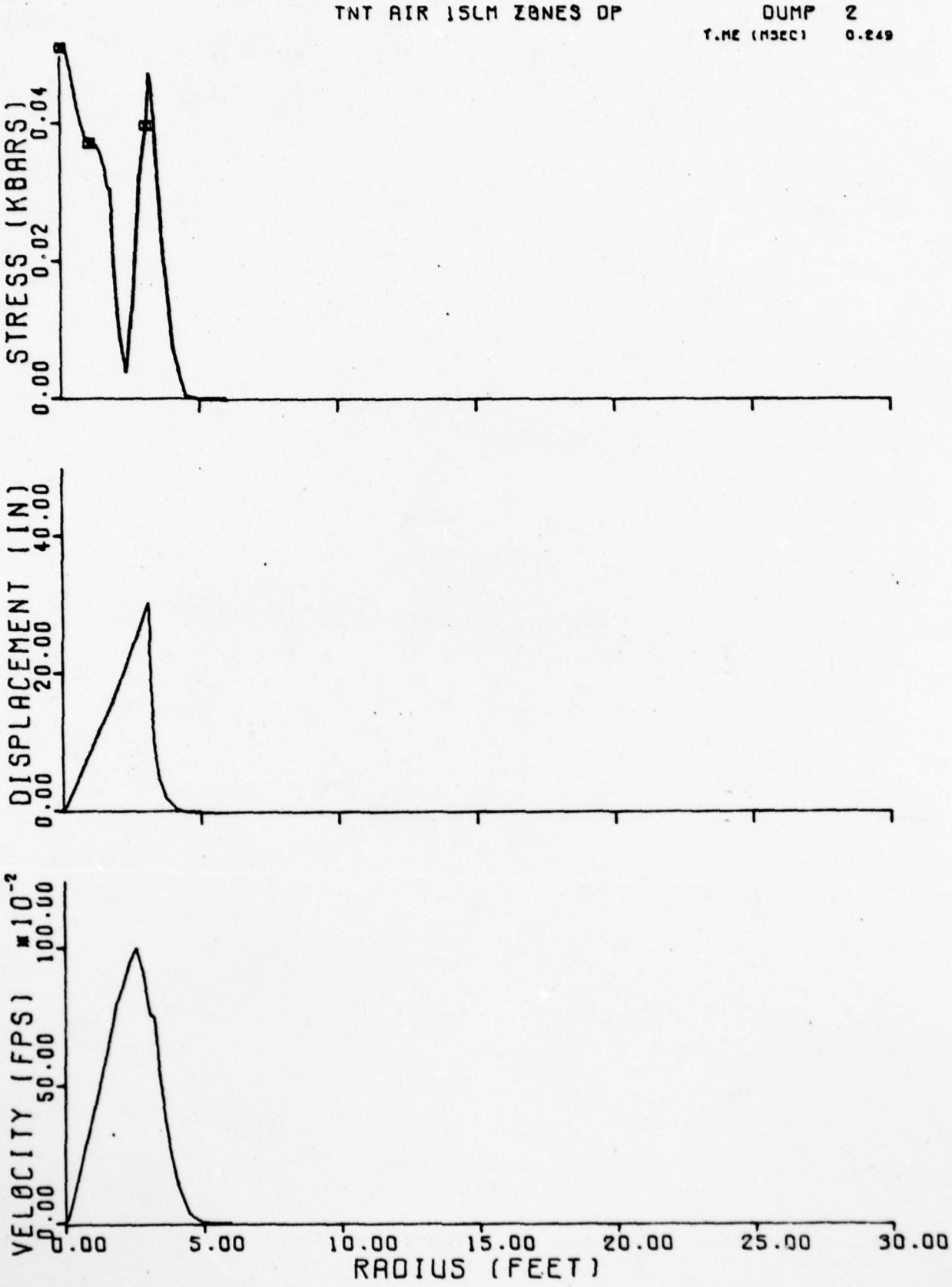
Figure 7.1 The Numerical Simulation of a Howitzer Blast.

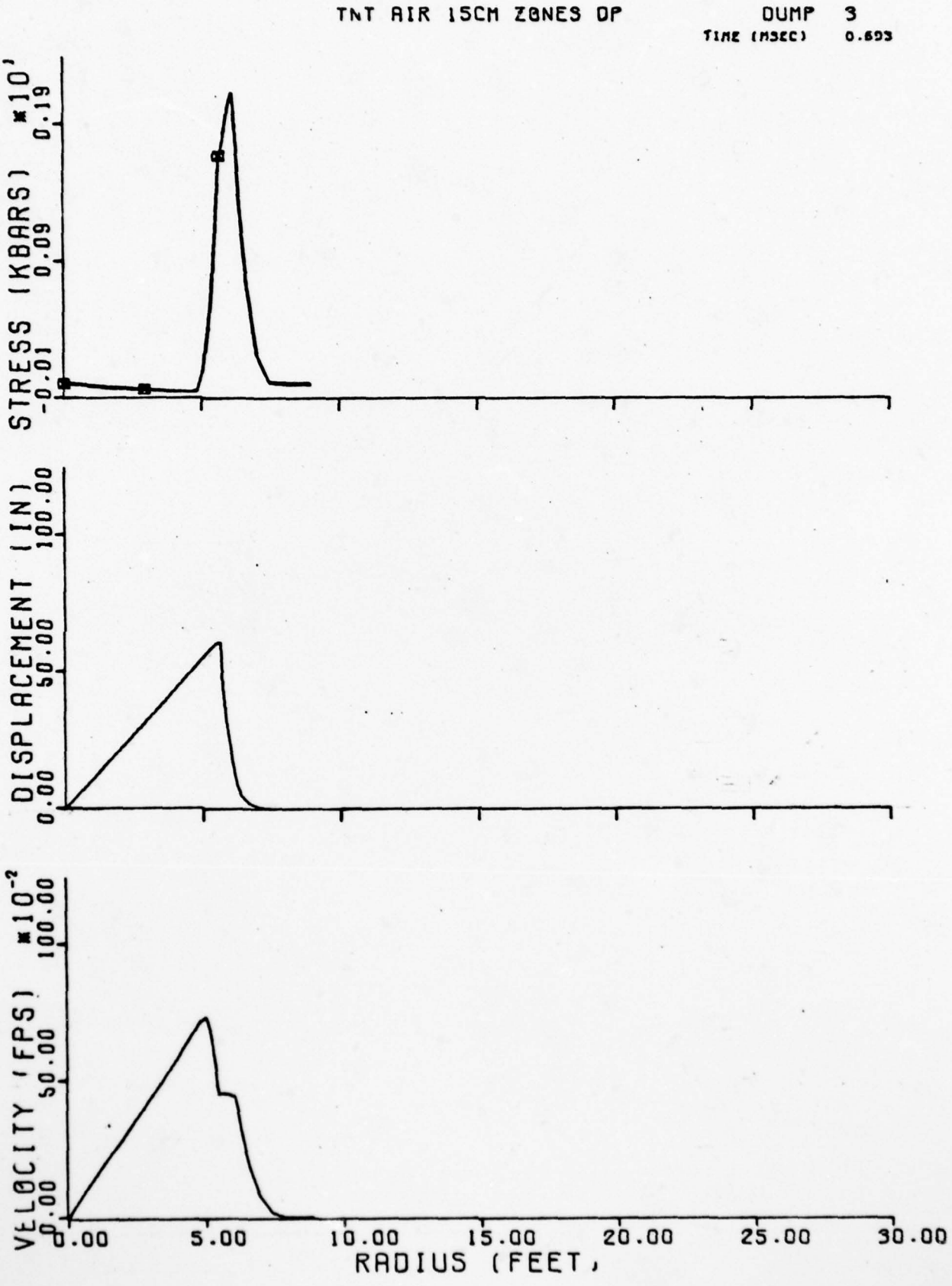
Each page shows spacial profiles of three quantities at a given time. The top profile is that of the stress, that is, the total pressure. The second is the parcel displacement, and the bottom is the velocity. Since the explosion is assumed sphericals the velocity is positive outward, negative inward, with the origin at the center of the explosion. The distance from this center is the abscissa, labeled "radius".

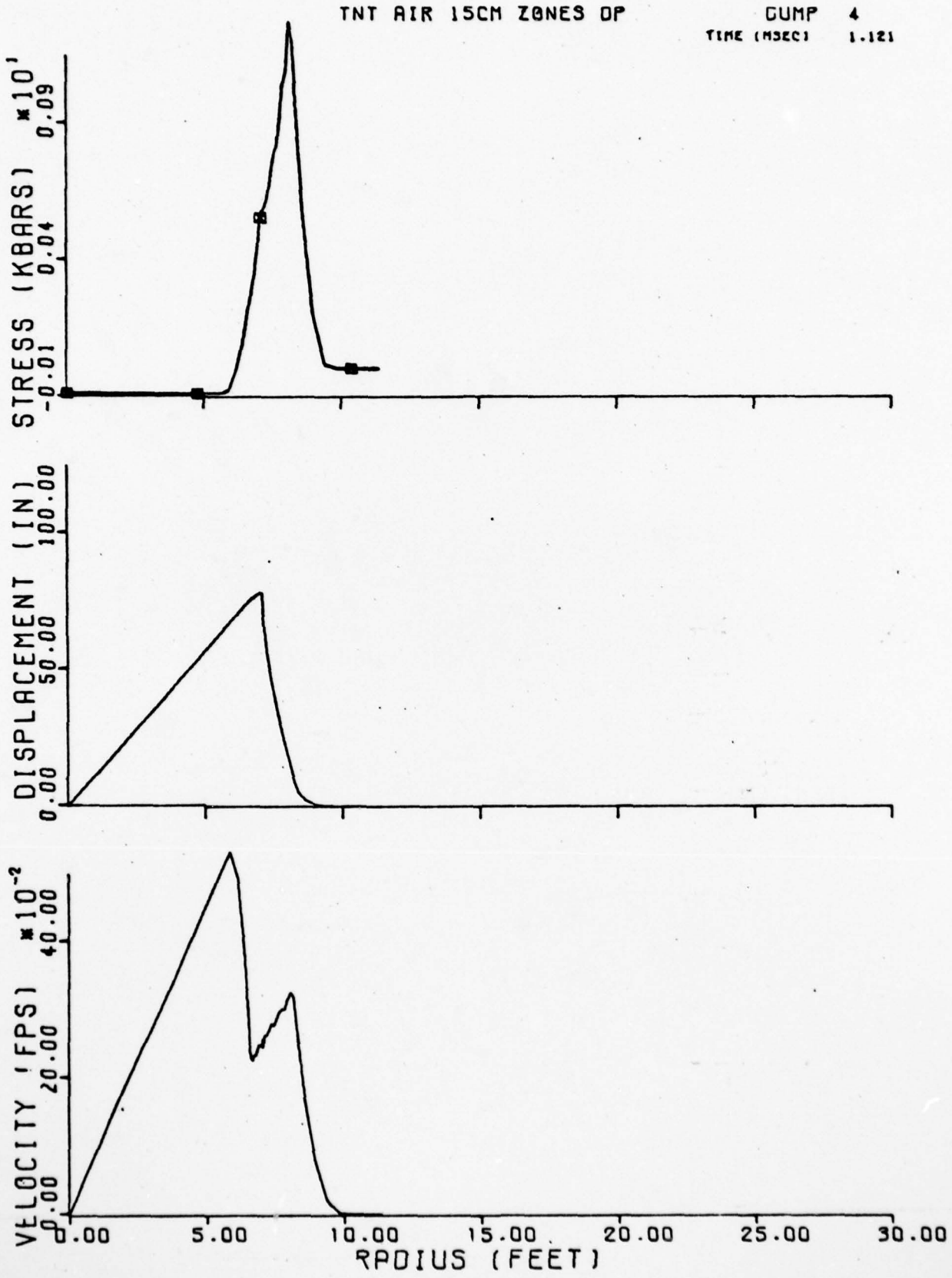
The scales and the zero positions are chosen to obtain a readable graph and should be consulted in viewing each profile.

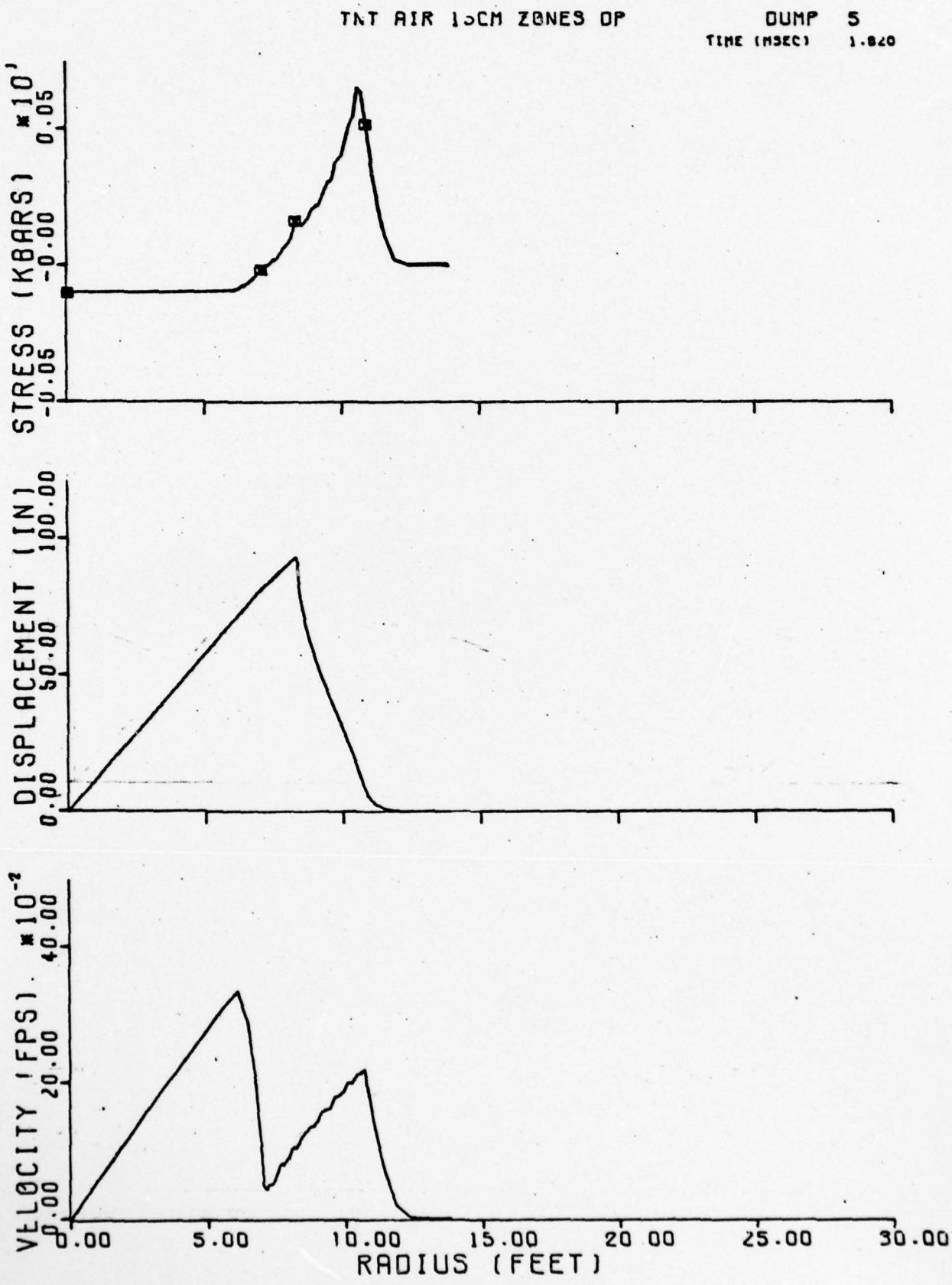
The time of each page is given at the top right in milliseconds.

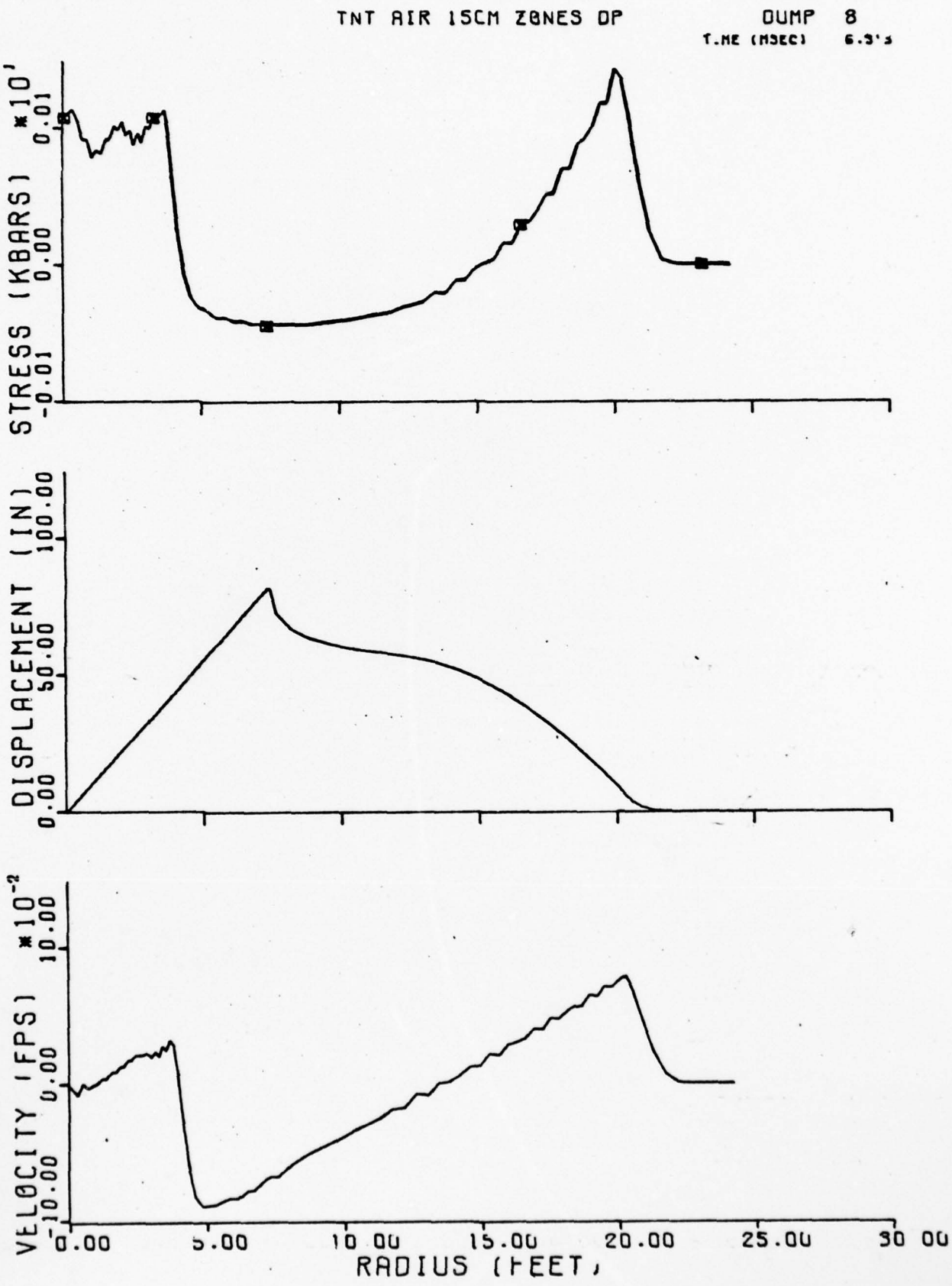

TNT AIR 15CM ZONES DP
DUMP 1
TIME (MSEC) 0.024
STRESS (KBARS)
0.00
50.00
100.00
DISPLACEMENT (IN)
0.00
1.00
2.00
VELOCITY (FPS) *10⁻¹
0.00
50.00
100.00
0.00
5.00
10.00
15.00
20.00
25.00
30.00
RADIUS (FEET)

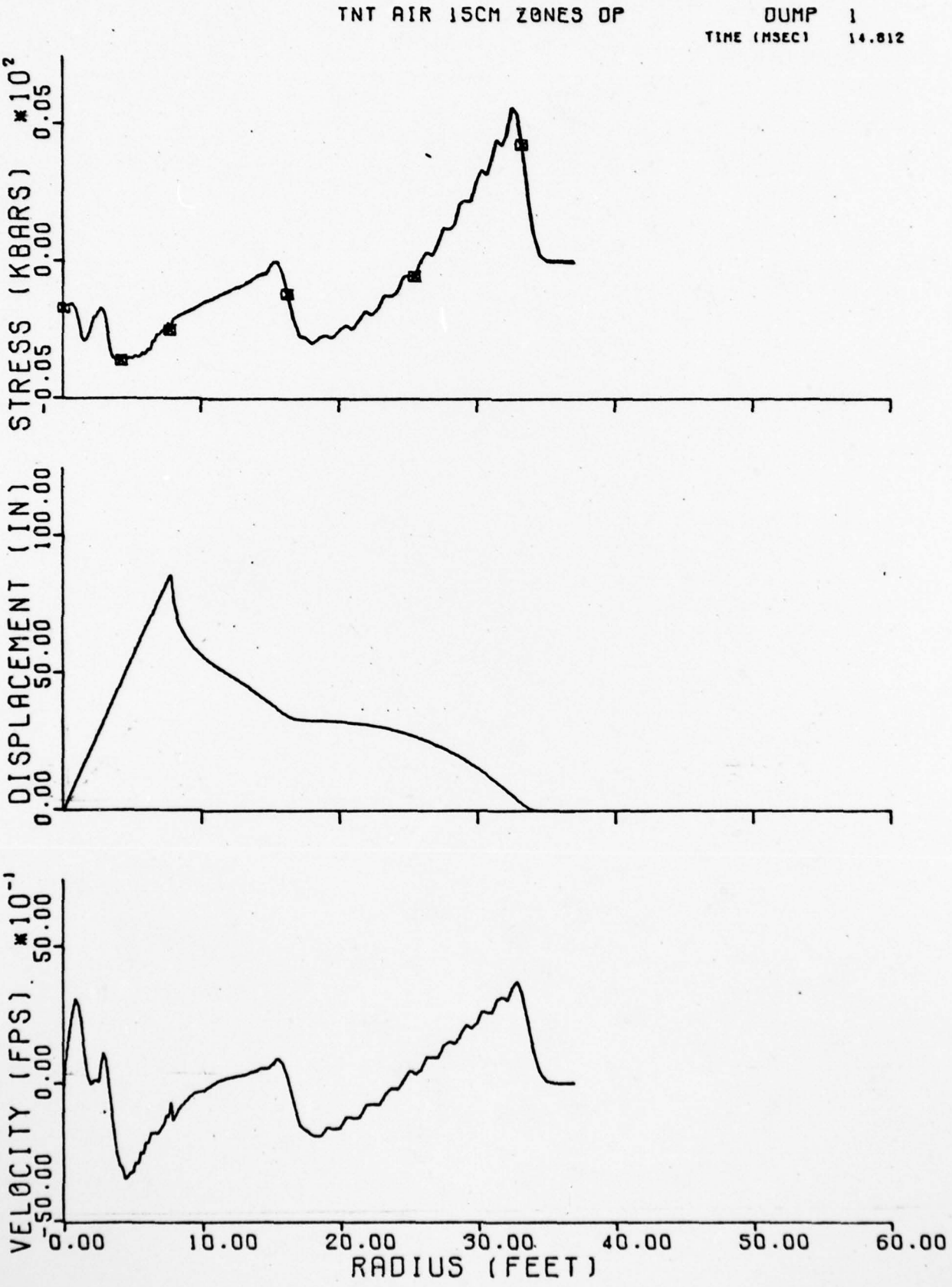

TNT AIR ISLM ZONES OP
DUMP 2
TIME (MSEC) 0.249
STRESS (KBARS)
0.00
0.02
0.04
DISPLACEMENT (IN)
0.00
20.00
40.00
VELOCITY (FPS) *10⁻²
0.00
50.00
100.00
0.00
5.00
10.00
15.00
20.00
25.00
30.00
RADIUS (FEET)

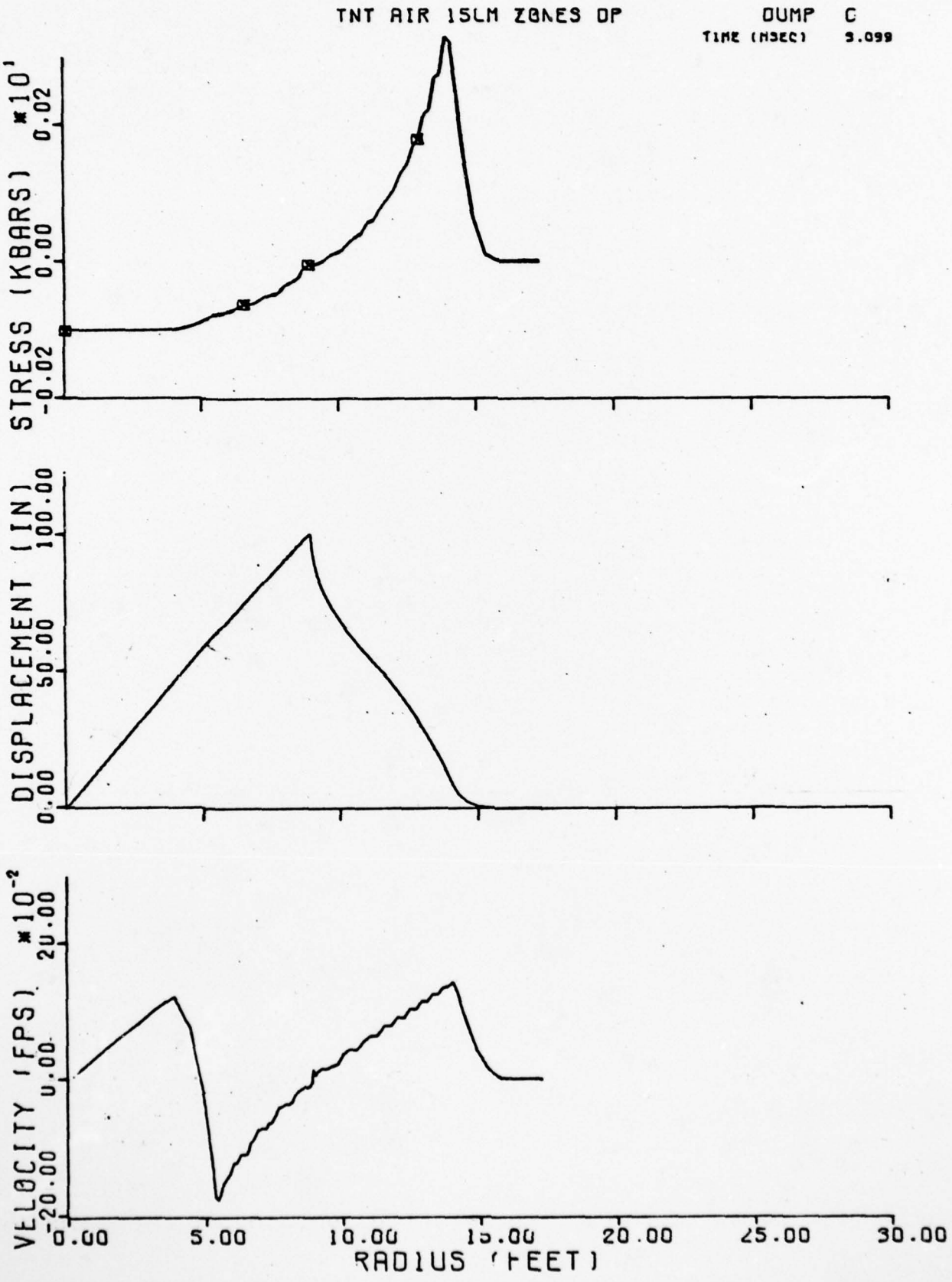

TNT AIR 15CM ZONES DP
DUMP 3
TIME (MSEC) 0.693
STRESS (KBARS) *10'
0.19
0.09
-0.01
DISPLACEMENT (IN)
100.00
50.00
0.00
VELOCITY (FPS) *10^-2
100.00
50.00
0.00
0.00
5.00
10.00
15.00
20.00
25.00
30.00
RADIUS (FEET)

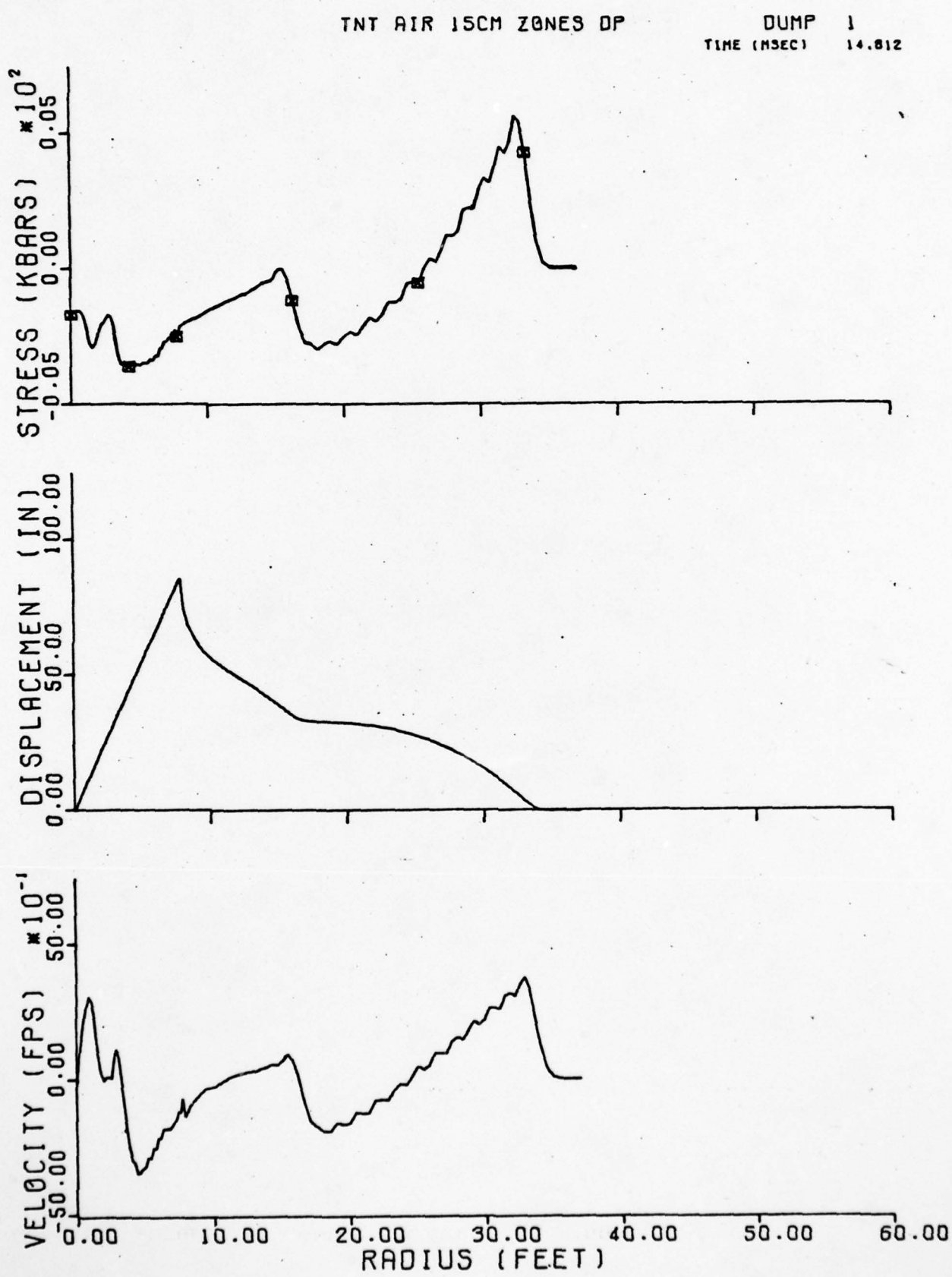

TNT AIR 15CM ZONES DP
DUMP 4
TIME (MSEC) 1.121
STRESS (KBARS) *10'
-0.01
0.04
0.09
DISPLACEMENT (IN)
0.00
50.00
100.00
VELOCITY (FPS) *10^-2
0.00
20.00
40.00
0.00
5.00
10.00
15.00
20.00
25.00
30.00
RADIUS (FEET)

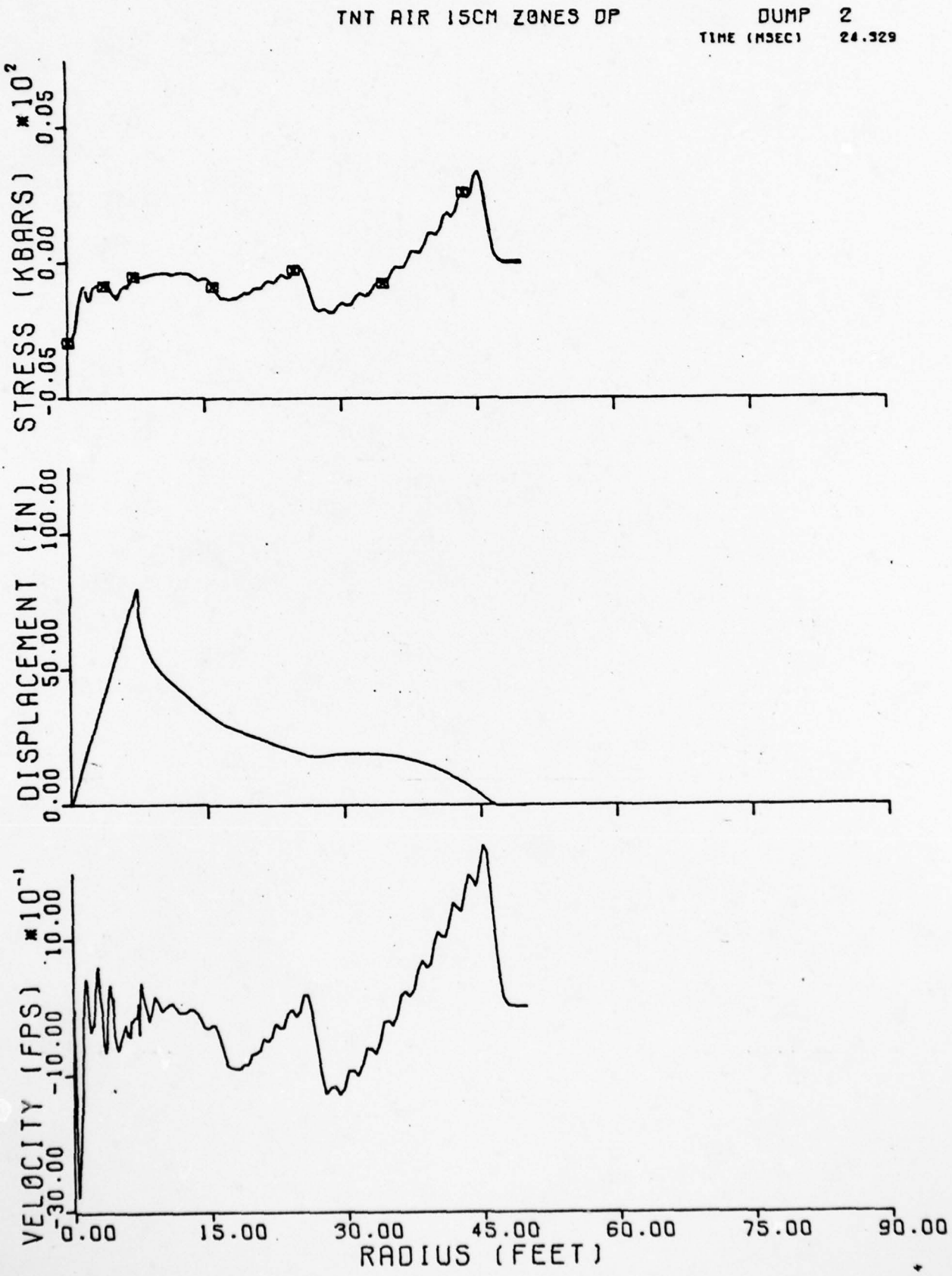

TNT AIR 15CM ZONES OP
DUMP 5
TIME (MSEC) 1.820
STRESS (KBARS) *10'
0.05
-0.00
-0.05
DISPLACEMENT (IN)
100.00
50.00
0.00
VELOCITY (FPS) *10-2
40.00
20.00
0.00
0.00
5.00
10.00
15.00
20.00
25.00
30.00
RADIUS (FEET)

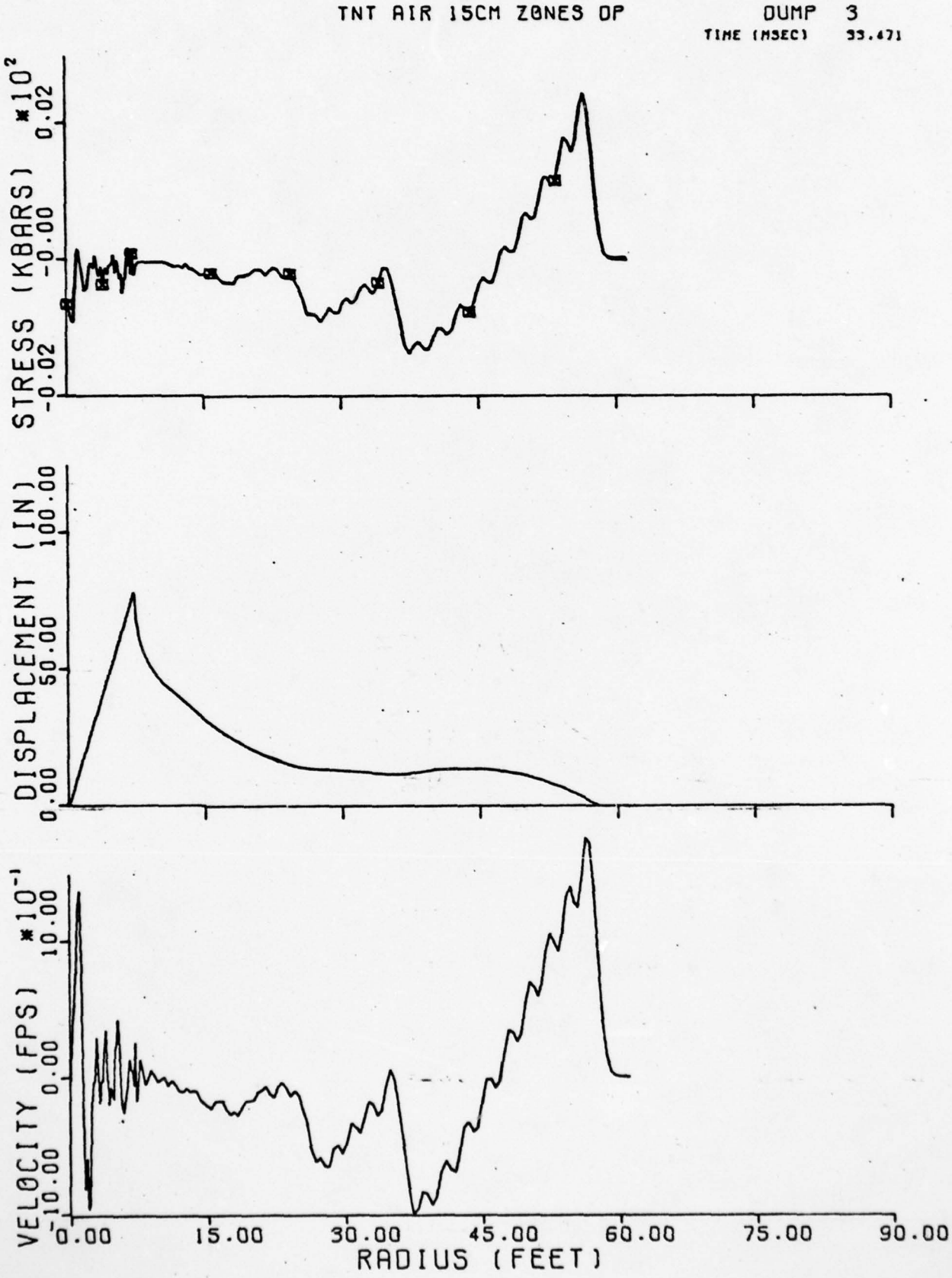

TNT AIR 1SCM ZONES DP
DUMP 8
TIME (MSEC) 6.3'5
STRESS (KBARS) *10'
0.01
0.00
-0.01
DISPLACEMENT (IN)
100.00
50.00
0.00
VELOCITY (FPS) *10^-2
10.00
0.00
-10.00
0.00
5.00
10.00
15.00
20.00
25.00
30.00
RADIUS (FEET)

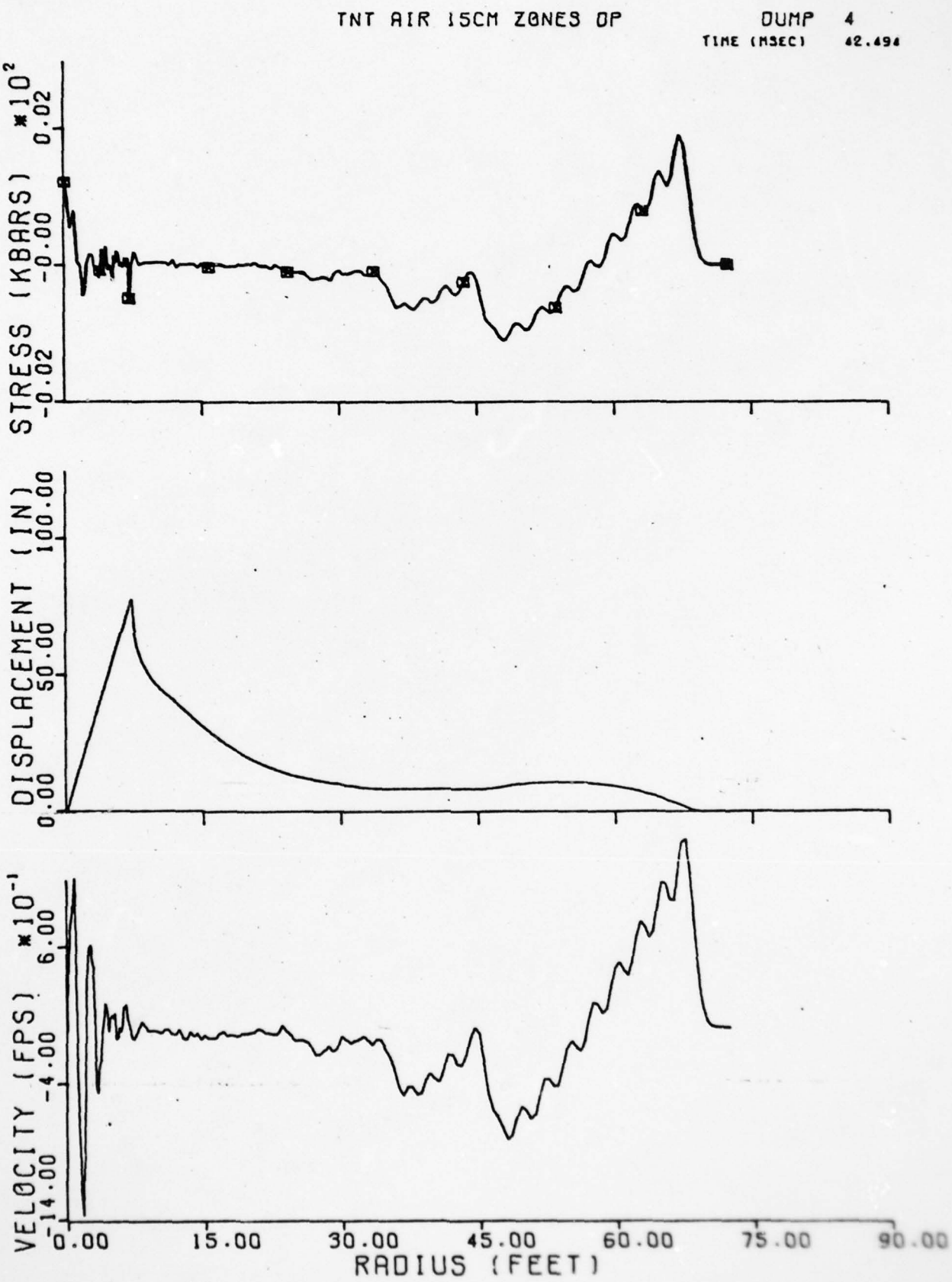

TNT AIR 15CM ZONES OP
DUMP 1
TIME (MSEC) 14.812
STRESS (KBARS) *10²
0.05
0.00
-0.05
DISPLACEMENT (IN)
100.00
50.00
0.00
VELOCITY (FPS) *10⁻¹
50.00
0.00
-50.00
0.00
10.00
20.00
30.00
40.00
50.00
60.00
RADIUS (FEET)


TNT AIR 15LM ZONES DP
DUMP C
TIME (MSEC) 9.099
STRESS (KBARS) *10¹
0.02
0.00
-0.02
DISPLACEMENT (IN)
100.00
50.00
0.00
VELOCITY (FPS) *10⁻²
20.00
0.00
-20.00
0.00
5.00
10.00
15.00
20.00
25.00
30.00
RADIUS (FEET)


TNT AIR 15CM ZONES DP
DUMP 1
TIME (MSEC) 14.812
STRESS (KBARS) *10²
0.05
0.00
-0.05
DISPLACEMENT (IN)
100.00
50.00
0.00
VELOCITY (FPS) *10⁻¹
50.00
0.00
-50.00
0.00
10.00
20.00
30.00
40.00
50.00
60.00
RADIUS (FEET)


TNT AIR 15CM ZONES DP
DUMP 2
TIME (MSEC) 24.329
STRESS (KBARS) *10²
0.05
0.00
-0.05
DISPLACEMENT (IN)
100.00
50.00
0.00
VELOCITY (FPS) *10⁻¹
10.00
-10.00
-30.00
0.00
15.00
30.00
45.00
60.00
75.00
90.00
RADIUS (FEET)


TNT AIR 15CM ZONES OP
DUMP 3
TIME (MSEC) 33.471
STRESS (KBARS) *10²
0.02
-0.00
-0.02
DISPLACEMENT (IN)
100.00
50.00
0.00
VELOCITY (FPS) *10⁻¹
10.00
0.00
-10.00
0.00
15.00
30.00
45.00
60.00
75.00
90.00
RADIUS (FEET)

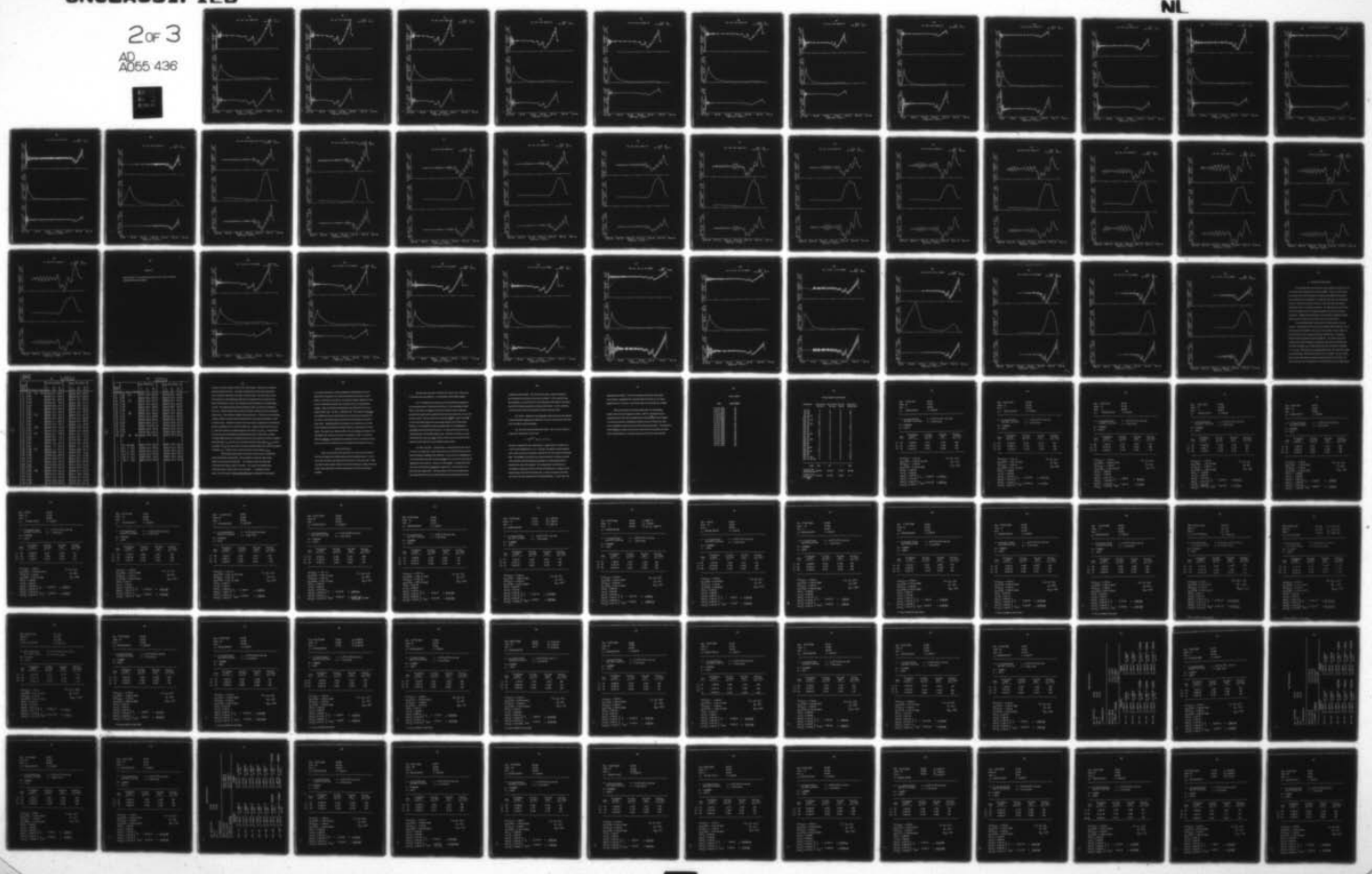

TNT AIR 15CM ZONES OP
DUMP 4
TIME (MSEC) 42.494
STRESS (KBARS) *10²
0.02
-0.00
-0.02
DISPLACEMENT (IN)
100.00
50.00
0.00
VELOCITY (FPS) *10⁻¹
6.00
-4.00
-14.00
0.00
15.00
30.00
45.00
60.00
75.00
90.00
RADIUS (FEET)

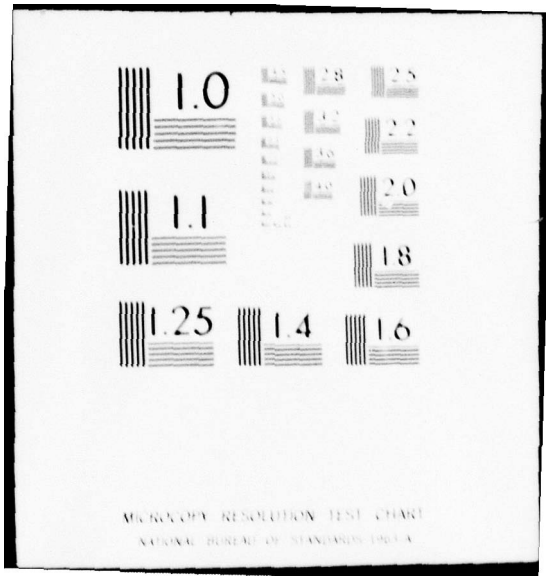
AD-A055 436 CALIFORNIA UNIV LOS ANGELES DEPT OF ATMOSPHERIC SCIENCES F/G 20/1
PROBLEMS AND TECHNIQUES OF SOUND RANGING.(U)
AUG 77 M G WURTELE, J ROE

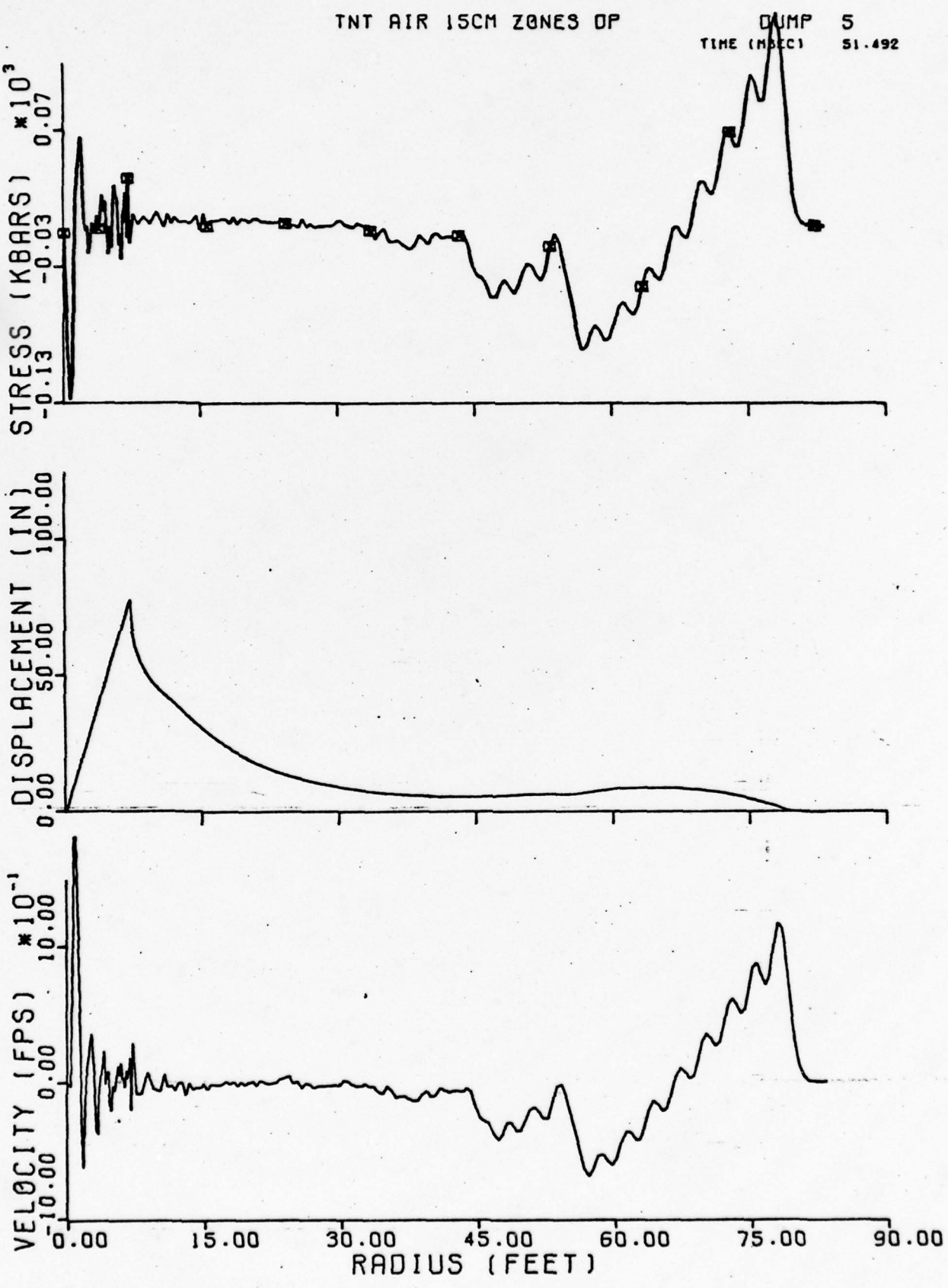
UNCLASSIFIED DAAD07-75-C-0087

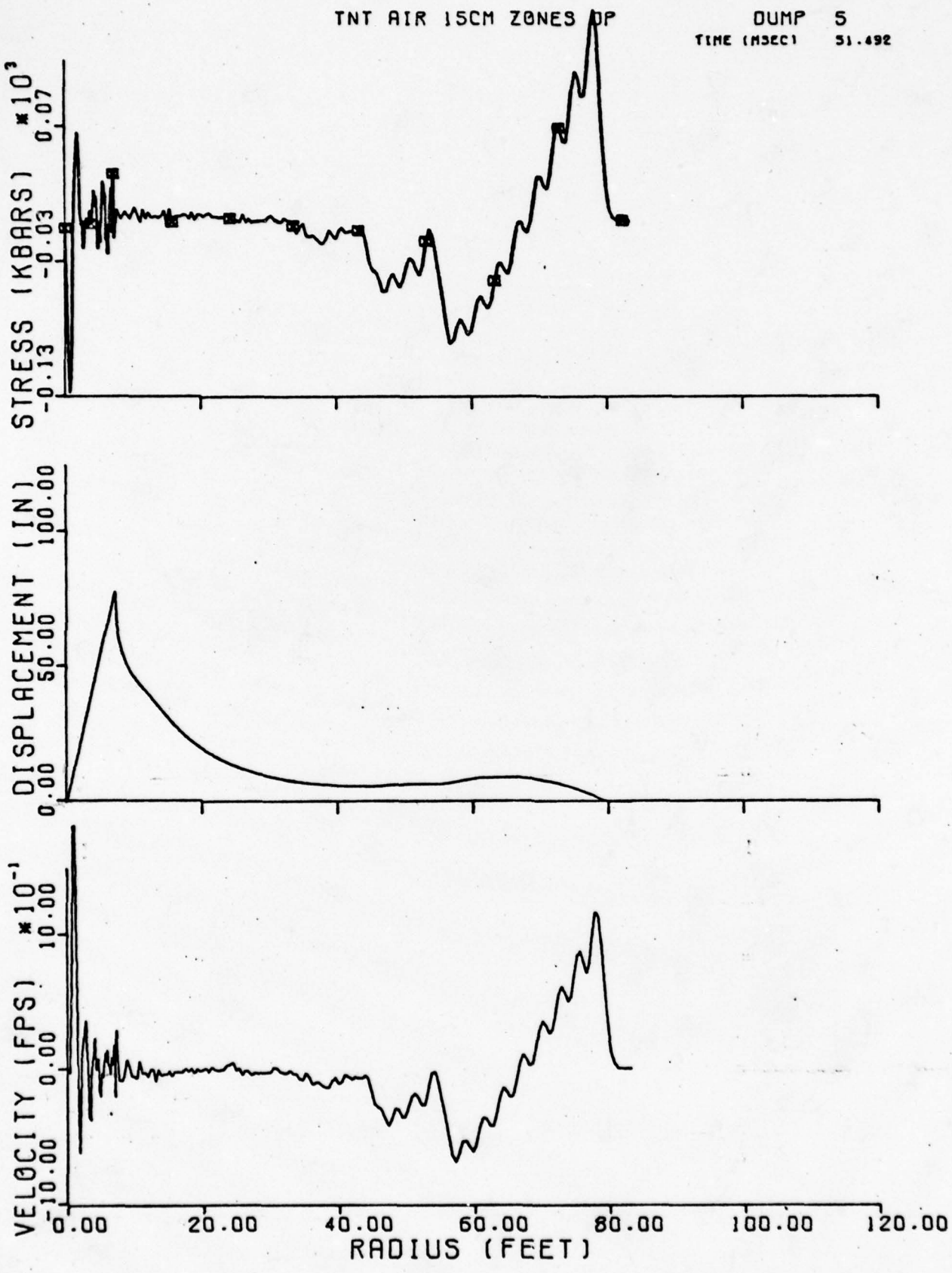
NL

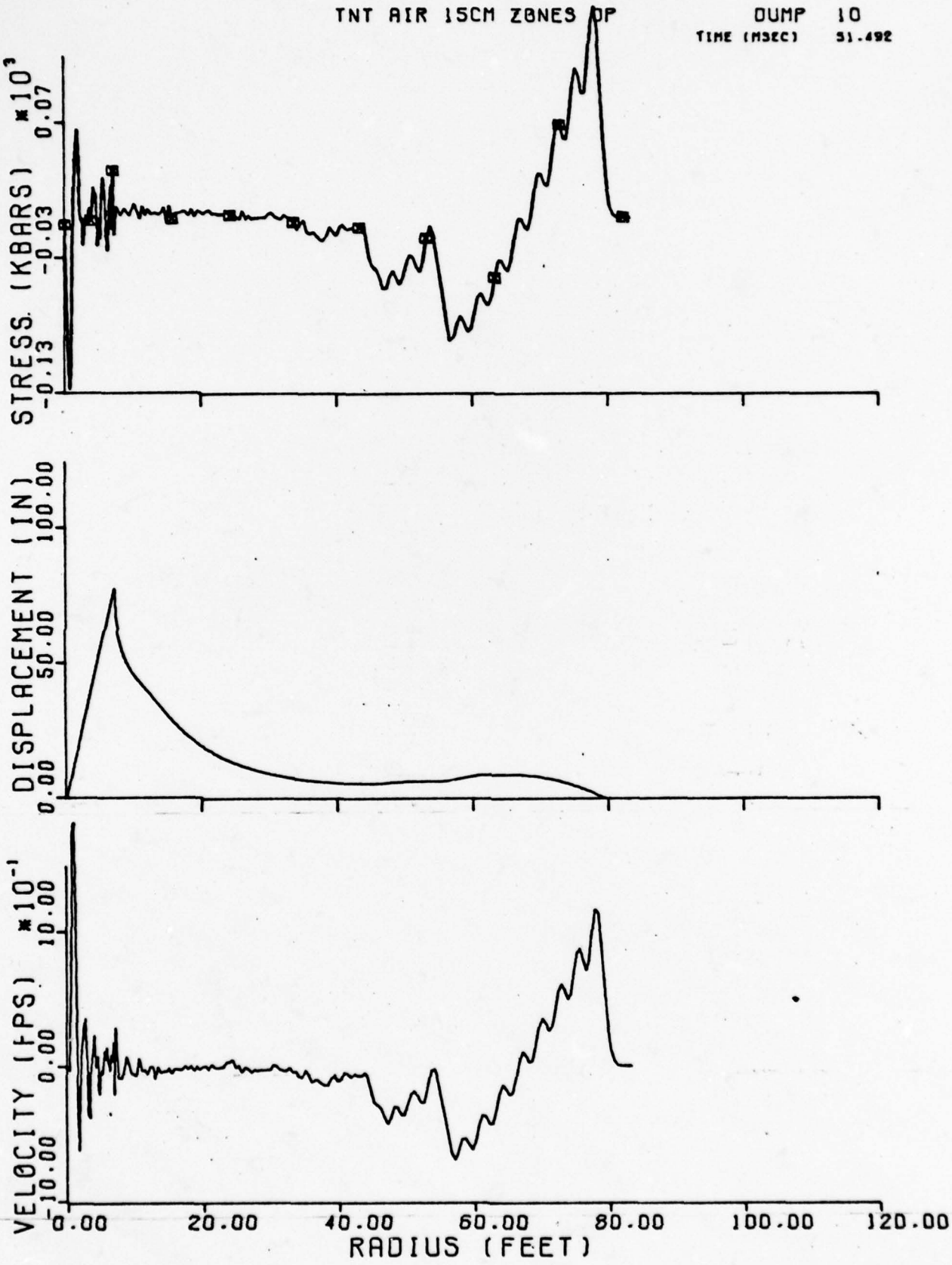
2 OF 3
AD
A055 436

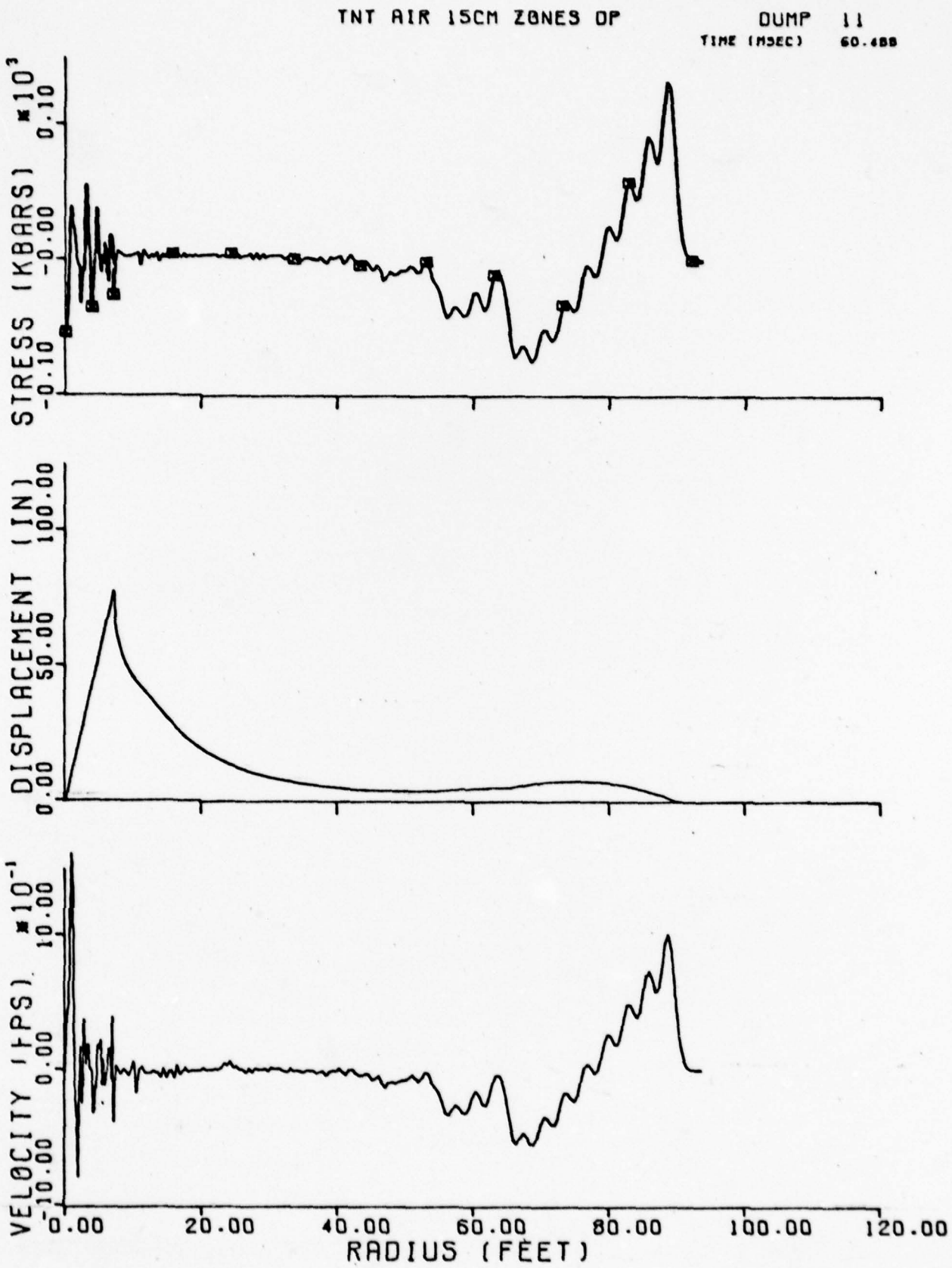


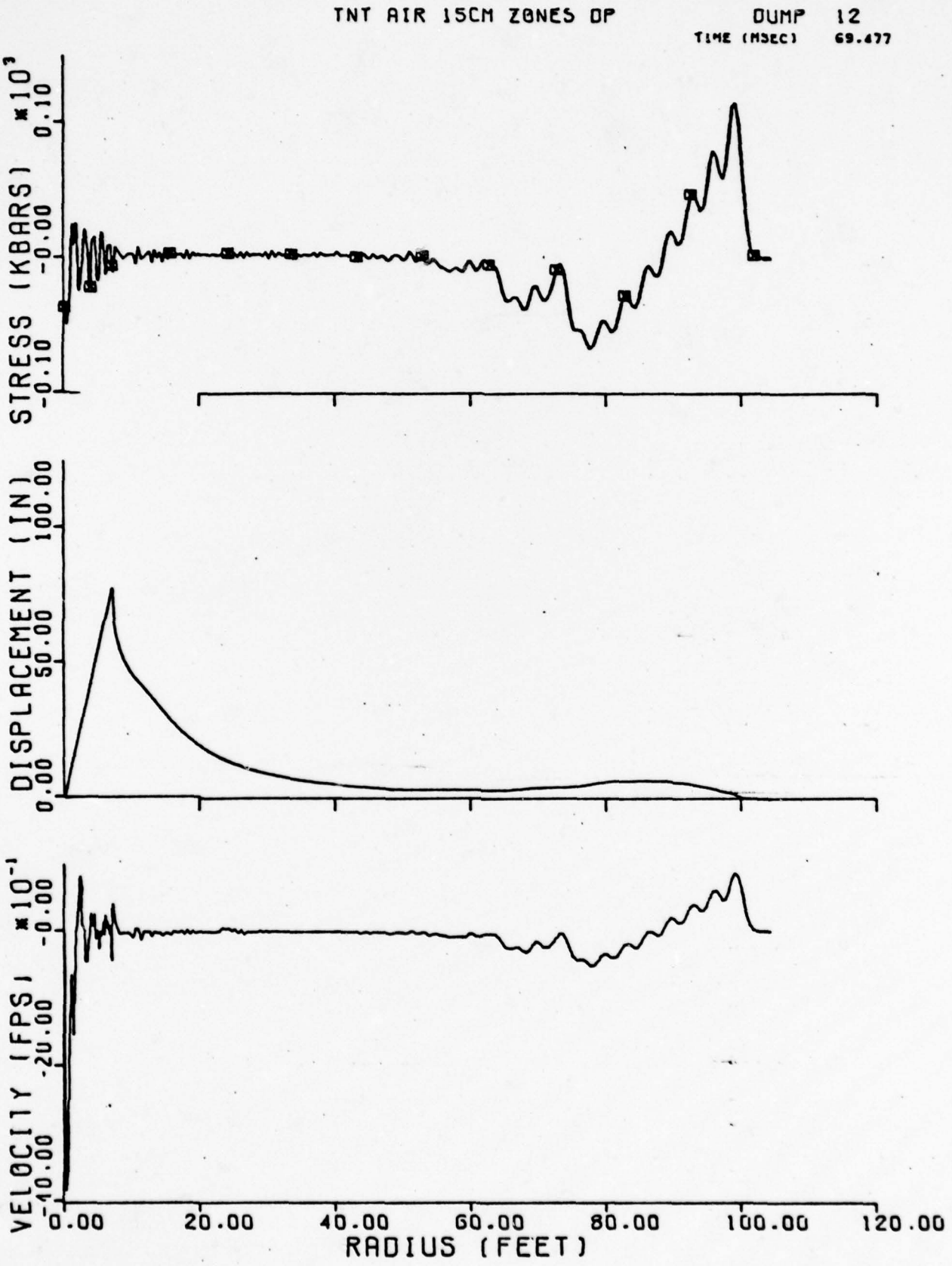

1.0
1.1
1.25
1.4
1.6
2.8
2.5
2.2
2.0
1.8
MICROCOPY RESOLUTION TEST CHART
NATIONAL BUREAU OF STANDARDS 1963-A

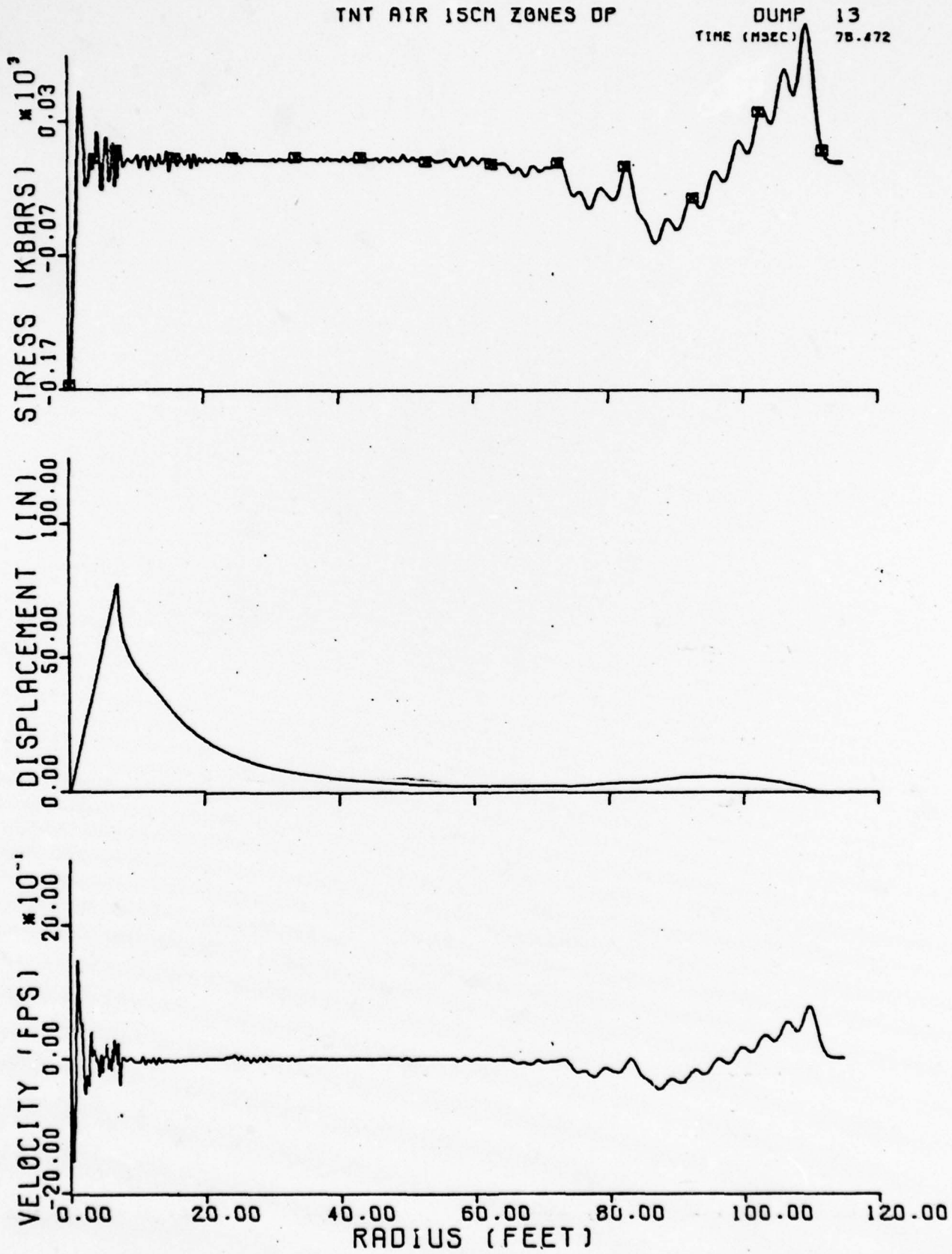

TNT AIR 15CM ZONES OP
DUMP 5
TIME (MSEC) 51.492
STRESS (KBARS) *10³
0.07
-0.03
-0.13
DISPLACEMENT (IN)
100.00
50.00
0.00
VELOCITY (FPS) *10⁻¹
10.00
0.00
-10.00
0.00
15.00
30.00
45.00
60.00
75.00
90.00
RADIUS (FEET)


TNT AIR 15CM ZONES OP
DUMP 5
TIME (MSEC) 51.492
STRESS (KBARS) *10³
0.07
-0.03
-0.13
DISPLACEMENT (IN)
100.00
50.00
0.00
VELOCITY (FPS) *10⁻¹
10.00
0.00
-10.00
0.00
20.00
40.00
60.00
80.00
100.00
120.00
RADIUS (FEET)


TNT AIR 15CM ZONES OP
DUMP 10
TIME (MSEC) 51.492
STRESS (KBARS) *10³
0.07
-0.03
-0.13
DISPLACEMENT (IN)
100.00
50.00
0.00
VELOCITY (FPS) *10⁻¹
10.00
0.00
-10.00
0.00
20.00
40.00
60.00
80.00
100.00
120.00
RADIUS (FEET)

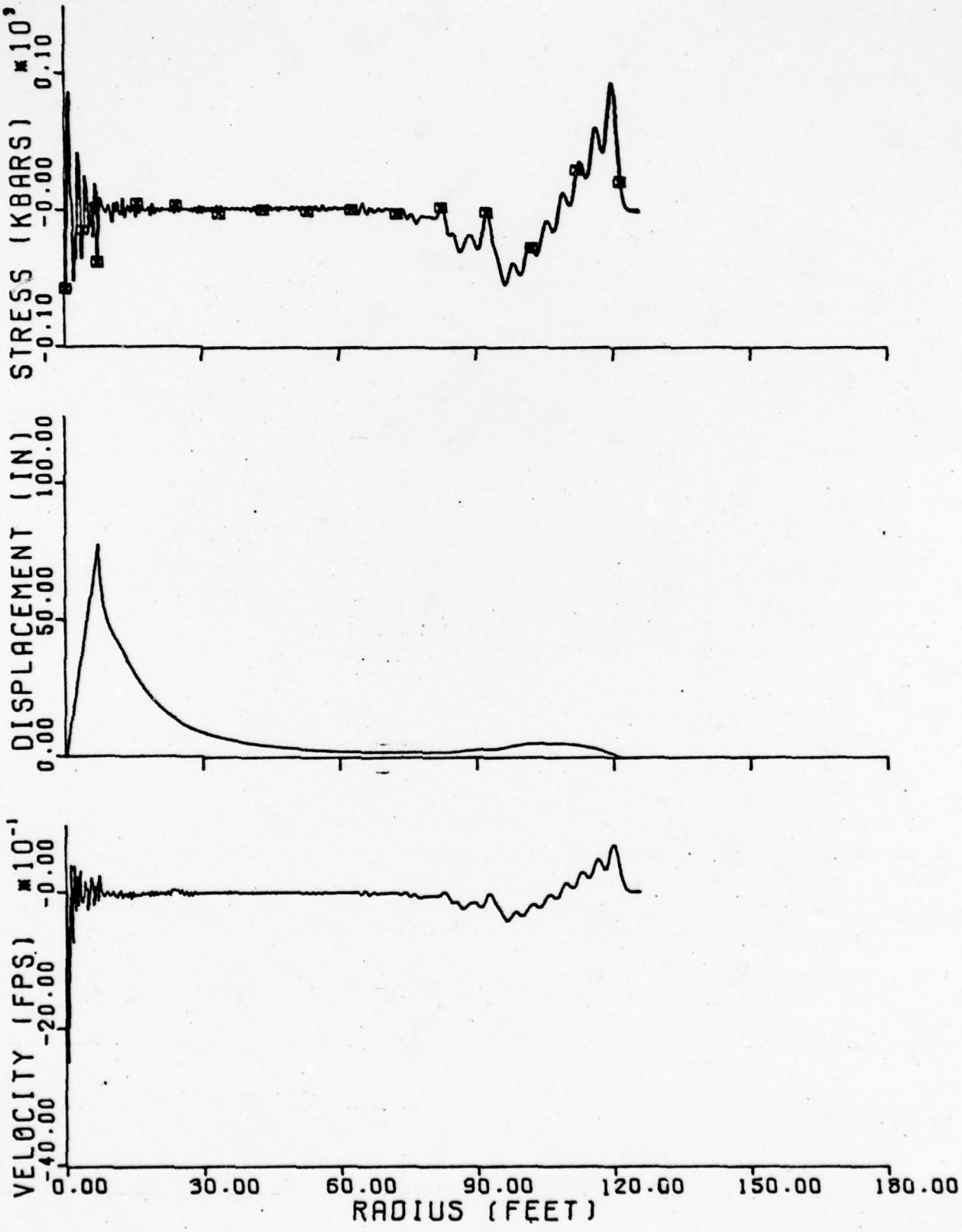

TNT AIR 15CM ZONES OP
DUMP 11
TIME (MSEC) 60.488
STRESS (KBARS) *10³
0.10
-0.00
-0.10
DISPLACEMENT (IN)
100.00
50.00
0.00
VELOCITY (IPS) *10⁻¹
10.00
0.00
-10.00
0.00
20.00
40.00
60.00
80.00
100.00
120.00
RADIUS (FEET)

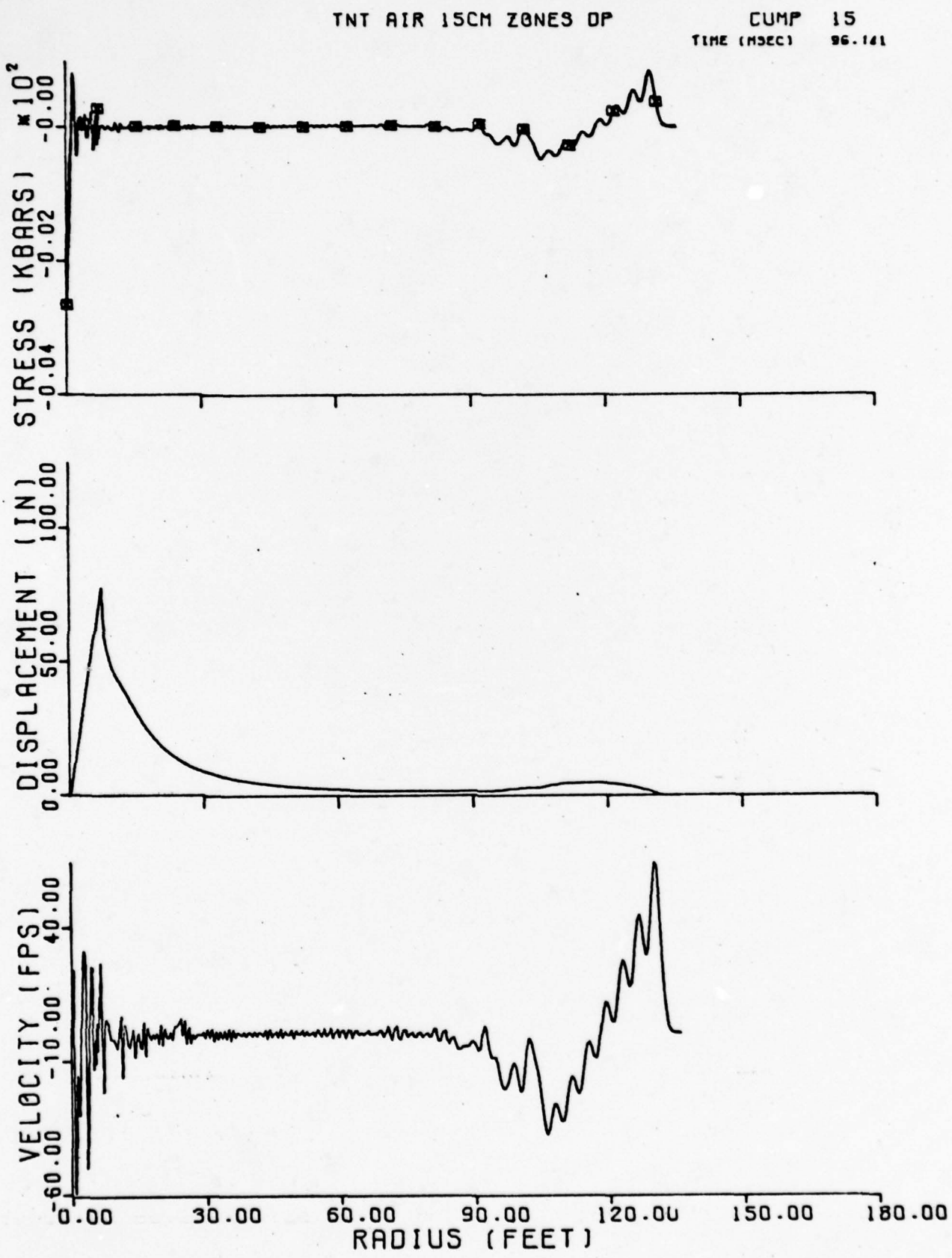

TNT AIR 15CM ZONES OP
DUMP 12
TIME (MSEC) 69.477
STRESS (KBARS) *10³
0.10
-0.00
-0.10
DISPLACEMENT (IN)
100.00
50.00
0.00
VELOCITY (FPS) *10⁻¹
-0.00
-20.00
-40.00
0.00
20.00
40.00
60.00
80.00
100.00
120.00
RADIUS (FEET)


TNT AIR 15CM ZONES DP
DUMP 13
TIME (MSEC) 78.472
STRESS (KBARS) *10³
0.03
-0.07
-0.17
DISPLACEMENT (IN)
100.00
50.00
0.00
VELOCITY (FPS) *10⁻¹
20.00
0.00
-20.00
0.00
20.00
40.00
60.00
80.00
100.00
120.00
RADIUS (FEET)

TNT AIR 15CM ZONES OP CUMP 14

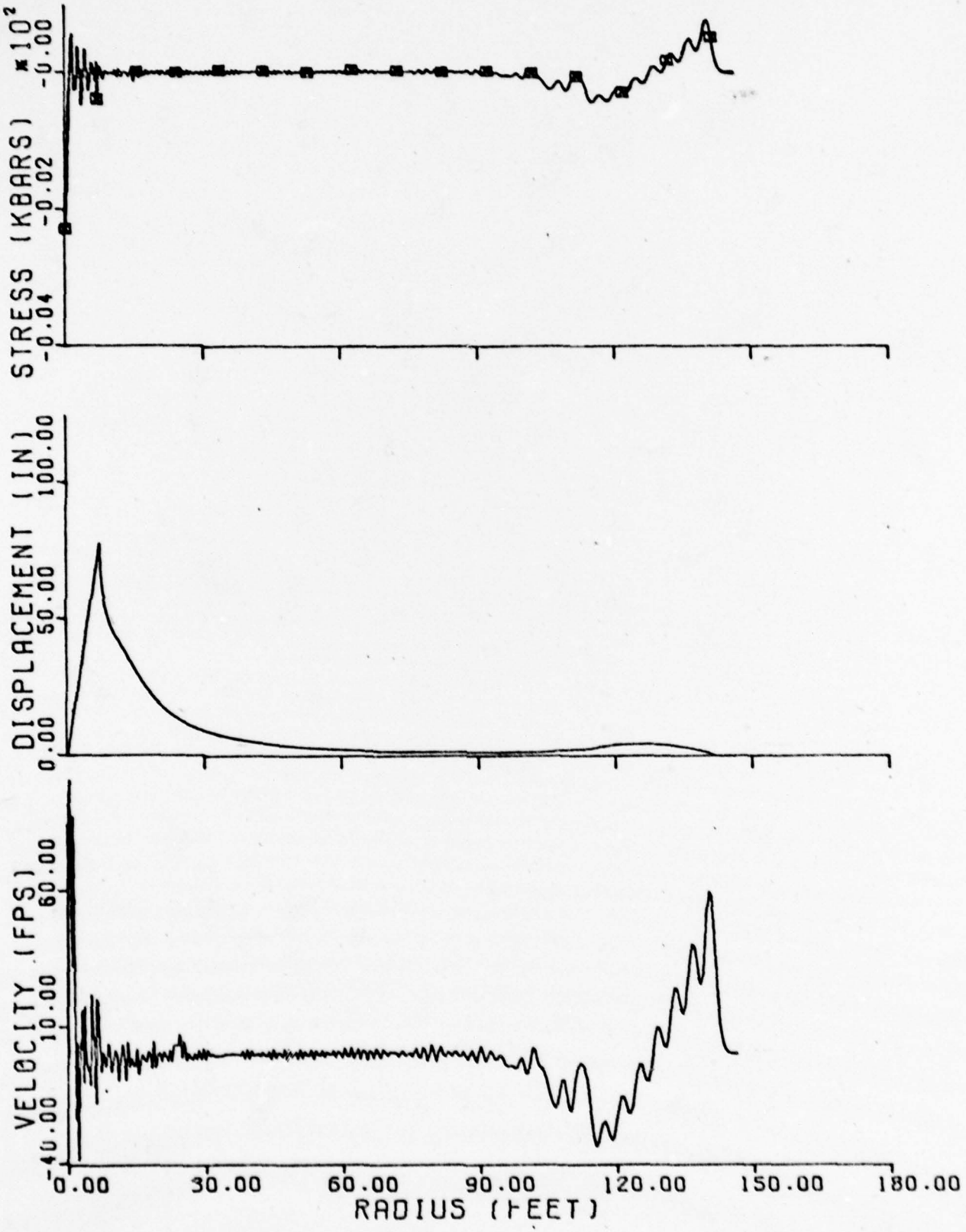
TIME (MSEC) 87.457




TNT AIR 15CM ZONES DP
CUMP 15
TIME (MSEC) 96.141
STRESS (KBARS) *10²
-0.00
-0.02
-0.04
DISPLACEMENT (IN)
100.00
50.00
0.00
VELOCITY (FPS)
40.00
-10.00
-60.00
0.00
30.00
60.00
90.00
120.00
150.00
180.00
RADIUS (FEET)

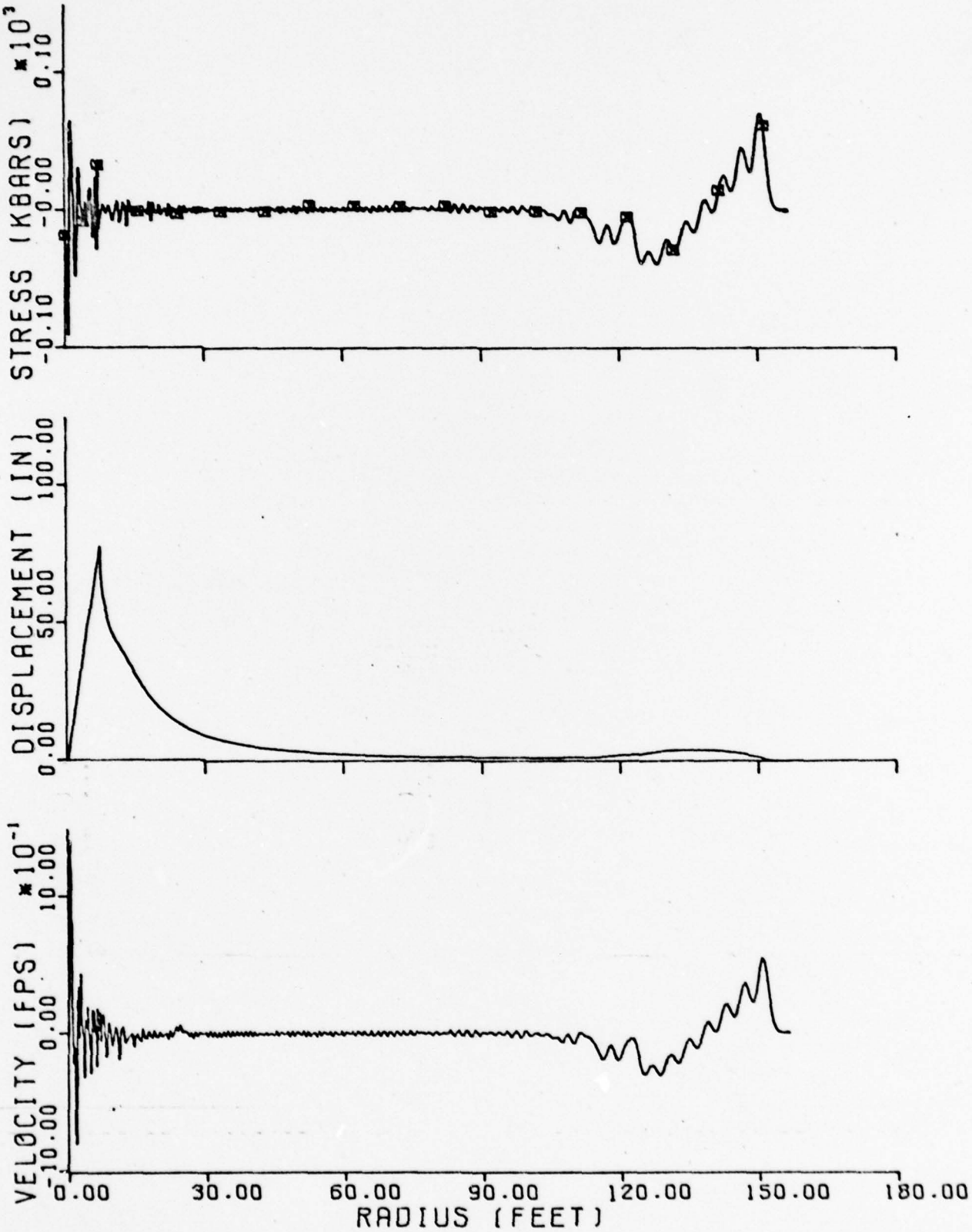
TNT AIR 15CM ZONES DP DUMP 16

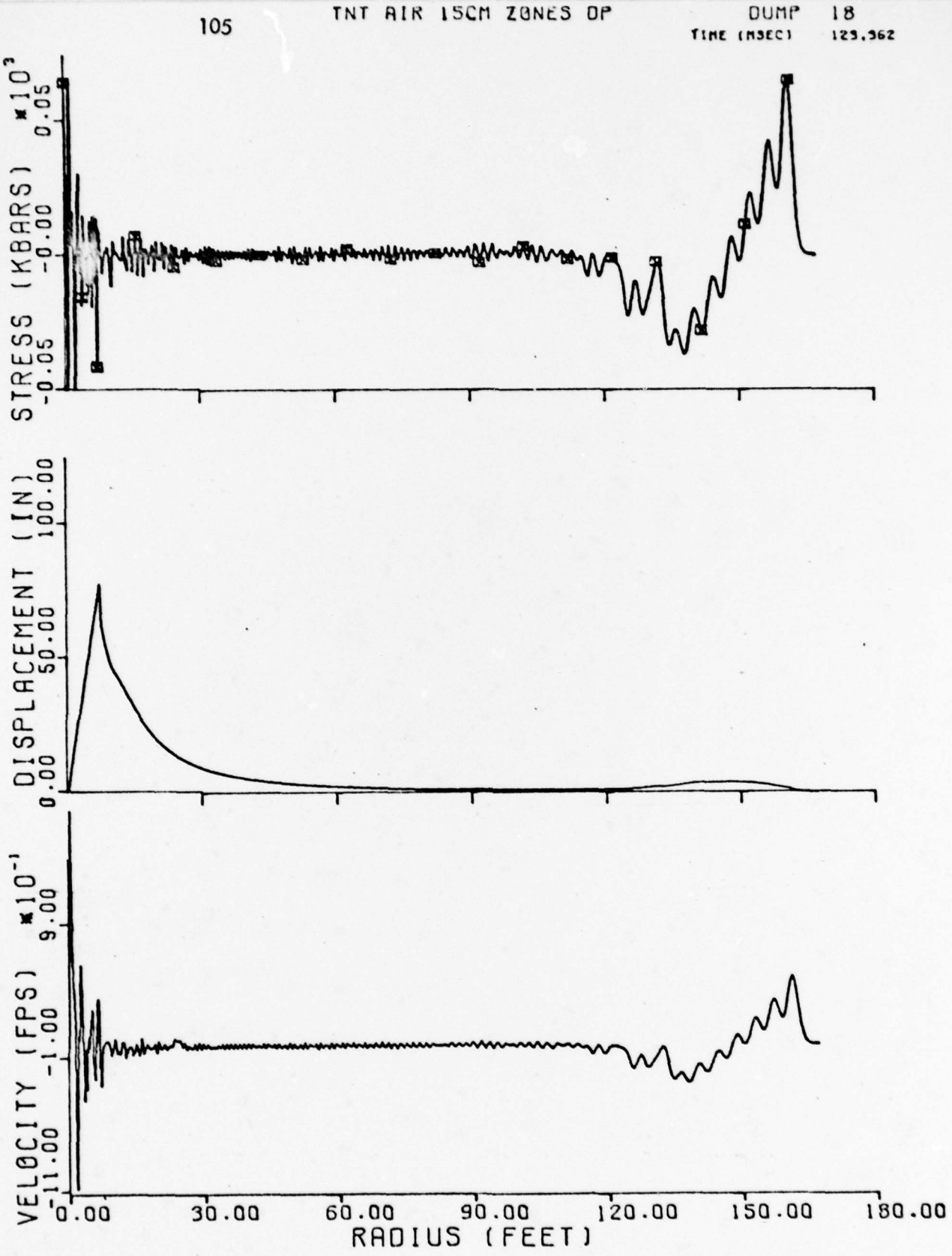
TIME (MSEC) 105.420

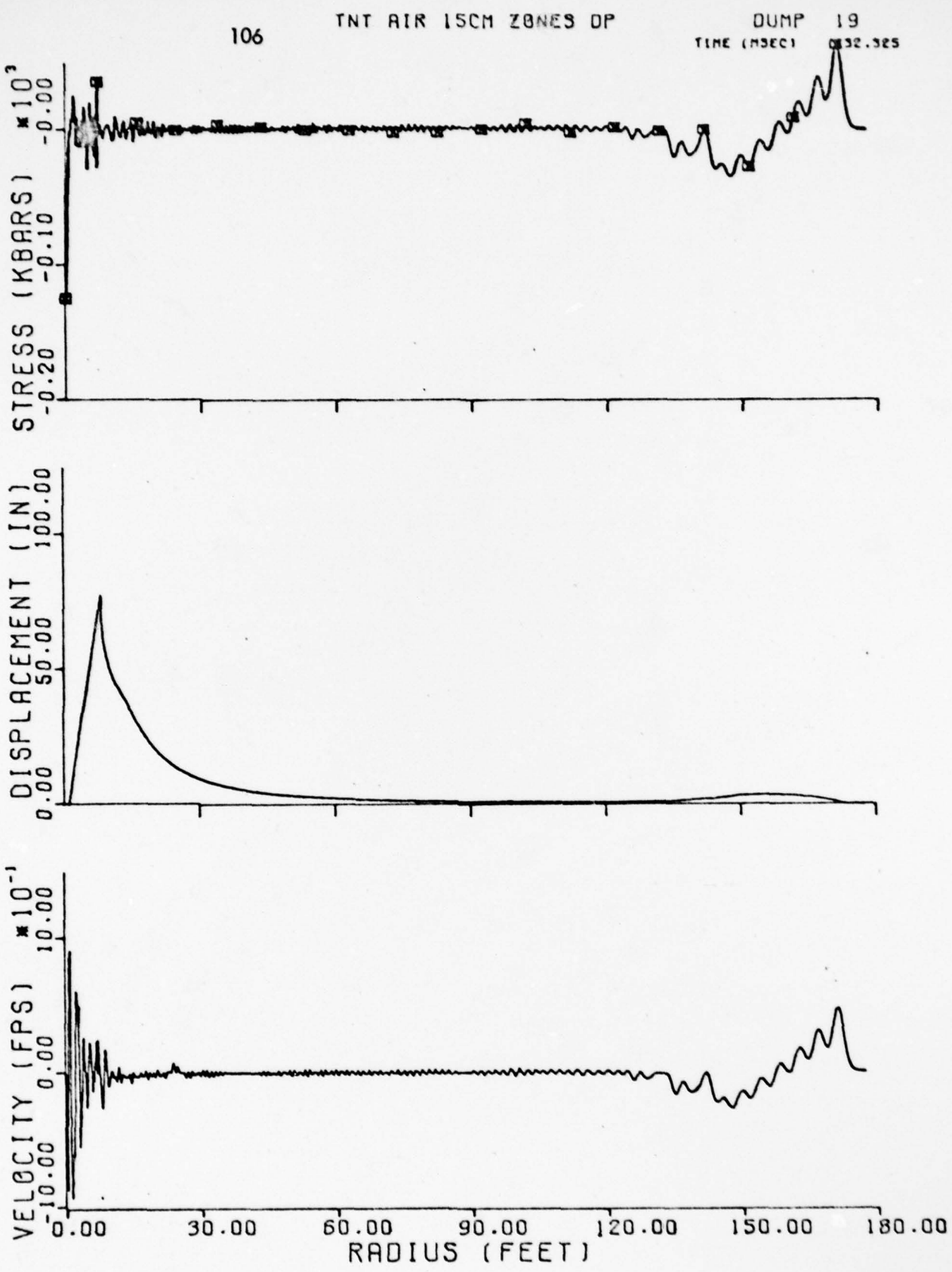


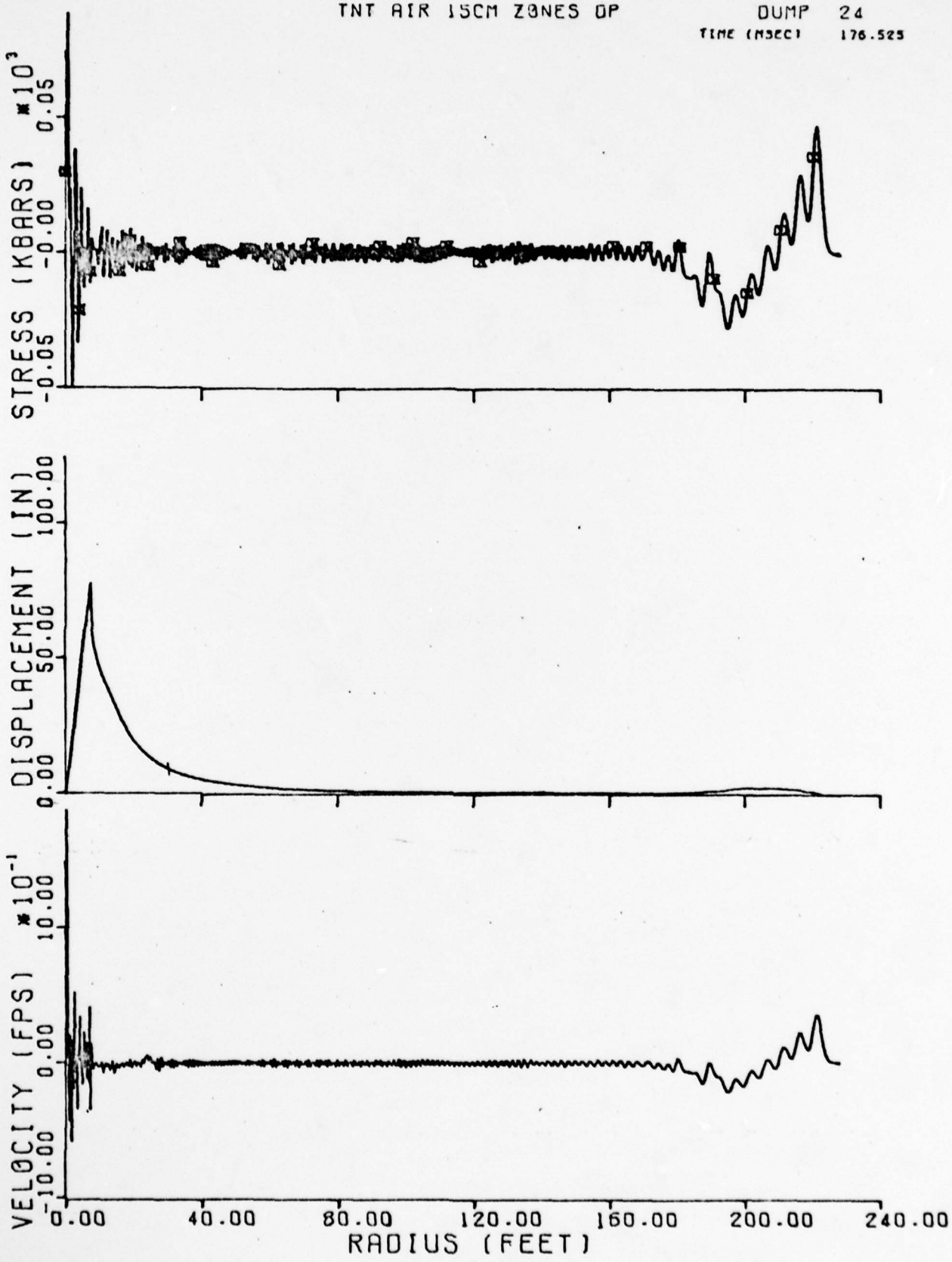
TNT AIR 15CM ZONES OP DUMP 17

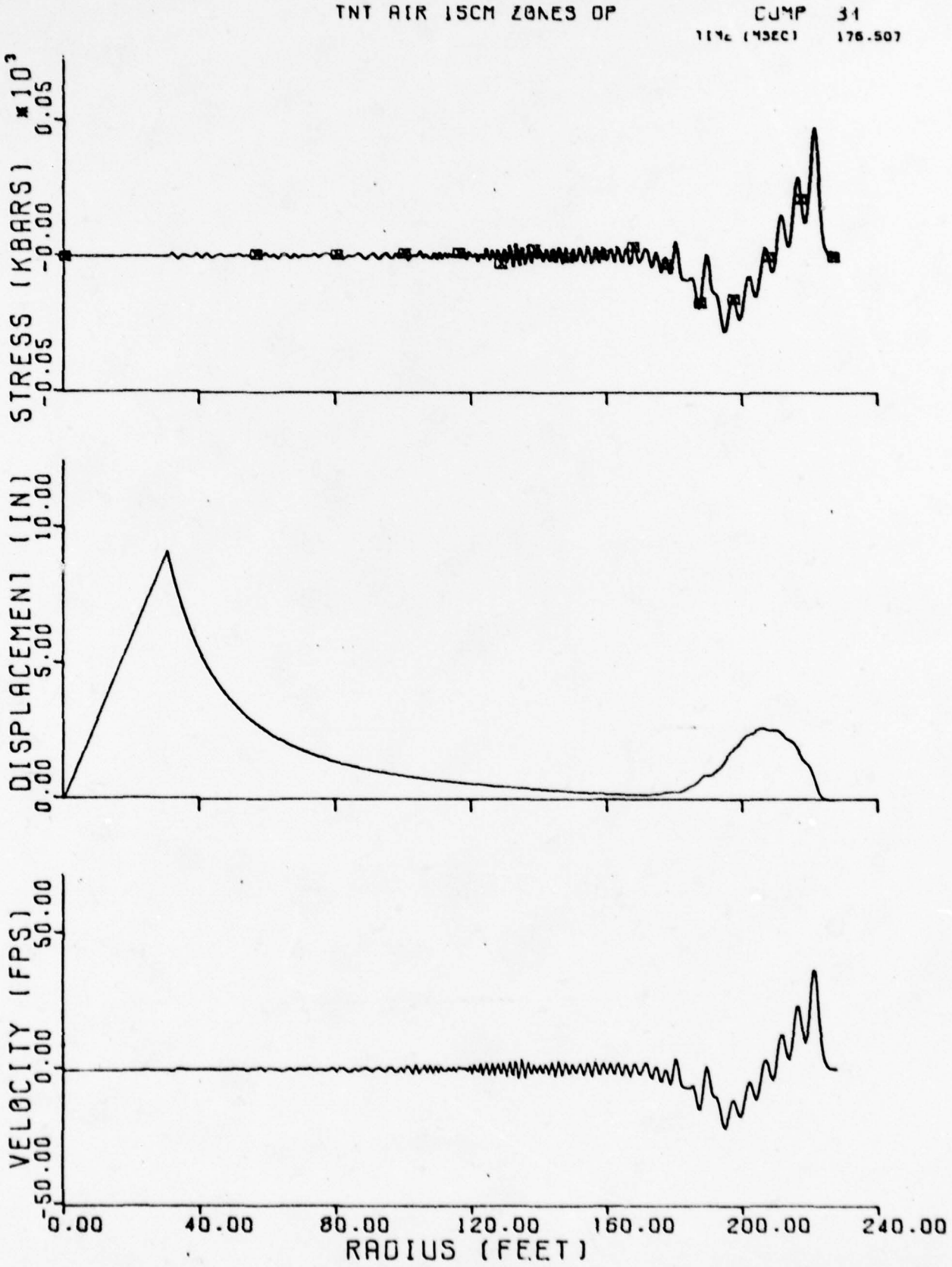
TIME (MSEC) 114.393

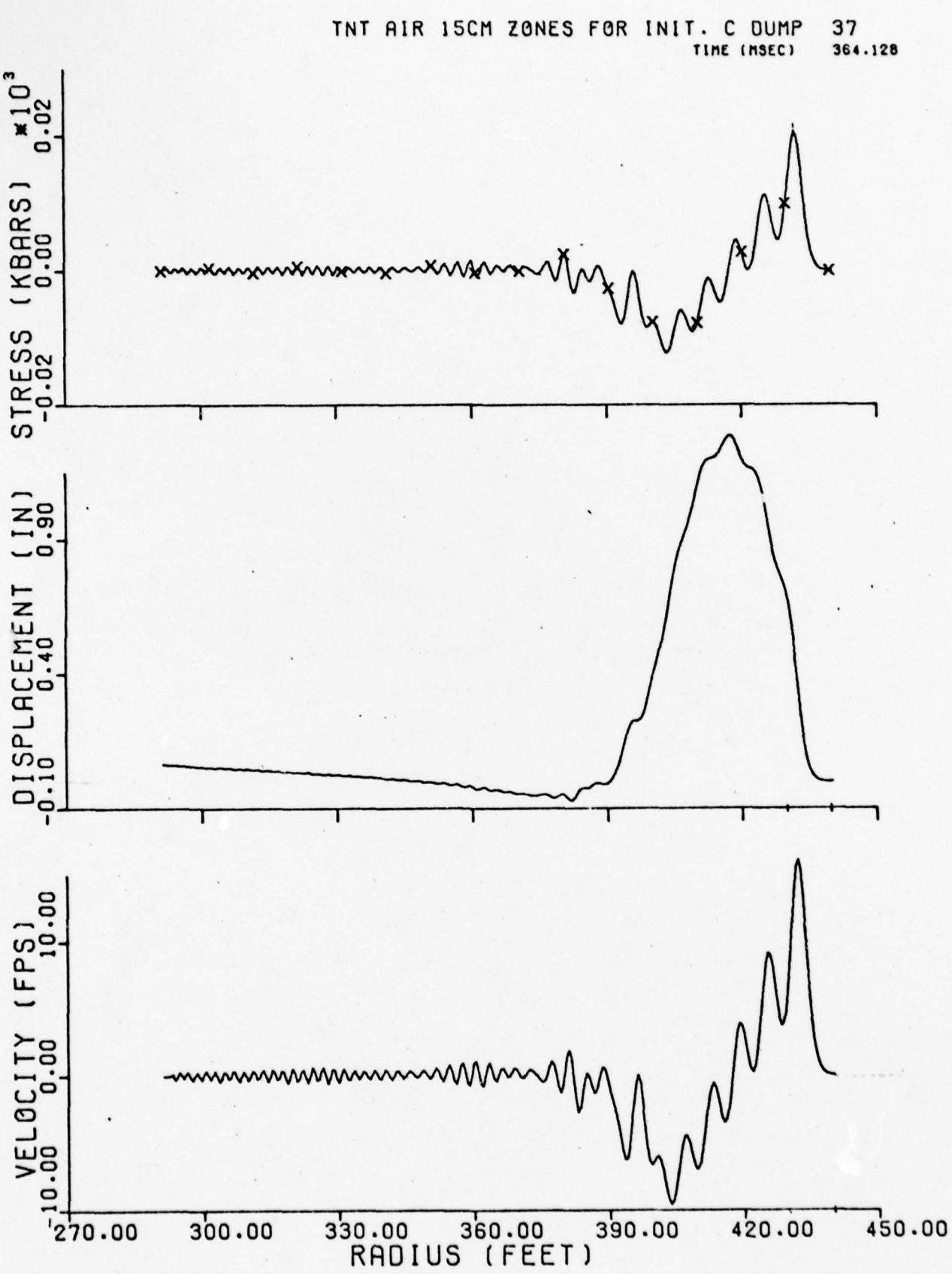


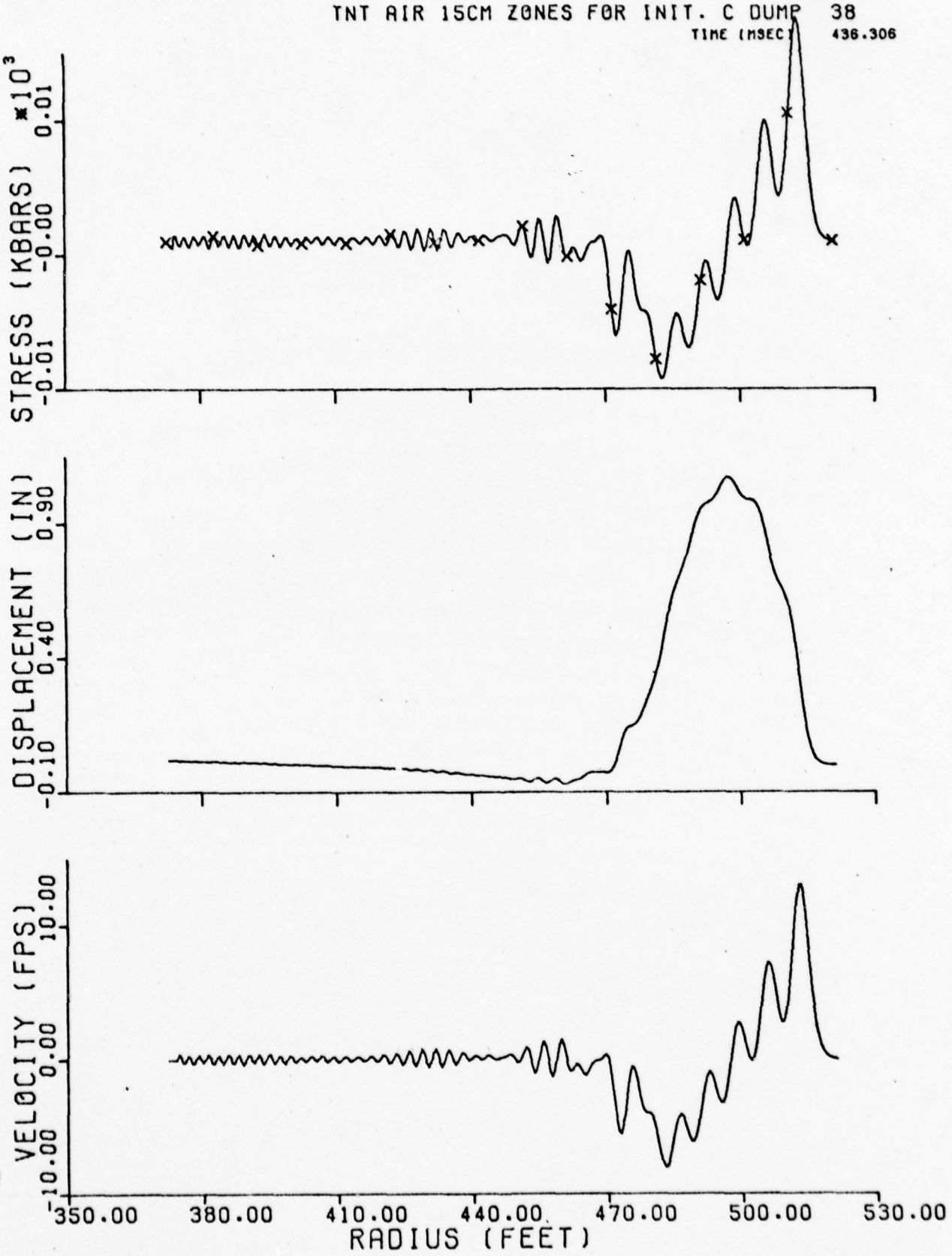

TNT AIR 15CM ZONES OP
DUMP 18
TIME (MSEC) 123.562
STRESS (KBARS) *10^3
0.05
-0.00
-0.05
DISPLACEMENT (IN)
100.00
50.00
0.00
VELOCITY (FPS) *10^-1
9.00
-1.00
-11.00
0.00
30.00
60.00
90.00
120.00
150.00
180.00
RADIUS (FEET)

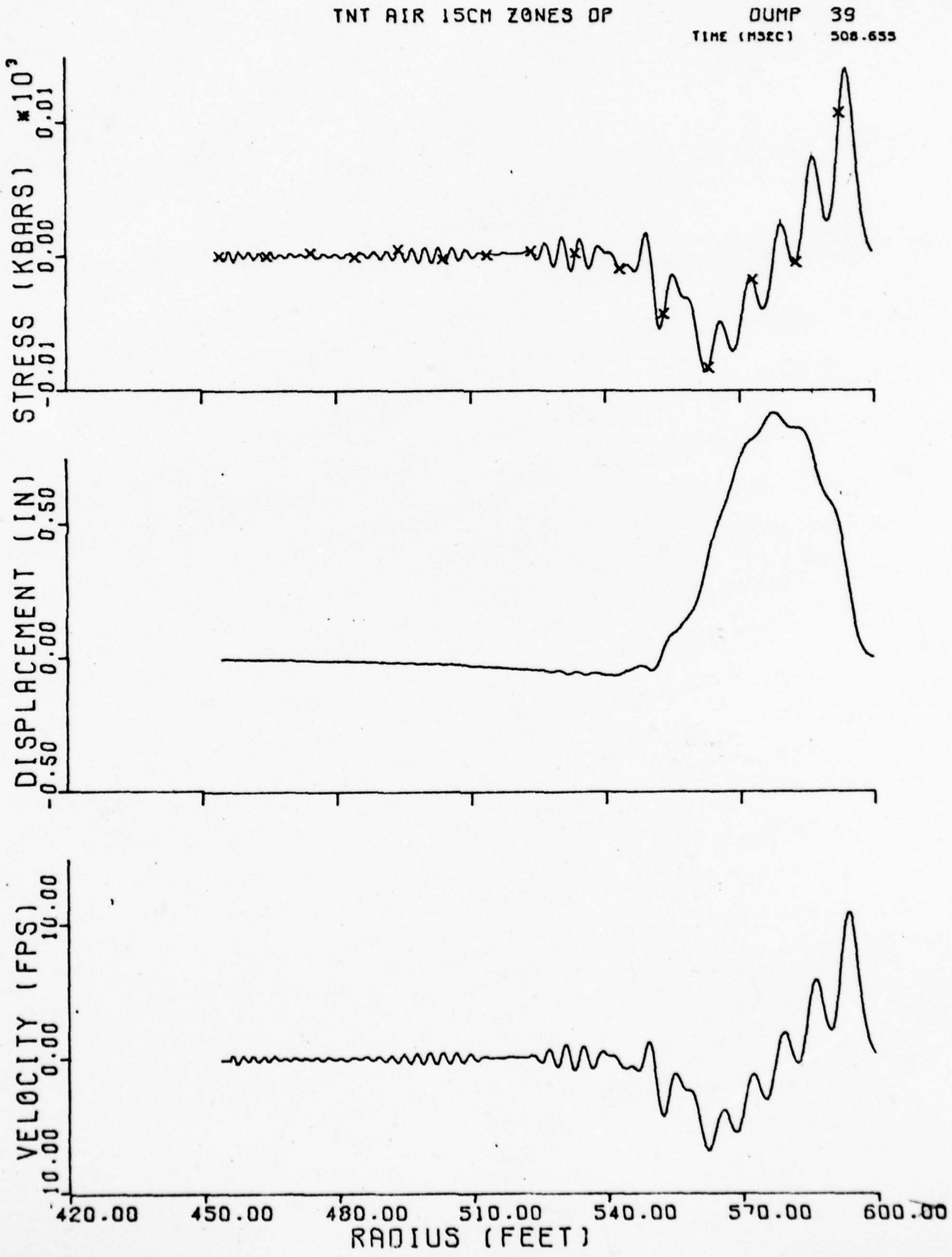

TNT AIR 15CM ZONES DP
DUMP 19
TIME (MSEC) 32.325
STRESS (KBARS) *10^3
-0.00
-0.10
-0.20
DISPLACEMENT (IN)
0.00
50.00
100.00
VELOCITY (FPS) *10^-1
10.00
0.00
-10.00
0.00
30.00
60.00
90.00
120.00
150.00
180.00
RADIUS (FEET)

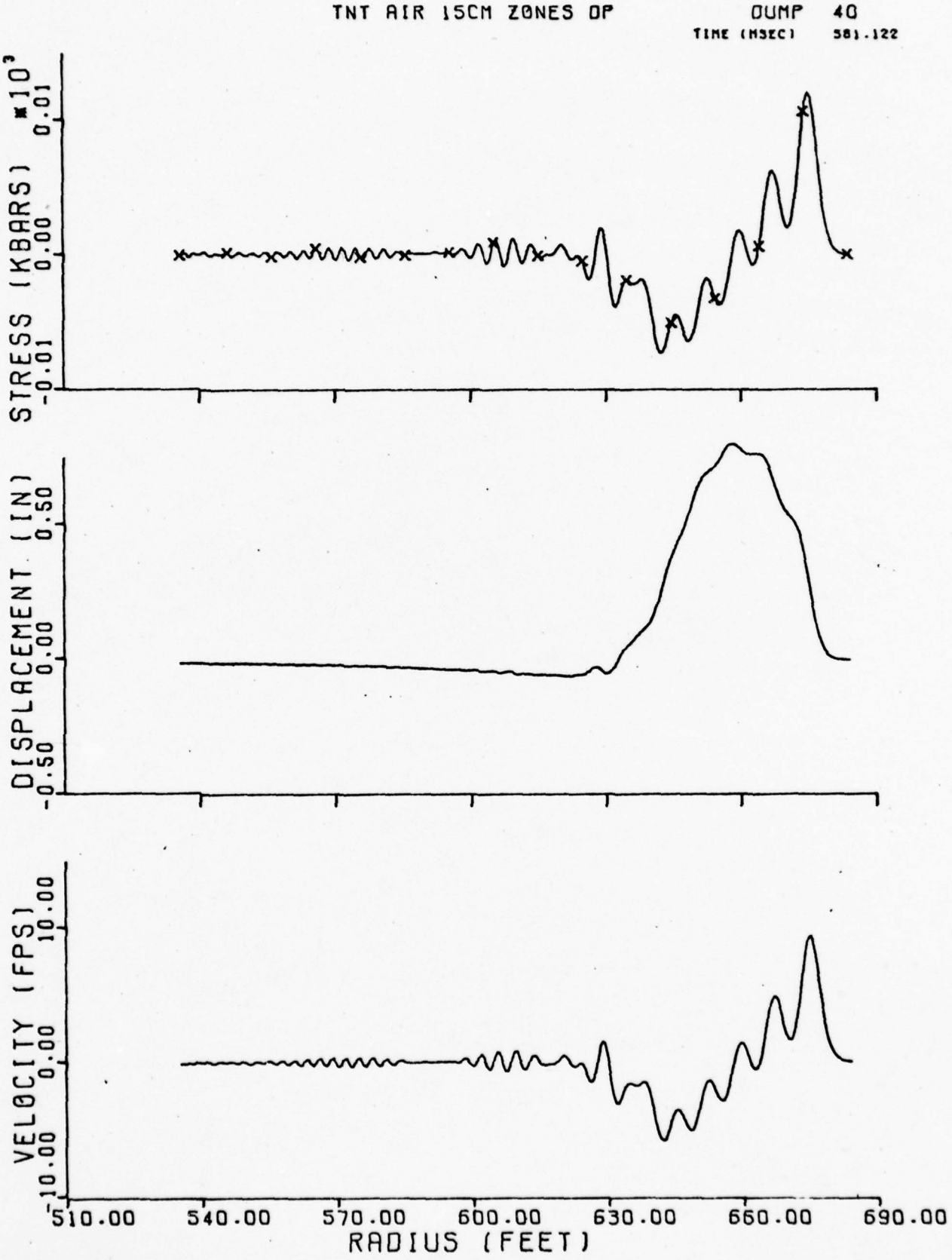

TNT AIR 15CM ZONES OP
DUMP 24
TIME (MSEC) 176.525
STRESS (KBARS) *10³
0.05
-0.00
-0.05
DISPLACEMENT (IN)
100.00
50.00
0.00
VELOCITY (FPS) *10⁻¹
10.00
0.00
-10.00
0.00
40.00
80.00
120.00
160.00
200.00
240.00
RADIUS (FEET)

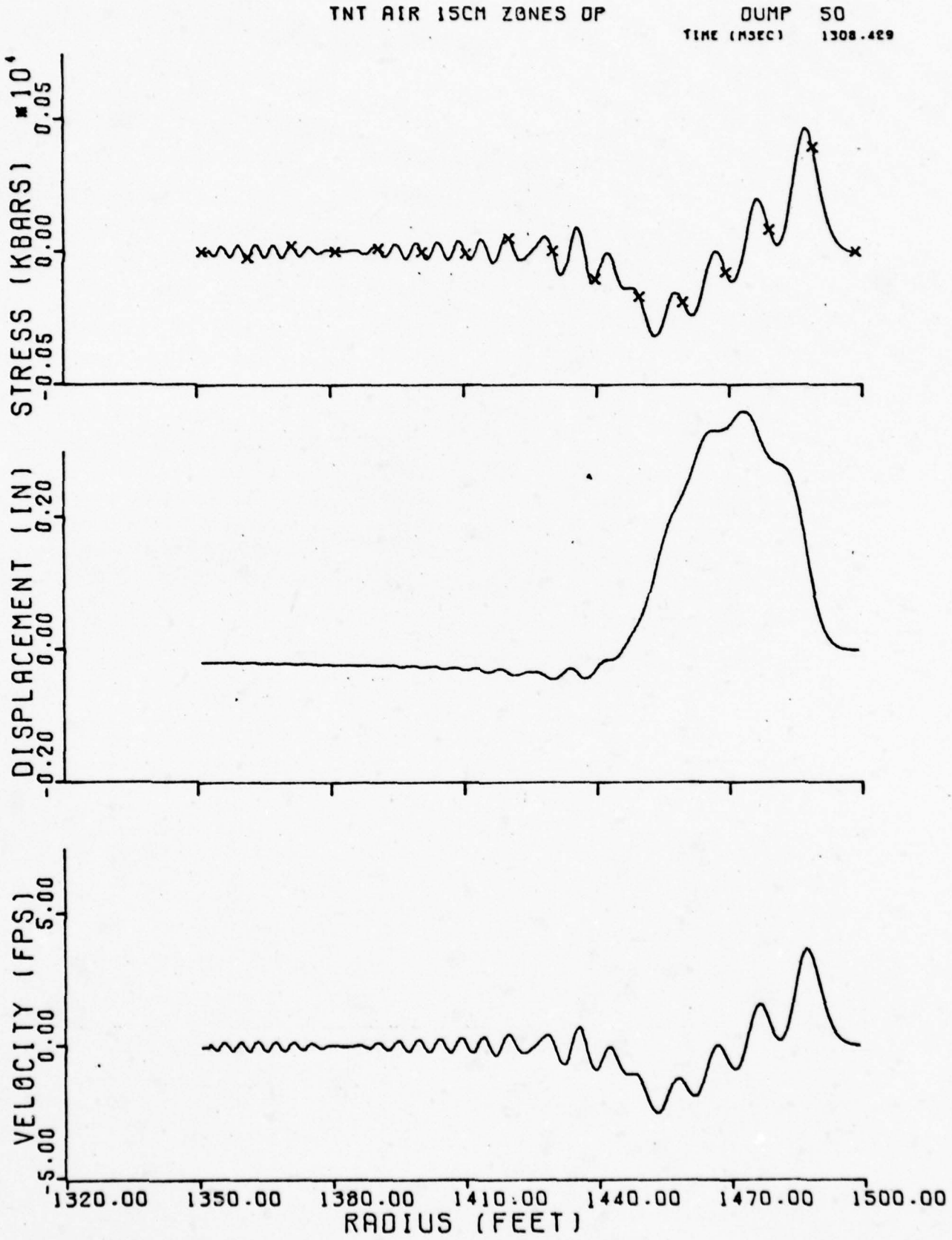

TNT AIR 15CM ZONES OP
CUMP 31
TIME (MSEC) 176.507
STRESS (KBARS) *10³
0.05
-0.00
-0.05
DISPLACEMENT (IN)
10.00
5.00
0.00
VELOCITY (FPS)
50.00
0.00
-50.00
0.00
40.00
80.00
120.00
160.00
200.00
240.00
RADIUS (FEET)

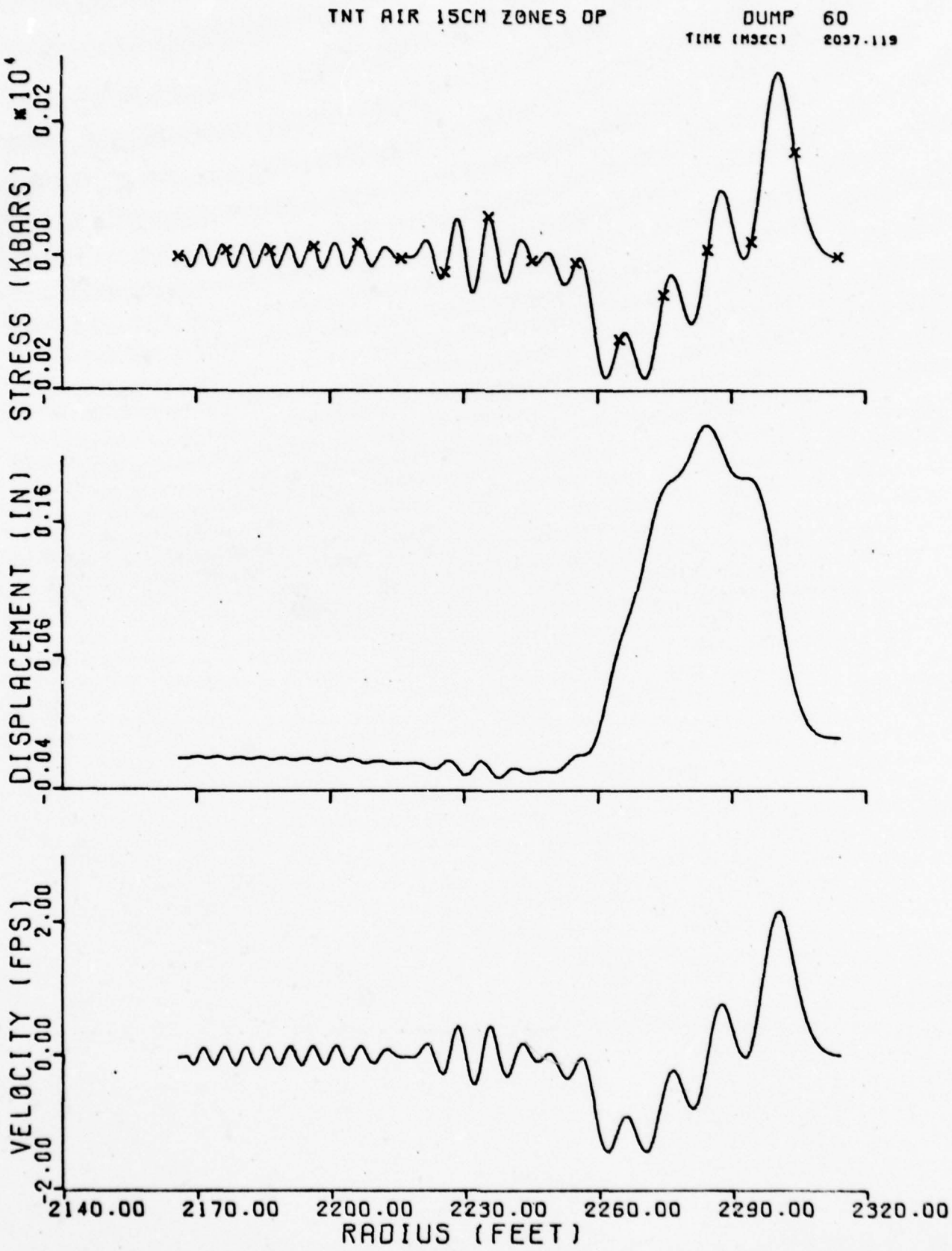

TNT AIR 15CM ZONES FOR INIT. C DUMP 37
TIME (MSEC) 364.128
STRESS (KBARS) *10³
0.02
0.00
-0.02
DISPLACEMENT (IN)
0.90
0.40
-0.10
VELOCITY (FPS)
10.00
0.00
-10.00
270.00
300.00
330.00
360.00
390.00
420.00
450.00
RADIUS (FEET)

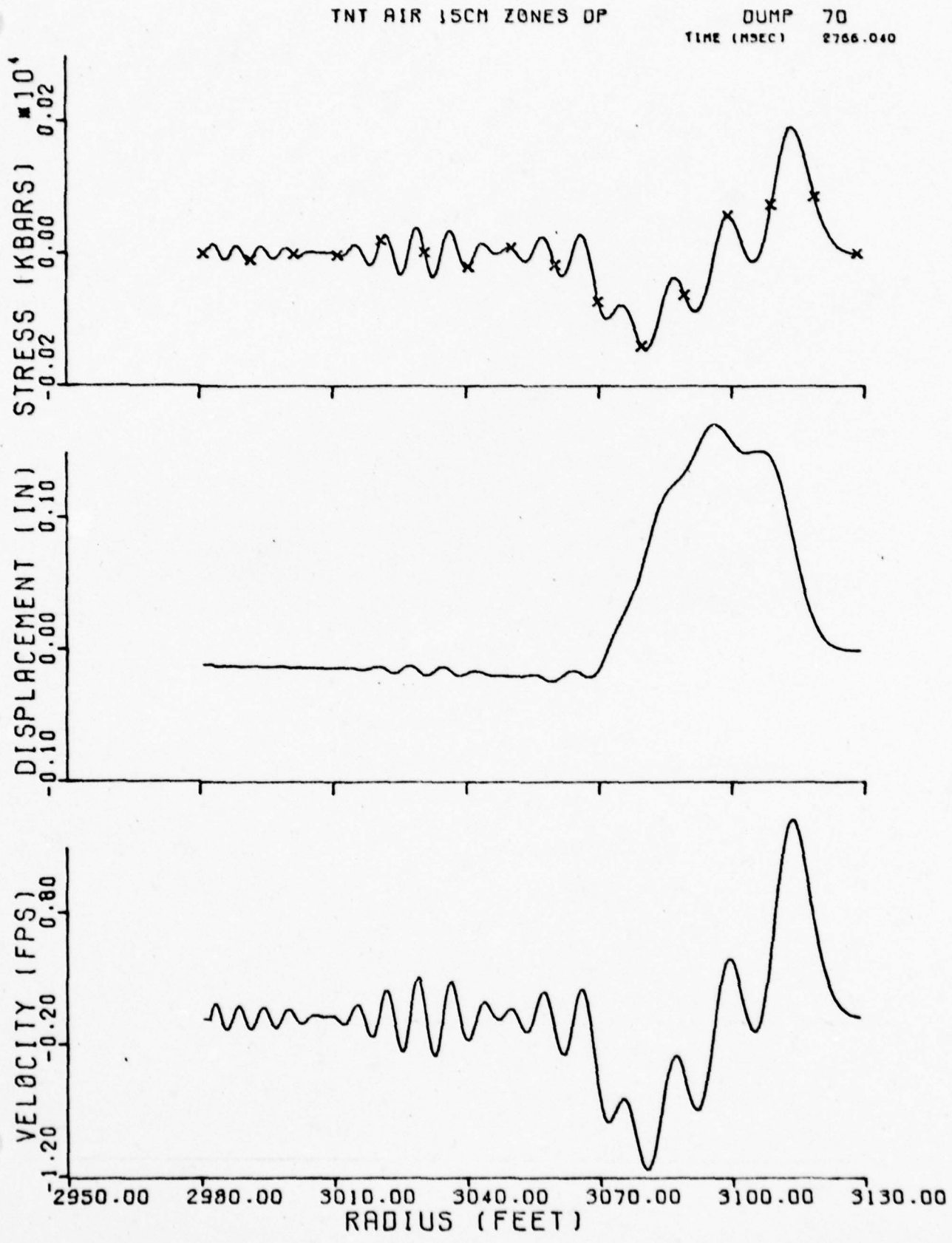

TNT AIR 15CM ZONES FOR INIT. C DUMP 38
TIME (MSEC) 436.306
STRESS (KBARS) *10^3
0.01
-0.00
-0.01
DISPLACEMENT (IN)
0.90
0.40
-0.10
VELOCITY (FPS)
10.00
0.00
-10.00
350.00
380.00
410.00
440.00
470.00
500.00
530.00
RADIUS (FEET)

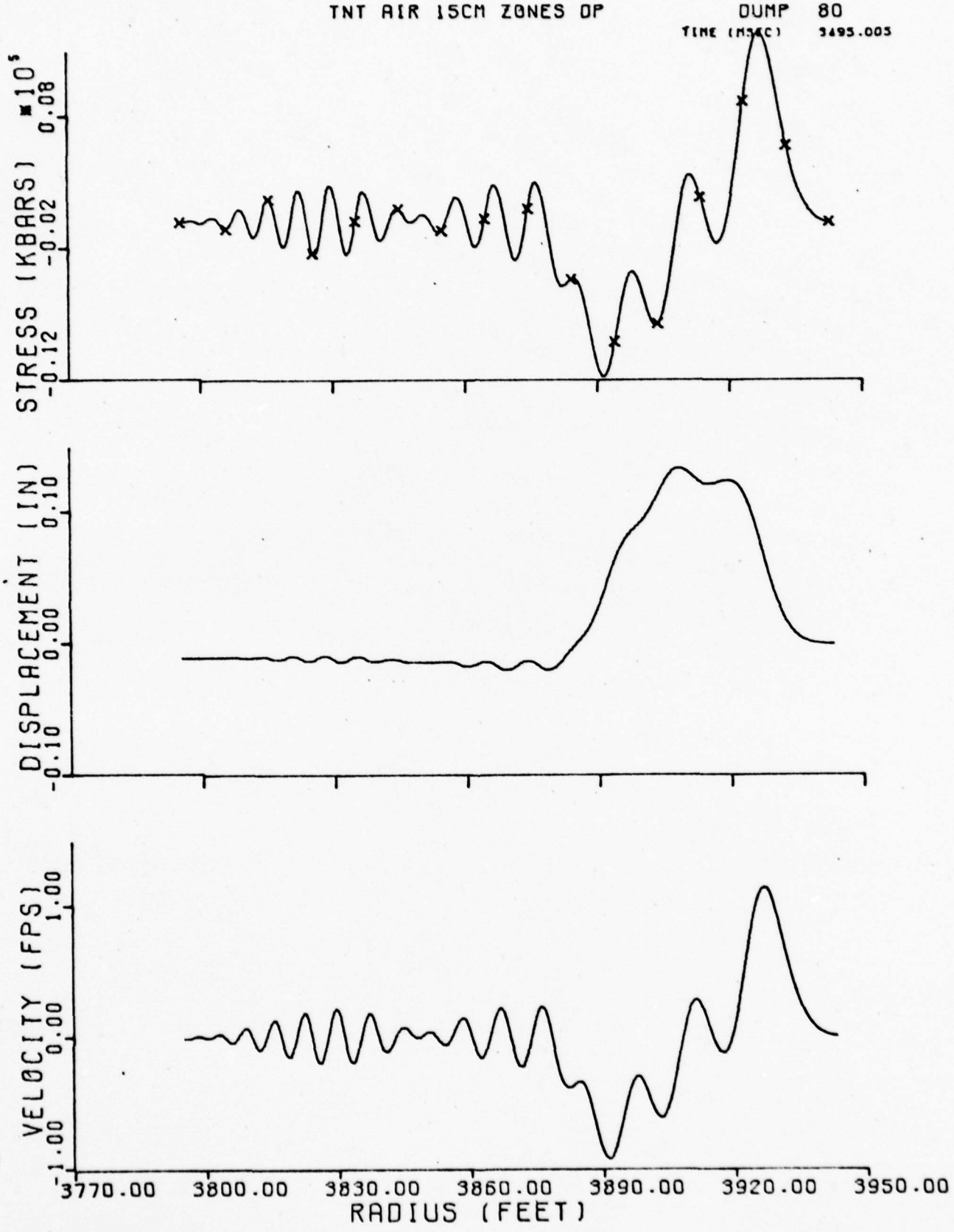

TNT AIR 15CM ZONES OP
DUMP 39
TIME (MSEC) 508.655
STRESS (KBARS) *10³
0.01
0.00
-0.01
DISPLACEMENT (IN)
0.50
0.00
-0.50
VELOCITY (FPS)
10.00
0.00
-10.00
420.00
450.00
480.00
510.00
540.00
570.00
600.00
RADIUS (FEET)

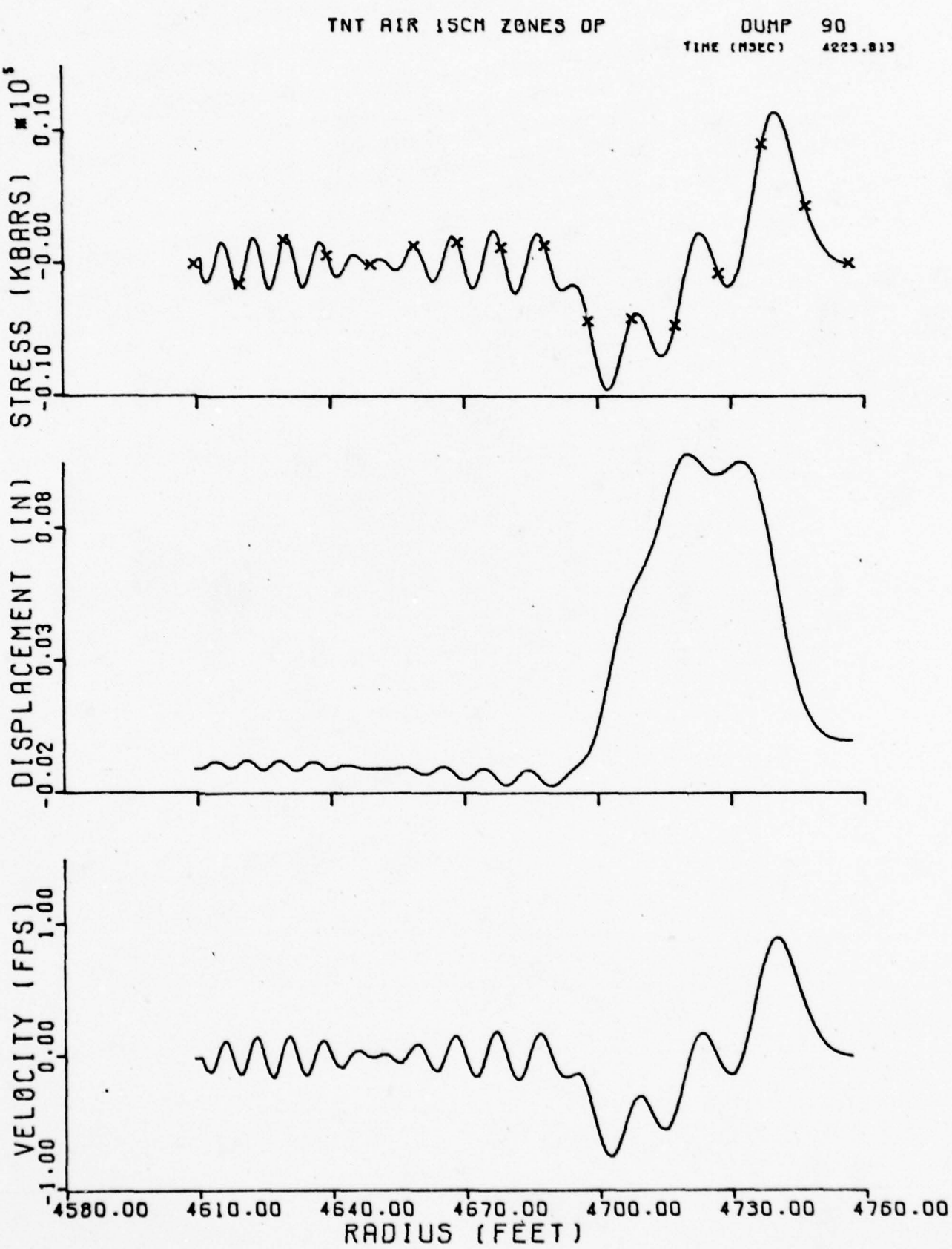

TNT AIR 15CM ZONES OP
DUMP 40
TIME (MSEC) 581.122
STRESS (KBARS) *10³
0.01
0.00
-0.01
DISPLACEMENT (IN)
0.50
0.00
-0.50
VELOCITY (FPS)
10.00
0.00
-10.00
510.00
540.00
570.00
600.00
630.00
660.00
690.00
RADIUS (FEET)

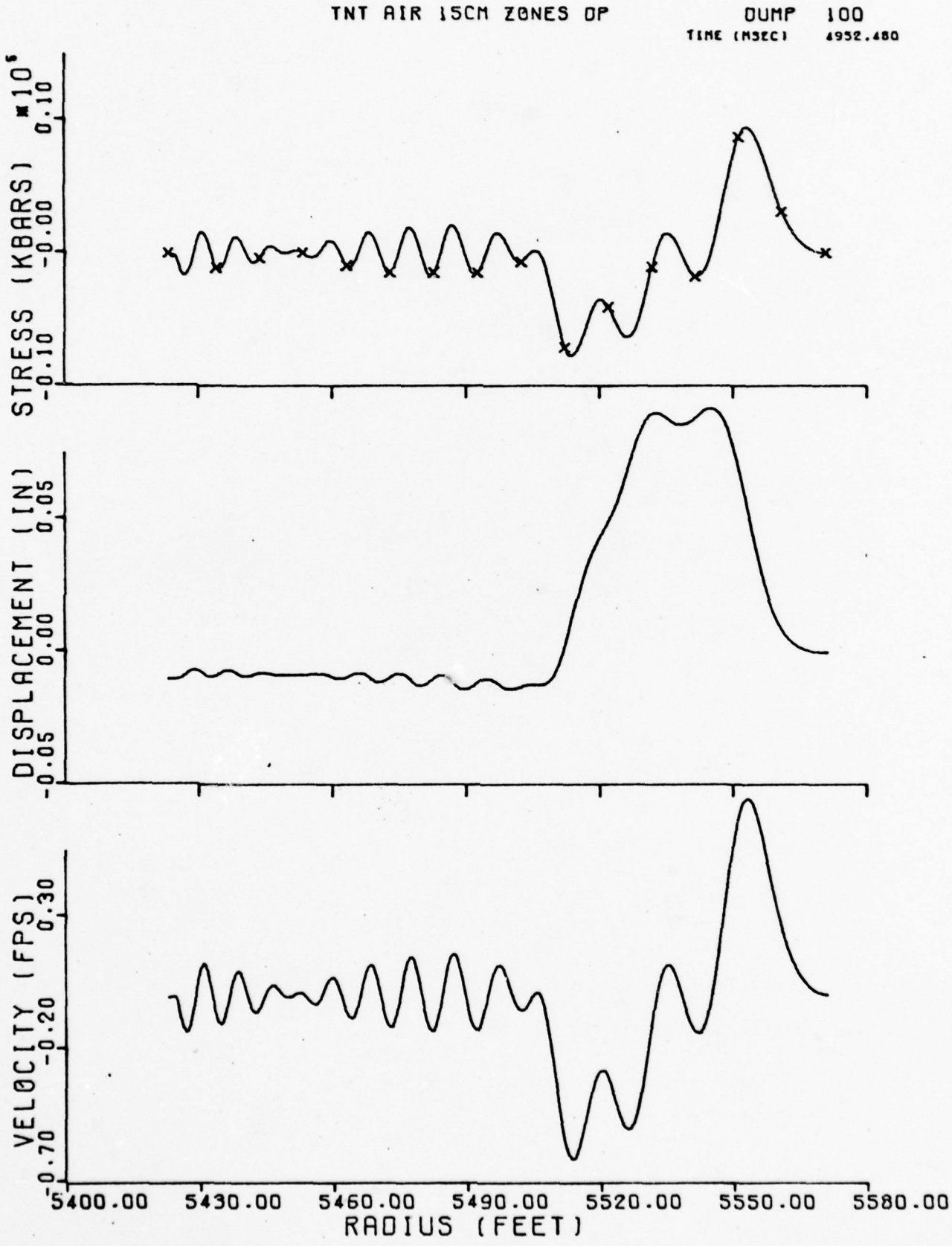

TNT AIR 15CM ZONES OP
DUMP 50
TIME (MSEC) 1308.429
STRESS (KBARS) *10⁴
0.05
0.00
-0.05
DISPLACEMENT (IN)
0.20
0.00
-0.20
VELOCITY (FPS)
5.00
0.00
-5.00
1320.00
1350.00
1380.00
1410.00
1440.00
1470.00
1500.00
RADIUS (FEET)

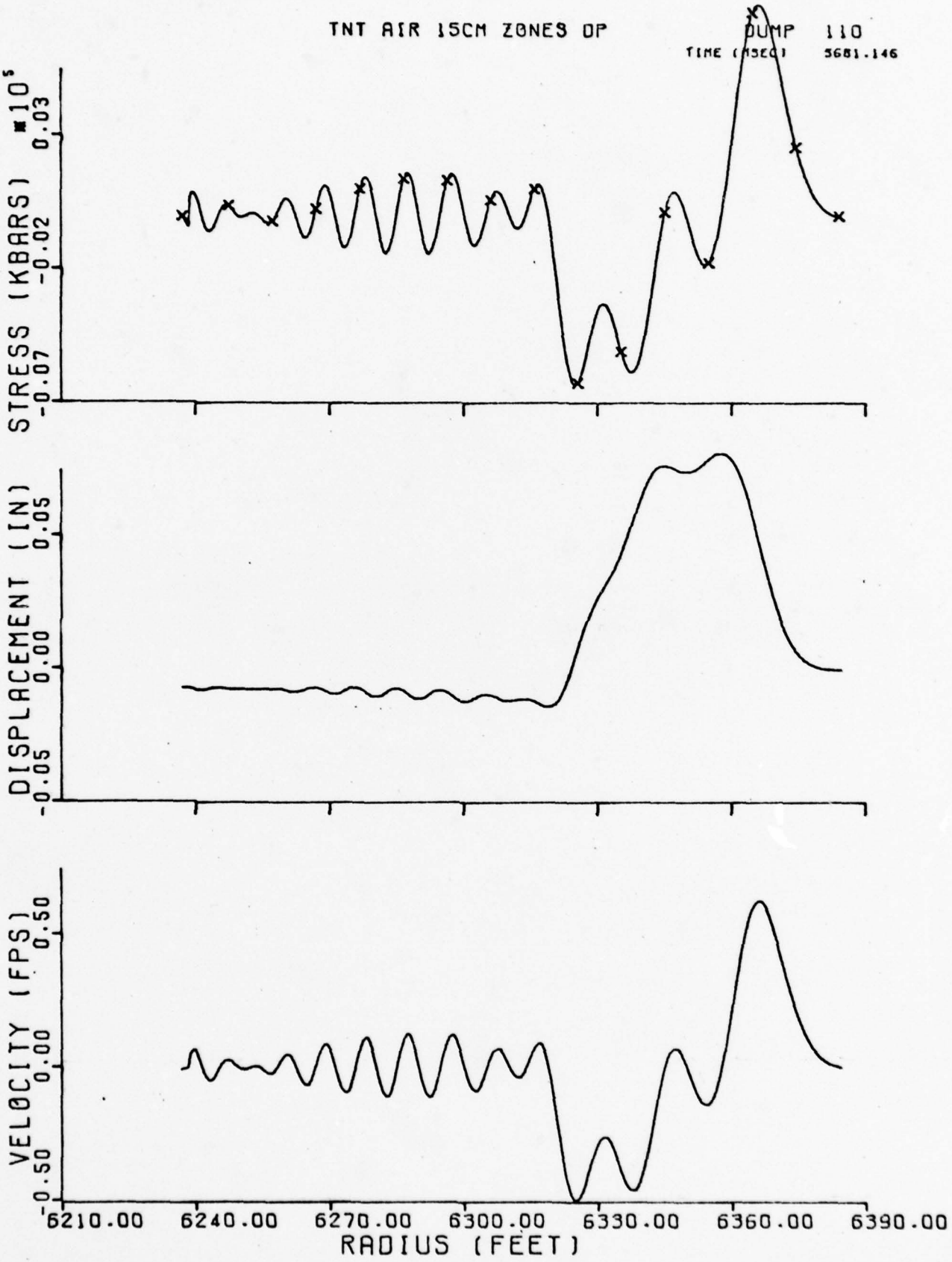

TNT AIR 15CM ZONES OP
DUMP 60
TIME (MSEC) 2037.119
STRESS (KBARS) *10⁴
0.02
0.00
-0.02
DISPLACEMENT (IN)
0.16
0.06
-0.04
VELOCITY (FPS)
2.00
0.00
-2.00
2140.00
2170.00
2200.00
2230.00
2260.00
2290.00
2320.00
RADIUS (FEET)

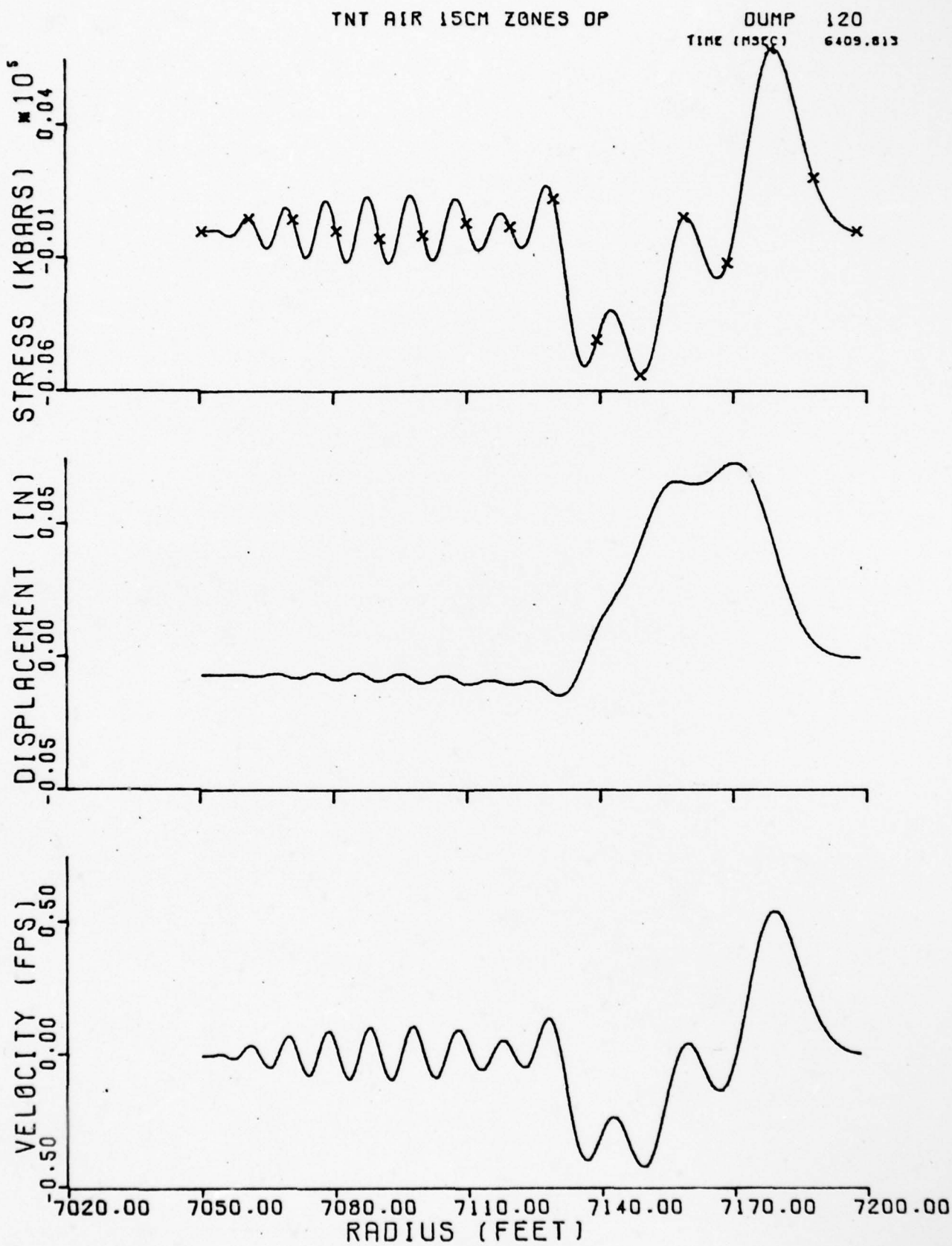

TNT AIR 15CM ZONES DP
DUMP 70
TIME (MSEC) 2766.040
STRESS (KBARS) *10⁴
0.02
0.00
-0.02
DISPLACEMENT (IN)
0.10
0.00
-0.10
VELOCITY (FPS)
0.80
-0.20
-1.20
2950.00
2980.00
3010.00
3040.00
3070.00
3100.00
3130.00
RADIUS (FEET)


TNT AIR 15CM ZONES OP
DUMP 80
TIME (MSEC) 3495.005
STRESS (KBARS) *10^5
0.08
-0.02
-0.12
DISPLACEMENT (IN)
0.10
0.00
-0.10
VELOCITY (FPS)
1.00
0.00
-1.00
3770.00
3800.00
3830.00
3860.00
3890.00
3920.00
3950.00
RADIUS (FEET)


TNT AIR 15CM ZONES OP
DUMP 90
TIME (MSEC) 4223.813
STRESS (KBARS) *10^5
0.10
-0.00
-0.10
DISPLACEMENT (IN)
0.08
0.03
-0.02
VELOCITY (FPS)
1.00
0.00
-1.00
4580.00
4610.00
4640.00
4670.00
4700.00
4730.00
4760.00
RADIUS (FEET)


TNT AIR 15CM ZONES OP
DUMP 100
TIME (MSEC) 4952.480
STRESS (KBARS) *10^5
0.10
-0.00
-0.10
DISPLACEMENT (IN)
0.05
0.00
-0.05
VELOCITY (FPS)
0.30
-0.20
-0.70
5400.00
5430.00
5460.00
5490.00
5520.00
5550.00
5580.00
RADIUS (FEET)


TNT AIR 15CM ZONES OP
DUMP 110
TIME (MSEC) 5681.146
STRESS (KBARS) *10^5
0.03
-0.02
-0.07
DISPLACEMENT (IN)
0.05
0.00
-0.05
VELOCITY (FPS)
0.50
0.00
-0.50
6210.00
6240.00
6270.00
6300.00
6330.00
6360.00
6390.00
RADIUS (FEET)


TNT AIR 15CM ZONES OP
DUMP 120
TIME (MSEC) 6409.813
STRESS (KBARS) *10^5
0.04
-0.01
-0.06
DISPLACEMENT (IN)
0.05
0.00
-0.05
VELOCITY (FPS)
0.50
0.00
-0.50
7020.00
7050.00
7080.00
7110.00
7140.00
7170.00
7200.00
RADIUS (FEET)

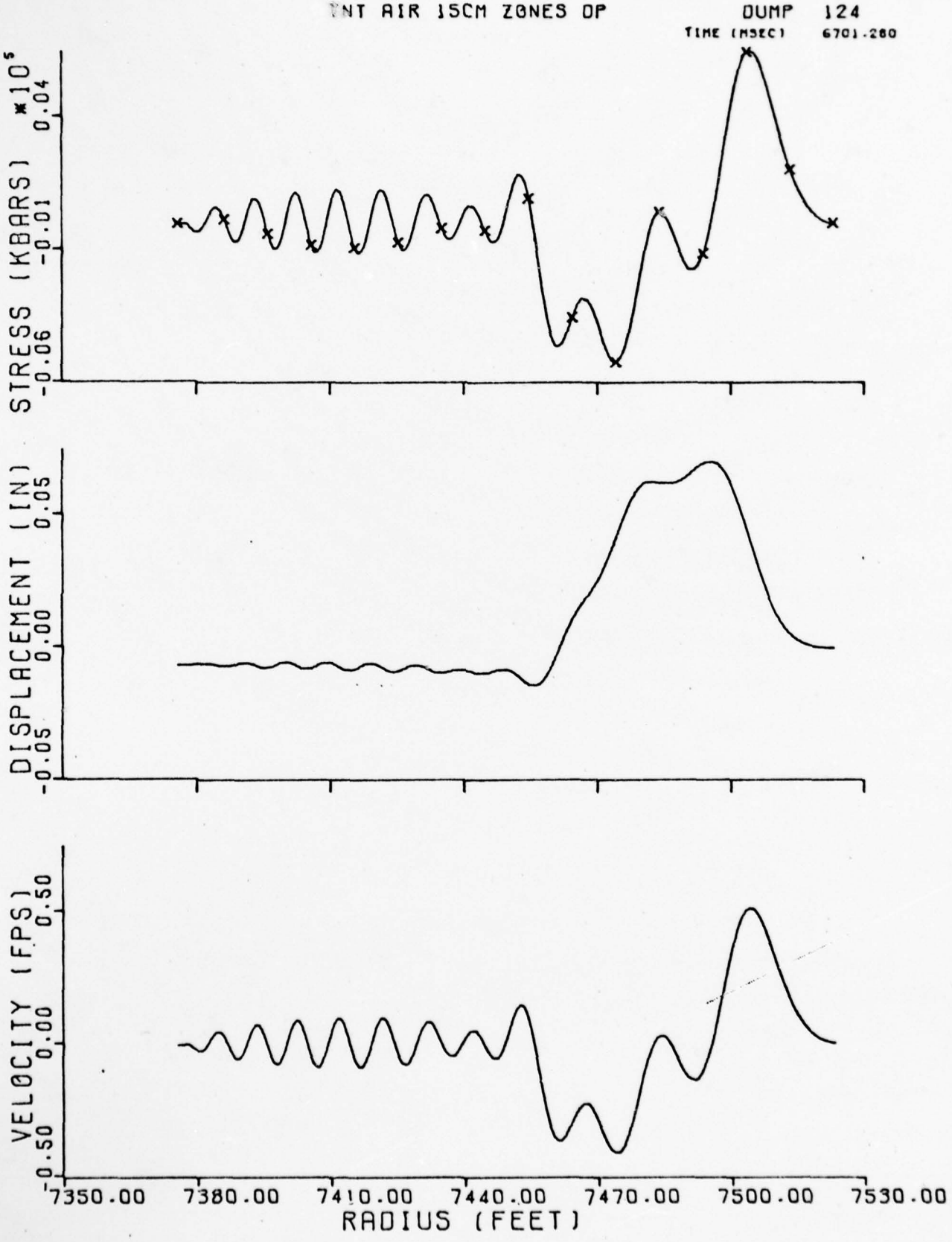
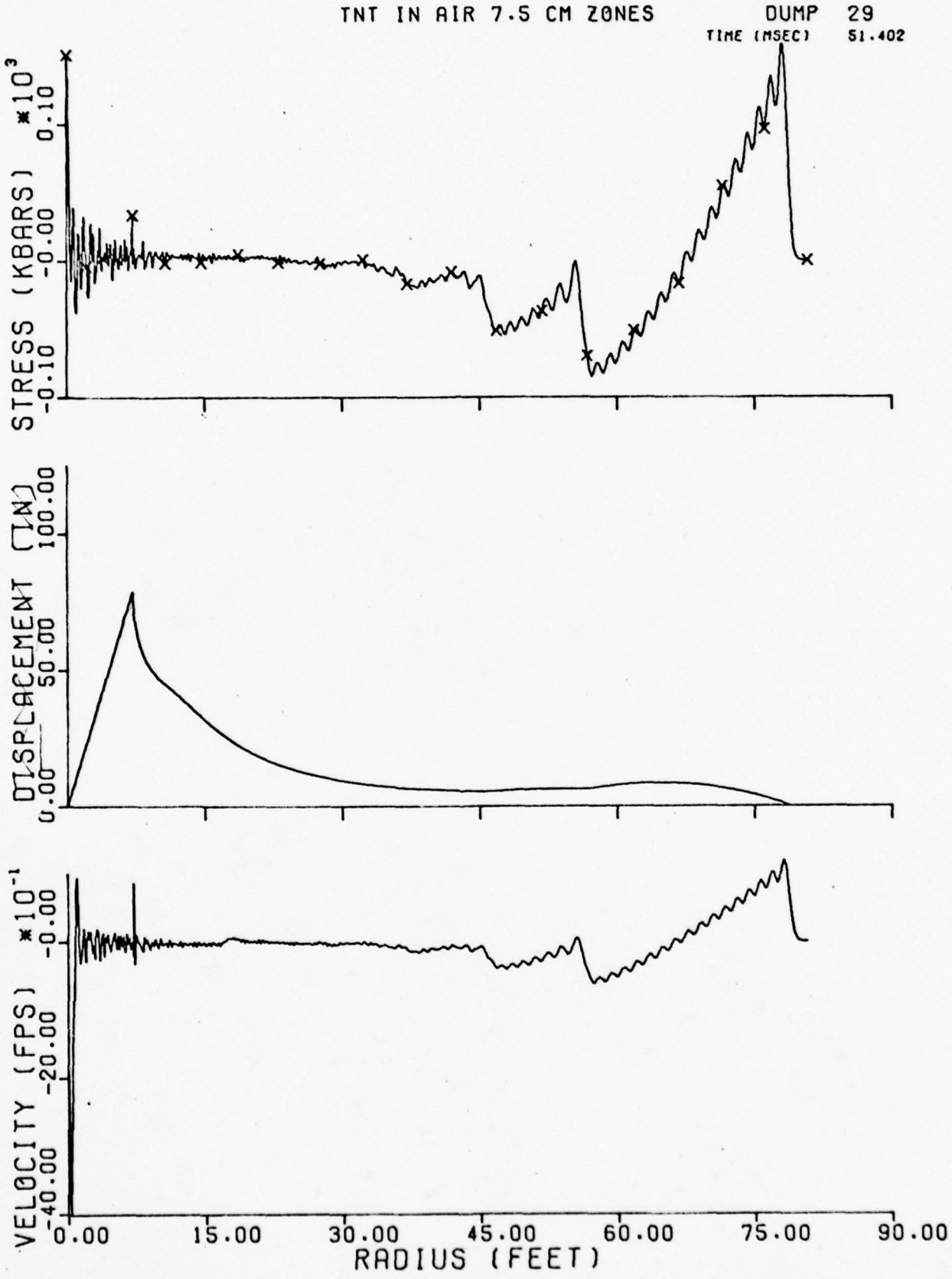
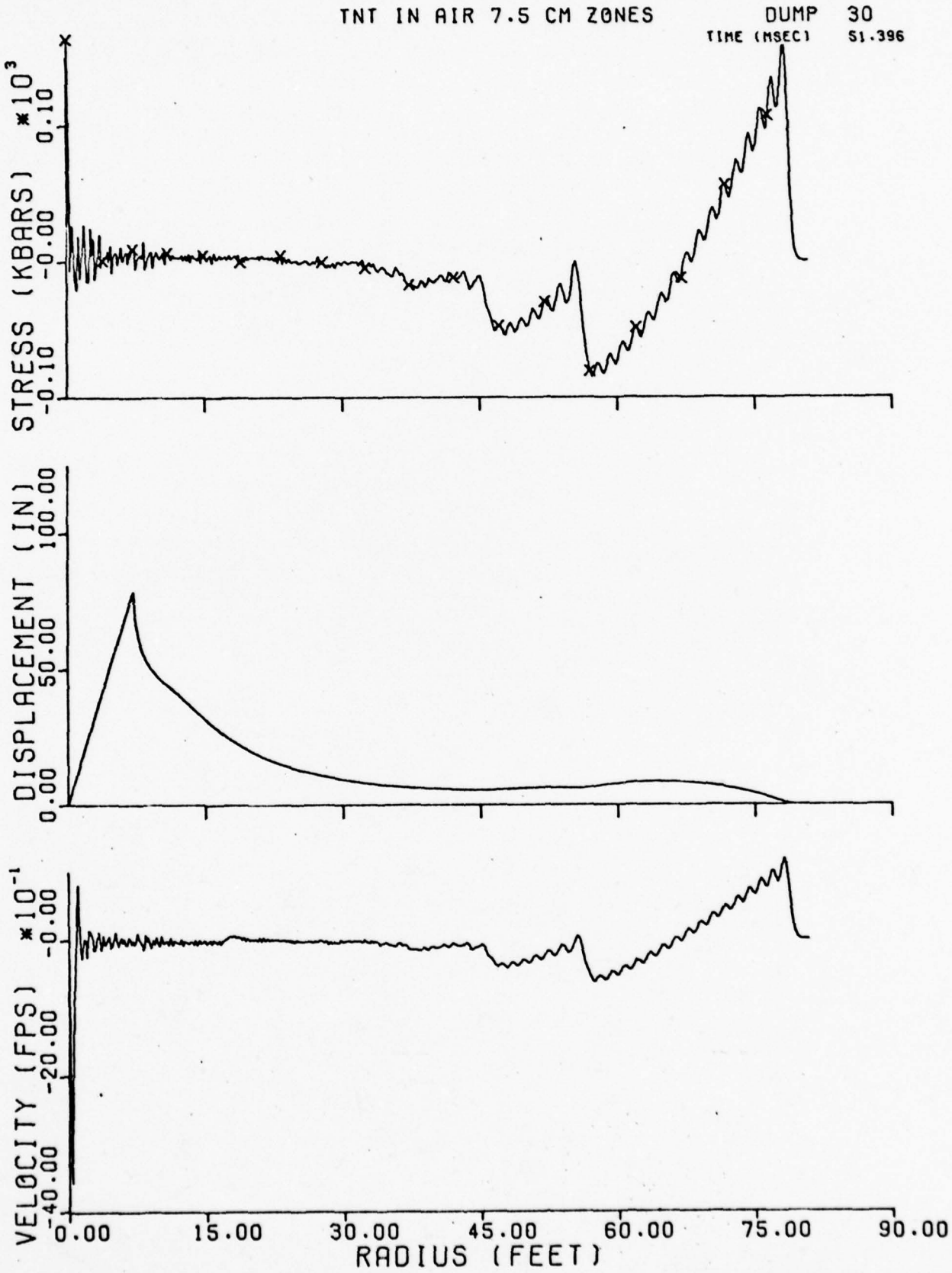

TNT AIR 15CM ZONES OP
DUMP 124
TIME (MSEC) 6701.280
STRESS (KBARS) *10^5
0.04
-0.01
-0.06
DISPLACEMENT (IN)
0.05
0.00
-0.05
VELOCITY (FPS)
0.50
0.00
-0.50
7350.00
7380.00
7410.00
7440.00
7470.00
7500.00
7530.00
RADIUS (FEET)

Figure 7.2

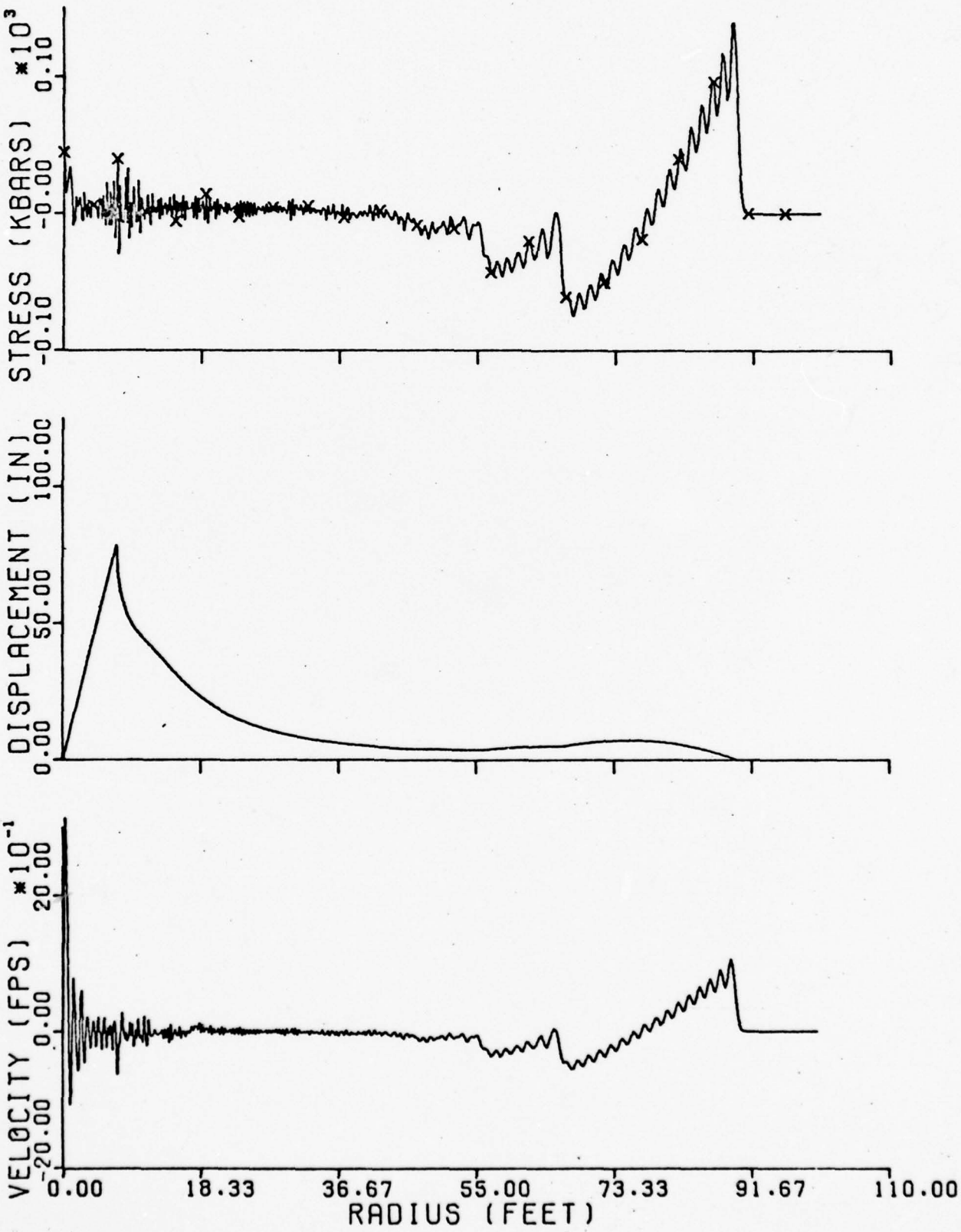
Same as Figure 7.1, but with space zones of 7.5 cm, that is, twice the resolution of the previous figure.

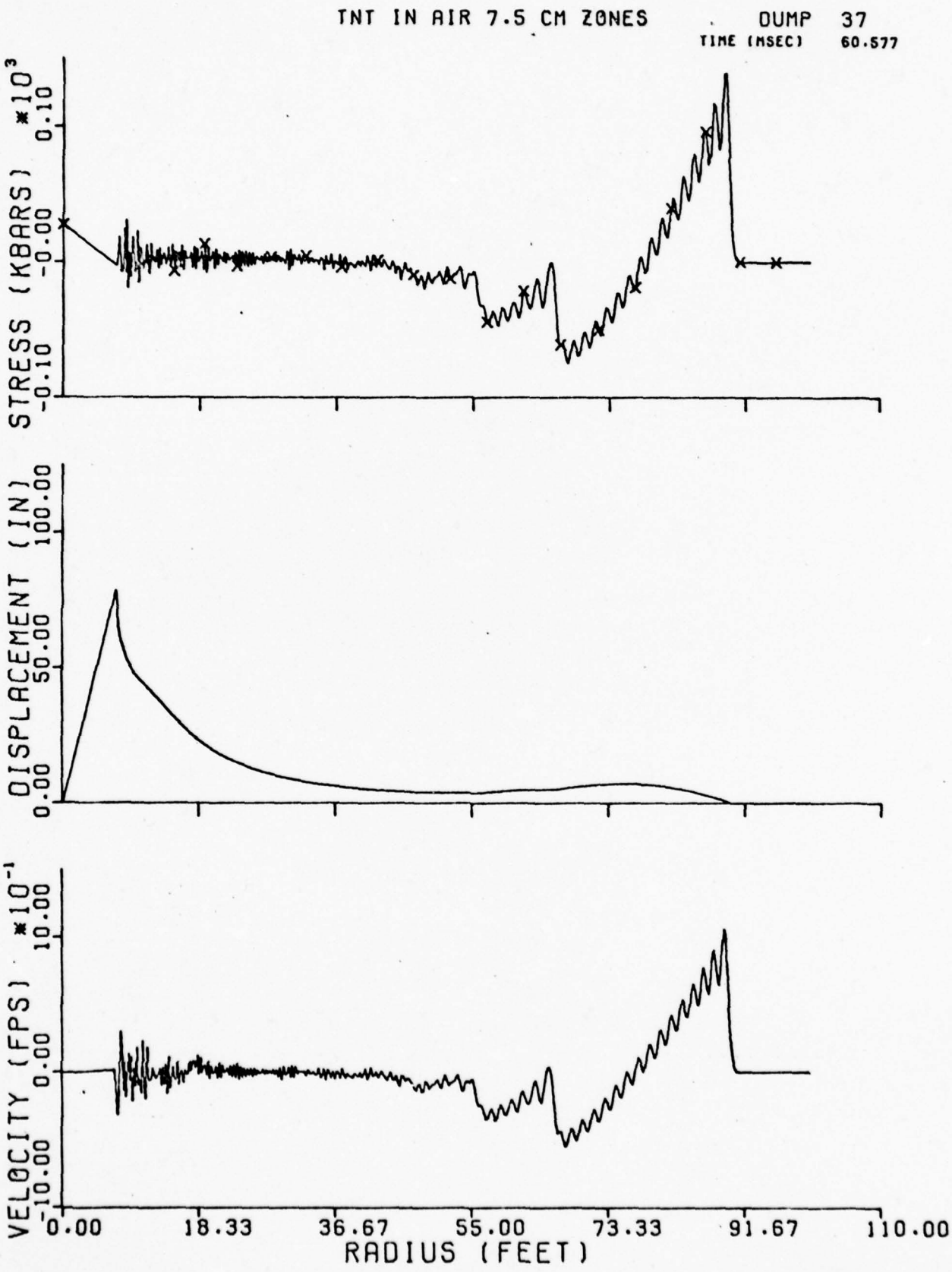

TNT IN AIR 7.5 CM ZONES
DUMP 29
TIME (MSEC) 51.402
STRESS (KBARS) *10³
0.10
-0.00
-0.10
DISPLACEMENT (IN)
100.00
50.00
0.00
VELOCITY (FPS) *10⁻¹
-0.00
-20.00
-40.00
0.00
15.00
30.00
45.00
60.00
75.00
90.00
RADIUS (FEET)

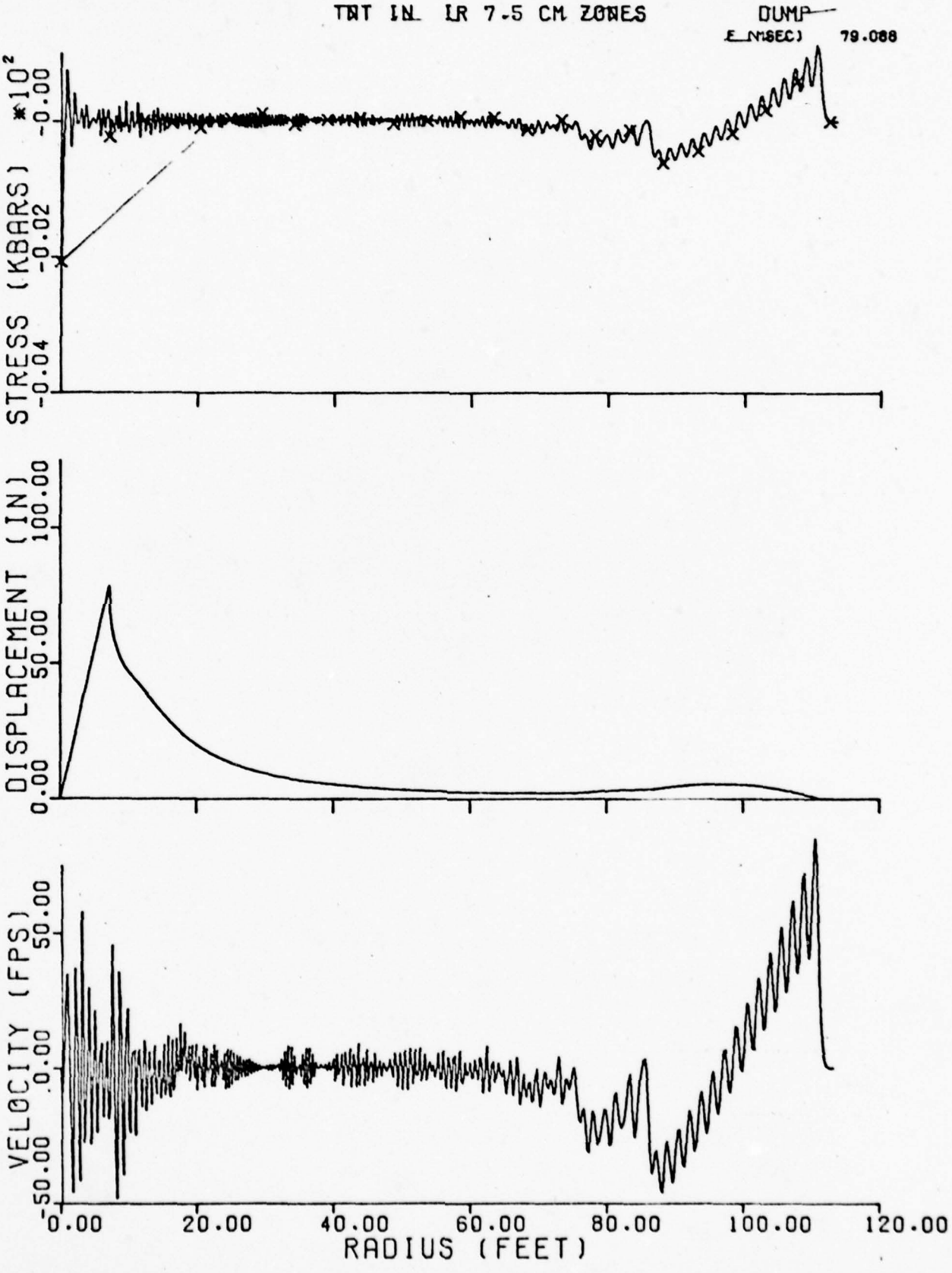

TNT IN AIR 7.5 CM ZONES
DUMP 30
TIME (MSEC) S1.396
STRESS (KBARS) *10^3
0.10
-0.00
-0.10
DISPLACEMENT (IN)
100.00
50.00
0.00
VELOCITY (FPS) *10^-1
-0.00
-20.00
-40.00
0.00
15.00
30.00
45.00
60.00
75.00
90.00
RADIUS (FEET)

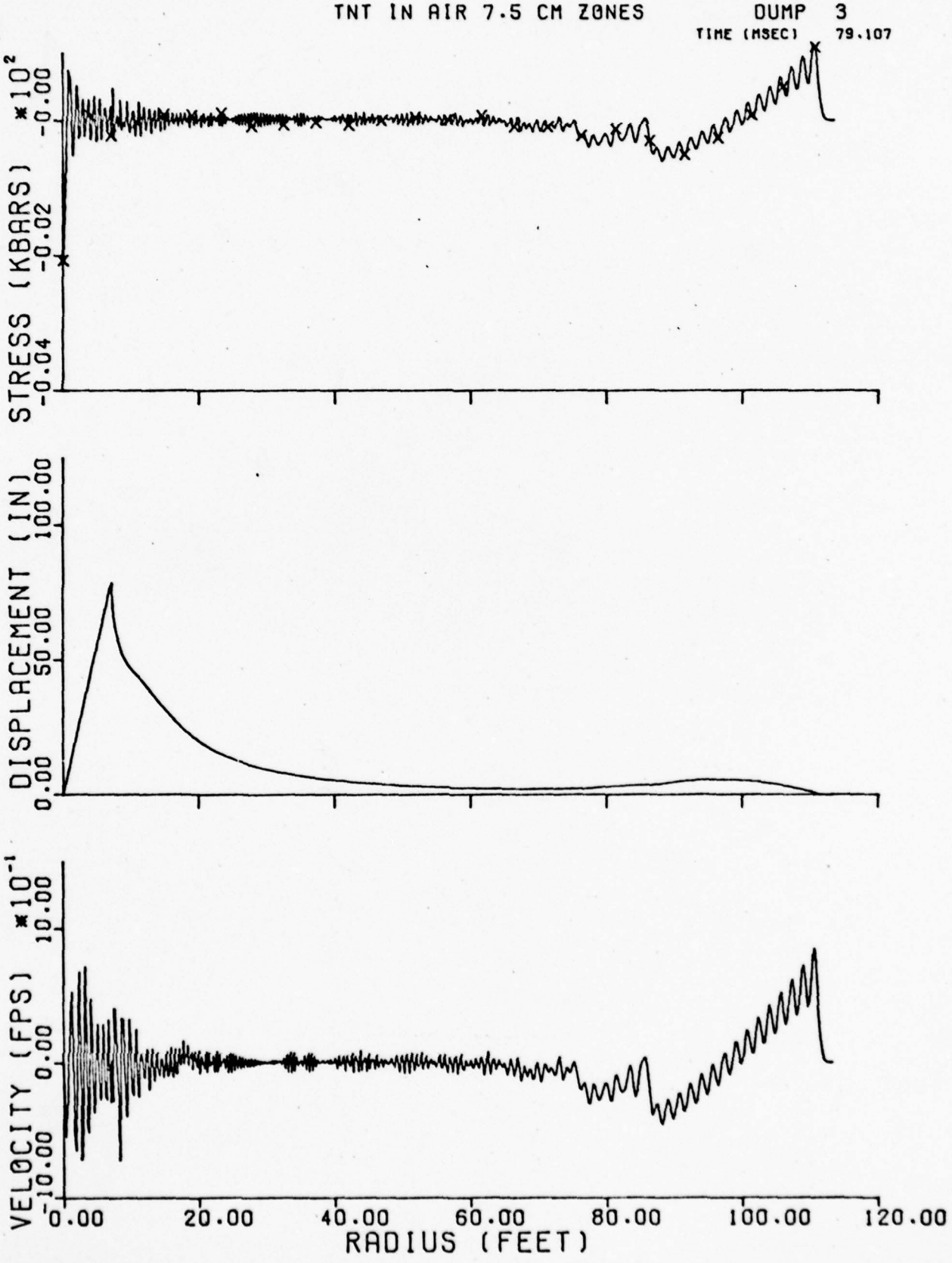
TNT IN AIR 7.5 CM ZONES DUMP 31

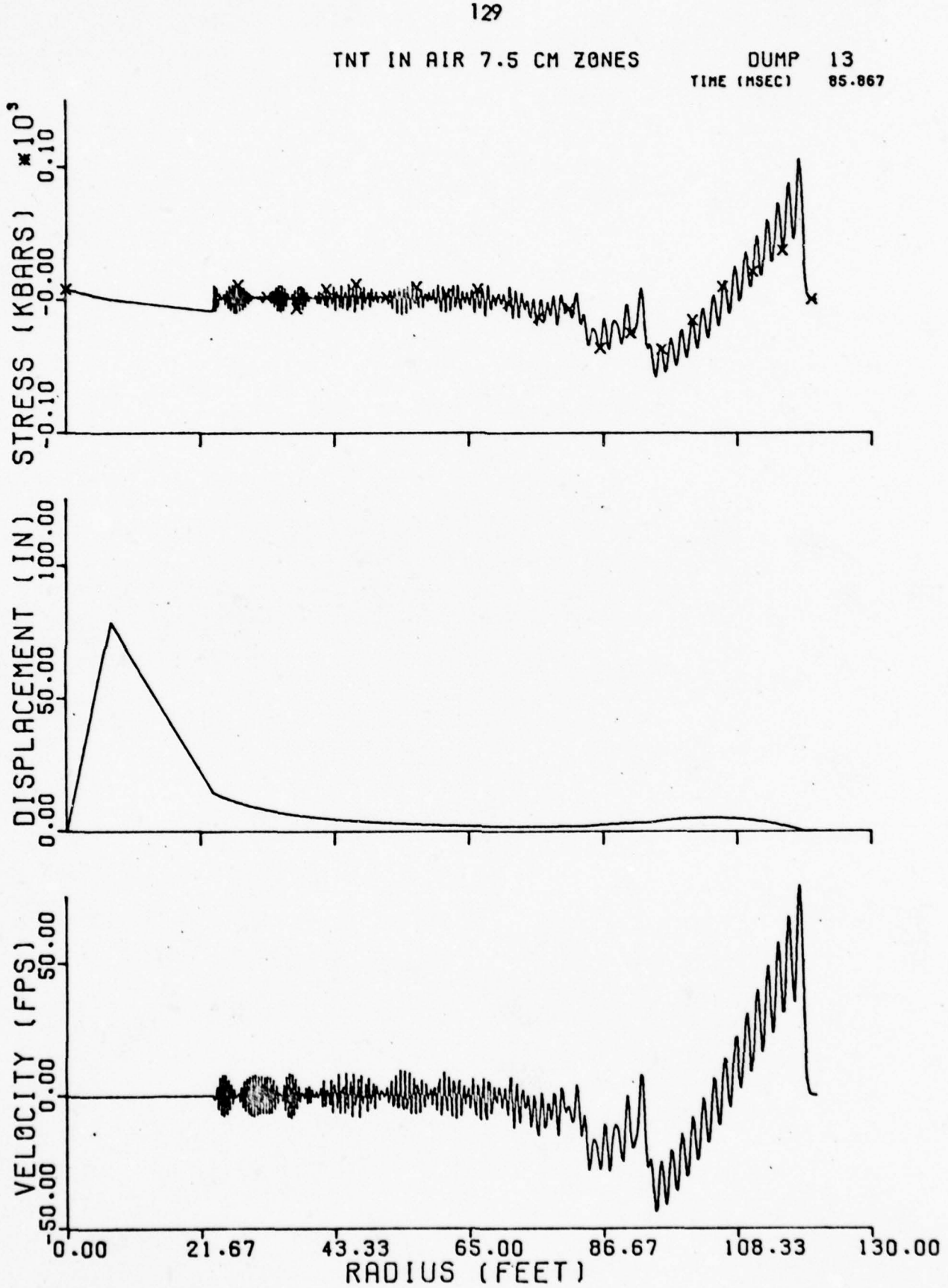
TIME (MSEC) 60.596

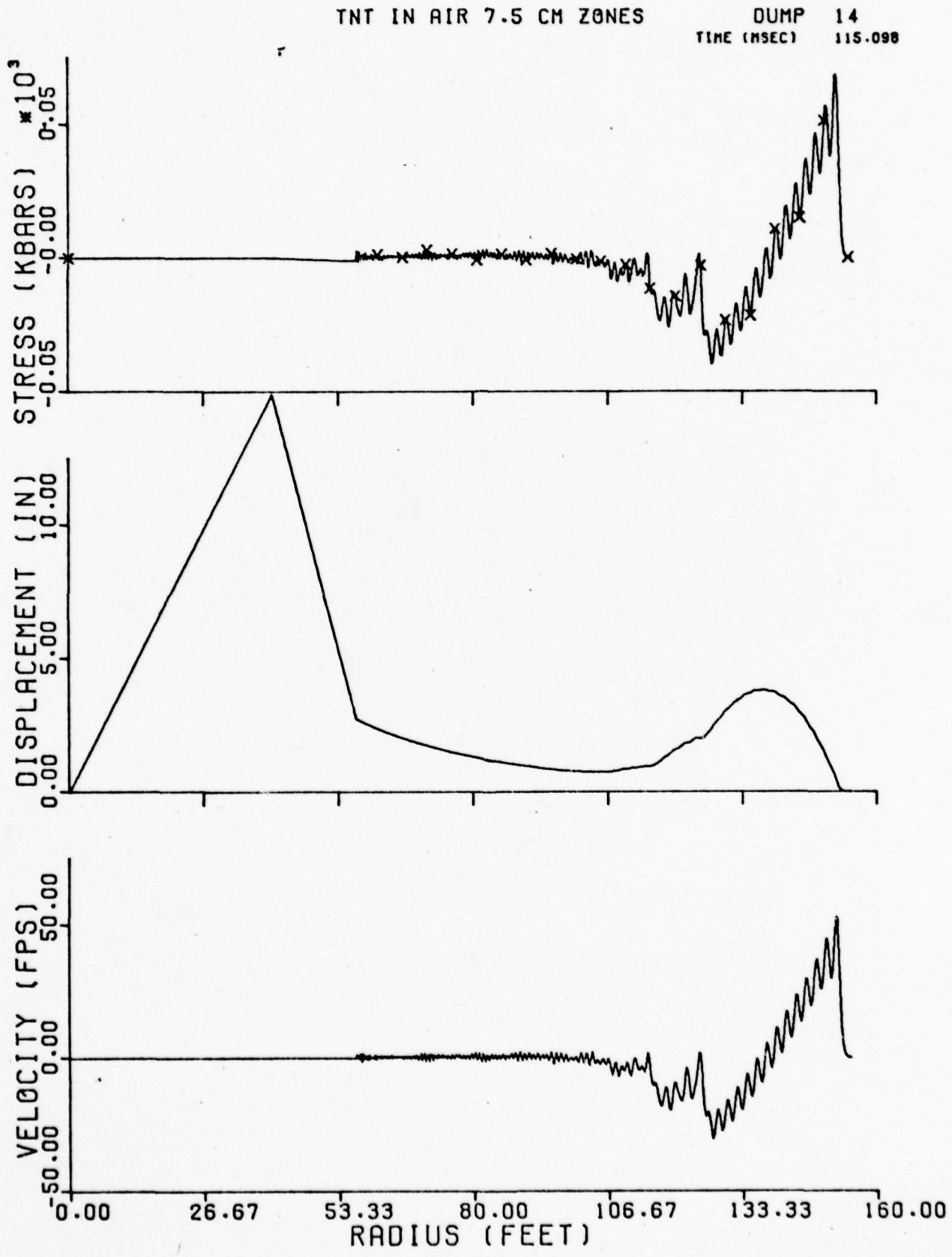


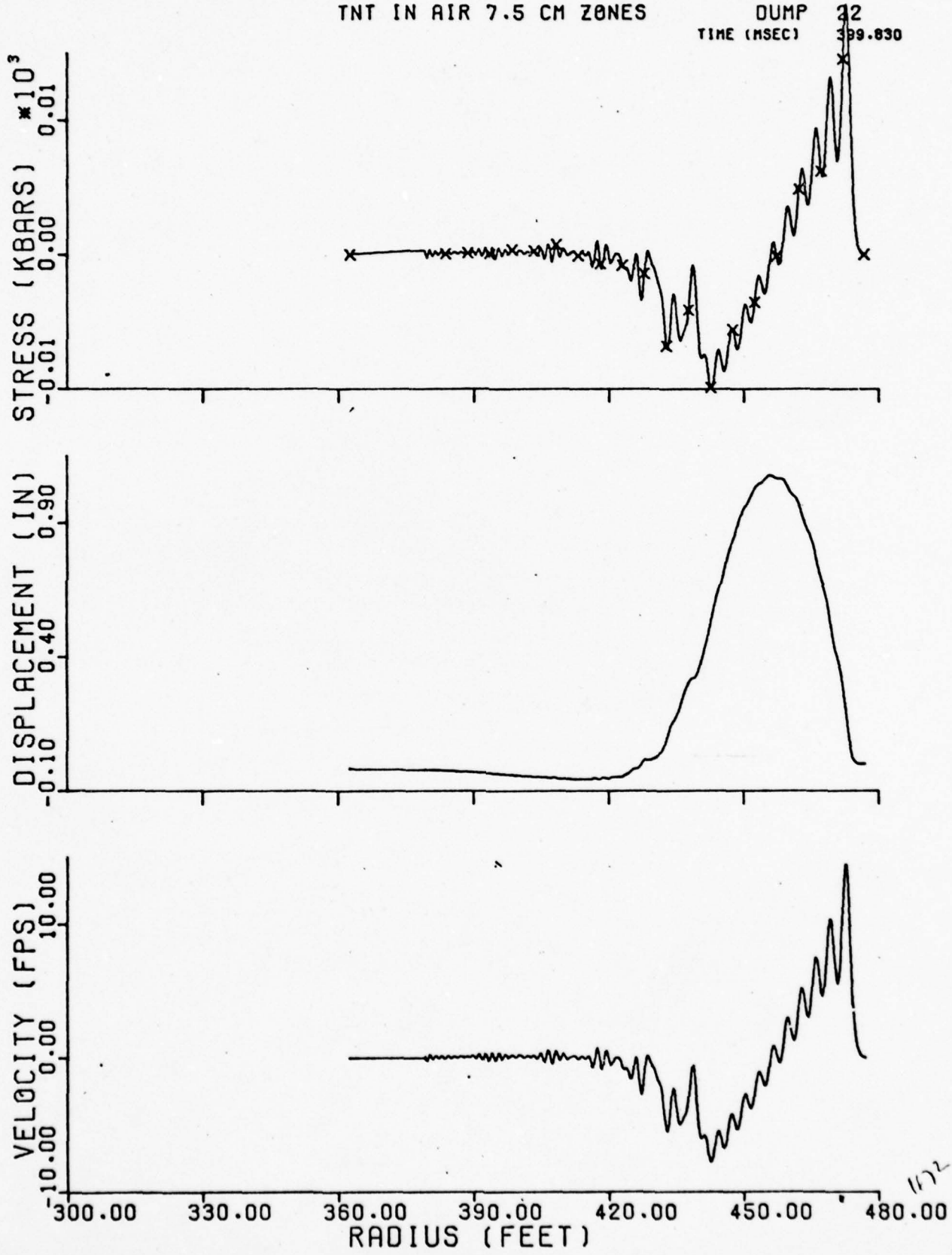

TNT IN AIR 7.5 CM ZONES
DUMP 37
TIME (MSEC) 60.577
STRESS (KBARS) *10^3
0.10
-0.00
-0.10
DISPLACEMENT (IN)
100.00
50.00
0.00
VELOCITY (FPS) *10^-1
10.00
0.00
-10.00
0.00
18.33
36.67
55.00
73.33
91.67
110.00
RADIUS (FEET)

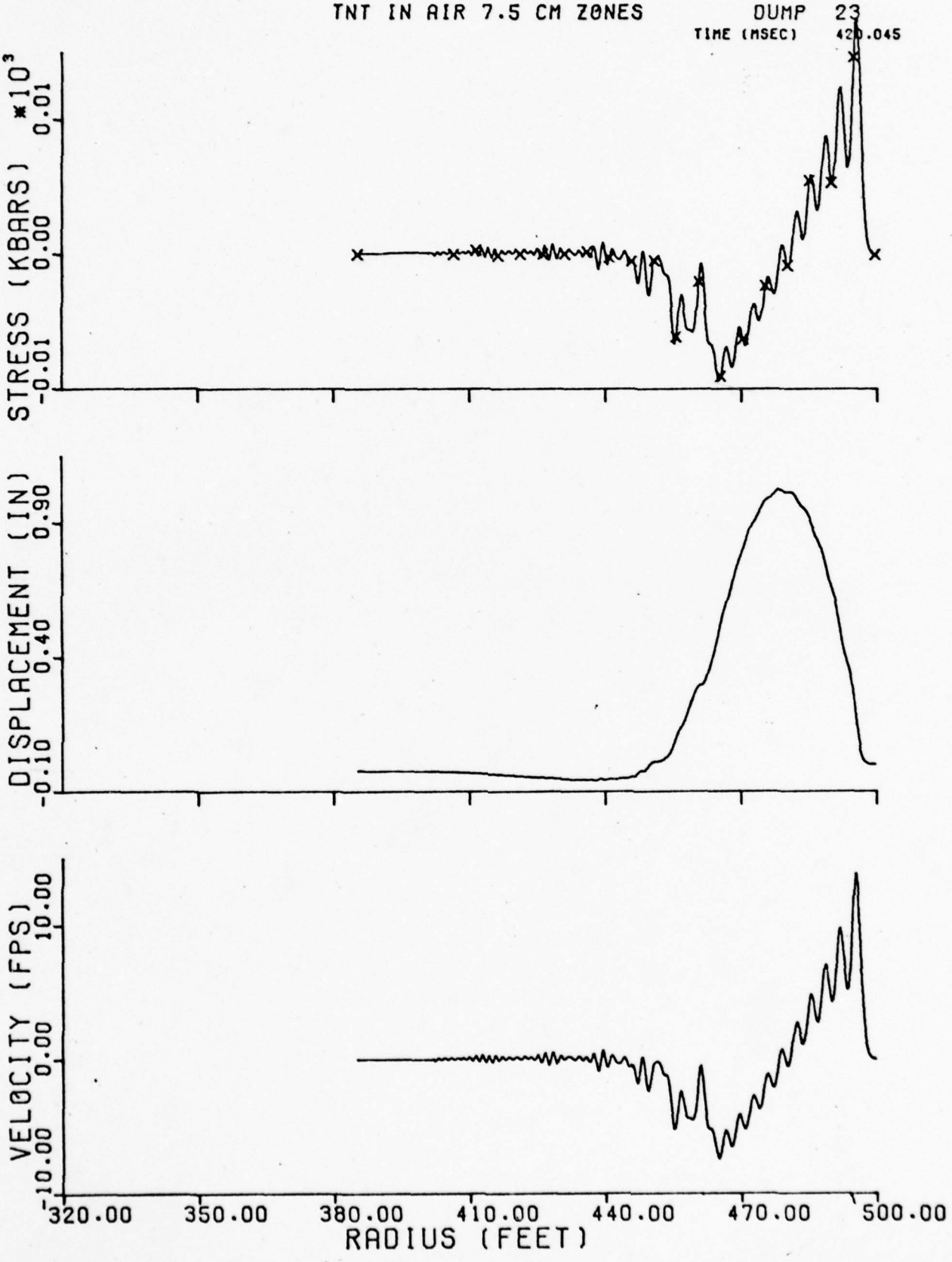

TNT IN LR 7.5 CM ZONES
DUMP
E (MSEC) 79.088
STRESS (KBARS) *10²
-0.00
-0.02
-0.04
DISPLACEMENT (IN)
100.00
50.00
0.00
VELOCITY (FPS)
50.00
0.00
-50.00
0.00
20.00
40.00
60.00
80.00
100.00
120.00
RADIUS (FEET)


TNT IN AIR 7.5 CM ZONES
DUMP 3
TIME (MSEC) 79.107
STRESS (KBARS) *10²
-0.00
-0.02
-0.04
DISPLACEMENT (IN)
100.00
50.00
0.00
VELOCITY (FPS) *10⁻¹
10.00
0.00
-10.00
0.00
20.00
40.00
60.00
80.00
100.00
120.00
RADIUS (FEET)


TNT IN AIR 7.5 CM ZONES
DUMP 13
TIME (MSEC) 85.867
STRESS (KBARS) *10³
0.10
-0.00
-0.10
DISPLACEMENT (IN)
100.00
50.00
0.00
VELOCITY (FPS)
50.00
0.00
-50.00
0.00
21.67
43.33
65.00
86.67
108.33
130.00
RADIUS (FEET)

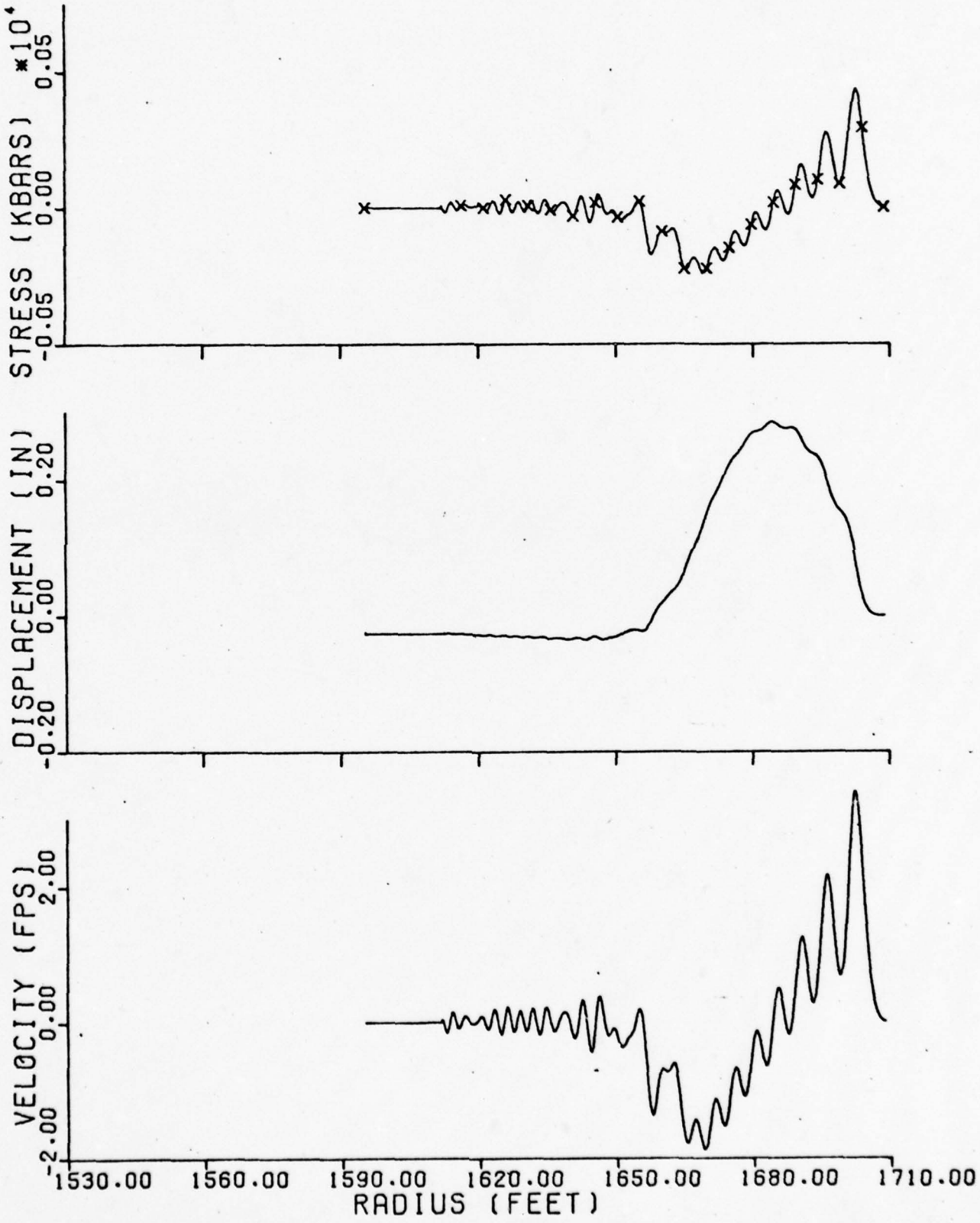

TNT IN AIR 7.5 CM ZONES
DUMP 14
TIME (MSEC) 115.098
STRESS (KBARS) *10³
0.05
-0.00
-0.05
DISPLACEMENT (IN)
10.00
5.00
0.00
VELOCITY (FPS)
50.00
0.00
-50.00
0.00
26.67
53.33
80.00
106.67
133.33
160.00
RADIUS (FEET)


TNT IN AIR 7.5 CM ZONES
DUMP 32
TIME (MSEC) 399.830
STRESS (KBARS) *10^3
0.01
0.00
-0.01
DISPLACEMENT (IN)
0.90
0.40
-0.10
VELOCITY (FPS)
10.00
0.00
-10.00
300.00
330.00
360.00
390.00
420.00
450.00
480.00
RADIUS (FEET)


TNT IN AIR 7.5 CM ZONES
DUMP 23
TIME (MSEC) 420.045
STRESS (KBARS) *10³
0.01
0.00
-0.01
DISPLACEMENT (IN)
0.90
0.40
-0.10
VELOCITY (FPS)
10.00
0.00
-10.00
320.00
350.00
380.00
410.00
440.00
470.00
500.00
RADIUS (FEET)

TNT IN AIR 7.5 CM ZONES DUMP 56

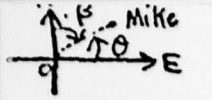
TIME (MSEC) 1500.033



8. ANALYSIS OF PASS DATA

Twenty separate Howitzer firing events were studied from the data, for two of which the actual microphone traces were available. These events were chosen by referring to the wind and temperature profiles from the 500 foot instrumented tower located near the two Howitzers. Conditions of near calm were preferred for all events, except for the eight on 12-5-74, so that wind velocities would not significantly enter into the range calculations. The eight events on 12-5-74 were chosen as the highest surface wind speeds available to test the wind correction calculation. Examples of the three typical vertical profiles of temperature (lapse, isothermal and inversion) were included in the twenty events studied.

We have tabulated each event studied in a format known as the Event Summary. The uppermost section of each event summary identifies the three microphones chosen for the baseline, the day, the event number, the gun number, the time of Howitzer firing, expressed as Mountain Standard Time, to the nearest millisecond and the distances between microphones. The distance between the closest and the middle microphone is labelled d_2, that between the farthest and the middle microphone d_3, and that between the closest and farthest microphone is $D = d_2 + d_3$. When d_2 and d_3 are approximately equal, their numerical average is expressed simply as d and the total distance D is not needed. The next section down on each event summary includes the speed and direction of the wind W at 25 feet elevation, the air temperature T at 26 feet elevation, the calculated speed



(H1 + H2 are 27.90 feet apart)

Sequential Mike Number	Grid Lettering Scheme	Origin At Howitzer 1 r_1 (feet)	θ_1 (°)	β_1 (°)	Origin At Howitzer 2 r_2 (feet)	θ_2 (°)	β_2 (°)
1	N1 W1 D1	21,942.02	111.9	338.1	21,921.59	111.9	338.1
2	N2	19,059.74	102.5	347.5	19,042.72	102.4	347.6
3	N3	16,862.68	90.2	359.8	16,850.77	90.1	359.9
4	N4	15,642.24	75.1	14.9	15,637.30	75.0	15.0
5	N5	15,629.05	58.8	31.2	15,632.00	58.7	31.3
6	N6	16,825.86	43.7	46.3	16,835.95	43.6	46.4
7	N7	19,005.48	31.3	58.7	19,020.91	31.3	58.7
8	N8 E1	21,876.10	21.8	68.2	21,895.15	21.8	68.2
9	W2	19,077.34	121.4	328.6	19,054.07	121.4	328.6
10	D2	15,675.69	112.0	338.0	15,655.26	111.9	338.1
11	E2	19,001.28	12.4	77.6	19,023.42	12.3	77.7
12	A1 W3	16,901.73	133.8	316.2	16,875.70	133.7	316.3
13	A2	12,944.68	126.1	323.9	12,917.24	126.0	324.0
14	A3 D3	9,410.51	112.1	337.9	9,390.03	112.0	338.0
15	A4	6,992.88	85.7	4.3	6,983.02	85.5	4.5
16	A5	6,963.40	48.7	41.3	6,971.24	48.4	41.6
17	A6	9,345.14	21.9	68.1	9,364.19	21.8	68.2
18	A7	12,862.16	7.8	82.2	12,885.60	7.7	82.3
19	A8 E3	16,916.25	0.0	90.0	16,841.52	359.9	90.1
20	W4	15,705.66	148.8	301.2	15,677.92	148.8	301.2
21	D4	3,145.89	112.8	337.2	3,125.24	112.4	337.6
22	E4	15,613.52	344.9	105.1	15,641.00	344.8	105.2
23	W5	15,713.66	165.0	285.0	15,686.19	165.0	285.0
24	D5	3,120.22	290.8	159.2	3,140.34	291.2	158.8
25	E5	15,621.54	328.5	121.5	15,649.27	328.6	121.4
26	B1 W6	16,924.14	180.0	270.0	16,898.89	180.1	269.9
27	B2	12,970.57	187.8	262.2	12,947.15	187.8	262.2
28	B3	9,451.63	201.7	248.3	9,432.57	201.9	248.1
29	B4	7,049.35	228.1	221.9	7,039.35	228.3	221.7
30	B5	7,016.80	264.8	185.2	7,026.36	265.0	185.0

(H1 + H2 are 27.90 feet apart)

Sequential Mike Number	Grid Lettering Scheme	Origin At Howitzer 1 r_1 (feet)	θ_1 (°)	β_1 (°)	Origin At Howitzer 2 r_2 (feet)	θ_2 (°)	β_2 (°)
31	B6 D6	9,385.47	291.5	158.5	9,405.76	291.6	158.4
32	B7	12,891.24	305.6	144.4	12,915.59	305.7	144.3
33	B8 E6	16,838.64	313.5	136.5	16,864.62	313.5	136.5
34	W7	19,109.90	192.3	257.7	19,087.77	192.4	257.6
35	D7	15,650.25	291.6	158.4	15,671.08	291.7	158.3
36	E7	19,034.19	301.1	148.9	19,057.40	301.2	148.8
37	S1 W8	21,981.98	201.8	248.2	21,962.93	201.8	248.2
38	S2	19,105.69	211.2	238.8	19,090.24	211.3	238.7
39	S3	16,914.64	223.5	226.5	16,904.49	223.6	226.4
40	S4	15,698.26	238.5	211.5	15,695.21	238.6	211.4
41	S5	15,685.12	254.8	195.2	15,689.93	254.9	195.1
42	S6	16,897.96	269.8	180.2	16,889.75	269.9	180.1
43	S7	19,051.44	282.2	167.8	19,068.36	282.2	167.8
44	S8 D8 E8	21,916.19	291.7	158.3	21,936.54	291.7	158.3
—	G1 (near B2)	12,970.57	187.8	262.2	12,947.15	187.8	262.2
—	G2 (" B3)	9,451.63	201.8	248.2	9,432.57	201.9	248.1
—	G3 (" B4)	7,047.35	228.1	221.9	7,038.35	228.3	221.7
—	G4 (" B5)	7,016.80	264.8	185.2	7,026.36	265.0	185.0
—	G5 (" B6)	9,385.47	291.5	158.5	9,405.76	291.6	158.4
—	G6 (" B7)	12,891.24	305.6	144.4	12,915.59	305.7	144.3

of sound C, the mach number of the wind M, and the angle θ between the microphone baseline and the wind vector. This angle is measured from the far end of the baseline back in toward the Howitzer to the head of the wind vector. The third section in each event summary is a self-explanatory table directly comparing the raw microphone time data to the predicted or correct time information using the temperature calculated speed of sound. The measured distance between Howitzer number one and any microphone is given as r_1 and the measured distance between Howitzer number two and any microphone is given as r_2. The raw-data microphone times are given as t. The time error column shows a negative number for late arrivals (recorded later than calculated) and a positive number for early arrivals. The bottom section of each event summary compares true time differences between microphones with raw data time differences, compares measured values of S_2 and S_3 (see wind correction and ranging diagrams) with values for S_2 and S_3 calculated from raw time data and the temperature calculated speed of sound, compares the raw-data-calculated angle between the microphone base line and line between the farthest microphone and the Howitzer, ψ_3, with the wind-corrected calculation of that angle, ψ_{3wind} and the true angle, True ψ_3, and compares the raw-data-calculated distance from nearest microphone to Howitzer, R_o, with the wind-corrected calculation of that distance, R_{wind}.

On the adjoining two pages to this written summary we have compiled the results of the twenty events studied. One quick glance reveals the rather serious problem of uncertain and missing data. This category accounts for nearly half of all possible microphone reports in the study. The criterion for deciding which arrivals were early, late and correct was very simple. I considered as correct results, those that exactly (to the nearest millisecond) corresponded to the predicted

or true values obtained by using the temperature calculated speed of sound. Under these circumstances one would not expect there to be many "correct" reports; indeed only one was found. But a good microphone might be one that has an even distribution between late and early arrivals, microphone B3 for example. After one discards the missing data, only 278 good results out of a possible 520 are seen. Of these, a striking 72.3% of the reports are too early. This compilation of twenty events would seem to filter out any systematic time error due to wind direction because nearly all wind directions are included in these results. Another possibility for systematic error would be an error in the timing mechanism of the Howitzer firings leading to a preponderance of "early" reports. This type of error should not affect the sound ranging calculations since the absolute error in the arrival times is not important in itself. It is the time differences between microphones that is important and this is not affected in any way by an error in the determination of the absolute time of Howitzer firing t_o.

Results of the Survey

When one surveys the event summaries, he cannot fail to be impressed with the very large errors sometimes produced by the ranging formulas. In not a few events, the error in the range was of the same size as the range itself. These cases stand in stark contrast to those in which the formulas give highly satisfactory results, quite sufficiently accurate for the purpose for which sound ranging is intended.

We have made every effort to identify the cause of error in those cases in which the error was significant. A brief summary of these efforts follows.

(1) Is it possible that a major source of error could be the ambiguity of the microphone traces in indicating arrival times, or in the misreading of these? Here we were able to investigate two of the 20 events for which we had been provided with copies of the microphone traces for the microphones D4, D5, A3, A6, A7, B2, and D7. The two events were on Day 323 (11/19/74, events 13 and 34). It will be noted that range errors were as large as 88 per cent in these events. However, it is not possible to ascribe any appreciable error to ambiguities or misreadings of arrival times from the traces. In every trace the arrival time was clearly indicated, and had been properly read. From this tiny sample we cannot conclude that the traces were never a source of error; but we can see that a well-marked and well-read trace can give highly erroneous results.

(2) Wind correction. As stated above, we had selected out the cases of no wind or very light wind, so that at the outset we can state that large errors can result under almost completely calm conditions. If we now turn to consideration of our cases selected on the basis of relatively high wind, we can survey the results of applying the wind correction. These are not encouraging. In roughly half of the cases, the wind correction increased the ranging error; in no case did it turn a poor result into a good result. The Mach numbers in all of these examples were quite small (less than 0.04); the PASS operation was conducted primarily under

conditions of little weather. When the wind was high, a large percentage of the microphones were missing or indicated as uncertain. In the remaining cases, those examined, we conclude that the wind represents a small signal in the general noise level of whatever processes are entering into the error. In such conditions, a wind correction would not be expected to produce improved results.

(3) Terrain. Reference to the topographic maps of the firing area indicates no physical features suggesting that diffraction by terrain could play any role in the errors recorded in the Events Summary.

(4) Non-linear and directional blast effects. Here we refer to Section 7 in particular, formulas (7.7) and (7.12):

$$\epsilon = K/R^{1.07} \quad \text{and} \quad S_i = (1 + \epsilon)\,\sigma_i$$

The theory, together with some approximations, suggests that the constant K has a value in the neighborhood of 1 to 5. However, this assumes a perfect spherical wave, which may not be an adequate model for the non-linear effect of a Howitzer blast. Accordingly we have followed a common procedure in selecting a formula such as the above that has theoretical grounding, but allowing experments to determine the value of the constant. For this experiment we selected the A microphones as being most directly in the line of Howitzer fire. Reference to the Event Summary will show that for these cases, a value of K between 10 and 50, but closer to 10, gave improvement in the ranging estimates. In some cases, this

improvement was marked. This does not guarantee that similar improvement can be made on independent data using this range of values for K, but it does suggest that such a correction is well worth trying if such data become available.

When all of the above factors have been taken into consideration, a large residue of cases of large error remains. When (i) the signal arrival is inexplicably early at the first microphone and (ii) the signal is sufficiently irregular in its arrival at the other microphones to produce an error of 100 per cent, then we are compelled to ascribe the errors to the timing instrumentation. No phenomenon of the atmosphere or feature of the terrain could account for this pattern of results, which was observable in a surprisingly large proportion of the events examined.

Events Studied

Day	Event Number
11-8-74 (312)	12
11-8-74 (312)	14
11-8-74 (312)	92
11-15-74 (319)	95
11-18-74 (322)	41
11-19-74 (323)	13
11-19-74 (323)	34
12-2-74 (336)	9
12-2-74 (336)	94
12-2-74 (336)	176
12-3-74 (337)	91
12-5-74 (339)	21
12-5-74 (339)	33
12-5-74 (339)	69
12-5-74 (339)	83
12-5-74 (339)	85
12-5-74 (339)	87
12-5-74 (339)	97
12-5-74 (339)	99
12-7-74 (341)	230

Twenty Separate Events Studied

Microphone	Arrival Times Too Short	Arrival Times Too Long	Arrivals Correct	Uncertain or Missing Data
(5) N5	9	3	0	8
(6) N6	4	0	0	16
(7) N7	3	0	0	17
(8) N8, E1	12	1	0	7
(11) E2	11	3	0	6
(12) A1, W3	6	5	0	9
(13) A2	10	3	0	7
(14) A3, D3	10	2	0	8
(15) A4	4	0	0	16
(16) A5	1	0	0	19
(17) A6	12	0	0	8
(18) A7	14	2	0	4
(19) A8, E3	13	1	0	6
(21) D4	12	0	0	8
(24) D5	3	8	0	9
(26) B1, W6	7	3	0	10
(27) B2	8	4	1	7
(28) B3	6	6	0	8
(30) B5	3	5	0	12
(31) B6, D6	8	5	0	7
(32) B7	13	4	0	3
(33) B8, E6	11	6	0	3
(34) W7	6	2	0	12
(36) E7	3	5	0	12
(37) S1, W8	7	3	0	10
(44) S8, D8, E8	5	5	0	10
Totals	201	76	1	242
% based on all 520 possibilities	(38.7%)	(14.6%)	(0.2%)	(46.5%)
% based on only good reports (278)	(72.3%)	(27.3%)	(0.4%)	-----

Day: 11/8/74 (312) B6 (31)

Event: 12 B7 (32)

Gun: 2 B8 (33)

t_o = 14:00:0.335 MST d = 4,430.30'

W = 2.6 kts (4.39 ft/sec) from 330°.2 at 25' elev.

T = 52.5°F (11.4°C) at 26' elev.

C = 1,109.9 ft/sec

M = 0.0039565

θ = 323°.0

	Mike	True Distance r_2 (feet)	True Time r_2/c (sec)	Time Data t(sec)	Time Error $r_2/c - t$ (sec)
1.)	B6	9,405.76	8.474	8.476	-.002
2.)	B7	12,915.59	11,637	11.638	-.001
3.)	B8	16,864.62	15.195	15.208	-.013

True (t_2-t_1) = 3.162 sec

(t_2-t_1) Data = 3.162 sec (no error)

True (t_3-t_1) = 6.720 sec

(t_3-t_1) Data = 6.732 sec (long)

True S_2 = 3,509.83'

True S_3 = 7,458.86'

Data S_2 = 3,509.50' } R_o = 8,898.92' → 5.39% low

Data S_3 = 7,471.85' }

Wind S_2 = 3,523.50' } R_{wind} = 8,653.50' → 8.00% low

Wind S_3 = 7,499.85' }

True Ψ_3 = 23°.3

Ψ_3 = 22°.9

Ψ_{3wind} = 22°.5

Day: 11/8/74 (312) W6 (26)

Event: 12 W7 (34)

Gun: 2 W8 (37)

t_o = 14:00: 0.335 MST d = 4,430.33'

W = 2.6 kts (4.39 ft/sec) from 330°.2 at 25' elv.

T = 52.5°F (11.4°C) at 26' elv.

C = 1,109.9 ft/sec

M = 0.0039565

θ = 53°.0

	Mike	True Distance r_2 (feet)	True Time r_2/c (sec)	Time Data t(sec)	Time Error $r_2/c-t$ (sec)
1.)	W6	16,898.89	15.226	15.189	.037
2.)	W7	19,087.77	17.198	17.164	.034
3.)	W8	21,962.93	19.788	19.760	.028

True (t_2-t_1) = 1.972 sec

(t_2-t_1) Data = 1.975 sec (long)

True (t_3-t_1) = 4.563 sec

(t_3-t_1) Data = 4.571 sec (long)

True S_2 = 2,188.88'

True S_3 = 5,065.04'

Data S_2 = 2,192.05'
Data S_3 = 5,073.35'
} R_o = 16,776.88' → 0.722% low

Wind S_2 = 2,202.60'
Wind S_3 = 5,094.45'
} R_{wind} = 16,688.52' → 1.24% low

True ψ_3 = 45.°0

ψ_3 = 44.°9

ψ_{3wind} = 44.°7

Day: 11/8/74 (312) B6 (31)

Event: 14 B7 (32)

Gun: 2 B8 (33)

t_o = 14:02:05.367 MST d = 4,430.30'

W = 2.6 kts (4.39 ft/sec) from 330°.2 at 25' elev.

T = 52.5°F (11.4°C) at 26' elev.

C = 1,109.9 ft/sec

M = 0.0039565

θ = 323°.0

	Mike	True Distance r_2 (feet)	True Time r_2/c (sec)	Time Data t(sec)	Time Error $r_2/c - t$ (sec)
1.)	B6	9,405.76	8.474	8.545	-.071
2.)	B7	12,915.59	11.637	11.633	+.004
3.)	B8	16,864.62	15.195	15.202	-.007

True (t_2-t_1) = 3.162 sec

(t_2-t_1) Data = 3.088 sec (short)

True (t_3-t_1) = 6.720 sec

(t_3-t_1) Data = 6.657 sec (short)

True S_2 = 3,509.83'

True S_3 = 7,458.86'

Data S_2 = 3,427.37' } R_o = 7,640.05' → 18.8% low

Data S_3 = 7,388.60' }

Wind S_2 = 3,441.37' } R_{wind} = 7,431.93' → 21.0% low

Wind S_3 = 7,416.60' }

True Ψ_3 = 23°.3

Ψ_3 = 22°.5

Ψ_{3wind} = 22°.1

Day: 11/8/74 (312) W6 (26)

Event: 14 W7 (34)

Gun: 2 W8 (37)

t_o = 14:02:05.367 MST d = 4,430.33'

W = 2.6 kts (4.39 ft/sec) from 330°.2 at 25' elev.

T = 52.5°F (11.4°C) at 26' elev.

C = 1,109.9 ft/sec

M = 0.0039565

θ = 53°.0

	Mike	True Distance r_2 (feet)	True Time r_2/c (sec)	Time Data t(sec)	Time Error r_2/c-t (sec)
1.)	W6	16,898.89	15.226	15.195	.031
2.)	W7	19,087.77	17.198	17.169	.029
3.)	W8	21,962.93	19.788	19.764	.024

True (t_2-t_1) = 1.972 sec

(t_2-t_1) Data = 1.974 sec (long)

True (t_3-t_1) = 4.563 sec

(t_3-t_1) Data = 4.569 sec (long)

True S_2 = 2,188.88'

True S_3 = 5,064.04'

Data S_2 = 2,190.94'
Data S_3 = 5,071.13'
} R_o = 16,786.16' → 0.667% low

Wind S_2 = 2,201.49'
Wind S_3 = 5,092.23'
} R_{wind} = 16,697.83' → 1.19% low

True Ψ_3 = 45.°0

Ψ_3 = 44.°9

Ψ_{3wind} = 44.°7

Day: 11/8/74 (312) B6 (31)

Event: 92 B7 (32)

Gun: 2 B8 (33)

t_o = 17:20:00.178 MST d = 4,430.30'

W = 3.9 kts (6.587 ft/sec) from 266°.4 at 25'elev. T = 52.1°F (11.2°C) at 26' elev.

C = 1,109.5 ft/sec

M = 0.0059368

θ = 26°.8

	Mike	True Distance r_2 (feet)	True Time r_2/c (sec)	Time Data t(sec)	Time Error r_2/c-t (sec)
1.)	B6	9,405.76	8.477	8.472	+.005
2.)	B7	12,915.59	11.641	11.645	-.004
3.)	B8	16,864.62	15.200	15.220	-.020

True (t_2-t_1) = 3.163 sec

(t_2-t_1) Data = 3.173 sec (long)

True (t_3-t_1) = 6.723 sec

(t_3-t_1) Data = 6.748 sec (long)

True Ψ_3 = 23°.3

Ψ_3 = 22°.8

Ψ_{3wind} = 22°.1

True S_2 = 3,509.83'

True S_3 = 7,458.86'

Data S_2 = 3,520.44'

Data S_3 = 7,486.91' R_o = 8,954.88' → 4.79% low

Wind S_2 = 3,543.92'

Wind S_3 = 7,533.86' R_{wind} = 8,536.40' → 9.24% low

Day: 11/8/74 W6 (26)

Event: 92 W7 (34)

Gun: 2 W8 (37)

t_o = 17:20:00.178 MST d = 4,430.33'

W = 3.9 kts (6.587 ft/sec) from 266°.4 at 25' elev.

T = 52.1°F (11.2°C) at 26' elev.

C = 1,109.5 ft/sec

M = 0.0059368

θ = 116°.8

	Mike	True Distance r_2 (feet)	True Time r_2/c (sec)	Time Data t(sec)	Time Error $r_2/c - t$ (sec)
1.)	W6	16,898.89	15.231	15.100	.131
2.)	W7	19,087.77	17.204	17.073	.131
3.)	W8	21,962.93	19.795	19.679	.116

True (t_2-t_1) = 1.973 sec

(t_2-t_1) Data = 1.973 sec (no error)

True (t_3-t_1) = 4.564 sec

(t_3-t_1) Data = 4.579 sec (long)

True S_2 = 2,188.88'

True S_3 = 5,064.04'

Data S_2 = 2,189.04' } R_o = 16,394.93' → 2.98% low

Data S_3 = 5,080.40' }

Wind S_2 = 2,177.18' } R_{wind} = 16,492.38' → 2.41% low

Wind S_3 = 5,056.68' }

True ψ_3 = 45°.0

ψ_3 = 44°.6

ψ_{3wind} = 44°.8

Day: 11/15/74 (319) A3 (14)

Event: 95 A2 (13)

Gun: 1 A1 (12)

t_o = 09:15:00.087 MST d = 4,430.70'

W = 2.9 kts (4.898 ft/sec) from 211°.4 at 25'elev. T = 51.4°F (10.8°C) at 26' elev.

C = 1,108.7 ft/sec

M = 0.0044178

θ = 261°.8

	Mike	True Distance r_1 (feet)	True Time r_1/c (sec)	Time Data t(sec)	Time Error $r_1/c - t$ (sec)
1.)	A3	9,410.51	8.488	8.456	+.032
2.)	A2	12,941.68	11.673	11.697	-.024
3.)	A1	16,901.73	15.245	15.280	-.035

True (t_2-t_1) = 3.185 sec

(t_2-t_1) Data = 3.241 sec (long)

True (t_3-t_1) = 6.757 sec

(t_3-t_1) Data = 6.824 sec (long)

True S_2 = 3,531.17'

True S_3 = 7,491.22'

Data S_2 = 3,593.30' } R_o = 10,344.88' → 9.93% high

Data S_3 = 7,565.77' }

Wind S_2 = 3,590.51' } R_{wind} = 10,403.32' → 10.6% high

Wind S_3 = 7,560.19' }

True ψ_3 = 23°.0

ψ_3 = 23°.0

ψ_{3wind} = 23°.0

Day: 11/15/74 (319)
Event: 95
Gun: 1
t_o = 09:15:00.087 MST

B6 (31)
B7 (32)
B8 (33)
d = 4,430.30'

W = 2.9 kts (4.898 ft/sec) from 211°.4 at 25' elev

M = 0.0044178

θ = 81°.8

T = 51.4°F (10.8°C) at 26'elev

C = 1,108.7 ft/sec

	Mike	True Distance r_1 (feet)	True Time r_1/c (sec)	Time Data t(sec)	Time Error $r_1/c-t$ (sec)
1.)	B6	9,385.47	8.465	8.478	-.013
2.)	B7	12,891.24	11.627	11.641	- .014
3.)	B8	16,838.64	15.188	15,210	- .022

True (t_2-t_1) = 3.162 sec
(t_2-t_1) Data = 3.163 sec (little long)
True (t_3-t_1) = 6.722 sec
(t_3-t_1) Data = 6.732 sec (long)
True S_2 = 3,505.77'
True S_3 = 7,453.17'
Data S_2 = 3,506.82' } R_o = 9,044.97' → 3.63% low
Data S_3 = 7,463.77' }
Wind S_2 = 3,509.61' } R_{wind} = 8,995.90' → 4.15% low
Wind S_3 = 7,469.35' }

True Ψ_3 = 23°.3
Ψ_3 = 23°.0
Ψ_{3wind} = 22°.9

Day: 11/15/74 (319)
Event: 95
Gun: 1
t_o = 09:15:00.087 MST

W6 (26)
W7 (34)
W8 (37)
d = 4,430.33'

W = 2.9 kts (4.898 ft/sec) from 211°.4 at 25' elev

M = 0.0044178

θ = 171°.8

T = 51.4°F (10.8°C) at 26' elev

C = 1,108.7 ft/sec

	Mike	True Distance r_1 (feet)	True Time r_1/c (sec)	Time Data t(sec)	Time Error $r_1/c-t$ (sec)
1.)	W6	16,924.14	15.265	15.273	-.008
2.)	W7	19,109.90	17.236	17.253	-.017
3.)	W8	21,981.98	19.827	19.854	-.027

True (t_2-t_1) = 1.971 sec
(t_2-t_1) Data = 1.980 sec (long)
True (t_3-t_1) = 4.562 sec
(t_3-t_1) Data = 4.581 sec (long)
True S_2 = 2,185.76'
True S_3 = 5,057.84'
Data S_2 = 2,195.23'
Data S_3 = 5,078.95'
R_o = 16,774.38' → 0.885% low
Wind S_2 = 2,175.86'
Wind S_3 = 5,040.21'
R_{wind} = 16,936.10' → 0.0707% high (12 feet off) Excellent

True ψ_3 = 45.°8
ψ_3 = 44.°8
ψ_{3wind} = 45.°2

Day: 11/18/74 (322) A3 (14)

Event: 41 A2 (13)

Gun: 2 A1 (12)

t_o = 06:34:00.293 MST d = 4,430.70'

W = 1.7 kts (2.87 ft/sec) from 173°.7 at 25' elev T = 45.8°F (7.7°C) at 26' elev

C = 1,102.7 ft/sec

M = 0.0026038

θ = 299°.5

	Mike	True Distance r_2 (feet)	True Time r_2/c (sec)	Time Data t(sec)	Time Error $r_2/c - t$ (sec)
1.)	A3	9,390.03	8.515	8.358	.157
2.)	A2	12,917.24	11.714	11.620	.094
3.)	A1	16,875.70	15.304	15.161	.143

True (t_2-t_1) = 3.199 sec

(t_2-t_1) Data = 3.262 sec (long)

True (t_3-t_1) = 6.788 sec

(t_3-t_1) Data = 6.803 sec (long)

True $\psi_3 = 23.^\circ 1$

$\psi_3 = 25.^\circ 3$

$\psi_{3wind} = 25.^\circ 2$

True S_2 = 3,527.21'

True S_3 = 7,485.67'

Data S_2 = 3,597.01'
Data S_3 = 7,501.67' } R_o = 14,406.17' → 53.4% high

Wind S_2 = 3,602.69'
Wind S_3 = 7,513.03' } R_{wind} = 14,261.88' → 51.9% high

Day: 11/18/74 (322) A6 (17) d_2 = 17,720.99'

Event: 41 A2 (13) d_3 = 4,430.45'

Gun: 2 A1 (12) D = 22,151.44'

t_o = 06:34:00.293 MST

W = 1.7 kts (2.87 ft/sec) from 173°.7 at 25'elev

T = 45.8°F (7.7°C) at 26' elev

C = 1,102.7 ft/sec

M = 0.0026038

θ = 299°.5

	Mike	True Distance r_2 (feet)	True Time r_2/c (sec)	Time Data t(sec)	Time Error r_2/c-t (sec)
1.)	A6	9,364.19	8.492	8.382	.110
2.)	A2	12,917.24	11.714	11.620	.094
3.)	A1	16,875.70	15.304	15.161	.143

True (t_2-t_1) = 3.222 sec

(t_2-t_1) Data = 3.238 sec (long)

True (t_3-t_1) = 6.812 sec

(t_3-t_1) Data = 6.779 sec (short)

True S_2 = 3,553.05'

True S_3 = 7,511.51'

Data S_2 = 3,570.54' }
Data S_3 = 7,475.20' } R_o = 9,661.13' → 3.17% high

Wind S_2 = 3,593.26' }
Wind S_3 = 7,503.60' } R_{wind} = 9,624.28' → 2.78% high

True ψ_3 = 23°.1

ψ_3 = 24°.5

ψ_{3wind} = 24°.3

Day: 11/18/74 (322) B5 (30) d_2 = 8861.11'

Event: 41 B7 (32) d_3 = 4,430.36'

Gun: 2 B8 (33) $D = d_2 + d_3$ = 13291.47'

t_o = 06:34:00.293 MST

W = 1.7 kts (2.87 ft/sec) from 173°.7 at 25' elev

T = 45.8°F (7.7°C) at 26' elev

C = 1,102.7 ft/sec

M = 0.0026038

θ = 119°.5

	Mike	True Distance r_2 (feet)	True Time r_2/c (sec)	Time Data t(sec)	Time Error $r_2/c - t$ (sec)
1.)	B5	7,026.36	6.372	6.368	.004
2.)	B7	12,915.59	11.713	11.693	.020
3.)	B8	16,864.62	15.294	15.279	.015

True (t_2-t_1) = 5.341 sec

(t_2-t_1) Data = 5.325 sec (short)

True (t_3-t_1) = 8.922 sec

(t_3-t_1) Data = 8.911 sec (short)

True S_2 = 5,889.23'

True S_3 = 9,838.26'

Data S_2 = 5,871.88'

Data S_3 = 9,826.16'

R_o = 6,897.74' → 1.83% low

Wind S_2 = 5,860.52'

Wind S_3 = 9,809.12'

R_{wind} = 6,963.86' → 0.605% low

True ψ_3 = 23°.3

ψ_3 = 23°.1

ψ_{3wind} = 23°.3

Day: 11/18/74 B6 (31)

Event: 41 B7 (32)

Gun: 2 B8 (33)

t_o = 06:34:00.293 MST d = 4,430.30'

W = 1.7 kts (2.87 ft/sec) from 173°.7 at 25' elev T = 45.8°F (7.7°C) at 26' elev

C = 1,102.7 ft/sec

M = 0.0026038

θ = 119°.5

	Mike	True Distance r_2 (feet)	True Time r_2/c (sec)	Time Data t(sec)	Time Error $r_2/c-t$ (sec)
1.)	B6	9,405.76	8.530	8.517	.013
2.)	B7	12,915.59	11.713	11.693	.020
3.)	B8	16,864.62	15.294	15.279	.015

True (t_2-t_1) = 3.183 sec

(t_2-t_1) Data = 3.176 (short)

True (t_3-t_1) = 6.764 sec

(t_3-t_1) Data = 6.762 (short)

True S_2 = 3,509.83'

True S_3 = 7,458.86'

Data S_2 = 3,502.18' } R_o = 9,054.25' → 3.74% low

Data S_3 = 7,456.46' }

Wind S_2 = 3,496.50' } R_{wind} = 9,153.54' → 2.68% low

Wind S_3 = 7,445.10' }

True ψ_3 = 23°.3

ψ_3 = 23°.1

ψ_{3wind} = 23°.3

Day: 11/18/74 (322) W6 (26)

Event: 41 W7 (34)

Gun: 2 W8 (37)

t_o = 06:34:00.293 MST d = 4,430.33'

W = 1.7 kts (2.87 ft/sec) from 173°.7 at 25' elev

T = 45.8°F (7.7°C) at 26' elev

C = 1,102.7 ft/sec

M = 0.0026038

θ = 209°.5

	Mike	True Distance r_2 (feet)	True Time r_2/c (sec)	Time Data t(sec)	Time Error $r_2/c - t$ (sec)
1.)	W6	16,898.89	15.325	15.260	.065
2.)	W7	19,087.77	17.310	17.247	.063
3.)	W8	21,962.93	19.917	19.864	.053

True (t_2-t_1) = 1.985 sec

(t_2-t_1) Data = 1.987 sec (long)

True (t_3-t_1) = 4.592 sec

(t_3-t_1) Data = 4.604 sec (long)

True S_2 = 2,188.88'

True S_3 = 5,064.04'

Data S_2 = 2,191.06' } R_o = 16,613.59' → 1.69% low

Data S_3 = 5,076.83' }

Wind S_2 = 2,181.02' } R_{wind} = 16,696.62 → 1.20% low

Wind S_3 = 5,056.75' }

True ψ_3 = 45.°0

ψ_3 = 44.°8

ψ_{3wind} = 44.°9

Day: 11/19/74 (323) A3 (14)

Event: 13 A2 (13)

Gun: 1 A1 (12)

t_o = 06:36:59.968 MST d = 4,430.70'

W = 5.9 kts (9.97 ft/sec) from 274°.8 at 25' elev

T = 56.4°F (13.5°C) at 26' elev

C = 1,114.0 ft/sec

M = 0.008945

θ = 198°.4

	Mike	True Distance r_1 (feet)	True Time r_1/c (sec)	Time Data t(sec)	Time Error $r_1/c - t$ (sec)
1.)	A3	9,410.51	8.447	8.325*	.122
2.)	A2	12,941.68	11.617	11.504*	.113
3.)	A1	16,901.73	15.172	15.099	.073

True (t_2-t_1) = 3.170 sec

(t_2-t_1) Data = 3.179 sec (long)

True (t_3-t_1) = 6.725 sec

(t_3-t_1) Data = 6.774 sec (long)

True S_2 = 3,531.17'

True S_3 = 7,491.22'

Data S_2 = 3,541.41'
Data S_3 = 7,546.24' } R_o = 7,983.73' → 15.2% low

Wind S_2 = 3,503.80'
Wind S_3 = 7,471.03' } R_{wind} = 8,630.37' → 8.29% low

True ψ_3 = 23°.0

ψ_3 = 21°.6

ψ_{3wind} = 22°.7

(* Traces available for these mikes)

Day: 11/19/74 (323) A6 (17)

Event: 13 A7 (18)

Gun: 1 A8 (19)

t_o = 06:36:59.968 MST d = 4,430.39'

W = 5.9 kts (9.97 ft/sec) from 274°.8 at 25' elev

T = 56.4° F (13.5°C) at 26' elev

C = 1,114.0 ft/sec

M = 0.008945

θ = 341°.6

	Mike	True Distance r_1 (feet)	True Time r_1/c (sec)	Time Data t(sec)	Time Error $r_1/c-t$ (sec)
1.)	A6	9,345.14	8.389	8.079*	.310
2.)	A7	12,862.16	11.546	11.116*	.430
3.)	A8	16,816.25	15.095	14.529	.566

True (t_2-t_1) = 3.157 sec

(t_2-t_1) Data = 3.037 sec (short)

True (t_3-t_1) = 6.707 sec

(t_3-t_1) Data = 6.450 sec (short)

True S_2 = 3,517.02'

True S_3 = 7,471.11'

Data S_2 = 3,383.22' } R_o = 12,558.53' → 34.4% high

Data S_3 = 7,185.30' }

Wind S_2 = 3,420.82' } R_{wind} = 11,872.09' → 27.0% high

Wind S_3 = 7,260.51' }

True Ψ_3 = 23°.2

Ψ_3 = 27°.4

Ψ_{3wind} = 26°.4

(* Traces available for these mikes)

Day: 11/19/74 (323) B3 (28)

Event: 13 B2 (27)

Gun: 1 B1 (26)

t_o = 06:36:59.968 MST d = 4,430.13'

W = 5.9 kts (9.97 ft/sec) from 274°.8 at 25' elev

T = 56.4°F (13.5°C) at 26' elev

C = 1,114.0 ft/sec

M = 0.008945

θ = 161°.6

	Mike	True Distance r_1 (feet)	True Time r_1/c (sec)	Time Data t(sec)	Time Error $r_1/c - t$ (sec)
1.)	B3	9,451.63	8.484	8.545	-.061
2.)	B2	12,970.57	11.643	11.643*	.000
3.)	B1	16,924.14	15.192	15.152	+.040

True (t_2-t_1) = 3.159 sec

(t_2-t_1) Data = 3.098 sec (short)

True (t_3-t_1) = 6.708 sec

(t_3-t_1) Data = 6.607 sec (short)

True S_2 = 3,518.94'

True S_3 = 7,472.51'

Data S_2 = 3,451.17' } R_o = 9,719.90' → 2.84% high

Data S_3 = 7,360.20' }

Wind S_2 = 3,413.57' } R_{wind} = 10,358.84' → 9.60% high

Wind S_3 = 7,285.00' }

True Ψ_3 = 23°.2

Ψ_3 = 24°.3

Ψ_{3wind} = 25°.4

(* Trace available for this mike)

Day: 11/19/74 (323)
Event: 13
Gun: 1
t_o = 06:36:59.968 MST

D4 (21)
A6 (17)
E2 (11)
d = 9,906.40'

W = 5.9 kts (9.97 ft/sec) from 274.°8 at 25' elev.
M = 0.008945
θ = 8.°2

T = 56.4°F (13.5°C) at 26' elev.
C = 1,114.0 ft/sec.

	Mike	True Distance r_1 (feet)	True Time r_1/c (sec)	Time Data t(sec)	Time Error $r_1/c - t$ (sec)
1.)	D4	3,145.89	2.824	2.775*	.049
2.)	A6	9,345.14	8.389	8.079*	.310
3.)	E2	19,001.28	17.057	16.447	.610

True (t_2-t_1) = 5.565 sec
(t_2-t_1) Data = 5.304 sec (short)
True (t_3-t_1) = 14.233 sec
(t_3-t_1) Data = 13.672 sec (short)
True S_2 = 6,199.25'
True S_3 = 15,855.39'
Data S_2 = 5,908.66' } R_o = 4,999.07' → 58.9% high
Data S_3 = 15,230.61' }
Wind S_2 = 5,996.37' } R_{wind} = 4,517.73' → 43.6% high
Wind S_3 = 15,406.03' }

True ψ_3 = 9.°0
ψ_3 = 14.°3
ψ_{3wind} = 13.°1

(*Traces available for these mikes)

Day: 11/19/74 (323)
Event: 13
Gun: 1
t_o = 06:36:59.968 MST

D5 (24) d_2 = 12,531.48'
A7 (18) d_3 = 6,265.36'
E2 (11) D = 18,796.84'

W = 5.9 kts (9.97 ft/sec) from 274°.8 at 25' elev.
M = 0.008945
θ = 333°.4

T = 56.4°F (13.5°C) at 26' elev.
C = 1,114.0 ft/sec.

	Mike	True Distance r_1 (feet)	True Time r_1/c (sec)	Time Data t(sec)	Time Error r_1/c-t (sec)
1.)	D5	3,120.22	2.801	2.804*	−.003
2.)	A7	12,862.16	11.546	11.116*	+.430
3.)	E2	19,001.28	17.057	16.447	+.610

True (t_2-t_1) = 8.745 sec
(t_2-t_1) Data = 8.312 sec (short)
True (t_3-t_1) = 14.256 sec
(t_3-t_1) Data = 13.643 sec (short)
True S_2 = 9,741.94'
True S_3 = 15,881.06'
Data S_2 = 9,259.57' } R_o = 5,876.57' → 88.3% high
Data S_3 = 15,198.30'
Wind S_2 = 9,359.80' } R_{wind} = 5,191.76' → 66.4% high
Wind S_3 = 15,348.64'

True ψ_3 = 9°.5
ψ_3 = 15°.6
ψ_{3wind} = 14°.3

(* Traces available for these mikes.)

Day: 11/19/74 (323)
Event: 13
Gun: 1
t_o = 06:36:59.968 MST

E6 (33)
E7 (36)
E8 (44)
d = 4,430.32'

W = 5.9 kts (9.97 ft/sec) from 274.8° at 25' elev.
M = 0.008945
θ = 251.6°

T = 56.4°F (13.5°C) at 26' elev.
C = 1,114.0 ft/sec

	Mike	True Distance r_1 (feet)	True Time r_1/c (sec)	Time Data t(sec)	Time Error $r_1/c - t$ (sec)
1.)	E6	16,838.64	15.115	14.739	.376
2.)	E7	19,034.19	17.086	16.789	.297
3.)	E8	21,916.19	19.673	19.461	.212

True (t_2-t_1) = 1.971 sec.
(t_2-t_1) Data = 2.050 sec. (long)
True (t_3-t_1) = 4.558 sec.
(t_3-t_1) Data = 4.722 sec. (long)
True S_2 = 2,195.55'
True S_3 = 5,077.55'
Data S_2 = 2,283.70' } R_o = 15,886.03' → 5.66% low
Data S_3 = 5,260.31'
Wind S_2 = 2,271.19' } R_{wind} = 15,993.29' → 5.02% low
Wind S_3 = 5,235.29'

True ψ_3 = 44.9°
ψ_3 = 43.2°
ψ_{3wind} = 43.4°

Day: 11/19/74 (323) A3 (14)

Event: 34 A2 (13)

Gun: 1 A1 (12)

t_o = 07:34:00.389 MST d = 4,430.70'

W = 5.4 kts (9.12 ft/sec) from 137°.3 at 25' elev T = 57.2°F (14.0°C) at 26' elev

C = 1,115.0 ft/sec

M = 0.008180

θ = 335°.9

	Mike	True Distance r_1 (feet)	True Time r_1/c (sec)	Time Data t(sec)	Time Error r_1/c-t (sec)
1.)	A3	9,410.51	8.440	8.445*	-.005
2.)	A2	12,941.68	11.607	11.698*	-.091
3.)	A1	16,901.73	15.159	15.329	-.170

True (t_2-t_1) = 3.167 sec

(t_2-t_1) Data = 3.253 sec (long)

True (t_3-t_1) = 6.719 sec

(t_3-t_1) Data = 6.884 sec (long)

True S_2 = 3,531.17'

True S_3 = 7,491.22'

Data S_2 = 3,627.10' } R_o = 7,898.92' → 16.1% low

Data S_3 = 7,675.66' }

Wind S_2 = 3,660.18' } R_{wind} = 7,260.43' → 22.8% low

Wind S_3 = 7,741.83' }

True ψ_3 = 23°.0

ψ_3 = 20°.4

ψ_{3wind} = 19°.3

(*Traces available for these mikes)

Day: 11/19/74 (323)
Event: 34
Gun: 1
t_o = 07:34:00.389 MST

A6 (17)
A7 (18)
A8 (19)
d = 4,430.39'

W = 5.4 kts (9.12 ft/sec) from 137°.3 at 25' elev

T = 57.2°F (14.0°C) at 26' elev

C = 1,115.0 ft/sec

M = 0.008180

θ = 204°.1

	Mike	True Distance r_1 (feet)	True Time r_1/c (sec)	Time Data t(sec)	Time Error $r_1/c-t$ (sec)
1.)	A6	9,345.14	8.381	8.238*	.143
2.)	A7	12,862.16	11.536	11.384*	.152
3.)	A8	16,816.25	15.082	14.806	.276

True (t_2-t_1) = 3.154 sec
(t_2-t_1) Data = 3.146 sec (short)
True (t_3-t_1) = 6.701 sec
(t_3-t_1) Data = 6.568 sec (short
True S_2 = 3,517.02'
True S_3 = 7,471.11'
Data S_2 = 3,507.79'
Data S_3 = 7,323.32'
R_o = 16,629.10' → 77.9% high
Wind S_2 = 3,474.71'
Wind S_3 = 7,257.16'
R_{wind} = 17,445.83' → 86.7% high

True ψ_3 = 23°.2
ψ_3 = 27°.7
ψ_{3wind} = 28°.6

(* Traces available for these mikes)

Day: 11/19/74 (323) B5 (30) d_2 = 8,860.58'

Event: 34 B3 (28) d_3 = 4,429.34'

Gun: 1 B2 (27) D = 13,289.92'

t_o = 07:34:00.389 MST

W = 5.4 kts (9.12 ft/sec) from 137°.3 at 25' elev

T = 57.2°F (14.0°C) at 26' elev

C = 1,115.0 ft/sec

M = 0.008180

θ = 24°.1

	Mike	True Distance r_1 (feet)	True Time r_1/c (sec)	Time Data t(sec)	Time Error $r_1/c-t$ (sec)
1.)	B5	7,016.80	6.293	6.311	-.018
2.)	B3	9,451.63	8.477	8.591	-.114
3.)	B2	12,970.57	11.633	11.793*	-.160

True (t_2-t_1) = 2.184 sec

(t_2-t_1) Data = 2.280 sec (long)

True (t_3-t_1) = 5.340 sec

(t_3-t_1) Data = 5.482 sec (long)

True S_2 = 2,434.83'

True S_3 = 5,953.77'

Data S_2 = 2,542.20'
Data S_3 = 6,112.43
} R_o = 6,783.77' → 3.32% low

Wind S_2 = 2,608.36'
Wind S_3 = 6,211.67'
} R_{wind} = 6,628.94' → 5.53% low

True ψ_3 = 31°.0

ψ_3 = 30°.0

ψ_{3wind} = 29°.3

(* Trace available for this mike)

Day: 11/19/74 (323) D4 (21)

Event: 34 A6 (17)

Gun: 1 E2 (11)

t_o = 07:34:00.389 MST d = 9,906.40'

W = 5.4 kts (9.12 ft/sec) from 137°.3 at 25' elev

T = 57.2°F (14.0°C) at 26' elev

C = 1,115.0 ft/sec

M = 0.008180

θ = 230°.7

	Mike	True Distance r_1 (feet)	True Time r_1/c (sec)	Time Data t(sec)	Time Error $r_1/c - t$ (sec)
1.)	D4	3,145.89	2.821	2.815*	.006
2.)	A6	9,345.14	8.381	8.238*	.143
3.)	E2	19,001.28	17.042	16.806	.236

True (t_2-t_1) = 5.560 sec

(t_2-t_1) Data = 5.423 sec (short)

True (t_3-t_1) = 14.220 sec

(t_3-t_1) Data = 13.991 sec

True ψ_3 = 9°.0

ψ_3 = 10°.8

ψ_{3wind} = 11°.6

True S_2 = 6,199.25'

True S_3 = 15855.39'

Data S_2 = 6,046.65' } R_o = 3,712.70' → 18.0% high

Data S_3 = 15,599.97' }

Wind S_2 = 5,995.32' } R_{wind} = 3,991.57' → 26.9% high

Wind S_3 = 15,497.32' }

(* Traces available for these mikes)

Day: 11/19/74 (323)
Event: 34
Gun: 1
t_o = 07:34:00.389 MST

D5 (24)
A7 (18)
E2 (11)

d_2 = 12,531.48'
d_3 = 6,265.36'
D = 18,796.84'

W = 5.4 kts (9.12 ft/sec) from 137°.3 at 25' elev

T = 57.2°F (14.0°C) at 26' elev
C = 1,115.0 ft/sec

M = 0.008180
θ = 110°.9

	Mike	True Distance r_1 (feet)	True Time r_1/c (sec)	Time Data t(sec)	Time Error $r_1/c - t$ (sec)
1.)	D5	3,120.22	2.798	2.791*	.007
2.)	A7	12,862.16	11.536	11.384*	.152
3.)	E2	19,001.28	17.042	16.806	.236

True (t_2-t_1) = 8.737 sec
(t_2-t_1) Data = 8.593 sec (short)
True (t_3-t_1) = 14.243 sec
(t_3-t_1) Data = 14.015 sec (short)
True S_2 = 9,741.94'
True S_3 = 15,881.06'
Data S_2 = 9,581.20'
Data S_3 = 15,626.73'
R_o = 4,489.48' → 43.9% high
Wind S_2 = 9,544.63'
Wind S_3 = 15,571.88'
R_{wind} = 4,753.21' → 52.3% high

True ψ_3 = 9°.5
ψ_3 = 12°.7
ψ_{3wind} = 13°.2

(* Traces available for these mikes)

Day: 11/19/74 (323)
Event: 34
Gun: 1
t_o = 07:34:00.389 MST

E6 (33)
E7 (36)
E8 (44)
d = 4,430.32'

W = 5.4 kts (9.12 ft/sec) from 137°.3 at 25' elev
M = 0.008180
θ = 114°.1

T = 57.2°F (14.0°C) at 26' elev
C = 1,115.0 ft/sec

	Mike	True Distance r_1 (feet)	True Time r_1/c (sec)	Time Data t(sec)	Time Error $r_1/c - t$ (sec)
1.)	E6	16,838.64	15.102	14.897	.205
2.)	E7	19,034.19	17.071	16.864	.207
3.)	E8	21,916.19	19.656	19.555	.101

True (t_2-t_1) = 1.969 sec
(t_2-t_1) Data = 1.967 sec (short)
True (t_3-t_1) = 4.554 sec
(t_3-t_1) Data = 4.658 sec (long)
True S_2 = 2,195.55'
True S_3 = 5,077.55'
Data S_2 = 2,193.21'
Data S_3 = 5,193.67'
R_o = 13,565.56' → 19.4% low
Wind S_2 = 2,178.41'
Wind S_3 = 5,164.07'
R_{wind} = 13,675.31' → 18.8% low

True ψ_3 = 44°.9
ψ_3 = 42°.2
ψ_{3wind} = 42°.4

Day: 12/2/74 (336) A3 (14)

Event: 9 A2 (13)

Gun: 2 A1 (12)

t_o = 06:32:02.083 MST d = 4,430.70'

W = 1.8 kts (3.04 ft/sec) from 200°.1 at 25' elev T = 36.3°F (2.4°C) at 26' elev

C = 1,092.2 ft/sec

M = 0.0027835

θ = 273°.1

	Mike	True Distance r_2 (feet)	True Time r_2/c (sec)	Time Data t(sec)	Time Error $r_2/c - t$ (sec)
1.)	A3	9,390.03	8.597	8.552	+.045
2.)	A2	12,917.24	11.827	11.882	-.055
3.)	A1	16,875.70	15.451	15.507	-.056

True (t_2-t_1) = 3.229 sec

(t_2-t_1) Data = 3.330 sec (long)

True (t_3-t_1) = 6.854 sec

(t_3-t_1) Data = 6.955 sec (long)

True S_2 = 3,527.21'

True S_3 = 7,485.67'

Data S_2 = 3,637.03' } R_o = 12,438.57' → 32.5% high

Data S_3 = 7,596.25' }

Wind S_2 = 3,637.70' } R_{wind} = 12,422.72' → 32.3% high

Wind S_3 = 7,597.58' }

True ψ_3 = 23°.1

ψ_3 = 23°.7

ψ_{3wind} = 23°.7

Day: 12/2/74 (336) B6 (31)

Event: 9 B7 (32)

Gun: 2 B8 (33)

t_o = 06:32:02.083 MST d = 4,430.30'

W = 1.8 kts (3.04 ft/sec) from 200°.1 at 25' elev T = 36.3°F (2.4°C) at 26' elev

C = 1,092.2 ft/sec

M = 0.0027835

θ = 93°.1

	Mike	True Distance r_2 (feet)	True Time r_2/c (sec)	Time Data t(sec)	Time Error r_2/c-t (sec)
1.)	B6	9,405.76	8.612	8.519	.093
2.)	B7	12,915.59	11.825	11.703	.122
3.)	B8	16,864.62	15.441	15.311	.130

True (t_2-t_1) = 3.214 sec

(t_2-t_1) Data = 3.184 sec (short)

True (t_3-t_1) = 6.829 sec

(t_3-t_1) Data = 6.792 sec (short)

True S_2 = 3,509.83'

True S_3 = 7,458.86'

Data S_2 = 3,477.56' } R_o = 9,082.24' → 3.44% low

Data S_3 = 7,418.22' }

Wind S_2 = 3,476.89' } R_{wind} = 9,093.29' → 3.32% low

Wind S_3 = 7,416.89' }

True ψ_3 = 23°.3

ψ_3 = 23°.4

ψ_{3wind} = 23°.5

Day: 12/2/74 (336) E6 (33)

Event: 9 E7 (36)

Gun: 2 E8 (44)

t_o = 06:32:02.083 MST d = 4,430.32'

W = 1.8 kts (3.04 ft/sec) from 200°.1 at 25' elev T = 36.3°F (2.4°C) at 26' elev

C = 1,092.2 ft/sec

M = 0.0027835

θ = 176°.9

	Mike	True Distance r_2 (feet)	True Time r_2/c (sec)	Time Data t(sec)	Time Error r_2/c-t (sec)
1.)	E6	16,864.62	15.441	15.311	.130
2.)	E7	19,057.40	17.449	17.385	.064
3.)	E8	21,936.54	20.085	19.985	.100

True (t_2-t_1) = 2.008 sec

(t_2-t_1) Data = 2.074 sec (long)

True (t_3-t_1) = 4.644 sec

(t_3-t_1) Data = 4.674 sec (long)

True S_2 = 2,192.78'

True S_3 = 5,071.92'

Data S_2 = 2,265.22' } R_o = 20,415.58' → 21.1% high

Data S_3 = 5,104.94' }

Wind S_2 = 2,252.91' } R_{wind} = 20,537.46' → 21.8% high

Wind S_3 = 5,080.31' }

True ψ_3 = 44°.9

ψ_3 = 46°.2

ψ_{3wind} = 46°.4

Day: 12/2/74 (336) A3 (14)

Event: 94 A2 (13)

Gun: 2 A1 (12)

t_o = 09:44:00.075 MST d = 4,430.70'

W = 1.4 kts (2.365 ft/sec) from 281°.7 at 25' elev

T = 42.3°F (5.7°C) at 26' elev

C = 1,098.7 ft/sec

M = 0.002152

θ = 191°.5

	Mike	True Distance r_2 (feet)	True Time r_2/c (sec)	Time Data t(sec)	Time Error r_2/c-t (sec)
1.)	A3	9,390.03	8.546	8.476	+.070
2.)	A2	12,917.24	11.757	11.751	+.006
3.)	A1	16,875.70	15.360	15.378	-.018

True (t_2-t_1) = 3.210 sec

(t_2-t_1) Data = 3.275 sec (long)

True (t_3-t_1) = 6.813 sec

(t_3-t_1) Data = 6.902 sec (long)

True S_2 = 3,527.21'

True S_3 = 7,485.67'

Data S_2 = 3,598.24' } R_o = 9,892.04' → 5.35% high

Data S_3 = 7,583.23' }

Wind S_2 = 3,588.90' } R_{wind} = 10,084.74' → 7.40% high

Wind S_3 = 7,564.54' }

True ψ_3 = 23°.1

ψ_3 = 22°.5

ψ_{3wind} = 22°.8

Shock Wave Influence

Day: 12/2/74 (336) A3 (14)

Event: 94 A2 (13)

Gun: 2 A1 (12)

t_o = 09:44:00.075 MST

Data S_2 = 3,598.24' True S_2 = 3,527.21'

Data S_3 = 7,583.23' True S_3 = 7,485.67'

R_o = 9,892.04' → 5.35% high True R = 9,390.03'

True ψ_3 = 23°.1

	Using True R		Using Ro	
(1) K = 1.5:	S_2 = 3599.32', S_3 = 7585.51'	→ R 9,864.36', ψ_3 = 22°.5	S_2 = 3599.26', S_3 = 7585.38'	→ R = 9,866.05', ψ_3 = 22°.5
(2) K = 5.0:	S_2 = 3601.84', S_3 = 7590.82'	→ R = 9,800.28', ψ_3 = 22°.4	S_2 = 3601.65', S_3 = 7590.41'	→ R = 9,805.54', ψ_3 = 22°.4
(3) K = 10:	S_2 = 3605.44', S_3 = 7598.41'	→ R = 9,708.62' → 3.39% high, ψ_3 = 22°.3	S_2 = 3605.05', S_3 = 7597.58'	→ R = 9,718.89 → 3.50% low, ψ_3 = 22°.3
(4) K = 50:	S_2 = 3634.25', S_3 = 7659.12'	→ R = 8,980.12' → 4.37% low, ψ_3 = 21°.3	S_2 = 3632.30', S_3 = 7655.00'	→ R = 9,029.70' → 3.84% low, ψ_3 = 21°.4
(5) K = 100:	S_2 = 3670.26', S_3 = 7735.01'	→ R = 8,078.08' → 14.0% low, ψ_3 = 20°.0	S_2 = 3666.35', S_3 = 7726.78'	→ R = 8,175.14' → 12.9% low, ψ_3 = 20°.2

Day: 12/2/74 (336) A6 (17)

Event: 94 A7 (18)

Gun: 2 A8 (19)

t_o = 09:44:00.075 MST d = 4,430.41'

W = 1.4 kts (2.365 ft/sec) from 281°.7 at 25' elev

T = 42.3°F (5.7°C) at 26' elev

C = 1,098.7 ft/sec

M = 0.002152

θ = 348°.5

	Mike	True Distance r_2 (feet)	True Time r_2/c (sec)	Time Data t(sec)	Time Error r_2/c-t (sec)
1.)	A6	9,364.19	8.523	8.462	.061
2.)	A7	12,885.60	11.728	11.694	.034
3.)	A8	16,841.52	15.329	15.295	.034

True (t_2-t_1) = 3.205 sec

(t_2-t_1) Data = 3.232 sec (long)

True (t_3-t_1) = 6.806 sec

(t_3-t_1) Data = 6.833 sec (long)

True S_2 = 3,521.41'

True S_3 = 7,477.33'

Data S_2 = 3,551.00' } R_o = 10,008.03' → 6.88% high

Data S_3 = 7,507.42' }

Wind S_2 = 3,560.34' } R_{wind} = 9,825.09' → 4.92% high

Wind S_3 = 7,526.11' }

True ψ_3 = 23°.1

ψ_3 = 23°.3

ψ_{3wind} = 23°.0

Shock Wave Influences

Day: 12/2/74 (336) A6 (17)

Event: 94 A7 (18)

Gun: 2 A8 (19)

t_o = 09:44:00.075 MST

Data S_2 = 3,551.00'

Data S_3 = 7,507.42'

R_o = 10,008.03' → 6.88% high

True S_2 = 3,521.41'

True S_3 = 7,477.33'

True R = 9,364.19'

True Ψ_3 = 23°.1

	Using True R		Using Ro	
(1) K = 1.5:	S_2 = 3552.07', S_3 = 7509.68'	→ R = 9,981.97', Ψ_3 = 23°.2	S_2 = 3552.00', S_3 = 7509.53'	→ R = 9983.77', Ψ_3 = 23°.2
(2) K = 5.0:	S_2 = 3554.56', S_3 = 7514.96'	→ R = 9920.46', Ψ_3 = 23°.2	S_2 = 3554.32', S_3 = 7514.44'	→ R = 9926.86', Ψ_3 = 23°.2
(3) K = 10:	S_2 = 3558.13', S_3 = 7522.49'	→ R = 9834.07' → 5.02% high, Ψ_3 = 23°.0	S_2 = 3557.64', S_3 = 7521.46'	→ R = 9845.77' → 5.14% high, Ψ_3 = 23°.1
(4) K = 50:	S_2 = 3586.64', S_3 = 7582.77'	→ R = 9141.42' → 2.38% low, Ψ_3 = 22°.1	S_2 = 3584.19', S_3 = 7577.60'	→ R = 9200.28' → 1.75% low, Ψ_3 = 22°.2
(5) K = 100:	S_2 = 3622.28', S_3 = 7658.12'	→ R = 8284.27' → 11.5% low, Ψ_3 = 20°.8	S_2 = 3617.39', S_3 = 7647.77'	→ R = 8401.78' → 10.3% low, Ψ_3 = 21°.0

Day: 12/2/74 (336) B6 (31)

Event: 94 B7 (32)

Gun: 2 B8 (33)

t_o = 09:44:00.075 MST d = 4,430.30'

W = 1.4 kts (2.365 ft/sec) from 281°.7 at 25'elev T = 42.3°F (5.7°C) at 26' elev

C = 1,098.7 ft/sec

M = 0.002152

θ = 11.°5

	Mike	True Distance r_2 (feet)	True Time r_2/c (sec)	Time Data t(sec)	Time Error r_2/c-t (sec)
1.)	B6	9,405.76	8.561	8.563	-.002
2.)	B7	12,915.59	11.755	11.753	+.002
3.)	B8	16,864.62	15.350	15.353	-.003

True (t_2-t_1) = 3.195 sec

(t_2-t_1) Data = 3.190 sec (short)

True (t_3-t_1) = 6.789 sec

(t_3-t_1) Data = 6.790 sec (long)

True S_2 = 3,509.83'

True S_3 = 7,458.86'

Data S_2 = 3,504.85' } R_o = 9,067.12' → 3.60% low

Data S_3 = 7,460.17' }

Wind S_2 = 3,514.19' } R_{wind} = 8,902.54' → 5.35% low

Wind S_3 = 7,478.86' }

True ψ_3 = 23.°3

ψ_3 = 23.°1

ψ_{3wind} = 22.°8

Day: 12/2/74 (336) E3 (19)

Event: 94 E2 (11)

Gun: 2 E1 (8)

t_o = 09:44:00.075 MST d = 4,430.33'

W = 1.4 kts (2.365 ft/sec) from 281°.7 at 25' elev T = 42.3°F (5.7°C) at 26' elev

C = 1,098.7 ft/sec

M = 0.002152

θ = 281°.5

	Mike	True Distance r_2 (feet)	True Time r_2/c (sec)	Time Data t(sec)	Time Error r_2/c-t (sec)
1.)	E3	16,841.52	15.329	15.295	.034
2.)	E2	19,023.42	17.314	17.271	.043
3.)	E1	21,895.15	19.928	19.780	.148

True (t_2-t_1) = 1.986 sec

(t_2-t_1) Data = 1.976 sec (short)

True (t_3-t_1) = 4.600 sec

(t_3-t_1) Data = 4.485 sec (short)

True Ψ_3 = 45°.0

Ψ_3 = 47°.6

$\Psi_{3\text{-wind}}$ = 47°.5

True S_2 = 2,181.90'

True S_3 = 5,053.63'

Data S_2 = 2,171.03' }
Data S_3 = 4,927.67' } R_o = 20,833.37' → 23.7% high

Wind S_2 = 2,172.93' }
Wind S_3 = 4,931.47' } R_{wind} = 20,815.48' → 23.6% high

Shock Wave Influence

Day: 12/2/74 (336) E3 (19)

Event: 94 E2 (11)

Gun: 2 E1 (8)

t_o = 09:44:00.075 MST

Data S_2 = 2,171.03'

Data S_3 = 4,927.67'

R_o = 20,833.37' → 23.7% high

True S_2 = 2,181.90'

True S_3 = 5,053.63'

True R = 16,841.52

True Ψ_3 = 45.°0

	Using True R	Using Ro
(1) K = 1.5:	S_2 = 2171.38', S_3 = 4928.46' → R = 20,826.12', Ψ_3 = 47.°5	S_2 = 2171.31', S_3 = 4928.30' → R = 20,827.65', Ψ_3 = 47.°5
(2) K = 5.0:	S_2 = 2172.19', S_3 = 4930.31' → R = 20,808.38', Ψ_3 = 47.°5	S_2 = 2171.96', S_3 = 4929.77' → R = 20,814.06', Ψ_3 = 47.°5
(3) K = 10:	S_2 = 2173.36', S_3 = 4932.95' → R = 20,784.20', Ψ_3 = 47.°5	S_2 = 2172.88', S_3 = 4931.87' → R = 20,793.98', Ψ_3 = 47.°5
(4) K = 50:	S_2 = 2182.66', S_3 = 4954.06' → R = 20,587.14, Ψ_3 = 47.°3	S_2 = 2180.29', S_3 = 4948.69' → R = 20,636.82', Ψ_3 = 47.°3
(5) K = 100:	S_2 = 2194.29', S_3 = 4980.46' → R = 20,342.37', Ψ_3 = 47.°0	S_2 = 2189.55', S_3 = 4969.70' → R = 20,441.91', Ψ_3 = 47.°1
(6) K = 500:	S_2 = 2287.31', S_3 = 5191.60' → R=18,449.96' → 9.55% high, Ψ_3 = 44.°8	S_2 = 2263.64', S_3 = 5137.87' → R = 18,921.10' → 12.4% high, Ψ_3 = 45.°4
(7) K = 1000:	S_2 = 2403.59', S_3 = 5455.53' → R = 16,231.46' → 3.62% low, Ψ_3 = 42.°1	S_2 = 2356.25', S_3 = 5348.08' → R = 17,116.27' → 1.63% high, Ψ_3 = 43.°2

Day: 12/2/74 (336) W6 (26)

Event: 94 W7 (34)

Gun: 2 W8 (37)

t_o = 09:44:00.075 MST d = 4,430.33'

W = 1.4 kts (2.365 ft/sec) from 281°.7 at 25' elev

T = 42.3°F (5.7°C) at 26' elev

C = 1,098.7 ft/sec

M = 0.002152

θ = 101°.5

	Mike	True Distance r_2 (feet)	True Time r_2/c (sec)	Time Data t(sec)	Time Error $r_2/c - t$ (sec)
1.)	W6	16,898.89	15.381	15.389	-.008
2.)	W7	19,087.77	17.373	17.376	-.003
3.)	W8	21,962.93	19.990	19.979	+.011

True (t_2-t_1) = 1.992 sec

(t_2-t_1) Data = 1.987 sec (short)

True (t_3-t_1) = 4.609 sec

(t_3-t_1) Data = 4.590 sec (short)

True S_2 = 2,188.88'

True S_3 = 5,064.04'

Data S_2 = 2,183.12' } R_o = 17,254.63' → 2.11% high

Data S_3 = 5,043.03' }

Wind S_2 = 2,181.22' } R_{wind} = 17,270.68' → 2.20% high

Wind S_3 = 5,039.23' }

True ψ_3 = 45°.0

ψ_3 = 45°.3

ψ_{3wind} = 45°.3

Day: 12/2/74 (336)
Event: 176
Gun: 2
t_o = 13:44:00.180 MST

B6 (31)
B7 (32)
B8 (33)
d = 4,430.30'

W = 2.4 kts (4.05 ft/sec) from 268°.3 at 25' elev
M = 0.0036465
θ = 24°.9

T = 54.1°F (12.3°C) at 26' elev
C = 1,111.6 ft/sec

	Mike	True Distance r_2 (feet)	True Time r_2/c (sec)	Time Data t(sec)	Time Error $r_2/c - t$ (sec)
1.)	B6	9,405.76	8.461	8.452	.009
2.)	B7	12,915.59	11.619	11.611	.008
3.)	B8	16,864.62	15.171	15.158	.013

True (t_2-t_1) = 3.157 sec
(t_2-t_1) Data = 3.159 sec (long)
True (t_3-t_1) = 6.710 sec
(t_3-t_1) Data = 6.706 sec (short)
True S_2 = 3,509.83'
True S_3 = 7,458.86'
Data S_2 = 3,511.54' } R_o = 9,678.67' → 2.90% high
Data S_3 = 7,454.39' }
Wind S_2 = 3,526.19' } R_{wind} 9,409.93' (4.17' off) → 0.0443% high
Wind S_3 = 7,483.70' }

True ψ_3 = 23°.3
ψ_3 = 23°.5
ψ_{3wind} = 23°.1

Day: 12/2/74 (336)
Event: 176
Gun: 2
t_o = 13:44:00.180 MST

W6 (26)
W7 (34)
W8 (37)
d = 4,430.33'

W = 2.4 kts (4.05 ft/sec) from 268°.3 at 25' elev
M = 0.0036465
θ = 114°.9

T = 54.1°F (12.3°C) at 26' elev
C = 1,111.6 ft/sec

	Mike	True Distance r_2 (feet)	True Time r_2/c (sec)	Time Data t(sec)	Time Error r_2/c-t (sec)
1.)	W6	16,898.89	15.202	15.186	.016
2.)	W7	19,087.77	17.171	17.168	.003
3.)	W8	21,962.93	19.758	19.731	.027

True (t_2-t_1) = 1.969 sec
(t_2-t_1) Data = 1.982 sec (long)
True (t_3-t_1) = 4.556 sec
(t_3-t_1) Data = 4.545 sec (short)
True S_2 = 2,188.88'
True S_3 = 5,064.04'
Data S_2 = 2,203.19'
Data S_3 = 5,052.22'
R_o = 18,145.99' → 7.38% high
Wind S_2 = 2,196.39'
Wind S_3 = 5,038.62'
R_{wind} = 18,205.91' → 7.73% high

True Ψ_3 = 45°.0
Ψ_3 = 45°.6
Ψ_{3wind} = 45°.8

Day: 12/3/74 (337)
Event: 91
Gun: 2
t_o = 10:13:59.771 MST

A3 (14)
A2 (13)
A1 (12)
d = 4,430.70'

W = 3.8 kts (6.42 ft/sec) from 183°.6 at 25' elev
M = 0.0058092
θ = 289°.6

T = 47.8°F (8.8°C) at 26' elev
C = 1,104.8 ft/sec

	Mike	True Distance r_2 (feet)	True Time r_2/c (sec)	Time Data t(sec)	Time Error r_2/c-t (sec)
1.)	A3	9,390.03	8.499	8.447	+.052
2.)	A2	12,917.24	11.692	11.689	+.003
3.)	A1	16,875.70	15.275	15.349	-.074

True (t_2-t_1) = 3.193 sec
(t_2-t_1) Data = 3.242 sec (long)
True (t_3-t_1) = 6.776 sec
(t_3-t_1) Data = 6.902 sec (long)
True S_2 = 3,527.21'
True S_3 = 7,485.67'
Data S_2 = 3,581.76' } R_o = 7,334.79' → 21.9% low
Data S_3 = 7,625.33' }
Wind S_2 = 3,590.39' } R_{wind} = 7,183.18' → 23.5% low
Wind S_3 = 7,642.60' }

True Ψ_3 = 23°.1
Ψ_3 = 20°.4
Ψ_{3wind} = 20°.1

Day: 12/3/74 (337) B6 (31)

Event: 91 B7 (32)

Gun: 2 B8 (33)

t_o = 10:13:59.771 MST d = 4,430.30'

W = 3.8 kts (6.42 ft/sec) from 183°.6 at 25' elev

T = 47.8°F (8.8°C) at 26' elev

C = 1,104.8 ft/sec

M = 0.0058092

θ = 109°.6

	Mike	True Distance r_2 (feet)	True Time r_2/c (sec)	Time Data t(sec)	Time Error r_2/c-t (sec)
1.)	B6	9,405.76	8.514	8.478	.036
2.)	B7	12,915.59	11.690	11.669	.021
3.)	B8	16,864.62	15.265	15.251	.014

True (t_2-t_1) = 3.177 sec

(t_2-t_1) Data = 3.191 sec (long)

True (t_3-t_1) = 6.751 sec

(t_3-t_1) Data = 6.773 sec (long)

True S_2 = 3,509.83'

True S_3 = 7,458.86'

Data S_2 = 3,525.42' } R_o = 9,398.62' → 0.0759% low

Data S_3 = 7,482.81' }

Wind S_2 = 3,516.79' } R_{wind} = 9,556.96' → 1.61% high

Wind S_3 = 7,465.54' }

True Ψ_3 = 23°.3

Ψ_3 = 23°.1

Ψ_{wind} = 23°.4

Day: 12/3/74 (337)
Event: 91
Gun: 2
t_o = 10:13:59.771 MST

W6 (26)
W7 (34)
W8 (37)
d = 4,430.33'

W = 3.8 kts (6.42 ft/sec) from 183°.6 at 25' elev

M = 0.0058092

θ = 199°.6

T = 47.8°F (8.8°C) at 26' elev

C = 1,104.8 ft/sec

	Mike	True Distance r_2 (feet)	True Time r_2/c (sec)	Time Data t(sec)	Time Error $r_2/c - t$ (sec)
1.)	W6	16,898.89	15.296	15.302	-.006
2.)	W7	19,087.77	17.277	17.269	+.008
3.)	W8	21,962.93	19.880	19.864	+.016

True (t_2-t_1) = 1.981 sec
(t_2-t_1) Data = 1.967 sec (short)
True (t_3-t_1) = 4.584 sec
(t_3-t_1) Data = 4.562 sec (short)
True S_2 = 2,188.88'
True S_3 = 5,064.04'
Data S_2 = 2,173.14'
Data S_3 = 5,040.10'
R_o = 16,789.74' → 0.646% low
Wind S_2 = 2,148.89'
Wind S_3 = 4,991.61
R_{wind} = 16,988.98' → 0.533% high

True ψ_3 = 45°.0
ψ_3 = 45°.1
ψ_{3wind} = 45°.5

Day: 12/5/74 (339)
Event: 21
Gun: 2
t_o = 12:48:00.133 MST

B5 (30)
B7 (32)
B8 (33)

d_2 = 8,861.11'
d_3 = 4,430.36'
D = 13,291.47'

W = 21.1 kts (35.64 ft/sec) from 74°.3 at 25' elev

M = 0.03198

θ = 218°.9

T = 56.5°F (13.6°C) at 26' elev

C = 1,114.2 ft/sec

	Mike	True Distance r_2 (feet)	True Time r_2/c (sec)	Time Data t(sec)	Time Error $r_2/c - t$ (sec)
1.)	B5	7,026.36	6.306	6.204	.102
2.)	B7	12,915.59	11.592	11.438	.154
3.)	B8	16,864.62	15.136	14.880	.256

True (t_2-t_1) = 5.286 sec
(t_2-t_1) Data = 5.234 sec (short)
True (t_3-t_1) = 8.830 sec
(t_3-t_1) Data = 8.676 sec (short)
True S_2 = 5,889.23'
True S_3 = 9,838.26'
Data S_2 = 5,831.72'
Data S_3 = 9,666.80'
R_o = 8,947.46' → 27.3% high
Wind S_2 = 5,611.18'
Wind S_3 = 9,336.00'
R_{wind} = 10,307.47' → 46.7% high

True Ψ_3 = 23°.3
Ψ_3 = 26°.4
Ψ_{3wind} = 29°.1

Day: 12/5/74 (339) E3 (19)

Event: 21 E2 (11)

Gun: 2 E1 (8)

t_o = 12:48:00.133 MST d = 4,430.33'

W = 21.1 kts (35.64 ft/sec) from 74°.3 at 25' elev T = 56.5°F (13.6°C) at 26' elev

C = 1,114.2 ft/sec

M = 0.03198

θ = 128°.9

	Mike	True Distance r_2 (feet)	True Time r_2/c (sec)	Time Data t(sec)	Time Error r_2/c-t (sec)
1.)	E3	16,841.52	15.115	14.689	.426
2.)	E2	19,023.42	17.074	16.607	.467
3.)	E1	21,895.15	19.651	19.068	.583

True (t_2-t_1) = 1.958 sec

(t_2-t_1) Data = 1.918 sec (short)

True (t_3-t_1) = 4.536 sec

(t_3-t_1) Data = 4.379 sec (short)

True S_2 = 2,181.90'

True S_3 = 5,053.63'

Data S_2 = 2,137.04' } R_o = 20,317.44' → 20.6% high

Data S_3 = 4,879.08' }

Wind S_2 = 2,048.06' } R_{wind} = 21,111.35' → 25.4% high

Wind S_3 = 4,701.11' }

True ψ_3 = 45°.0

ψ_3 = 47°.7

ψ_{3wind} = 49°.2

Day: 12/5/74 (339) B6 (31)

Event: 33 B7 (32)

Gun: 2 B8 (33)

t_o = 13:29:59.917 MST d = 4,430.30'

W = 18.7 kts (31.58 ft/sec) from 91°.2 at 25' elev

T = 57.9°F (14.4°C) at 26' elev

C = 1,115.7 ft/sec

M = 0.02831

θ = 202°.0

	Mike	True Distance r_2 (feet)	True Time r_2/c (sec)	Time Data t(sec)	Time Error $r_2/c - t$ (sec)
1.)	B6	9,405.76	8.430	8.386	.044
2.)	B7	12,915.59	11.576	11.456	.120
3.)	B8	16,864.62	15.116	14.874	.242

True (t_2-t_1) = 3.146 sec

(t_2-t_1) Data = 3.070 sec (short)

True (t_3-t_1) = 6.685 sec

(t_3-t_1) Data = 6.488 sec (short)

True S_2 = 3,509.83'

True S_3 = 7,458.86'

Data S_2 = 3,425.20' } R_o = 13,287.81' → 41.3% high

Data S_3 = 7,238.66' }

Wind S_2 = 3,308.92' } R_{wind} = 15,536.59' → 65.2% high

Wind S_3 = 7,006.11' }

True ψ_3 = 23°.3

ψ_3 = 27°.3

ψ_{3wind} = 30°.2

Day: 12/5/74 (339) A4 (15) d_2 = 8,860.63'

Event: 69 A6 (17) d_3 = 4,430.59'

Gun: 2 A7 (18) D = 13,291.22'

t_o = 14:47:00.051 MST

W = 21.9 kts (36.99 ft/sec) from 79°.5 at 25' elev

T = 57.6°F (14.2°C) at 26' elev

C = 1,115.3 ft/sec

M = 0.03316

θ = 146°.3

	Mike	True Distance r_2 (feet)	True Time r_2/c (sec)	Time Data t(sec)	Time Error r_2/c-t (sec)
1.)	A4	6,983.02	6.261	5.668	.593
2.)	A6	9,364.19	8.396	8.117	.279
3.)	A7	12,885.60	11.553	11.260	.293

True (t_2-t_1) = 2.135 sec

(t_2-t_1) Data = 2.449 sec (long)

True (t_3-t_1) = 5.292 sec

(t_3-t_1) Data = 5.592 sec (long)

True S_2 = 2,381.17'

True S_3 = 5,902.58'

Data S_2 = 2,731.37' } R_o = 7,286.71' → 4.35% high

Data S_3 = 6,236.76' }

Wind S_2 = 2,486.90' } R_{wind} = 7,877.07' → 12.8% high

Wind S_3 = 5,870.04 }

True ψ_3 = 30°.9

ψ_3 = 31°.5

ψ_{3wind} = 33°.8

Day: 12/5/74 (339) N6 (6)

Event: 69 N7 (7)

Gun: 2 N8 (8)

t_o = 14:47:00.051 MST d = 4,430.34'

W = 21.9 kts (36.99 ft/sec) from 79°.5 at 25' elev

T = 57.6°F (14.2°C) at 26' elev

C = 1,115.3 ft/sec

M = 0.03316

θ = 146°.3

	Mike	True Distance r_2 (feet)	True Time r_2/c (sec)	Time Data t(sec)	Time Error r_2/c-t (sec)
1.)	N6	16,835.95	15.095	14.768	.327
2.)	N7	19,020.91	17.055	16.697	.358
3.)	N8	21,895.15	19.632	19.040	.592

True (t_2-t_1) = 1.959 sec

(t_2-t_1) Data = 1.929 sec (short)

True (t_3-t_1) = 4.536 sec

(t_3-t_1) Data = 4.272 sec (short)

True S_2 = 2,184.96'

True S_3 = 5,059.20'

Data S_2 = 2,151.41' } R_o = 27,950.71' → 66.0% high

Data S_3 = 4,764.56' }

Wind S_2 = 2,029.17' } R_{wind} = 29,301.95' → 74.0% high

Wind S_3 = 4,520.08' }

True Ψ_3 = 45°.0

Ψ_3 = 50°.7

Ψ_{3wind} = 52°.6

AD-A055 436 CALIFORNIA UNIV LOS ANGELES DEPT OF ATMOSPHERIC SCIENCES F/G 20/1
PROBLEMS AND TECHNIQUES OF SOUND RANGING.(U)
AUG 77 M G WURTELE, J ROE DAAD07-75-C-0087

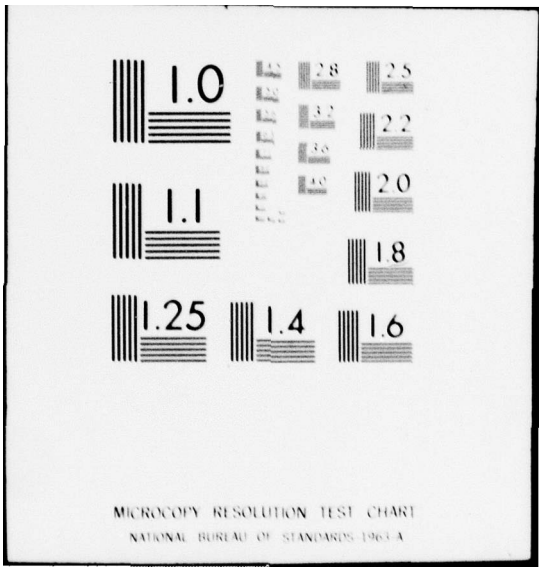
UNCLASSIFIED NL

3 OF 3
AD
A055 436



END
DATE FILMED
8-78
DDC

END
DATE FILMED
8-78
DDC


1.0
1.1
1.25
1.4
1.6
2.8
3.2
3.6
4.0
2.5
2.2
2.0
1.8
MICROCOPY RESOLUTION TEST CHART
NATIONAL BUREAU OF STANDARDS-1963-A

Day: 12/5/74 (339) A5 (16) d_2 = 4,430.18'

Event: 83 A6 (17) d_3 = 8,860.79'

Gun: 2 A8 (19) D = 13,290.97'

t_o = 15:32:00.261 MST

W = 21.4 kts (36. 14 ft/sec) from 82°.9 at 25' elev

T = 56.8°F (13.8°C) at 26' elev

C = 1,114.6 ft/sec

M = 0.03243

θ = 149°.7

	Mike	True Distance r_2 (feet)	True Time r_2/c (sec)	Time Data t(sec)	Time Error r_2/c-t (sec)
1.)	A5	6,971.24	6.254	6.082	.172
2.)	A6	9,364.19	8.401	8.093	.308
3.)	A8	16,841.52	15.110	14.572	.538

True (t_2-t_1) = 2.147 sec

(t_2-t_1) Data = 2.011 sec (short)

True (t_3-t_1) = 8.855 sec

(t_3-t_1) Data = 8.490 sec (short)

True S_2 = 2,392.95'

True S_3 = 9,870.28'

Data S_2 = 2,241.46' } R_o = 7,905.12' → 13.4% high

Data S_3 = 9,462.95'

Wind S_2 = 2,117.43' } R_{wind} = 8,869.67' → 27.2% high

Wind S_3 = 9,090.83'

True ψ_3 = 23°.1

ψ_3 = 25°.8

ψ_{3wind} = 28°.3

Day: 12/5/74 (339) A6 (17)

Event: 85 A7 (18)

Gun: 2 A8 (19)

t_o = 15:34:00.224 MST d = 4,430.39'

W = 22.8 kts (38.51 ft/sec) from 83°.4 at 25' elev

T = 56.8°F (13.8°C) at 26' elev

C = 1,114.6 ft./sec

M = 0.03455

θ = 150°.2

	Mike	True Distance r_2 (feet)	True Time r_2/c (sec)	Time Data t(sec)	Time Error $r_2/c - t$ (sec)
1.)	A6	9,364.19	8.401	8.088	.313
2.)	A7	12,885.60	11.561	11.268	.293
3.)	A8	16,841.52	15.110	14.635	.475

True (t_2-t_1) = 3.159 sec

(t_2-t_1) Data = 3.180 sec (long)

True (t_3-t_1) = 6.709 sec

(t_3-t_1) Data = 6.547 sec (short)

True S_2 = 3,521.41'

True S_3 = 7,477.33'

Data S_2 = 3,544.43' } R_o = 26,704.98' → 185% high

Data S_3 = 7,297.29' }

Wind S_2 = 3,411.61' } R_{wind} = 31,405.13' → 235% high

Wind S_3 = 7,031.64' }

True Ψ_3 = 23°.1

Ψ_3 = 30°.1

Ψ_{3wind} = 33°.3

Day: 12/5/74 (339) B5 (30)

Event: 85 B6 (31)

Gun: 2 B7 (32)

t_o = 15:34:00.224 MST d = 4,430.55'

W = 22.8 kts (38.51 ft/sec) from 83°.4 at 25' elev

T = 56.8°F (13.8°C) at 26' elev

C = 1,114.6 ft/sec

M = 0.03455

θ = 209°.8

	Mike	True Distance r_2 (feet)	True Time r_2/c (sec)	Time Data t(sec)	Time Error $r_2/c - t$ (sec)
1.)	B5	7,026.36	6.304	6.356	-.052
2.)	B6	9,405.76	8.439	8.428	+.011
3.)	B7	12,915.59	11.588	11.431	+.157

True (t_2-t_1) = 2.135 sec

(t_2-t_1) Data = 2.072 sec (short)

True (t_3-t_1) = 5.284 sec

(t_3-t_1) Data = 5.075 sec (short)

True S_2 = 2,379.40'

True S_3 = 5,889.23'

Data S_2 = 2,309.45' } R_o = 8,639.08' → 22.9% high

Data S_3 = 5,656.60' }

Wind S_2 = 2,176.62' } R_{wind} = 9,478.97' → 34.9% high

Wind S_3 = 5,390.94' }

True Ψ_3 = 31°.1

Ψ_3 = 34°.7

Ψ_{3wind} = 37°.2

Day: 12/5/74 (339)
Event: 87
Gun: 2
t_o = 15:36:00.237 MST

A4 (15)
A6 (17)
A7 (18)

d_2 = 8,860.63'
d_3 = 4,430.59'
D = 13,291.22'

W = 25.7 kts (43.41 ft/sec) from 77°.6 at 25' elev

T = 56.8°F (13.8°C) at 26' elev
C = 1,114.6 ft/sec

M = 0.03894
θ = 144°.4

	Mike	True Distance r_2 (feet)	True Time r_2/c (sec)	Time Data t(sec)	Time Error $r_2/c - t$ (sec)
1.)	A4	6,983.02	6.265	5.626	.639
2.)	A6	9,364.19	8.401	8.123	.278
3.)	A7	12,885.60	11.561	11.225	.336

True (t_2-t_1) = 2.136 sec
(t_2-t_1) Data = 2.497 sec (long)
True (t_3-t_1) = 5.300 sec
(t_3-t_1) Data = 5.599 sec (long)
True S_2 = 2,381.17'
True S_3 = 5,902.58'
Data S_2 = 2,783.16'
Data S_3 = 6,240.65'
R_o = 7,638.95' → 9.39% high
Wind S_2 = 2,502.59'
Wind S_3 = 5,819.79'
R_{wind} = 8,329.02' → 19.3% high

True ψ_3 = 30°.9
ψ_3 = 32°.6
ψ_{3wind} = 35°.2

Day: 12/5/74 (339) E3 (19)
Event: 97 E2 (11)
Gun: 2 E1 (8)
t_o = 15:46:00.549 MST d = 4,430.33'

W = 22.1 kts (37.33 ft/sec) from 78°.4 at 25' elev
T = 56.7°F (13.7°C) at 26' elev
C = 1,114.4 ft/sec
M = 0.03349
θ = 124°.8

	Mike	True Distance r_2 (feet)	True Time r_2/c (sec)	Time Data t(sec)	Time Error r_2/c-t (sec)
1.)	E3	16,841.52	15.113	14.657	.456
2.)	E2	19,023.42	17.071	16.476	.595
3.)	E1	21,895.15	19.647	18.884	.763

True (t_2-t_1) = 1.958 sec
(t_2-t_1) Data = 1.819 sec (short)
True (t_3-t_1) = 4.535 sec
(t_3-t_1) Data = 4.227 sec (short)
True S_2 = 2,181.90'
True S_3 = 5,053.63'
Data S_2 = 2,027.09' } R_o = 19,260.17' → 14.4% high
Data S_3 = 4,710.57' }
Wind S_2 = 1,942.40' } R_{wind} = 19,941.71' → 18.4% high
Wind S_3 = 4,541.19' }

True ψ_3 = 45°.0
ψ_3 = 48°.4
ψ_{3wind} = 49°.8

Day: 12/5/74 (339)
Event: 99
Gun: 2
t_o = 15:48:00.215 MST

N5 (5)
N7 (7)
N8 (8)

d_2 = 8,860.67'
d_3 = 4,430.34'
D = 13,291.01

W = 20.1 kts (33.95 ft/sec) from 81°.0 at 25' elev
M = 0.03046
θ = 147°.8

T = 56.7°F (13.7°C) at 26' elev
C = 1,114.4 ft/sec

	Mike	True Distance r_2 (feet)	True Time r_2/c (sec)	Time Data t(sec)	Time Error $r_2/c - t$ (sec)
1.)	N5	15,632.00	14.027	13.705	.322
2.)	N7	19,020.91	17.068	16.570	.498
3.)	N8	21,895.15	19.647	19.141	.506

True (t_2-t_1) = 3.041 sec
(t_2-t_1) Data = 2.865 sec (short)
True (t_3-t_1) = 5.620 sec
(t_3-t_1) Data = 5.436 sec (short)
True S_2 = 3,388.91'
True S_3 = 6,263.15'
Data S_2 = 3,192.76' } R_o = 14,769.15' → 5.52% low
Data S_3 = 6,057.88' }
Wind S_2 = 2,964.35' } R_{wind} = 15,527.35' → 0.67% low
Wind S_3 = 5,715.27' }

True ψ_3 = 45°.0
ψ_3 = 44°.9
ψ_{3wind} = 46°.8

Day: 12/7/74 (341)
Event: 230
Gun: 1
t_o = 15:48:00.435 MST

A3 (14)
A2 (13)
A1 (12)
d = 4,430.70'

W = 8.4 kts (14.19 ft/sec) from 354°.3 at 25' elev
M = 0.01277
θ = 118°.9

T = 53.4°F (11.9°C) at 26' elev
C = 1,110.9 ft/sec

	Mike	True Distance r_1 (feet)	True Time r_1/c (sec)	Time Data t(sec)	Time Error $r_1/c - t$ (sec)
1.)	A3	9,410.51	8.471	8.356	.115
2.)	A2	12,941.68	11.650	11.553	.097
3.)	A1	16,901.73	15.214	15.098	.116

True (t_2-t_1) = 3.179 sec
(t_2-t_1) Data = 3.197 sec (long)
True (t_3-t_1) = 6.743 sec
(t_3-t_1) Data = 6.742 sec (short)
True S_2 = 3,531.17'
True S_3 = 7,491.22'
Data S_2 = 3,551.55' } R_o = 10,856.16' → 15.4% high
Data S_3 = 7,489.69' }
Wind S_2 = 3,524.20' } R_{wind} = 11,410.96' → 21.3% high
Wind S_3 = 7,435.00' }

True Ψ_3 = 23°.0
Ψ_3 = 23°.9
Ψ_{3wind} = 24°.7

Day: 12/7/74 (341) B6 (31)

Event: 230 B7 (32)

Gun: 1 B8 (33)

t_o = 15:48:00.435 MST d = 4,430.30'

W = 8.4 kts (14.19 ft/sec) from 354°.3 at 25' elev

T = 53.4°F (11.9°C) at 26' elev

C = 1,110.9 ft/sec

M = 0.01277

θ = 298°.9

	Mike	True Distance r_1 (feet)	True Time r_1/c (sec)	Time Data t(sec)	Time Error $r_1/c - t$ (sec)
1.)	B6	9,385.47	8.449	8.534	-.085
2.)	B7	12,891.24	11.604	11.700	-.096
3.)	B8	16,838.64	15.158	15.274	-.116

True (t_2-t_1) = 3.156 sec

(t_2-t_1) Data = 3.166 sec (long)

True (t_3-t_1) = 6.709 sec

(t_3-t_1) Data = 6.740 sec (long)

True S_2 = 3,505.77'

True S_3 = 7,453.17'

Data S_2 = 3,517.11' } R_o = 8,751.28' → 6.76% low

Data S_3 = 7,487.47' }

Wind S_2 = 3,544.45' } R_{wind} = 8,270.30' → 11.9% low

Wind S_3 = 7,542.16' }

True Ψ_3 = 23°.3

Ψ_3 = 22°.6

Ψ_{3wind} = 21°.8

9. A MORE GENERAL VIEW OF THE SOUND RANGING PROBLEM

The foregoing sections show conslusively that to a greater or lesser extent, a number of commonly occurring circumstances can distort the acoustic signal of the Howitzer blast. These include atmospheric temperature gradient, an absorbant ground surface, and terrain features of the scale of hundreds of feet. It remains true that in theory the pulse front of the signal arrives at time R/c where R is the shortest distance from source to microphone and c is the local sound speed. However, the effect of diffraction by any of the agencies mentioned above is to deform a relatively sharp pulse-front --ideally a step function--into a signal that arrives with zero amplitude and gradually increases to the amplitude given by the theory without diffraction. If the arriving signal has the signature of an N-wave, it may not rise to this amplitude at all.

Thus the microphone may or may not be able to detect the true arrival time, depending on (1) the sensitivity of the instrumentation, and (2) the background noise level at the time of arrival. The uncertainties in arrival time at a number of microphones do not cancel out, but may lead to serious ranging errors,

One may express this situation in a general way in formulas. If the signal is an undiffracted pulse

$$p = P_o \frac{H(t - R/c)}{R}$$

and is detectable at any two similar microphones. Then

$$t_1 - R_1/c = t_2 - R_2/c$$

or

$$R_2 - R_1 = c(t_2 - t_1) \qquad (9.1)$$

the basic sound-ranging assumption (Section I).

However, if now

$$P = P_o\, H(t - R/c)\; F(R, t)$$

where $F(R, t)$ is the shape factor introduced by diffraction, then (9.1) no longer is valid. We now equate the pressure detectable above noise level by the two microphones, and obtain an equation of the form

$$F(R_1, t_1) = F(R_2, t_2). \qquad (9.2)$$

If $F(R, t)$ were expressible as a function solely of the single variable $t - R/c$, the form of F would not matter: we could always recover (9.1). However, the signatures associated with diffraction do not permit this, for example, that given by (6.3). Thus R_1, t_1, R_2, and t_2 are all unknown, and manipulations and, ultimately, approximations are required to obtain the desired functional form,

$$R_2 - R_1 = G(t_2 - t_1)\,. \qquad (9.3)$$

To produce such a formulation might not be impossible. But success in this would imply that on the whole the diffraction effects were small. The essential feature of a general functional equation (9.2), from the present point of view, is that the difference $t_2 - t_1$ does <u>not</u> uniquely determine the difference $R_2 - R_1$. The basic sound-ranging hypothesis is not valid.

This situation brings us face to face with the most general problem of sound ranging. A beginning has been made on a general approach by Miller and Engebos (1976), but it is not clear that their technique can accommodate to the phenomenon of strong diffraction. <u>The physics of the problem is such that observed signal arrival</u>

time differences are not in general sufficient information to determine source location, even assuming ideal instrumentation. If assumptions of classical sound ranging theory are not valid under conditions that produce diffractive effects, the ranging procedure must be rethought and a much more complicated information-processing system designed. The information would have to consist of the time signatures of pressure at two or more stations, that is, amplitude vs. time as well as time of arrival information. This in turn means careful calibration of the microphones. Supposing that the instrumentation for such a system existed. How would the calculations be performed?

First, we must have a functional form for the pressure signatures, derived from a combination of theory, computation, and observation. Let us say

$$p = F(R, t - t_a)$$

where t_a is the time of first arrival at the microphone, unknown, of course. Let microphone number k have the signature,

$$p^{(k)} = F(R^{(k)}, t - t_a^{(k)}).$$

Then for each microphone there are two unknowns, R and t_a. Two observations P_i at times t_i are in principle adequate to determine the two unkowns, and two microphones are sufficient to determine the source location:

$$P_i^{(k)} = F(F^{(k)}, t_i - t_a^{(k)}) \qquad (9.4)$$

In practice, as is usual in sound ranging, more observations will be useful: the source location is over-determined, but because of inaccuracies in practice, a weighted mean of these estimates is likely to be better than any single estimate.

The solution of (9.4), in general a transcendental equation, would have to be done by a pre-programmed calculator, but is within the capabilities of current hand-held equipment.

10. CONCLUSIONS AND RECOMMENDATIONS

(1) The exact ranging formulas, without approximation, should replace the graphical approximation scheme of FM 6-122. The formulas, including correction for constant wind, can be expressed correct to the first order in the Mach number. These formulas are all derived from first principles in Section 1, and the appropriate FORTRAN softwear is provided in Annex 1.

(2) We emphasize that these formulas referred to in (1) are, or soon will be, within the capability of hand-held programmable calculators, and recommend that this possibility be given serious consideration.

(3) The Howitzer blast begins as a shock front and rather rapidly decays to a sound pulse. However, both theory and computation (Section 7) show that the arrival time of the pulse at sound-ranging distances is measurably in advance of that predicted by linear theory. This suggests the form of a correction term in the sound ranging formulas. In Section 8 it was shown that the incorporation of this term improved the ranging estimates on which it was tested.

It is recommended that further tests of the correction term (7.12) be made on independent data in order to ascertain whether it should be routinely incorporated into the sound ranging formulas.

(4) In Section 3 it is shown that the character of the soil surface significantly lowers the impedance of the boundary for higher frequencies than those used in sound ranging.

This results in a diffractive effect that disguises the true arrival time and causes ranging errors.

It is recommended that the impedance of various surfaces be determined for sound-ranging frequencies, in order to ascertain whe ther this effect should be incorporated into the procedure.

(5) The theoretical solution of a sound pulse propagating in an atmosphere with vertical temperature gradient is exhibited in Section 5. Some cases were numerically computed and it was concluded that diffraction by normal atmospheric temperature gradients are probably not a significant source of error in sound ranging.

(6) In Section 6 it is shown both analytically and computationally that terrain features of the scale of hundreds of meters have a profound effect on the form of the signal. The result of this diffraction is that the signal has zero amplitude at the time of arrival and increases relatively slowly as it is reinforced continuously by later arrivals. Depending on the sensitivity of the microphones, the sound ranging formulas will be more or less in error.

It is recommended that an empirical study be undertaken to determine the threshhold of response and the subsequent record of the microphone exposed to a signal with the characteristic of the diffracted wave. With this information, together with the computations of this report, it would be easy to verify the extent of the error introduced by terrain features, and to design for their correction.

(7) In Section 8, a subset of the PASS data was examined. The atmospheric conditions in those events selected were most nearly conforming to the assumptions underlying sound ranging technique. Although the ranging formulas were highly successful in target acquisition in certain of these cases, in some others the ranging errors were off by as much as 50 to 100 percent. Using different sets of microphones, we obtained both excellent and poor ranging estimates in the same event. After eliminating other sources of error, we concluded that the source was instrumental, most likely in the timing system.

It is recommended that a controlled experiment be designed to test the quantitative reliability of the instrumentation in the field, in order to obtain a better understanding of the source of ranging errors.

(8) This report has not been able to treat the problem of diffraction by wind shear. It is clear, however, that this effect can be of the same importance as diffraction by terrain features, but that the theoretical methods of dealing with it are quite different. It is therefore recommended that diffraction by windshear be investigated in relation to the problem of sound ranging.

(9) In Section 9 it is pointed out that the use of further information (that is, other than arrival time) from the microphone records could improve ranging estimates. This point is also made by W.S.M.R. personnel Miller and Engebos (1976).

It is highly recommended that the possibility of obtaining and using quantitative signal information be investigated. This research effort would necessarily involve

the interaction of expertise in instrumentation, in atmospheric physics, and in mathematics; but the chief hope of improvement in sound ranging lies in this direction.

11. REFERENCES

Brekhovskikh, L. M., 1960: Waves in Layered Media, Academic Press.

Brode, H., 1959: "Blast wave from a spherical charge," Phys. Fluids, 2, 217-229.

Campbell, R. G., 1958: "Initial wave phenomena in a weak spherical blast," J. Appl. Phys., 29, 55-60.

Carlson, M., and Hunt, J. T., 1974: "Effect of geometric symmetry on acoustic scattering in the shadow region," J. Acoust. Soc. Am., 55, 964-967.

Chessell, C. I., 1976: "Observations of the effects of atmospheric turbulence on low-frequency sound propagation," J. Acoust. Soc. Am., 60, 29-33.

Chien, C. F., and Soroka, W. W., 1975: "Sound propagation along an impedance plane," J. Sound Vib., 43, 9-20.

Delaney, M. E., and Bazley, E. N., 1970: "Monopole radiation in the presence of an absorbing plane," J. Sound Vib., 13, 269-279.

Dickenson, P. J., and Doak, P. E., 1970: "Measurements of the normal acoustic impedance of ground surfaces," J. Sound Vib., 13, 309-322.

Doak, P. E., 1952: "The reflexion of a spherical acoustical pulse by an absorbant plane," Proc. Royal Soc., A, 215, 233-254.

Donato, R. J., 1960b: "Spherical wave reflection from a boundary of reactive impedance using a modification of Cagniard's method," J. Acost. Soc. Am.

Donato, R. J., 1976a: "Propagation of a spherical wave near a plane boundary with complex impedance," J. Acost. Soc. Am., 60, 34-39.

Embleton, T. F.W., 1956: "The propagation and reflection of sound pulses of finite amplitude," Proc. Phys. Soc. London, B69, 382-395.

Embleton, T. F. W., and Piercy, J. E., 1974: "Effect of ground on near-horizontal sound propagation," Society of Automotive Engineers, Congress, Detroit, Michigan, 1974.

Embleton, T. F. W., Piercy, J. T., and Olson, N., 1976: "Outdoor sound propagation over ground of finite impedance," J. Acoust. Soc. Am., 59, 267-277.

Embleton, T. F. W., Thiessen, G. T., and Piercy, J. E., 1976: "Propagation in an inversion and reflections at the ground," J. Acost. Soc. Am., 59, 278-282.

Field Manual FM 6-122, 1964: "Artillery Sound Ranging and Flash Ranging", Department of the Army, Washington, D.C.

Franck, H., and Sager, G., 1975: "Zur Schallwegverteilung in der unteren Grundschicht bei Vorhandsein einer Bodeninversion," Z. für Meteor., 24, 130-137.

Friedlander, F. G., 1958: Sound Pulses, Cambridge University Press.

Huang, H., 1975: "Scattering of spherical pulses by a hard cylinder," J. Acoust. Soc. Am., 58, 310-317.

Ingard, U., 1951: "On the reflection of a spherical sound wave from an infinite plane," J. Acost. Soc. Am., 23, 329-335.

Kinney, G. F., 1962: Explosive Shocks in Air, Macmillan Co.

Krasilnikov, V. A., 1963: Sound and ultrasound waves in air, water, and solid bodies, Published for the National Science Foundation by the Israel Program for Scientific Translation, Jerusalem.

Lawhead, R. B., and Rudnick, I., 1951: "Measurements of an acoustic wave propagated along a boundary," J. Acost. Soc. Am., 23, 541-549.

Lee, E. L., Hoinig, H. C., and Kury, J. W., 1968: "Adiabatic expansion of high explosive detonation products," UCRL-50422, Lawrence Radiation Laboratory, Univ. of California.

McNicholas, J. V., Überall, H., and Choate, K., 1968: "Pulse shapes of creeping waves around soft cylinders," J. Acost. Soc. Am., 44, 752-764.

Meecham, W. C., 1956: "On the use of the Kirchhoff approximation for the solution of reflection problems", J. Rational Mech. Anal., 5, 323-334.

Meecham, W. C., 1957: "Varational method for the calculation of the distribution of energy reflected from a periodic surface," J. Acost. Soc. Am., 27, 361-367.

Miles, J. M., 1967: "Decay of spherical blast waves," Phys. Fluids, 10, 2707-2708.

Miller, W., and Engebos, B., 1976: "A mathematical structure for refinement of sound ranging estimates," R and D Tech Rept. ECOM-5805, ASL, White Sands Missile Range.

Milne, E. A., 1921: "Sound waves in the atmosphere," Phil. Mag., 6th ser., 42, 96-114.

Morse, P. M., and Ingard, U., 1968: Theoretical Acoustics, McGraw-Hill Book Co.

Naugolnykh, K. A., 1966: "Compression wave radiated by an expanding sphere," Soviet Physics-Acoustics, 11, 296-301.

Piercey, J. E., and Embleton, T. F. W., 1974: "Effect of weather and topography on the propagation of noise at Vancouver Airport," National Research Council of Canada, Division of Physics, Acoustics Section.

Proud, J. M., Tamarkin, P., and Meecham, W. C., 1958: "Reflection of sound from a surface of saw-tooth profile," J. App. Phys., 28, 1298-1301.

Rudgers, A. J., and Überall, H., 1970: "Pulses specularly reflected by a soft cylinder," J. Acoust. Soc. Am., 48, 3710381.

Rudnick, I., 1947: "The propagation of an acoustic wave along a boundary," J. Acost. Soc. Am., 19, 348-356.

Sedov, L. I., 1959: Similarity and dimensional methods in mechanics, Academic Press.

Taylor, G. I., 1946: "The air wave surrounding an expanding sphere," Proc. Royal Soc., A, 186, 273-292.

Taylor, G. I., 1950: "The dynamics of the combustion products behind plane and spherical detonation fronts in explosives," Proc. Royal Soc., A, 200, 235-247.

Taylor, G. I., 1950: "The formation of a blast wave by a very intense explosion," Proc. Roy. Soc. London, A 201, 159-186.

Trulio, J. G., Perl, N. K., and Balanis, G. N., 1976: "The Afton 2A computer code revised user's manual, AFWL-TR-75-111, Defense Nuclear Agency, A.F. Weapons Laboratory, Kirtland A.F.B., N.M.

Überall, H., Doolittle, R. D., and McNicholas, J. V., 1966: "Use of sound pulses for a study of circumferential waves," J. Acoust. Soc. Am., 39, 564-578.

Thomasson, S.-I., 1976: "Reflection of waves from a point source by an impedance boundary", J. Acost. Soc. Am., 59, 780-785.

U. S. Army Field Artillery School, 1972: "Development of the Field Artillery Observation (Target Acquisition) Battalions," Fort Sill, Oklahoma.

Wenzel, Alan R., 1974: "Propagation of waves along an impedance boundary", J. Acost. Soc. Am., 55, 956-963.

Whitham, G. B., 1974: Linear and Nonlinear Waves, John Wiley and Sons.

Whitham, G. B., 1950: "The propagation of spherical blast," Proc. Royal Soc. A, 203, 571-581.

Wurtele, M. G., 1961: "On the problem of truncation error," Tellus, 13, 379-391.

ANNEX I

FORTRAN CODE FOR SOUND RANGING ESTIMATES

```
FORTRAN IV G LEVEL  21                MAIN              DATE = 77033          08/07/14          PAGE 0001

                C
                C       INPUT VALUES ARE TDEL2,TDEL3,T,V,THETA,D
                C
                C       TYPE DECLARATIONS
                C
                C
0001                    REAL*8 C,M,SIGMA2,SIGMA3,GAMMA2,GAMMA3,X12,X13,D,RHO
0002                    REAL*8 LAMBD1,LAMBD2,LAMBDA,MU,T,V,THETA
0003                    REAL*8 SIGMA(2),GAMMA(2),PSI(2),R(2),TDEL(2),DVAL(2)
0004                999 FORMAT(1H1/1H ,9X,'INDEX',21X,'PSI',22X,'R'/1H0)
0005                    EQUIVALENCE (SIGMA2,SIGMA(1)),(SIGMA3,SIGMA(2)),(GAMMA2,GAMMA(1)),
                       A (GAMMA3,GAMMA(2))
                C
                C       COMPUTATIONS
                C
0006                    WRITE(6,999)
0007                    READ(5,800)ITER
0008                800 FORMAT(I5)
0009                    DO 200 N=1,ITER
0010                    READ(5,850)IDN,(DVAL(I),I=1,IDN)
0011                850 FORMAT(I5/8F10.5)
0012                    DO 200 NN=1,IDN
0013                    D=DVAL(NN)
0014                    READ(5,900) TDEL,V,T,THETA
0015                900 FORMAT(8F10.5)
0016                    THETA=THETA/57.29578
0017                    C =(1.4 * 287. * T)**.5
0018                    M=V/C
0019                    DO 100 I=1,2
0020                100 SIGMA(I)= C * TDEL(I)+M*D*DCOS(THETA)
0021                    GAMMA2 = (SIGMA3/D)*((D**2.-SIGMA2*(SIGMA3-SIGMA2))/
                       A (2.*D**2.+2.*SIGMA2*SIGMA3-SIGMA3**2.-2.*SIGMA2**2.))
0022                    GAMMA3=(SIGMA2*SIGMA3*( SIGMA3-SIGMA2)+D**2.*
                       A (4.*SIGMA2-3.*SIGMA3))/(D*(4.*SIGMA2*SIGMA3-2.*SIGMA2**2.-
                       B SIGMA3**2.-2.*D**2.))
0023                    RHO = .5   * (2.*D**2.-SIGMA3**2+2.*SIGMA2**2.)/(SIGMA3-2.*SIGMA2)
0024                    DO 120 I=1,2
0025                    R(I)=RHO+SIGMA(I)
0026                120 PSI(I) =  DARCOS(GAMMA(I))
0027                    DO 130 I=1,2
0028                    J=I+1
0029                130 WRITE(6,1000)J,PSI(I),R(I)
0030               1000 FORMAT(1H ,10X,I4,2X,2(10X,E18.8))
0031                200 CONTINUE
0032                    STOP
0033                    END
```

SUBPROGRAMS CALLED

SYMBOL	LOCATION	SYMBOL	LOCATION	SYMBOL	LOCATION	SYMBOL	LOCATION	SYMBOL	LOCATION
IBCOM#	AB	FDXPD#	AC	DCOS	B0	DARCOS	B4		

EQUIVALENCE DATA MAP

SYMBOL	LOCATION	SYMBOL	LOCATION	SYMBOL	LOCATION	SYMBOL	LOCATION	SYMBOL	LOCATION
SIGMA2	118	SIGMA	118	SIGMA3	120	GAMMA2	128	GAMMA	128
GAMMA3	130								

SCALAR MAP

SYMBOL	LOCATION	SYMBOL	LOCATION	SYMBOL	LOCATION	SYMBOL	LOCATION	SYMBOL	LOCATION
D	138	V	140	T	148	THETA	150	C	158
M	160	R40	168	ITER	170	N	174	IDN	178
I	17C	NN	180	J	184				

ARRAY MAP

SYMBOL	LOCATION	SYMBOL	LOCATION	SYMBOL	LOCATION	SYMBOL	LOCATION	SYMBOL	LOCATION
PSI	188	R	198	TDEL	1A8	DVAL	1B8		

FORMAT STATEMENT MAP

SYMBOL	LOCATION	SYMBOL	LOCATION	SYMBOL	LOCATION	SYMBOL	LOCATION	SYMBOL	LOCATION
999	1C8	800	1EA	850	1EE	900	1F8	1000	1FF

OPTIONS IN EFFECT ID,EBCDIC,SOURCE,NOLIST,NODECK,LOAD,MAP
OPTIONS IN EFFECT NAME = MAIN , LINECNT = 56
STATISTICS SOURCE STATEMENTS = 33,PROGRAM SIZE = 1686
STATISTICS NO DIAGNOSTICS GENERATED

IEW2061 STEP RETURN CODE = 0000

CCN3011 QUICKRUN PRINTED 2 TOTAL PAGES, REQUIRED 0 TRACKS.

REGION ALLOCATION	CORE USED	MAIN STORAGE	EXTENDED STORAGE
150K	138K	150K	00K
REGION CHARGED			
150K			

STEP CPU TIME	JOB CPU TIME	STEP I/O COUNT	JOB I/O COUNT
0.60S	0.60S	63	63

OS/360 LOADER

OPTIONS US_ _ PRINT,MAP,NOLET,CALL,RES,NOTERM,SIZE=120832,NAME=**GO

NAME	TYPE	ADDR	NAME	TYPE	ADDR	NAME	TYPE	ADDR	NAME	TYPE	ADDR	NAME	TYPE	ADDR
MAIN	SD	6C810	IHDLASCN*	SD	6CEAB	DARCOS *	LR	6CEAB	IH$DARCS*	LR	6CEAB	DARSIN *	LR	6CEC0
IH$DARSN*	LR	6CEC0	IHDLSCN *	SD	6D110	DCOS *	LR	6D110	IH$DCOS *	LR	6D110	DSIN *	LR	6D134
IH$DSIN *	LR	6D134	IHDFDXPD*	SD	6D3A0	FDXPD# *	LR	6D3A0	IHDECOMM*	SD	6D558	IBCOM# *	LR	6D584
IB081971*	LR	6D584	FDIOCS# *	LR	6D640	INTS#TCH*	LR	6E328	FIOAP# *	SD	6E3E8	AP081971*	LR	6E85C
IHDCOMH2*	SD	6EAE0	SEQDASD *	LR	6EE92	IHDFCVTM*	SD	5F4A0	ADCON# *	LR	5F4A0	FCVADUTP*	LR	6F54A
FCVLOUTP*	LR	6F5DA	FCVZOUTP*	LR	6F736	FCVIOUTP*	LR	6FAE4	FCVEOUTP*	LR	5F8D5	FCVCOUTP*	LR	6F8D6
INT6S#CH*	LR	6FE30	IHDERNTH*	SD	6FEB0	ARITH# *	LR	6FEB0	ADJS#TCH*	LR	70448	IHDEFIOS*	SD	70630
FIOCS# *	LR	70680	FIOCSBEP*	LR	70686	IHDFIOS2*	SD	71828	IHDUOPT *	SD	71E08	IHDFCONI*	SD	72140
FQCONI# *	LR	72140	IHDFCONQ*	SD	72440	FQCONQ# *	LR	72440	IHDERRM *	SD	72910	ERRMON *	LR	72910
IHDERRE *	LR	72928	IHDUATBL*	SD	72F38	IHDFTEN *	SD	73570	FTEN# *	LR	73570	IHDETRCH*	SD	73708
IHDTRCH *	LR	73708	ERRTRA *	LR	73710	IHD_EXP *	SD	73980	DEXP *	LR	73980	IH$DEXP *	LR	73980
IHDLLOG *	SD	73C60	DLOG10 *	LR	73C60	IH$DLOG0*	LR	73C60	D_OG *	LR	73C78	IH$DLOG *	LR	73C78
IHDLSQRT*	SD	73E88	DSQRT *	LR	73E88	IH$DSQRT*	LR	73E88						

TOTAL LENGTH 77E0
ENTRY ADDRESS 6C810

PSI

0.95504953D+00
0.78504060D+00

R

0.56117125D+04
0.64850654D+04